Freezing of Lakes and the Evolution of their Ice Cover

Matti Leppäranta

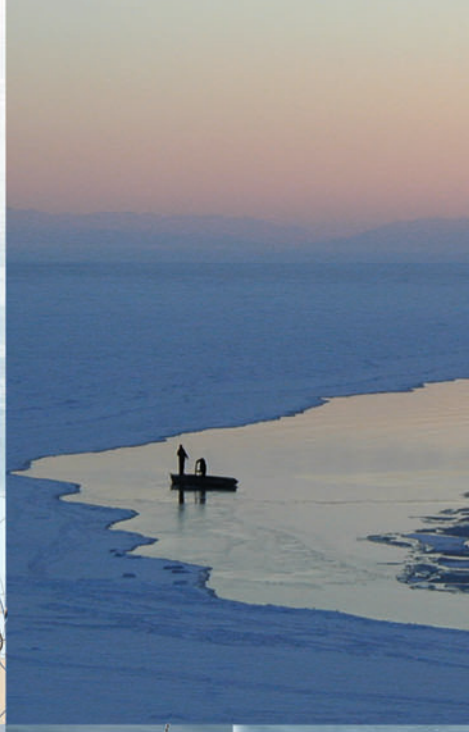

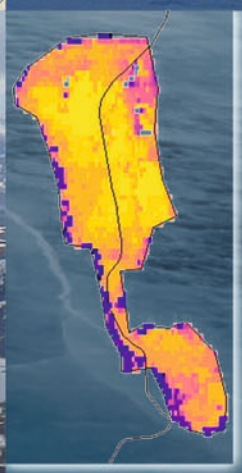

Springer

PRAXIS

Freezing of Lakes and the Evolution of their Ice Cover

Cover: Picture Information

Lake landscape in the middle
Lake Kilpisjärvi, northern Finland, taken from top of neighbouring fell 540 m above the lake surface (Photograph by Matti Leppäranta).

Map above
Isolines of 180 days and 100 days long ice season and 0 °C January mean temperature (this figure was prepared by graphics assistant Salla Jokela for the book).

Image on the right side
Surface radiative temperature field of Lake Peipsi, at the border of Estonia and Russia based on MODIS data (prepared by professor John E. Lewis, Ottawa, Canada).

Lake on the upper right corner
Lake Baikal landscape (Photograph by Dr. Oleg Timoshkin, Irkutsk, Russia).

Back Cover Photo

Winter limnology course students taking water samples in an ice-covered lake in Lammi, southern Finland. (photograph by Matti Leppäranta).

Matti Leppäranta

Freezing of Lakes and the Evolution of their Ice Cover

Springer

PRAXIS

Matti Leppäranta
Department of Physics
University of Helsinki
Helsinki
Finland

ISBN 978-3-642-29080-0 ISBN 978-3-642-29081-7 (eBook)
DOI 10.1007/978-3-642-29081-7

Library of Congress Control Number: 2014951667

Springer Heidelberg New York Dordrecht London

Published in association with Praxis Publishing Chichester, UK

Printed on acid-free paper

Springer is part of Springer Science+Business Media (www.springer.com)

Preface

Ice cover is an essential element in cold climate lakes. To a large degree it isolates the water body from the atmosphere and sunlight and slows down physical and biological processes. In the boreal zone, tundra, and mountain regions the ice cover is seasonal, while in very high altitudes and high polar latitudes perennially ice-covered lakes are found. Ice formation results in different ice types and stratigraphy, which further influence the ice properties. Ice sheets of freshwater lakes are poor in impurities. However, they may possess liquid layers or inclusions, which serve as habitats of biota. Freezing of lakes also brings both practical advantages and problems to human living conditions in cold regions. It is of great interest to know the physics and ecology of lake ice, to monitor and predict ice conditions in lakes, and to evaluate what can be the impact of climate changes to lake ice seasons.

The present book, *Freezing of Lakes and the Evolution of their Ice Cover*, provides the status of knowledge in the physics of lake ice and the interactions between the ice cover and the liquid water body underneath. Historical developments in lake ice research are also discussed. Chapter 1 gives a brief overview and presents the research fields. The Chap. 2 contains the classification of ice-covered lakes, and in Chap. 3 the structure and properties of lake ice are presented. Ice growth and melting are treated in Chap. 4, while the following chapter focuses on ice mechanics. Chapter 6 goes into the more exotic environment of pro-glacial lakes. The last three chapters consider important lake topics related to the presence of ice in lakes. Chapter 7 contains the physics of the water body beneath lake ice, Chap. 8 discusses the winter ecology of freezing lakes and the lake ice interface toward the society including the impact of climate change on lake ice seasons. The book ends with a brief closing chapter and a list of references. Examples of research problems for student learning are listed throughout the book.

The underlying idea behind the book has been to include the whole story of lake ice into a single volume. There is a crying need for such synthesis, as winter limnology research and applications are increasing and, apart from review papers, no comprehensive monograph exists on this topic in English. The author has contributed to lake ice research since the 1980s. In particular, his topics of interest have been lake ice structure and thermodynamics, light transfer in ice and snow, ice mechanics in large lakes, and lake ice climatology. Mathematical modeling of ice growth, drift, and decay are covered in this research.

This book has grown from the author's research, collaborative visits to several universities and research institutions, and intensive international courses—winter schools—in lake ice and winter limnology. These visits concern in particular the Estonian Marine Institute of Tartu University (Tallinn, Estonia), Institute of Limnology of the Russian Academy of Sciences (Sankt Petersburg, Russia), Institute of Low Temperature Science of Hokkaido University (Sapporo, Japan), Leibniz-Institute of Freshwater Ecology and Inland Fisheries (Berlin, Germany), Marine Systems Institute of Tallinn University of Technology (Tallinn, Estonia), Northern Water Problems Institute of the Russian Academy of Sciences (Petrozavodsk, Russia), and the State Key Laboratory of Coastal and Offshore Engineering of Dalian University of Technology (Dalian, China). The winter schools have been arranged in Lammi Biological Station and Kilpisjärvi Biological Station of the University of Helsinki, in the Saroma-ko field site of the Hokkaido University, and in the Dalian University of Technology. Very recently, the author joined the Global Ice Modeling Project of the Global Lake Ecological Observatory Network (GLEON).

In the progress of his research the author has learned about lake ice from a large number of colleagues. Especially, he wants to thank Professor Erkki Palosuo as well as Professors Lauri Arvola, Nikolai N. Filatov, Robert V. Goldstein, Hardy B. Granberg, Timo Huttula, Toshiyuki Kawamura, John E. Lewis, Zhijun Li, Anu Reinart, Kalevi Salonen, Matti Tikkanen, Kunio Shirasawa and Juhani Virta, and Drs. Helgi Arst, Cheng Bin, Christof Engelhardt, Ants Erm, Glen George, Sergey Golosov, Sergey Karetnikov, Georgiy Kirillin, Esko Kuusisto, Nikolai M. Osipenko, William Rizk and Arkady Terzhevik. He is also deeply thankful to his present and former students, in particular Ms. Elina Jaatinen, Mr. Juho Jakkila, Dr. Onni Järvinen, Ms. Anni Jokiniemi, Mr. Tom Kokkonen, Dr. Ruibo Lei, Ms. Elisa Lindgren, Dr. Shi Liqiong, Dr. Ioanna Merkouriadi, Dr. Jari Uusikivi, Dr. Caixing Wang, Dr. Keguang Wang, and Dr. Yu Yang. The scientists and technicians, who have participated in lake ice research programs from this institute and from several other organizations, are gratefully acknowledged, as well as students of the summer and winter schools. Ms. Elisa Lindgren is thanked for a very careful review of the manuscript, and Dr. Salla Jokela is thanked for several graphics products for this book.

The home institute of the author since 1992, the Department of Geophysics (fused to Department of Physics in 2001) of the University of Helsinki, is deeply thanked for good working conditions and support. This work is a contribution of the Nordic Center of Excellence Cryosphere–atmosphere interactions in a changing Arctic climate (CRAICC), and the results are based on several research projects, primarily Ficca and Finnarp programs of the Academy of Finland and Clime project of the EU V Framework. The preparation of this book was made possible by financial support for a sabbatical year from the Finnish Cultural Foundation, which is gratefully acknowledged.

Helsinki, August 2014 Matti Leppäranta

Contents

Introduction

1

At a hole in lake ice, painting from the year 1900 by Finnish artist Pekka Halonen (1865–1933), who is well known especially of his winter landscapes. In cold regions the normal life has adapted to the presence of frozen lakes. Holes in ice cover have been used for household water, for washing clothes, and for cold bathing.

M. Leppäranta, *Freezing of Lakes and the Evolution of their Ice Cover*,
DOI 10.1007/978-3-642-29081-7_1

Fig. 1.1 Ice break-up takes place in spring in boreal lakes. In a few weeks before, the ice cover is weak and patchy and impossible to cross by foot or boat

A lake is a liquid water body in a depression on the surface of the Earth. It is associated with a water balance, which largely determines the lake volume and the quality of the water. Most lakes contain fresh water,[1] and their size ranges from small ponds to large intra-continental basins with area more than 10^4 km^2. The global water storage of lakes is 125,000 km^3, and about 80 % of that is fresh water, accounting for the fraction of 0.3 % of the Earth's fresh water resources (Henderson and Henderson 2009). In the boreal zone, tundra, and high mountain regions in lower latitudes, lakes freeze over in winter. The ice season may last more than half a year, and the thickness of the ice can reach 1 m. In high polar zones and at very high altitudes, there are perennially ice-covered lakes, with ice cover several meters thick. Sub-glacial lakes are located at the base of the 3–4 km thick Antarctic ice sheet and represent an extreme ice coverage condition.

Frozen lakes have belonged to people's normal life in the cold regions. Solid ice cover has been an excellent base for traffic across lakes and to travel and to transport cargo, provided the ice has been thick enough. Indeed, ice cover isolates island inhabitants from the mainland in periods, when the ice is too weak to walk but still limits boating (Fig. 1.1). These periods bear in Finnish language an old word *kelirikko* (from 'keli' = traffic

[1] Fresh water refers to natural water with low concentration of dissolved substances. There is no strict upper limit for the concentration but 0.5 ‰ (or about 0.5 g L^{-1}) serves as a convenient reference. This limit is also often used for the upper limit of the salinity of drinking water.

conditions, 'rikko' = broken); in Russian language there is a corresponding word распутица (rasputica) for land crossing. One of the first records of lake ice events is 'The battle on the ice', a winter clash between the forces of the Norwegian king Áli and the Swedish king Aðals on the ice of Lake Vänern in Sweden, about year 530 AD (Osborn and Mitchell 2007). The chart and booklet of Olaus Magnus Gothus (1539) also showed drawings of crossing over ice-covered lakes by skis, skates and horses in the Middle Ages.

In wood industry logs have been stored in winter on ice to be dragged or flown along streams to factories after ice melt. Until about mid-20th century, when refrigerators were not common, the cold content of lake ice was utilized. Ice blocks were cut in winter, stored under a sawdust cover to protect against melting, and used as a cooler for foods in summer. Openings were sawed into the lake ice cover for household water and for washing clothes at the site. For ice-covered lakes, special techniques were developed for domestic and commercial winter fishing.

Scientific research on lake ice was commenced in the 1800s along with the birth of physical limnology and lake hydrology. Scientists in the European Alpine countries have played a strong role in physical limnology, and therefore it is natural that lake ice has been considered as an important topic from the beginning (e.g., Götzinger 1909; Verescagin 1925). Lake ice monitoring was also commenced in northern Europe in the 1800s (Simojoki 1978). The lake ice season modifies the hydrological year in cold regions by its influence on the annual distribution of runoff and by the problems caused by ice to the management of water resources. Ice engineering problems were included in scientific research from the late 1800s (Barnes 1928), concerning shipping, ice forces on structures, and the bearing capacity of ice.

Lake ice phenology[2] has been a major topic, since ice seasons show large variability, which is a critical issue to the local population (Simojoki 1940). Collection of ice phenology time series of inland waters was commenced in the 1800s (Hällström 1839; Levänen 1894), and now they are of great importance in the research of climate history. Long time series are available, e.g., from 1443 for Lake Suwa, Japan (Arakawa 1954), from 1833 for Lake Kallavesi, Finland (Simojoki 1959), and from 1850 for Lake Mendota, Wisconsin (Wing 1943). Records of lake ice in Central Europe have been used to examine the occurrence of extreme cold winters (Maurer 1924). Winter temperature conditions in lakes were also investigated in the early lake research (Homén 1903). Ecology of frozen lakes gained more attention only later (see, e.g., Greenbank 1945; Hutchinson 1957; Vanderploeg et al. 1992). In all, the research of ice-covered lakes turned out to be for long, until about 1970s, scattered and occasional. The annual cycle of lakes was taken into the topics of the International Hydrological Decade 1965–1974 with ice season then considered in cold regions (e.g., Falkenmark 1973). Thereafter, more effort was made on polar lakes as the access to reach them was better and measurement techniques had become feasible.

[2] Phenology refers to studies of dates of recurring phenomena; it originates from the Greek word φαίνω (*phainō*), 'to make appear'.

After the year 2000, lake ice science has re-gained much attention, due to environmental problems and due to climate change impact questions (Magnuson et al. 2000; Leppäranta 2009a; Bengtsson 2011; Kirillin et al. 2012). The leading research topics have been light transfer through ice, interaction between the ice and the water body, mathematical modelling, remote sensing, and ice phenology time series analysis. Characteristics of lake ice seasons are quite sensitive to climate variations. For human living conditions, shorter ice seasons, while extending the open water season, with also thinner ice would severely or even drastically limit traditional on-ice activities. Climate change issues also necessitate a better understanding of the role played by lake ice cover in the emission of greenhouse gases, especially methane, into the atmosphere, and in the global carbon budget.

Research on winter biology of lakes has largely increased (Melnik et al. 2008; Salonen et al. 2009; Shuter et al. 2012). Questions of life in extreme conditions have brought in more research of lakes with perennial ice and pro-glacial lakes (Vincent and Laybourn-Parry 2008; Keskitalo et al. 2013), especially in the Antarctic continent (Fig. 1.2). The ecosystem of subglacial lakes has been largely unknown (Christner et al. 2006), but the

Fig. 1.2 Supraglacial Lake Suvivesi in the western Dronning Maud Land, Antarctica. The *photograph* was taken from Basen nunatak about 300 m above the lake surface. The lake surface is blue ice, the length of the lake is 3 km, its maximum depth is about 1.5 m, and it possesses a thin ice cover of 5–10 cm (see Leppäranta et al. 2013)

first samples ever were taken from these lakes in 2013 showing signs of life, mainly bacteria (Rogers et al. 2013).

A seasonal lake ice cover is normally thin as compared with the lake depth. Its physical properties show large variability due to the high homologous temperature,[3] the large size of individual crystals, and the presence of impurities. Lake ice sheets show a simple stratification pattern consisting mainly of congelation ice and snow-ice (e.g., Michel and Ramseier 1971). Snow accumulation on lake ice is a common, and essential feature. Only in cold and very dry climate regions, the ice cover is snow-free (e.g., Huang et al. 2012). Even a thin layer of snow significantly weakens the heat exchange between the lake water body and the atmosphere and the transfer of sunlight into the water. Also snow and liquid water may form slush, which transforms into snow-ice in cold weather (e.g., Palosuo 1965). In freezing lakes, frazil ice seems to be a very rare form of ice, and no observations have been reported of the occurrence of anchor ice.

The evolution of a lake ice season is primarily a thermodynamic process (see Leppäranta and Wang 2008; Leppäranta 2009a). When the ice is thick enough, it spans a stable cover across the lake. Ice breakage and mechanical displacements take place in very large lakes and also in smaller lakes when the ice is weak. In the melting period, ice loses its bearing capacity due to internal deterioration (Fig. 1.3). Decay of a lake ice cover is a thermo-mechanical process, starting from the shoreline. Melting of near-shore ice releases the ice from solid boundaries, and the ice cover may then shift as forced by winds and currents. The movement of ice causes further breakage of ice that speeds the decay process.

Land-ice interaction due to thermal expansion and onshore ride-up or piling-up is an important environmental and practical issue. It has attracted geographers for more than 100 years (Buckley 1900; Helaakoski 1912; Alestalo and Häikiö 1979). Due to thermal and mechanical stresses, lake ice deforms shore areas and loads man-made structures. In shallow areas, bottom scouring by ice and freezing through the whole water column give rise to deformation and erosion of the lake bottom. Land-ice interaction has therefore geological as well as biological consequences.

In the lake water body, physical phenomena and processes are very different under ice cover from the open water conditions. The ice cover cuts the transfer of momentum from the wind to the water body that damps turbulence and mixing. The surface water temperature is at the freezing point, and there is very little vertical transfer of heat, apart from geothermal lakes. In all, the temperature structure and circulation are quite stable. However, in very large lakes, the ice sheet may experience episodic movements and disturb the water body. In spring, solar radiation provides a strong downward flux of heat, which constitutes the strongest heat flux into fully ice-covered lakes, and the ice melt water with its impurities is released into the water column.

The volumetric changes in the liquid water body, associated with formation and growth of ice are of no consequence in deep lakes, but in very shallow lakes, there may be

[3] Absolute temperature of a medium relative to its melting point.

Fig. 1.3 The bearing capacity of lake ice is a major safety question for on-ice traffic. The *photograph* shows a rescue operation of a car in Lake Päijänne, Finland in spring 2005. Published in newspaper *Etelä-Suomen Sanomat* on March 31, 2005, *photograph* by Mr. Pertti Louhelainen. Printed by permission

substantial proportional reductions in the volume of liquid water. Also in shallow lakes the bottom sediments have an important role in the ice season. They store heat in summer and release the heat back into the water body in winter. The release of heat and gas from the lake bottom makes a contribution to the circulation in the water body and the structure of the ice sheet. Impurities may dissolve from the sediments to the near-bottom waters and create a thin bottom boundary layer due to the salinity stratification. This layer also has impact on the near-bottom living conditions.

Lake ice formation and growth have influence on the water quality as well as on the lake ecology (see, e.g., Salonen et al. 2009). The concentration of suspended matter decreases in the water column during the ice season, since inflow and turbulence are weak, and sedimentation is not compensated by resuspension. At the time of ice breakup, the load of impurities peaks from the snow and ice meltwater. Sunlight is the main limitation for primary production under ice cover. Photosynthesis is paused for the polar night, and in the case of a thick snow cover on ice, the dark season can be much longer and extend to sub-polar latitudes. Another critical factor is that the ice cover reduces the level of dissolved oxygen in the water body by cutting the influx from the atmosphere (Greenbank 1945; Hargrave 1969; Golosov et al. 2006). This results sometimes in anoxic conditions in the deep water and fish kills (Fig. 1.4). At the beginning of the ice season, the oxygen

Fig. 1.4 Fish kill in Lake Äimäjärvi, southern Finland, March 2003. Ice season 2002–2003 began exceptionally early (late October), and the oxygen storage was not sufficient for the whole ice season. *Photograph* by Mr. Jouni Tulonen, printed with permission

content depends on the strength of the autumn mixing. In windy autumn conditions the whole water body may cool down to 1–2 °C, and the cold water will then contain a large amount of oxygen. Stratification conditions can be favourable for primary production beneath the ice cover, and an under-ice bloom may form if the bare ice period lasts long enough in spring.

Mathematical modelling applications in lake ice research have concerned ice growth and decay, radiation transfer, ice forces, and ice drift or ice displacements (Fig. 1.5). The models are used in basic science, forecasting, ice engineering, and environmental and climate research. Two classical, analytical models, which are still applicable as first approximations, are the ice growth model by Stefan (1891) and the bearing capacity model by Hertz (1884). The former model predicts ice thickness proportional to the square root of the freezing-degree-days, and the latter model predicts bearing capacity of a point load to be proportional to square of the ice thickness.

Until 1990s, thermodynamic lake ice models were mostly semi-analytical, based on the freezing-degree-days for ice growth and positive degree-days for melting (e.g., Ashton 1986; Leppäranta 2009a). Thereafter also numerical models have been employed (e.g.,

Fig. 1.5 Learning frozen lakes in the field is an essential corner stone of knowledge. Students of winter limnology field course taking samples under guidance of teachers in Lake Pääjärvi, Finland

Croley and Assel 1994; Leppäranta 1983; Yang et al. 2012) for the evolution of ice thickness and temperature. Numerical sea ice models had been developed earlier (Maykut and Untersteiner 1971; Semtner 1976; Saloranta 2000) and they could be utilized for lake ice as well. The snow layer, which plays an important, interactive role in the evolution of the thickness of ice, forms the most difficult part of lake ice thermodynamic models. Mechanical models have been developed for ice forces in the scales of man-made structures (Korzhavin 1962; Michel 1978) and for drift ice for whole lake basins (Ovsienko 1976; Wake and Rumer 1983; Leppäranta and Wang 2008). Ice drifts in very large lakes, such as Caspian Sea and Lake Superior, as in oceanic basins, and also in this field sea ice models were the basis of lake ice models (Doronin 1970; Hibler 1979; Coon 1980; Wang et al. 2003). The drift of ice is forced by winds and currents, and the mobility of ice is determined by its yield strength.

The Earth's surface waters are classified into lakes, rivers and seas. In cold regions, ice occurs in these basins as lake ice, river ice, sea ice, and blocks of land ice[4] origin forming the category of *floating ice*. Rivers have a dynamic ice cover due to their permanent and turbulent flow, resulting in abundance of frazil ice, anchor ice and ice jams. Sea ice forms of saline water and contains brine, and sea ice basins have large length scale with drifting ice. Small blocks of land ice can be found in proglacial lakes, but massive icebergs belong

[4] Land ice is glacial, brought to water bodies by calving of glaciers.

to the polar oceans. Much of the research history in lake ice tells of applications of earlier results of sea ice and river ice research to lake environment. This is largely because lake ice has less scientific history due to the less practical significance. For the background references, the status of sea ice physics is presented in Wadhams (2000), Weeks (2010) and Leppäranta (2011), and for river ice a good coverage is contained in Ashton (1986), Ferrick and Prowse (2002) and Shen (2006).

Lake ice is a degree more simple as compared with sea ice and river ice. Lake ice cover is mostly immobile, circulation in the water body beneath the ice cover is weak, and freshwater lake ice is poor in impurities. But lakes with strong through flow may have river ice type processes, ice structure in brackish and saline lakes is similar to sea ice, and drift ice occurs in very large lakes. Our knowledge of ice in saline waters comes mainly from marine research, and these results are to a large degree applicable for brackish and saline lakes.

This book, *Freezing of lakes and the evolution of their ice cover*, presents an up-to-date (year 2014) status of knowledge of the physics of lake ice with applications. The focus is in freshwater lakes, with river ice and sea ice results utilized where necessary. The role of dissolved substances of the parent water is explained here on the basis of the results of sea-ice research. A historical view is embedded with material from the more than 100 years long period in lake ice research. Earlier literature of the physics of ice-covered lakes is quite sparse. The important earlier books include Barnes (1928), Shumskii (1956), Pivovarov (1973), Michel (1978), and Ashton (1986), and also the book of Pounder (1965) contains much general material on ice in natural waters. Pivovarov (1973) presented a scientific monograph on freezing lakes and rivers with weight on the liquid water body, while Ashton (1986) had a more engineering point of view on this topic [see also Ashton (1980) for a condensed review paper on the topic]. More recent material is given in the article collections by Vincent and Laybourn-Parry (2008), George (2009), and in the reviews of Kirillin et al. (2012) and Shuter et al. (2012).

This chapter introduces the topic with a brief historical overview. Chapter 2 presents lakes, their classification, and the zones of ice-covered lakes. Ice formation and the structure and properties of lake ice are treated in Chap. 3, with ice impurities and ice mass balance. Chapter 4 contains lake ice thermodynamics from the freezing of lakes to ice melting, with thermodynamic models included. Lake ice mechanics is the topic of Chap. 5 with engineering questions such as ice forces and bearing capacity of ice. A section is included on drift ice in large lakes. Glaciers and pro-glacial lakes are treated in Chap. 6. Quite exotic lakes are introduced, in particular lakes at the top and bottom of glaciers and ice sheets. Chapter 7 focuses on the water body beneath lake ice cover with water balance, stratification, and circulation. Ecology of ice-covered lakes is treated in Chap. 8, considering the limitations brought by ice cover and considering life inside the ice cover. Also environmental and practical questions with lake ice are treated, and the chapter ends at evaluating the climate change impact on lake ice seasons. Final closing words are written in Chap. 9, and the book ends with references. Study problems with solutions are given as

examples in the text. Properties of ice and liquid water and useful constants and formulae have been collected in the annex.

Lake ice belongs to the cryosphere part, which closely interacts with human living conditions. The ice cover has caused problems but people have learnt to live with them and also to utilize the ice. Especially, in the present time this is true for on-ice traffic and recreation activities. Ice fishing has become a widely enjoyed winter hobby. Winter sports such as skiing, skating and ice sailing are now popular activities on frozen lakes. Lake ice—human interface is to stay so in future, but modifications may be brought along the evolution of the climate. The lake ice response to climate warming will appear as the shortening of the ice season due to the increasing air temperature and also as changing the quality of the ice seasons via the climate influence on the thickness and structure of the ice.

Freezing of Lakes

2

Terra/Aqua – MODIS (Moderate Resolution Imaging Spectroradiometer) image of the eastern Great Lakes region on February 28, 2004. White sheets of ice float on Lake Huron, top left, and Lake Erie, bottom center. Lake Ontario, right, remains free of ice because of its depth, though the land around it is in winter's icy grip. The mean depth is 19 m in Lake Erie and 86 m in Lake Ontario.

NASA. Production by The Visible Earth team (http://visibleearth.nasa.gov/).

M. Leppäranta, *Freezing of Lakes and the Evolution of their Ice Cover*,
DOI 10.1007/978-3-642-29081-7_2

2.1 Lake Types and Characteristics

2.1.1 Classification and Geometry of Lakes

Lakes are found in all climate zones. A first-order zonation of potentially freezing freshwater lakes can be taken as the continental areas where the January (Northern Hemisphere) or July (Southern Hemisphere) mean air temperature is less than 0 °C (Fig. 2.1). This region is called the *cold climate zone* in the present book. There, at least very shallow freshwater lakes freeze in normal years (Fig. 2.2). The cold climate zone covers most of Eurasia and North America down to around 40°N at sea level (see Hutchinson and Löffler 1956; Bates and Bilello 1966). In the Asian mountains the boundary is more south, while in the Western Europe it is more north. Apart from Antarctica, in the Southern Hemisphere only some mountain areas are included in the zone of freezing lakes. Actually, between 45°S and the Antarctic continent the only land masses are the southern corner of New Zealand and some small islands with eventual minor freezing inland water basins; e.g., Lake Alta, a small and deep cirque lake in the New Zealand Southern Alps at 45°03′S 168°49′E, 1,800 m above sea level. In the high Andes, the cold zone even reaches the Equator.

However, in the cold climate zone there are lakes, which do not freeze. Very deep lakes have thermal time scale longer than the winter, geothermal heating influences the surface temperature due to convective mixing in the water body, and salinity depresses the freezing point. Examples of these lakes are the very deep Lake Shikotsu (mean depth 266 m) in Hokkaido (http://www.ilec.or.jp/database/asi/asi-16.html), the geothermal Lake Hévíz in Hungary, where the water temperature is above 20 °C in winter although other lakes in the region are normally frozen (http://www.lakeheviz.hu), and the hypersaline Don Juan Pond (salinity 440 ‰) in McMurdo Dry Valley in Antarctica, generally unfrozen in winter even at temperatures below −50 °C (Meyer et al. 1962).

For lake ice climatology, it is convenient to define *the ice year* as the time between the maxima in the summer heat storage in two consequent summers. In the Northern Hemisphere the maximum occurs normally in July–August, while in the south it is January–February. The ice years are labelled as the year they begin, i.e. ice year 2006 is the period between the summer maxima of 2006 and 2007. In this way ice-free years and *perennial ice* periods can be properly treated in ice phenology analyses. Perennial ice or *multi-year ice* is ice that has survived at least one summer, while ice-free ice year is such where no ice occurs between two summer maxima.

A natural *geological classification* of lakes is according to the origins of the depressions, where lakes have formed (Table 2.1). The time scale of the depressions is usually very long. On a short time-scale, new ones can be created by landslides or environmental engineering. The formation of glacial lakes has taken place at glaciers and ice sheets. In the Northern Europe and North America there are large lake districts, which originate from ice sheet–land processes after the Last Glacial Maximum. Epiglacial, supraglacial and subglacial lakes constitute the class of proglacial lakes, which are found at existing

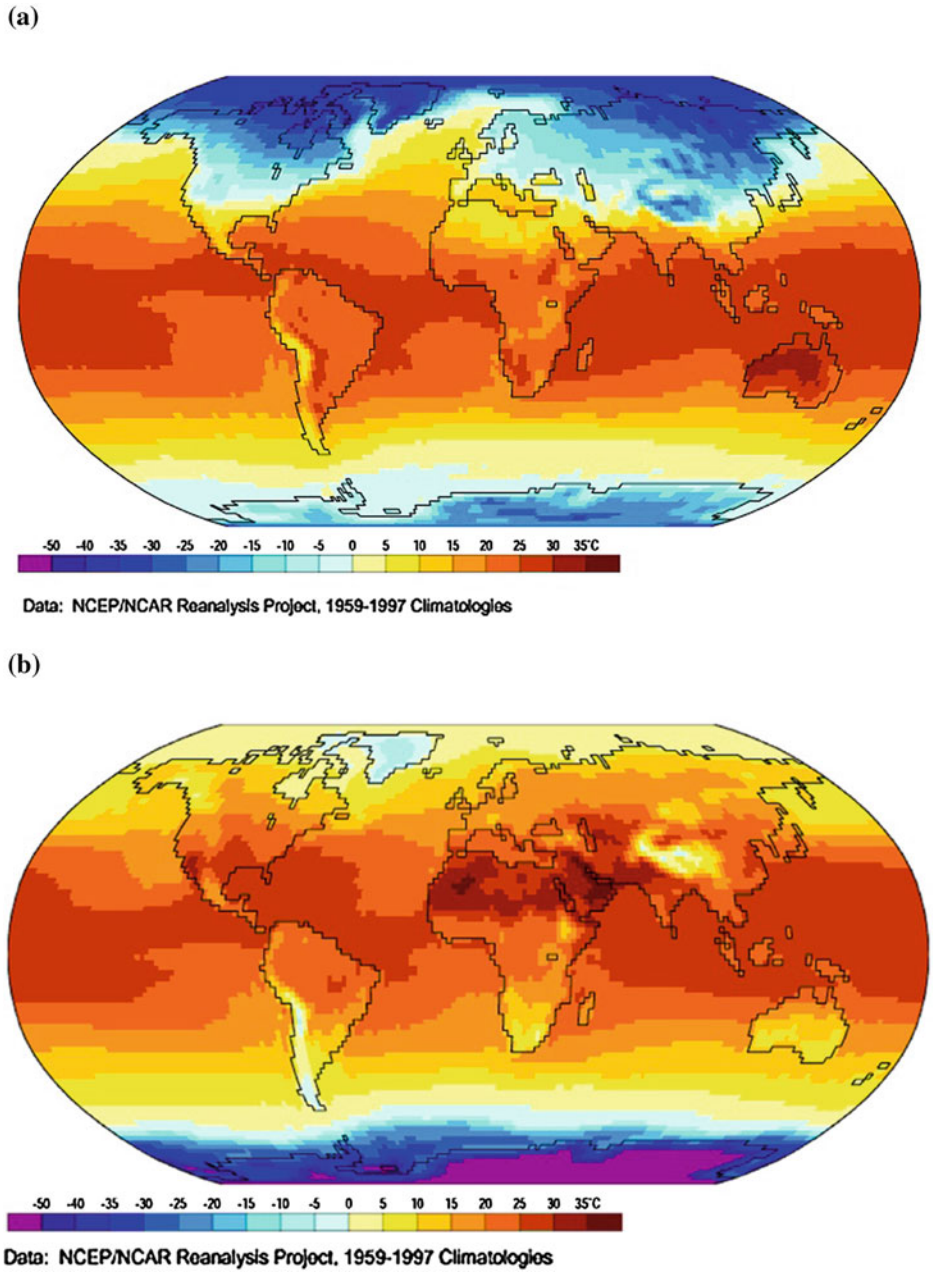

Fig. 2.1 Mean **a** January and **b** July air temperature (°C) on the Earth's surface, 1959–1997 (Global climate animations, Department of Geography, University of Oregon based on NCEP/NCAR Reanalysis Project 1959–1997 Climatologies data, see http://geography.uoregon.eduenvchange/clim_animations/index.html). © Department of Geography, University of Oregon

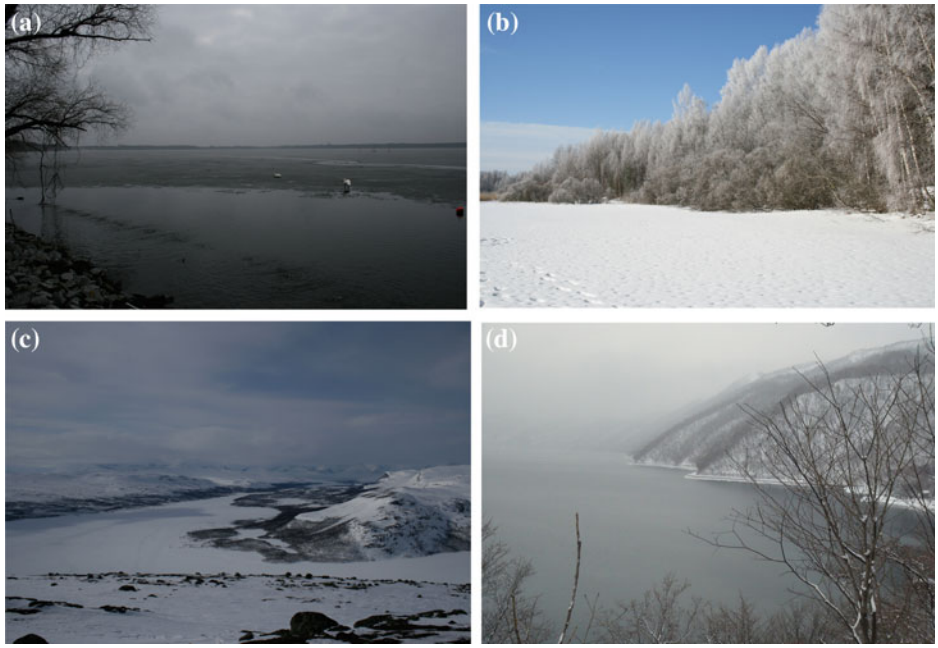

Fig. 2.2 Lakes in the cold climate zone: **a** Ephemeral, Lake Müggelsee, Berlin; **b** Boreal, Lake Pääjärvi, southern Finland; **c** Tundra, Lake Kilpisjärvi, Lapland; **d** Deep, non-freezing lake, Lake Shikotsu, Hokkaido

Table 2.1 The origins of lake basins with examples from the cold climate zone

Class	Mechanism for depression	Examples
Tectonic	Plate shifts	Lake Baikal (Russia)
Volcanic	Volcano crater	Lake Shikotsu (Hokkaido, Japan)
Meteorite	Impact crater	Lake Lappajärvi (Finland)
Landslide	Land mass accumulation	Attabad Lake (Pakistan)
Reservoir	Man-made	Rybinsk reservoir (Volga basin, Russia)
Glacial	Ice sheet dynamics	Lake Saimaa (Finland)
Epiglacial	Ice sheet dynamics	Lake Mandrone (Italy)
Supraglacial	Solar radiation	Lake Suvivesi (Dronning Maud Land)
Subglacial	Glacial pressure	Lake Vostok (East Antarctica)

glaciers and ice sheets, and glacial meltwater forms the main part of their water balance. Supraglacial lakes are a particular category in that their base is ice rather than rock or soil. Sometimes epishelf lakes are taken as their own category, accounting for freshwater lakes at the surface of ice shelves and a marine basin underneath.

Example 2.1. The Baltic Sea has a dynamic history since the retreat of the Fennoscandian ice sheet, beginning 15,000 years ago, due to the positive fresh water balance and rebound of the ground from the pressure of the ice sheet (see Leppäranta and Myrberg 2009). First, the basin was an epiglacial lake (the Baltic Ice Lake), then a brackish sea (the Yoldia Sea, connected to Atlantic), and again an epiglacial lake (Ancylus Lake, Fig. 2.3). About 8,000 years ago Ancylus Lake turned into a brackish marine basin, which has developed to the present Baltic Sea. The land uplift is still in progress in the northern Baltic Sea, and after 1,000 years the northern basin, the Bay of Bothnia, will be isolated from the oceanic connection and become the largest lake in Europe. The presently largest lake of Europe, Lake Ladoga, was part of the Baltic Ice Lake but became isolated in the Yoldia Sea phase.

The *physical classification* of the lake basins concerns their size and shape. A simple approach is to consider the magnitudes of the geometric size, both horizontal and vertical

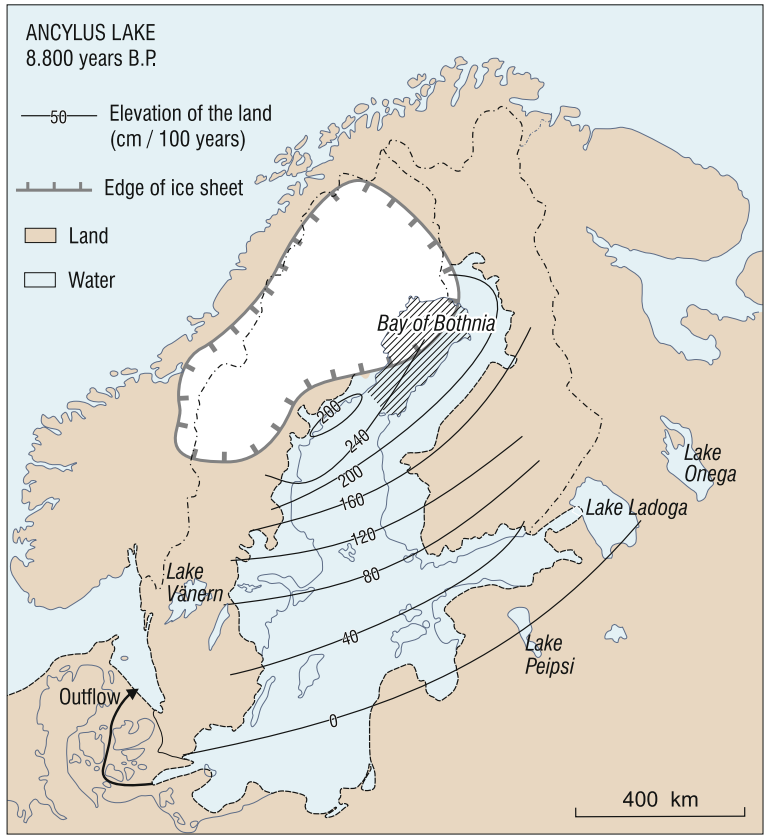

Fig. 2.3 Ancylus Lake. Also shown are the largest lake of Europe, the Lake Ladoga, which separated at the formation of the Yoldia Sea about 10,000 years ago, and the Bay of Bothnia, the largest lake in Europe after 1,000 years. The contour inside the lake shows the present Baltic Sea. Modified from Leppäranta and Myrberg (2009)

extent. The following system corresponds to the present terminology as well as to the common language (Table 2.2).

Table 2.2 Classification of lakes for their lateral and vertical size

Lateral	Very large	Large	Medium	Small	Very small
	1,000 km	100 km	10 km	1 km	100 m
Vertical	Very deep	Deep		Shallow	Very shallow
	1,000 m	100 m		10 m	1 m

Note 'medium deep' concept is not used for lakes in general

The lateral dimension is taken as the length of the major axis of the lake, $\ell_{\max}$, and the vertical dimension is taken as the maximum depth $H_{\max}$. Lakes with horizontal extent much smaller than 100 m are ponds or pools. The minor axis $\ell_{\min}$ is defined as the minimum width of the 'opening' through which the lake could penetrate. These two axes together with the area and depth define the elongation γ, the shape factor κ, and the aspect ratio δ:

$$\gamma = \frac{\ell_{\max}}{\ell_{\min}}, \quad \kappa = \frac{A}{\ell_{\max}\ell_{\min}}, \quad \delta = \frac{H_{\max}}{\ell_{\max}} \tag{2.1}$$

where A is the surface area of the lake. For a square lake, $\gamma = 1$, and for a rectangular lake $\kappa = 1$. The aspect ratio is normally $\delta \sim 10^{-3}$. Example medium-size lakes have depth of 10 m and lateral extent of 10 km. Lakes are defined open or closed whether there is outflow or not, respectively.

The horizontal size of a lake influences the mixing conditions, since long wind fetches create more turbulence and higher waves. Freshwater lakes are vertically mixed at the temperature of maximum density, and therefore the depth of a lake is one of the principal characteristics to influence the timing of the freezing. The deeper or larger the lake, the later will the freezing be and, consequently, the shorter the ice season. In brackish and saline lakes, the temperature of maximum density depends on the salinity and mixing by cooling reaches halocline. In the freeze-up of a lake, the distribution of depth influences the lateral growth of the ice cover. The whole depth distribution is given by the hypsographic curve

$$\Pi(H) = \int_{H}^{\infty} \pi(H')dH' \tag{2.2}$$

where $\Pi(H)$ is the relative are of the lake deeper than H, and π is the spatial density of depth.

A single lake is connected so that liquid water particles can circulate throughout. There may be sub-basins with straits between, and sometimes such basins are taken as separate lakes. The geometry of lakes has fractal characteristics (Korvin 1992). The length of the

Table 2.3 Classification of lakes based on the salinity (S) of the water

Freshwater lakes	$S < 0.5$ ‰	Salinity of concern only in ice season
Brackish lakes	0.5 ‰ $\leq S < 24.6$ ‰	Freezing point < temperature of max density
Saline lakes	24.6 ‰ $\leq S < 35$ ‰	Freezing point ≥ temperature of max density, salinity at most at the oceanic level
Hypersaline lakes	$S \geq 35$ ‰	Salinity greater than the oceanic level

shoreline increases as a power law $l \propto (\Delta s)^{1-D}$, where $D > 1$ is the fractal dimension or the Hausdorff dimension of the shoreline; thus $l \to \infty$ as $\Delta s \to 0$. Therefore the length of the shoreline is not a well-defined geometrical property of a lake. Similarly, the number of lakes in an area depends on the resolution of the map and is a questionable quantity. Instead, the surface area and the lengths of the major and minor axes of a lake are well defined. Apart from the descriptive geometry, however, the fractal concept has not brought much new applicable information to lake research. It is clear that the coastline geometry is an important factor during the ice season but the length scale of this factor is finite and process dependent.

The *geochemical classification* of the water quality is firstly based on the salinity[1] (S), which is, by definition, the relative mass of dissolved salts and expressed in parts per thousand or per mille (‰). Salinity is a state variable of natural waters and influences on the mixing, circulation, cooling, and freezing. The classification reads (Table 2.3).

Brackish water salinity is much less than the salinity of normal seawater (35 ‰); the transition at 24.6 ‰ is often chosen, because this is the salinity where the temperature of maximum density equals the freezing point (see Sect. 2.1.2). The chemical composition of the lake water plays an especially significant role in hypersaline lakes, for which lake-specific equations of state would be desirable to describe the growth and properties of the ice. Additional geochemical classifiers are pH and concentrations of specific substances; e.g., oxygen, nutrients, organic matter. A specific class of lakes are tidal lakes, such as lagoons, which exchange water with the ocean (Shirasawa et al. 2005). In the northern part of the Baltic Sea, due to glacial land uplift lakes become slowly isolated from the sea and the salinity consequently decreases (e.g., Lindholm et al. 1989). These lakes are called *fladas*.

2.1.2 Physical Properties of Lake Waters

A fundamental property of lake water is its density, denoted by ρ. This is provided by the equation of state, which is written in general form as

$$\rho = \rho(T, S, p) \tag{2.3}$$

[1] In limnology, the amount of dissolved salts (c_d) is normally expressed in mass/volume (grams/litre). Clearly $c_d = \rho S$, where ρ is the density of the solution.

where T is temperature and p is pressure.[2] Salinity is usually ignored in the case of freshwater bodies, but even there it may be significant under a complete ice cover when turbulence is absent. Results from marine research are mainly used to obtain the properties of water in brackish and saline lakes. Seawater is a chemically uniform solution, where only the total concentration of dissolved salts varies, but lake waters are lake-specific, and therefore each lake would need an own equation of state. However, the seawater case is usually taken as the approximation. Standard seawater formulae are valid for the salinity range from 0 to 40 ‰, and therefore another approach needs to be employed for hypersaline lakes. The influence of pressure on density is significant only in very deep lakes.

The equation of state of seawater is an empirical function with about 40 parameters (UNESCO 1981, see Appendix 1). It can be formulated as:

$$\rho(T,S,p) = \frac{\rho(T,0,0) + \Delta(T,S,0)}{1 - p/K(T,S,p)} \tag{2.4}$$

where $\rho(T, 0, 0)$ is the density of pure water and $\Delta(T, S, 0)$ is salinity correction at zero gauge pressure, and the secant bulk modulus $K = K(T, S, p)$ gives the pressure effect.

The pressure distribution in a lake can be obtained from the hydrostatic law

$$\frac{dp}{dz} = -\rho g \tag{2.5}$$

where z is the vertical co-ordinate positive up, and $g = 9.81$ m s^{-2} is the acceleration due to gravity. The surface ($z = \zeta$) boundary condition for the gauge pressure is $p(\zeta) = 0$; note that $\zeta - z$ is the depth below the lake surface, and if the density is constant, we have $p = \rho g \cdot (\zeta - z)$. In fresh water, $p(10\text{ m}) = 0.98$ bar, i.e. a 10-m water column corresponds approximately to the pressure of one standard atmosphere ≈1 bar. Since $K \approx 2 \times 10^4$ bar, the density increase due to pressure is about 0.5 % per 10 kbar or about 1 km depth. The pressure effect can be ignored in lakes less than 100 m deep ($p < 10$ bar).

In deep lakes also the *adiabatic temperature change* is an important factor in the vertical stratification. When a water parcel rises up, its temperature decreases due to decreasing pressure, and in sinking down adiabatic warming takes place in a symmetric manner. The adiabatic change of temperature can be expressed as $\Gamma \equiv -\mathrm{d}T/\mathrm{d}z|_{\mathrm{ad}} = \alpha g T/c_{\mathrm{p}}$, where α is the coefficient of thermal expansion, and c_{p} is the specific heat at constant pressure (see Curry and Webster 1999); in fresh water, $\Gamma \sim 0.12$ °C km^{-1}. The temperature corresponding to the surface temperature after adiabatic cooling is called the *potential temperature*. In a neutrally stratified deep fresh water lake, the potential temperature is constant, and therefore the in situ temperature increases by the adiabatic lapse rate with depth.

[2] Pressure is taken as the 'gauge pressure', which is the pressure above the sea level atmospheric pressure. Usually pressure is given in bars; the SI unit is Pascal and 1 bar = 100 kPa. The pressure of one standard atmosphere is 1013.25 mbars.

When salinity variations are ignored, the following simple form can be used for the density of lake water:

$$\rho(T, 0, 0) = \rho_0 - \alpha(T - T_m)^2 \tag{2.6}$$

where $\rho_0 = \rho(T_m, 0, 0) = 999.98$ kg m^{-3} is the fixed reference density, T_m is the temperature of maximum density of fresh water, $T_m(S = 0, p = 0) = 3.98$ °C, and $\alpha \approx 8.0 \times 10^{-3}$ kg m^{-3} °C^{-2} is an empirical parameter (Fig. 2.4). The parameter α can be further tuned fitting the density to the UNESCO (1981) formula after selecting the applicable temperature range. The first-order approximation for low salinities is obtained just by adding the term $\beta \cdot S$, $\beta \approx 0.81$ kg m^{-3} to the right-hand side of Eq. (2.6). In cold waters the influence of temperature on density is at smallest. Under a stable ice cover, even small salinity variations can be important, and then it is better to stick to the full UNESCO (1981) formula.

Example 2.2. The average density of a human body is 1,062 kg m^{-3} (Krywicki and Chinn 1966). If the water salinity is more than 75 ‰, the water is denser and human bodies float free. There are many hypersaline lakes, which satisfy this requirement, perhaps the most famous ones are the Dead Sea ($S \approx 315$ ‰, $\rho \approx 1{,}240$ kg m^{-3}) and the Great Salt Lake in Utah ($S \sim 100$ ‰, $\rho \sim 1{,}100$ kg m^{-3}).

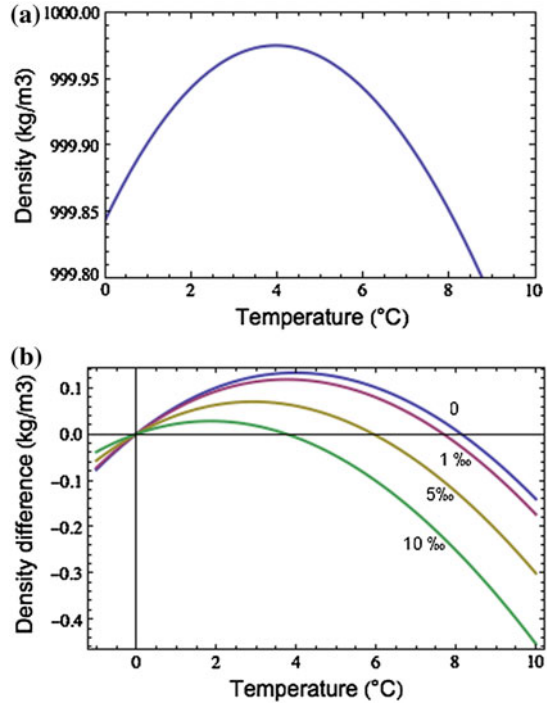

Fig. 2.4 Density of water as a function of temperature for different salinities at zero gauge pressure: **a** Pure water density as a function of temperature, **b** Density difference from the density at 0 °C in fresh and brackish water (salinities 0, 1, 5 and 10 ‰). The plots are based on the UNESCO (1981) standard equation of state

Salinity and pressure also influence on the temperature of maximum density and the freezing point, T_f. The former can be obtained from the equation of state (Eq. 2.4) (in principle, but the mathematics is cumbersome and lower order fits are therefore employed), while the latter is an independent formula given in UNESCO (1981). The fit for T_m by Caldwell (1978) and the UNESCO freezing point formula are:

$$T_m[^\circ\mathrm{C}] = 3.982 - 0.2229 \cdot S - 0.02004 \cdot p \cdot (1 + 0.00376 \cdot S) \cdot (1 + 0.000402 \cdot p) \tag{2.7a}$$

$$T_f[^\circ\mathrm{C}] = -0.0575 \cdot S + 1.710523 \times 10^{-3} S^{3/2} - 2.154996 \times 10^{-4} S^2 - 7.53 \times 10^{-3} p \tag{2.7b}$$

where the salinity is taken in parts per thousand (‰) and the pressure in bars. These equations are valid for the salinity up to 40 ‰, where $T_f = -2.21\,^\circ$C and $T_m = -4.93\,^\circ$C at the zero gauge pressure. It is seen that both the freezing point and the temperature of maximum density decrease with increasing salinity, the latter one even more rapidly. For $p = 0$, the curves meet at $T = -1.28$ °C, $S = 24.6$ ‰. This salinity is normally taken as the boundary between brackish and saline waters; then in brackish water $T_m \geq T_f$, and in saline water the opposite is true. Even though brackish water has a maximum density above the freezing point, the maximum is weaker the larger is the salinity (Fig. 2.4b). In freshwater lakes, the freezing point is between −0.03 and 0 °C, and the temperature of maximum density is between 3.87 and 3.98 °C.

Linear approximations of Eq. (2.7a, b) are:

$$T_m = 3.98 - 0.223 \cdot S - 0.0207 \cdot p \tag{2.8a}$$

$$T_f = -0.0549 \cdot S - 7.53 \times 10^{-3} \cdot p \tag{2.8b}$$

The pressure term in Eq. (2.8a) is a linear fit to the outcome from the equation of state, exact at $p = 0$ and 100 bar, showing that the temperature of maximum density decreases with increasing pressure by about 0.1 °C/5 bar. The freezing point is exact at $p = 0$, $S = 0$ and $S = 35$ ‰.

Example 2.3. Lake Baikal is a deep, freezing fresh water lake in Siberia. At 1-km depth, the temperature of maximum density is 1.91 °C, and at this temperature and depth the density of water is 1004.9 kg m^{-3}. The freezing point is –0.75 °C at this depth. The subglacial Lake Vostok is beneath the Antarctic ice sheet. The pressure is of the order of 350 bar (Siegert et al. 2001), and, consequently, if the water is fresh, then T_f = –2.64 °C and T_m = –3.95 °C.

In hypersaline waters, the freezing point depends more strongly on the chemical composition of the dissolved substances. At high salinities, the freezing point depression is no more linear, and different salts crystallize at their individual eutectic temperatures

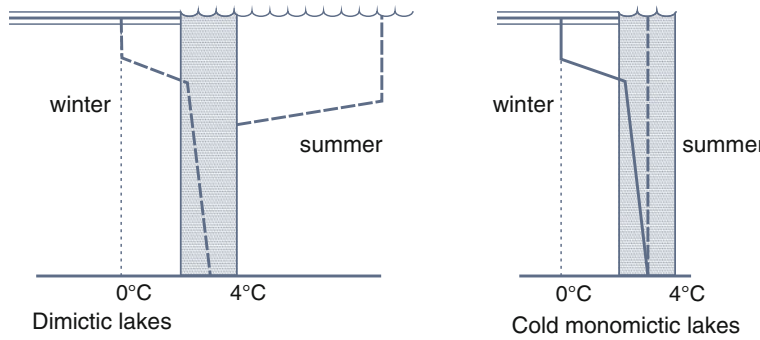

Fig. 2.5 Temperature stratification in dimictic and cold monomictic lakes. The *dotted rectangle* denotes for autumn and spring overturn of the water mass

(for seawater, see Assur 1958). Therefore the freezing point formula is more clearly lake-specific. The Great Salt Lake of Utah does not freeze although there is snow around in winter. Also it is well known that Don Juan Pond with the salinity 440 ‰ in Antarctica does not freeze at −50 °C during the austral winter (Meyer et al. 1962).

Unstable density stratification does not hold in natural conditions, and therefore increase of surface water density leads to convective mixing. The temperature of maximum density of fresh water is close to 4 °C, and when the surface temperature reaches this level, the whole water column is mixed by vertical convection. This is also called the *water mass turnover*. The oxygen storage of fresh water lakes is renewed in turnover events, which are necessary for aquatic life.

In the response of freshwater lakes to thermal forcing, overturn events are crucial. This event is especially strong in the cooling season, starting from the deepening of the mixed layer in the autumn. Convective mixing deepens until the surface water temperature reaches the temperature of maximum density, and then mixing can continue by wind forcing to lower temperatures. The water temperature lags behind the air temperature forcing with the 'thermal memory' depending on the lake depth. For shallow lakes the memory is less than 1 month, and for deep lakes it can be several months. Water volumes are fairly small, but if the annual cycle is strong, lakes may store much heat in the summertime to be released in winter. Summer heat is also stored in the bottom sediments in shallow lakes.

The annual frequency of the turnover events is the basis of *limnological classification* of lakes (Fig. 2.5). Most seasonally freezing lakes have two turnover events—in spring and fall—and thus are *dimictic*. The summer stratification[3] shows warm upper layer and cold lower layer with a thermocline layer between, where the temperature changes sharply. In winter, the stratification is inversed. However, the time between spring and fall mixing becomes shorter with colder climate, and when cold enough they merge together

[3] In limnology the upper layer is called epilimnion and the lower layer is called hypolimnion.

—the lakes are then cold *monomictic*. Lake with perennial ice can be *polymictic* or *amictic*, but if they are completely ice-covered the oxygen storage is not renewed.

In shallow brackish, saline or hypersaline lakes, wind-driven or wave-driven mixing can drive the turnover. But in deep lakes, vertical mechanical mixing may be limited, and permanent salinity stratification develops. The layer with a sharp change in salinity is called a *halocline*, analogous to the thermocline. If the halocline is very weak, the bottom water may be renewed locally by increase of salinity due to evaporation or salt rejection in freezing. If this is not the case, the lake is classified as *meromictic*, referring to the existence of a lower layer of water, which does not intermix and hence is anoxic. In principle, ventilation of such layer could take place by inflow of more saline water, but that is possible only in particular environmental conditions. Example in Finland there are small meromictic lakes, where the stratification has developed after the Last Ice Age.

Example 2.4. Consider a cold lake with temperature T_b and salinity S_b in the lower layer and salinity $S_0 < S_b$ in the upper layer. Vertical ventilation of the water body is possible, if $\rho(T_m, S_0) > \rho(T_b, S_b)$. This can be exactly solved from the equation of state (Eq. 2.4), but a first-order approximation can be made using Eq. (2.5) with a salinity term $\beta \cdot S_b$, $\beta \sim 0.8$ kg m^{-3} added. Then we can obtain the ventilation condition (salinity in ‰):

$$S_b - S_0 < \frac{\alpha}{\beta}[T_b - T_m(S_b)]^2$$

Since $\alpha/\beta \sim 10^{-2}$ °C^{-2}, it is seen that for $T_b - T_m(S_b) = 3$ °C, we must have $S_b - S_0 < 0.1$ ‰.

The temperature pair of the maximum density and the freezing point (T_m, T_f) is the basis of the classification of the cooling process in lakes. In fresh and brackish lakes, as soon as $T_0 < T_m$, the lake is potentially capable to freeze, because then the density decreases in cooling, and in calm conditions only a short, cold period may result in a thin ice cover. Kirillin et al. (2012) called ‘pre-winter’ the period, when the surface temperature is below T_m and the surface is still ice-free. The condition $T_0 \leq \max(T_m, T_f)$ means always a risk of ice formation. However, the strength of the inverse stratification becomes weaker with increasing salinity (Fig. 2.4b). In saline and hypersaline lakes, the potential freezing condition comes only when the surface temperature has reached the freezing point. Lakes can be classified for the ice season (see also Fig. 2.2) into (Table 2.4).

Proglacial lakes form a special group of ice-covered lakes. They form in front (epiglacial lakes), on top (supraglacial lakes) or underneath (subglacial lakes) of glaciers and ice sheets, and glacial melt water is their main water source (Menzies 1995). Epiglacial lakes have normally a seasonal ice cover, and they are much as normal cold region lakes. Supraglacial lakes have seasonal or perennial ice cover and the body is in liquid state usually in summer only (e.g., Leppäranta et al. 2013). Subglacial lakes have a perennial, glacial ice cover, and they are usually under a heavy pressure caused by the thick ice.

Table 2.4 Classification of lakes according to the quality of the ice season

Ice cover	Explanation	Surface temperature T_0	Limnological type
Ephemeral	Ice formation possible	Winter $T_0 \leq \max(T_m, T_f)$	DM, MM
Seasonal	Ice forms and melts	Winter $T_0 = T_f$	DM, CM, PM, MM
Perennial	Multi-year ice	Summer $T_0 \approx T_f$	CM, AM, PM, MM

DM Dimictic; *CM* Cold monomictic; *PM* Polymictic; *AM* Amictic; *MM* Meromictic

Physical properties of fresh water can be taken constants for many applications (Table 2.5). Temperature, salinity and pressure modify the physical properties of water, but apart from electromagnetic properties the influence is small. The density is, however, an important exception, since beneath the ice cover very small differences have a major role in the circulation of lake water masses. Very high pressure, or equivalently great depth, needs to be considered in subglacial lakes and cooling of very deep lakes. In the other extreme, at the surface of high mountain lakes the pressure is low that has influence primarily on the saturation levels of dissolved gases.

Optical classification of lake waters goes for the colour and transparency (Arst 2003; Arst et al. 2008). Coloured dissolved organic matter (CDOM), suspended matter, and chlorophyll *a* are the basis of this classification. The strength of brown colour is related to the concentration of CDOM, while turbidity is related to the concentration of suspended matter. Because humic substances give a large contribution to CDOM in boreal lakes, in classical limnology, the colour of water is given by the degree of brown colour in filtered water samples, obtained by comparing the water sample colour with the colour of platinum

Table 2.5 Physical properties of fresh water ($S < 0.5$ ‰) at the temperature of 0 °C and comments on the variability of these properties in cold water. Standard atmospheric pressure is assumed

Property	Value (T = 0 °C, S = 0)	Variability
Molecular weight	18.02 g mol^{-1}	–
Density	1,000 kg m^{-3}	Equation of state
Thermal expansion	-6.7×10^{-5}	→0 at 3.98 °C, >0 at higher T
Viscosity	1.79×10^{-3} N s m^{-1}	1.57×10^{-3} N s m^{-1} at 4 °C
Surface tension	75.6 N m^{-1}	<1 % (75.1 N m^{-1} at 4 °C)
Compressibility	0.51×10^{-10} Pa^{-1}	Very small
Speed of sound	1,402 m s^{-1}	1,421 m s^{-1} at 4 °C
Specific heat	4.22 kJ kg^{-1} $°C^{-1}$	<1 ‰
Thermal conductivity	0.561 W m^{-1} $°C^{-1}$	≈1 %
Latent heat of freezing	333.5 kJ kg^{-1}	–
Latent heat of evaporation	2.49 MJ kg^{-1}	<1 %
Electric conductivity	<1 μS cm^{-1}	Highly sensitive to salinity[a]
Relative permittivity	87.9	Sensitive to salinity

[a]In pure water the electric conductivity is extremely small but then rises fast with salinity

Table 2.6 Lake classification systems

Background	Object	Basis
Geological	Lake basin	Origin of the depression where the lake has formed
Physical	Size	Horizontal extent and depth
Geochemical	Salinity	Influence on water density and other properties
Limnological	Mixing	Frequency of convective overturn of the water mass
Optical	Colour	Optically active substances
Biological	Trophic status	Level of nutrients
Cryospheric	Ice	Quality of ice season

solutions (the unit is mg Pt, which refers to the concentration of dissolved platinum). Generally, in clear lake waters the Secchi depth[4] is more than 5 m, while it is less than 1 m in strongly brown, turbid or eutrophic water. The *optical thickness* of lake water, defined as the e-folding distance of light intensity, provides the scale for the mixing depth in calm waters due to solar heating.

The *biological classification* is based on the trophic status. This contains the *ultra-oligotrophic*, *oligotrophic*, *mesotrophic*, *eutrophic*, and *hyper-eutrophic* categories. The trophic status is related to the concentrations of phosphorus and nitrogen, that is reflected in the optical quality of the water. Therefore the response of a water body to the ice period depends on the trophic status. Consumption of oxygen is much faster in eutrophic or hyper-eutrophic lakes and they reach more easily anoxic conditions in winter.

A summary of the lake classification systems is given in Table 2.6. There have been approaches to classify the size of lakes on the basis of physical processes. Example the background can be the Coriolis acceleration, which leads to the use of the Rossby radius of deformation as the size criterion (Kirillin et al. 2012). Ashton (1980) classified freezing lakes into small lakes (lakes with stable ice cover), reservoirs (stable ice cover and significant through flow), and large lakes (lakes with drift ice).

2.2 Weather and Climate

2.2.1 General Regional Climate

The local climatology determines to a large degree whether a lake freezes over or not. However, geothermal, hypersaline, and very deep lakes are able to stay ice-free in cold winters. The world's climate conditions are classified according to the Köppen–Geiger

[4] Secchi depth is the maximum depth where a white disk, diameter 30 cm, is visible from the surface.

system into five main classes depending on the temperature T and precipitation P (Fig. 2.6):

A Equatorial climates	$T_{min} > 18$ °C
B Arid climates	Threshold depends on T_{mean} and P
C Warm temperate climates	-3 °C $< T_{min} < 18$ °C
D Snow climates	$T_{min} < -3$ °C
E Polar climates	$T_{max} < 10$ °C

There are further subclasses based on temperature and precipitation criteria. It is clear that freezing lakes are found in snow climates and polar climates. Also, there are cold regions in the arid climate zone, and at the cold boundary of the warm climate zone lakes may freeze in some winters. Thus climatic conditions have a very large variability across the zones where lakes freeze. Apart from very large lakes, the size of lakes is small compared to weather systems, and therefore the atmospheric conditions over a given lake are fairly homogeneous. However, more variability may be seen in the drainage basins, which are often much larger than the lake where the water is collected.

Large-scale weather systems are described by various indexes based on the atmospheric pressure distribution. In Europe, widely used is the NAO (North Atlantic Oscillation) index, which tells of the intensity of the westerlies. In exact terms, NAO equals the

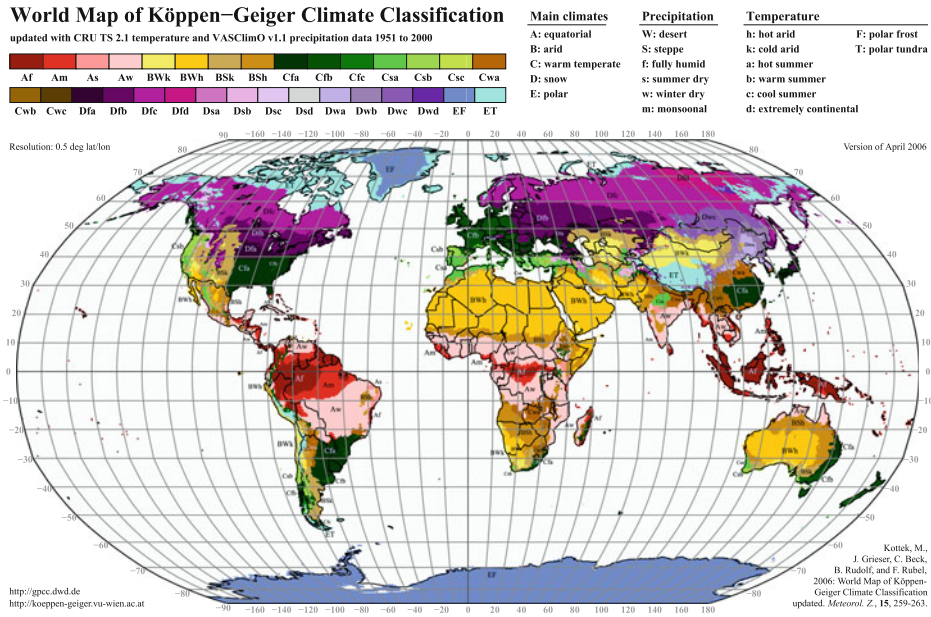

Fig. 2.6 Köppen-Geiger classification of climates (Kottek et al. 2006)

normalized anomaly of the difference in the heights of the 500 mbar atmospheric pressure surfaces between the Azores (Ponta Delgada) and Iceland (Stykkisholmur). The NAO-index is positive, when the westerly winds are stronger than normal and these winters in Europe are typically much warmer than on average; when the NAO-index is negative, the westerlies are weaker and the winters are cold. The index value 1 (−1) means that the westerly winds at 500 mbar level between Iceland and the Azores are one standard deviation stronger (weaker) than on average. Much of the variability of lake ice seasons in Europe is correlated with NAO. This is trivial but it is noteworthy that the correlation is quite high and therefore general regional climate overcomes the individual characteristics of lakes (e.g., Blenckner et al. 2004). In land regions around the Pacific Ocean, El Niño–Southern Oscillation (ENSO) is connected to anomalously warm and cold winters (e.g., Mishra et al. 2011).

The influence of weather and climate on frozen lakes is by the exchange of mass, heat and momentum between lakes and atmosphere and solar radiation. These fluxes between the atmosphere and lakes depend on the precipitation, air pressure, cloudiness, air temperature and humidity, and wind. The standard weather station data include air pressure, temperature and humidity at 2 m altitude, and wind speed and direction at 10 m altitude; some stations also provide cloudiness. Since direct measurements of solar and terrestrial radiation components are rarely available, cloudiness becomes a key variable for their indirect estimation. Table 2.7 presents climatological data from stations Jokioinen (snow climate, boreal zone) and Utsjoki (polar climate, tundra zone).

The atmospheric mass flux to a lake is given by the difference between precipitation and evaporation/sublimation. Precipitation is obtained directly from weather observations, but evaporation and sublimation need to be estimated using atmospheric boundary layer and surface temperature data.

Absolute humidity is given by the mass proportion of water vapour (q) or by the partial atmospheric pressure due to water vapour (e). They are related by

$$q = 0.622 \frac{e}{p} \tag{2.9}$$

The maximum amount of water vapour depends strongly on the temperature (Fig. 2.7; for the exact formulae, see Annex); at temperatures below zero, the saturation level is given both for liquid water surface and for ice surface. Example the saturation water vapour pressure at the standard atmospheric pressure is 12.27 mbar at the temperature of 10 °C, 6.11 mbar at 0 °C, and 2.86 mbar (water surface) or 2.60 mbar (ice surface) at −10 °C. The relative humidity is the actual humidity in relation to the saturation value:

$$R = \frac{q}{q_s} = \frac{e}{e_s} \tag{2.10}$$

Table 2.7 Climatological data from the normal period 1981–2010 for Jokioinen (60°48′N 23°30′E) and Utsjoki Kevo (69°45′N 27°00′E)

Jokioinen	Temperature (°C)	Precipitation (mm)	Incoming solar radiation (W m^{-2})	Relative humidity (%)	Cloudiness (1/8)	Wind	
						m/s	direction
January	−5.6	46	11	89	6.4	3.6	165
February	−6.3	32	38	87	6.0	3.5	171
March	−2.4	32	87	82	5.5	3.5	168
April	3.5	30	152	72	5.6	3.5	153
May	9.8	41	208	65	5.1	3.5	163
June	14.0	63	225	68	4.9	3.3	235
July	16.7	75	218	71	5.3	3.1	201
August	15.0	80	162	77	5.6	3.1	150
September	9.9	58	97	83	5.9	3.3	194
October	4.9	66	41	88	6.2	3.5	194
November	−0.2	57	13	91	6.7	3.7	164
December	−3.9	47	6	91	6.6	3.7	173

Utsjoki	Temperature (°C)	Precipitation (mm)	Incoming solar radiation (W m^{-2})	Relative humidity (%)	Wind	
					m/s	direction
January	–14.0	27	1	85	2.8	165
February	–12.8	24	15	83	2.9	171
March	–8.2	21	66	81	3.0	168
April	–2.5	25	146	76	2.9	153
May	3.7	27	181	72	3.0	163
June	9.6	50	195	68	3.2	235
July	13.1	72	170	74	2.9	201
August	10.7	57	116	80	2.6	150
September	5.7	38	61	85	2.6	194
October	–0.5	39	29	88	2.7	194
November	–8.3	28	1	88	2.6	164
December	–12.3	25	0	86	3.7	173

The data are from Pirinen et al. (2012) expect cloudiness is from 1971–1980 (FMI 1982)

where q_s and e_s are the saturation levels of specific humidity and water vapour pressure, respectively. Annual variations in relative humidity are usually small, but the absolute humidity follows largely the air temperature.

Solar radiation has a strong annual cycle in high-latitude lakes, so that the radiation balance is switched from positive to negative for the cold season. It reflects the presence of polar summer and polar winter in the north. Over lakes, the sensible and latent heat losses to the atmosphere are strong in fall and winter as long as the surface is ice-free but go down after the ice has formed. Transport of warm air from lower latitudes by intensive cyclone activity may delay ice formation. This transport is especially strong for central and northern Europe since the North Atlantic Current brings warm water and adds heat into the atmosphere. When the westerlies are strong (positive NAO index), they are able to transport this oceanic heat to lakes in the European continent.

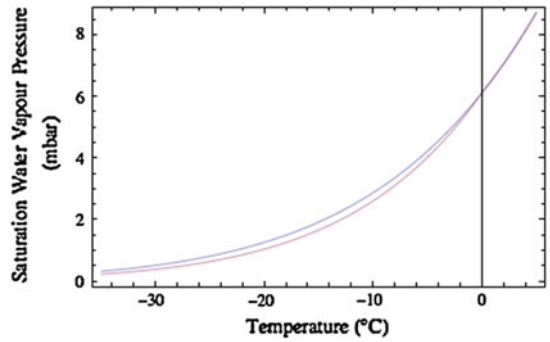

Fig. 2.7 Saturation water vapour pressure as a function of temperature at water surface, and at ice surface

Momentum, heat and moisture transfer between lakes and atmosphere are determined by atmospheric boundary layer processes. Wind velocity gives the momentum transfer in terms of the tangential surface stress, and to estimate the drag properly, temperature and humidity distributions are also needed to account for the stability of the atmospheric surface layer. True weather data over lakes can be obtained from floats (Fig. 2.8). Routine weather stations are located on land, and using their data for the lake surface needs particular consideration.

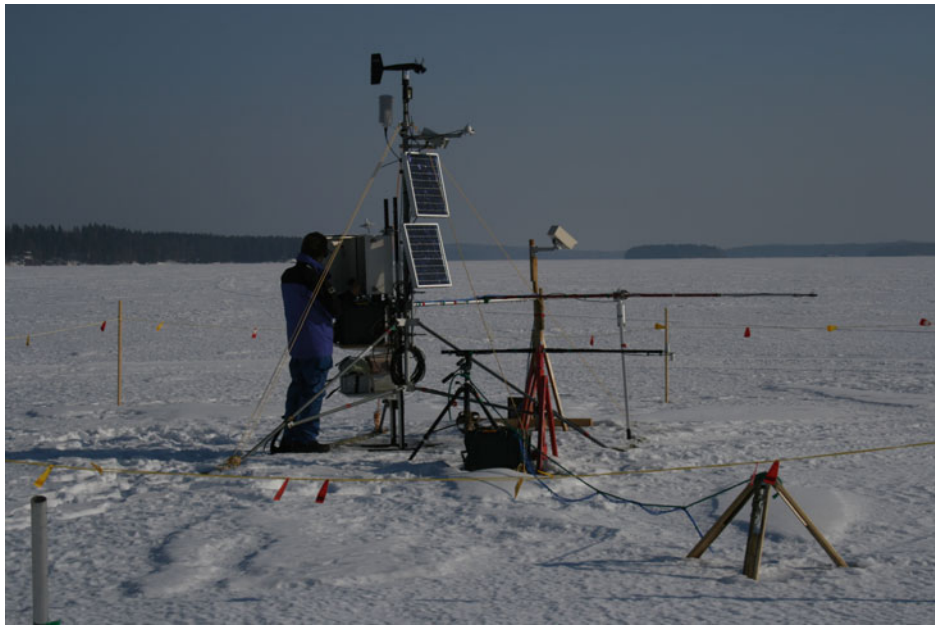

Fig. 2.8 Ice station *Lotus*, Lake Pääjärvi in southern Finland (e.g., Wang et al. 2005; Jakkila et al. 2009). Solar power panels and atmospheric surface layer instrumentation is seen *above* the lake surface. Also included are the instrumentations for ice (temperature and light) and water body (temperature, light, conductivity, flow velocity)

2.2.2 Air Pressure

The influence of air pressure in lake physics steps in primarily by its influence on the physical properties of air across large altitudinal differences. Also horizontal air pressure variations may induce seiches in ice-covered lakes (Kirillin et al. 2012). At the sea surface level, air pressure is within 900 and 1,100 mbar, while the standard atmospheric pressure is 1013.25 mbar. In weather station records, the atmospheric pressure is normally reduced to the sea surface level.

By the hydrostatic law (Eq. 2.5), air pressure decreases with height. Since air is compressible, the pressure–height relation is a little complicated. With decreasing pressure, temperature and density also decrease. The equation of state for dry air is $p = \rho R_d T$, where $R_d = 287$ J K^{-1} kg^{-1} is the gas constant of dry air. Then the temperature decreases with pressure and follows the dry adiabatic lapse rate

$$\Gamma = \frac{g}{c_{pd}(1 + 0.87q)} \tag{2.11}$$

where $c_{pd} = 1{,}004$ J K^{-1} kg^{-1} is the specific heat of dry air at constant pressure, and q is the specific humidity. For $q = 0$, $\Gamma = 9.8$ K km^{-1}. In air saturated with water vapour, the lapse rate is less, because condensation releases heat to partly compensate for the influence of pressure release. In the troposphere, the normal adiabatic lapse rate is $\Gamma = 6.5$ K km^{-1} (e.g., Holton 1979; Curry and Webster 1999). The pressure distribution is given by:

$$p(z) = p(0)\left(1 - \frac{\Gamma}{T_0} z\right)^{\frac{g}{R_d \Gamma}} \tag{2.12}$$

where T_0 is the surface temperature. The power in Eq. (2.12) is 5.25 for $\Gamma = 6.5$ K km^{-1}. In mountain lakes the ambient pressure needs to be accounted for the surface conditions. The primary influence of the reduced pressure goes in the solubility of gases into water.

Example 2.5. Equation (2.12) tells that in the troposphere the pressure decreases by about 100 mbar/1 km increase in elevation. Thus at 5 km altitude the air pressure is around 500 mbar. This equation can be also solved for the height as a function of pressure when the surface temperature and pressure are known. The adiabatic lapse rate provides the temperature decrease with altitude in neutral conditions: $T(z) = T_0 - \Gamma z$. At 5 km altitude, the temperature is 32.5 K lower than at the sea surface level. If $T_0 > T_f$, the freezing point is reached at the altitude of $(T_0 - T_f) \cdot \Gamma^{-1}$.

2.2.3 Precipitation

Precipitation provides the external mass flux to drainage basins. The level of precipitation is connected to atmospheric humidity, temperature and circulation, and orography, since the saturation water vapour pressure is sensitive to temperature (Fig. 2.7). Therefore precipitation is usually lower in colder climate (see Table 2.8). The main exceptions are in the tropics, where descending air masses produce very small amount of precipitation, and at mountains, where orographic effects may force air masses upward and result in heavy precipitation. The highest precipitation levels over ice-covered lakes are observed in mid-latitude mountain areas, e.g. in European Alps, Rocky Mountains in North America, and Japanese Alps, where the annual precipitation is 2,000–3,000 mm. Toward the polar regions, the precipitation level decreases, and as an extreme case, there is no precipitation in Antarctic dry valleys.

Precipitation data are available from most weather stations. It is given in terms of accumulation rate of an equivalent liquid water layer, normally in millimetres per time. Precipitation gauges are used for the measurements. There are large difficulties to determine the solid precipitation, especially during snowstorms due to turbulent transport of snowflakes, and the recorded snow accumulation data are often biased down. Instead of simple cylindrical gauges, in cold climate regions precipitation gauges are equipped with specific structures to manage the snowfall aerodynamics properly (Fig. 2.9).

In cloud altitudes the air temperature is typically below the freezing point due to adiabatic cooling. Because the saturation water vapour pressure is lower at ice surface than at water surface (Fig. 2.7), deposition of water vapour into ice crystals is more likely than condensation into water droplets. If the atmosphere is cold down to the Earth's surface, precipitation lands in the solid phase. Hailstones fall fast and can reach the ground even in warm conditions. The shape of the falling ice or snow crystals depends on the temperature and the degree of oversaturation in clouds (Fig. 2.10). If the phase of precipitation is unknown, a practical approach is to take it solid when the air temperature is below a specified level, e.g. below −1 °C.

Table 2.8 Quality of ice season in different cold climate zones

	P(I) = 0	0 < P(I) < 1	P(I) = 1
P(O) = 0	X	X	Perennial
0 < P(O) < 1	X	Perennial/seasonal/ephemeral	Perennial/seasonal
P(O) = 1	Ice free	Ephemeral	Seasonal

P(I) and P(O) are the probabilities of the annual occurrences of ice and open lake, respectively; X stands for 'not possible'

Fig. 2.9 Tretyakov model precipitation gauge with a snowfall capture system (*left side*). The metal slices around the cylinder constitute the specific design for aerodynamics to obtain good snowfall data. On the right, an old gauge behind the cabled box

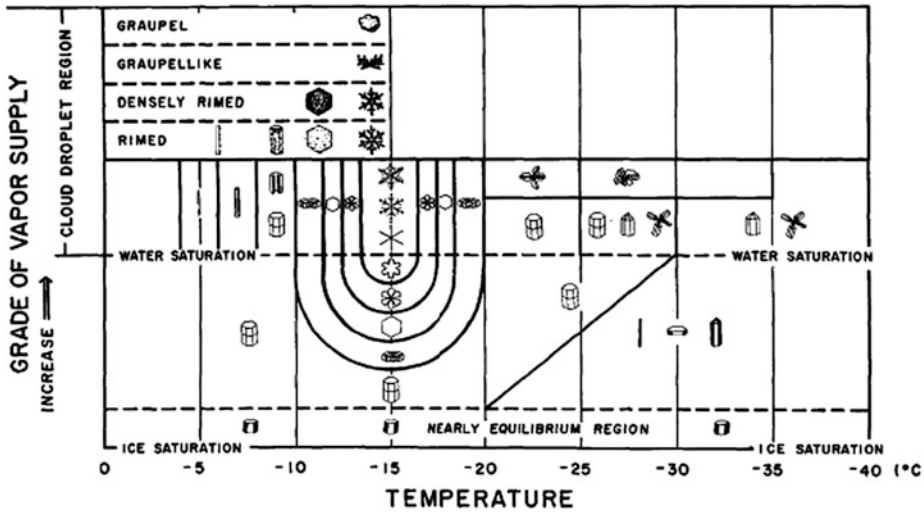

Fig. 2.10 Snow crystal structure as a function of temperature and oversaturation (modified from Magano and Lee 1966)

2.2.4 Air Temperature, Humidity and Wind

Air temperature is a widely used characteristic in geoscience and ecology. It is a quite stable quantity, its measurement is easy to perform and can be made accurately, and there are long-term data available for[5] many observation stations around the world. Humidity is normally expressed as the relative humidity, and it is a key factor in evaporation/condensation and sublimation/deposition, which are important in the mass and heat budgets of lakes. Temperature and humidity are recorded in all weather stations, and their reference altitude has been defined as 2 m above the surface. Wind, measured in most weather stations, refers to two-dimensional, horizontal airflow and is expressed by its speed and direction at the standard altitude of 10 m above the surface.[6]

The annual cycle of the air temperature largely follows the solar radiation (Table 2.7). In summer, the Sun and warm air heat lakes and the surface temperature reaches maximum, while in fall the situation is reversed, as lake waters are warmer than the cooling atmosphere. In general, the amplitude of the annual cycle of air temperature is larger in land areas than in lake districts. Apart from geothermal and deep lakes, the difference between the air temperature and surface temperature is small except for transient events. Thus, for a lake to freeze, in practice the air temperature cannot be much above the freezing point. As long as the drainage basin is snow-covered, the air temperature can be significantly above 0 °C only due to advection of warm air.

In cold climate the absolute humidity of air is small, and therefore mass and heat fluxes due to evaporation/sublimation or condensation/deposition are much smaller than in warm climate, order of 1 mm water equivalent[7] per day. But due to the large latent heat of phase transitions of water, these fluxes are always significant in the heat balance. In dry and cold climate regions, also mass losses due to sublimation can be significant. Deposition of water vapour onto ice surface is sometimes observed as beautiful 'frost flowers'. However, it takes place rarely so that it is insignificant in the heat and mass balance.

Wind velocity shows large local and regional variations depending on the surface topography, vegetation and stratification of the atmospheric surface layer. Therefore wind velocity is sensitive to local conditions at an observation station, and the difference in wind between a lake and nearby land station can be large. Sometimes correction factors are employed to estimate the wind velocity on a lake from land station measurements.

---

[5] Celcius (°C) is a convenient temperature unit in investigations of freezing lakes and mostly used in this book. The absolute temperature (Kelvin) is the natural scale for thermodynamics and used here where considered preferable. These units transform by 273.15 K = 0 °C.

[6] Wind direction (WD, degrees) tells from where the wind blows in the compass angle, zero toward north and turning clockwise. Mathematical right-hand coordinate system has zero direction toward east (x-axis) and turns counter-clockwise. Wind vector direction (to where the wind blows) is in the right-hand system 270°–WD.

[7] Water equivalent refers to the thickness of a layer of liquid water with corresponding volume.

Air temperature, humidity and wind speed determine the turbulent transfer of momentum, heat and moisture between the atmosphere and lakes. The bulk formulae to estimate these fluxes are, respectively,

$$\tau_a = \rho_a C_a U_a U_a \tag{2.13a}$$

$$Q_c = \rho_a c_p C_H (T_a - T_0) U_a \tag{2.13b}$$

$$Q_e = \rho_a L^* C_e (q_a - q_0) U_a \tag{2.13c}$$

where ρ_a is the air density, C_a, C_H and C_E are the bulk exchange coefficients for momentum, heat and moisture, and L^* is the latent heat of evaporation ($L^* = L_e$) or latent heat of sublimation ($L^* = L_f + L_e$) depending on the quality of the moisture transfer, and U_a is the wind speed. We can assume that the humidity is at the saturation level at the surface, $q_0 = q_s(T_0)$. The magnitude of the turbulent exchange coefficients is 10^{-3}, and in general they depend on the surface roughness and stratification of the atmospheric surface boundary layer (see Sect. 4.1.4 for more details). In the neutral case, 1.2×10^{-3} is a good reference value (Andreas 1998). Example for the wind speed of 5 m s^{-1}, the momentum transfer is 0.039 Pa, the sensible heat exchange is 7.8 W m^{-2}/1 °C temperature difference between air and the surface, and the latent heat exchange is 12.1 W m^{-2} (evaporation/condensation) or 13.7 W m^{-2} (sublimation/deposition) per 1 mbar difference in the water vapour pressure.

The characteristics of the atmospheric surface boundary layer have a clear seasonal dependence. In autumn, lakes are usually warmer than the air, and the boundary layer is unstable. Then the turbulent fluxes are strong. In spring and early summer the air is warmer than lake surface, the boundary layer is stable and winds usually remain weak, and, consequently, turbulent transfer is weak. Routine weather station observations provide the atmospheric information needed to evaluate the air–lake interaction except for the surface temperature.

2.2.5 Radiation Balance

The radiation balance consists of solar and terrestrial radiation, and the net radiation provides the governing forcing to the annual course of the freezing lakes. The physical basis is the Planck's law of black body radiation, which provides the distribution of thermal radiation as a function of temperature and wavelength. When this law is integrated over the wavelengths, we have the *Stefan-Boltzmann law*, which tells that the radiative heat flux is proportional to the fourth power of the absolute temperature. Natural objects radiate a little less than a black body; if the spectral distribution of radiation is similar to the black body law, the object is called *a grey body*. The radiative flux of a grey body

equals the radiative flux of a black body, at the same temperature, multiplied by its *emissivity* ε ($0 \le \varepsilon \le 1$):

$$Q = \varepsilon \sigma T_0^4 \tag{2.14}$$

where $\sigma = 5.6704 \times 10^{-8}\,\mathrm{W\,m^{-2}\,K^{-4}}$ is the Stefan-Boltzmann constant, and T_0 is the surface temperature. The black body case comes with ε = 1 in Eq. (2.14). Sun and lake surface (whether liquid water, ice or snow) radiate almost as black bodies (ε > 0.95). For a grey body, the *radiative temperature* T_R is defined from $\sigma T_R^4 = \varepsilon \sigma T^4$.

The *solar constant* is defined as the annual average of solar radiation incident on a plane perpendicular to the solar rays on the top of the atmosphere. Its value is equal to 1367 W m^{-2} (e.g., Iqbal 1983). On the way through the atmosphere, this radiation is reduced by 30–80 % due to absorption and scattering. Solar radiation makes a strong seasonal cycle over freezing lakes (Table 2.7). Part of the *incoming solar radiation* is reflected and scattered back at the lake surface, called as the *outgoing solar radiation*. The ratio of outgoing to incoming radiation is the *albedo* (α,$0 \le \alpha \le 1$), which has a very important role during the lake ice season, in particular in the melting period.

Incoming and outgoing solar radiation are in exact terms downwelling and upwelling, respectively, planar *irradiances* at the surface (see, e.g., Arst 2003). These irradiances integrate the radiance coming from a hemisphere onto a horizontal plane element. Downwelling and upwelling solar irradiances[8] are measured directly by using a pyranometer. Only few weather stations provide direct measurements of solar radiation on a routine basis but simple formulae are available to estimate it using routine weather data (see Sect. 3.4.1).

In terrestrial radiation, lake surface acts as a grey body with emissivity ε_0 in the range 0.96–0.98. For $\varepsilon_0 = 0.97$, the emitted thermal radiation is 306 W m^{-2} at 0 °C (the range is 303–309 W m^{-2} for $\varepsilon_0 = 0.96$–0.98), and for the temperature range from –20 to 20 °C the emitted radiation varies through 226–406 W m^{-2}. Thermal radiation from the atmosphere is more complicated since it comes from atmospheric gas molecules, aerosols, water vapour, water droplets and ice crystals, from different altitudes with different temperatures. An analogous formula to grey body radiation, for parameterization from normal weather data, is used with 'effective emissivity' and the surface air temperature (altitude 2 m) as the representative temperature. This effective emissivity is $\varepsilon_a = 0.7$–0.9, giving the radiation at 0 °C in the range of 221–284 W m^{-2}, and, consequently, the net terrestrial radiation is then negative.

Terrestrial radiation can be measured with pyrgeometers, but such data are not available in routine weather records. To estimate the atmospheric thermal radiation is a key problem in the heat balance evaluation since indirect estimates based on the routine weather data are not so accurate. Cloudiness is the key factor, which is available at some weather stations but good data are coming less and less as they are produced only by

[8] The total downwelling solar irradiance on a horizontal plane is also called *global radiation*.

visual observations of trained personnel. Secondary influence on the radiation level is due to water vapour, other greenhouse gases, and aerosols.

In the polar zone, sunlight is absent in mid-winter, while in the polar summer the daily maximums of solar radiation become up to 500–800 W m^{-2}. Albedo of open water, ice and snow are of the order of 0.1, 0.5 and 0.9, respectively, and therefore the quality of the surface makes a major contribution to the net solar radiation absorbed by a lake: the net daily maximum is 50–500 W m^{-2}. The net terrestrial radiation

$$Q_{\mathrm{nL}} = \varepsilon_0\sigma(\varepsilon_{\mathrm{a}}T_{\mathrm{a}}^4 - T_0^4) = \varepsilon_0\sigma\left(T_{\mathrm{Ra}}^4 - T_0^4\right) \tag{2.15}$$

is of the order of −50 W m^{-2}. It is in practice always negative and varies during the annual cycle mostly from −20 to −80 W m^{-2}. The wavelength band of solar radiation is in practice 0.3–3 μm, while the terrestrial radiation band is 5–15 μm. This is why they are also called short-wave and long-wave radiation, respectively.

Example 2.6. A simple planetary climate model (no atmosphere) is based on the balance between the net solar radiation and the emitted terrestrial radiation from the surface. The balance and the solution are:

$$\varepsilon_0\sigma T_0^4 = \frac{1}{4}\cdot(1-\alpha)Q_{sc} \text{ or } T_0 = 4\sqrt{\frac{(1-\alpha)Q_{sc}}{4\varepsilon_0\sigma}}$$

where the factor ¼ comes from averaging the solar radiation over the planet. The planetary albedo of the Earth is 0.3, and taking $\varepsilon_0 = 0.97$, we have $T_0 = -16$ °C. For other planets, the albedo can be different and the 'solar constant' is inversely proportional to the square of the distance between the planet and the Sun.

We can extend this model by adding atmosphere, with emissivity ε_a, and letting the solar radiation be absorbed at the surface (b_0) and in the atmosphere (b_1), $b_0 + b_1 = 1 - \alpha$. Then we have a pair of equations for the temperatures at the surface and in the atmosphere, and the surface temperature becomes:

$$T_0 = 4\sqrt{\frac{b_0 + \frac{1}{2}\varepsilon_0 b_1}{\left(1 - \frac{1}{2}\varepsilon_0\varepsilon_a\right)(b_0 + b_1)}\cdot\frac{(1-\alpha)Q_{sc}}{4\varepsilon_0\sigma}}$$

where the factor ½ comes from the atmosphere losing heat by radiation to its both sides. On the right-hand side, the first factor constitutes the atmospheric correction, and the second factor is the no-atmosphere solution. Taking $\varepsilon_a = 0.8$, $b_0 = 0.65$ and $b_1 = 0.05$, corresponding to planetary albedo of 0.3, we have $T_0 = 12.6$ °C, which is not far from the present global average (about 15 °C). It is clear that the result is sensitive to the atmospheric emissivity and albedo.

Example 2.7. In the tropical zone, in the coldest month T_a = 300 K. Taking the adiabatic lapse rate as Γ = 6.5 K km^{-1}, the air temperature reaches the freezing point at the altitude of 4.1 km. For the scaling magnitude, we can take $Q_s \propto \cos Z_0 \times t_{day}$, where Z_0 is the solar zenith angle at noon and t_{day} is the length of the day. In the northern hemisphere mid-winter, we have approximately $Q_s = Q_{s0} \times \cos(\phi - \delta), \phi - \delta \leq 90°$, where Q_{s0} is the scale of radiation in the tropics, ϕ is latitude, and $\delta \sim -15°$ is declination. Assuming $T_0 = T_a$, the surface temperature is obtained from the radiation balance as

$$T_0^4(\phi) = \frac{(1-\alpha)Q_{s0}}{\varepsilon_0(1-\varepsilon_a)\sigma}\cos(\phi - \delta)$$

The temperature decreases with altitude and latitude as $T_0(z, \phi) = T_0(0, \phi) - \Gamma z$. We can then solve for $z = z(\phi)$ where $T_0(z, \phi) = T_f$ as:

$$z = \frac{1}{\Gamma}\left[\sqrt[4]{\frac{(1-\alpha)Q_{s0}}{\varepsilon_0(1-\varepsilon_a)\sigma}\cos(\phi - \delta)} - T_f\right]$$

The altitude increases towards lower latitudes from zero at $\phi \sim 40°$–$50°$.

2.3 Water Budget of Lakes

2.3.1 General Form

Lakes are associated with a water budget. The lake water storage S changes by precipitation (P), evaporation/sublimation (E), inflow (I) and outflow (O):

$$\frac{dS}{dt} = (P - E)A + I - O \tag{2.16}$$

where A is the area of the lake. Inflow and outflow consist of surface and groundwater components. The term E is normally positive but occasionally, in case of condensation or solid deposition of water vapour, it may appear negative. Sometimes it is desirable to express the storage as $S = AH$, where H is the mean depth. The relative magnitudes of inflow and precipitation are related to the size of the drainage basin of the lake.

The water storage is easy to monitor from the water level elevation, which changes due to the external fluxes. Precipitation is directly measured (Sect. 2.2.3), while evaporation/sublimation can be obtained directly only in special campaigns, and normally it is estimated indirectly from weather station data (Sect. 2.2.4). The most difficult parts are usually the groundwater fluxes and the surface runoff. Figure 2.11 shows an example of the annual course of the water budget in Lake Vanajanselkä, southern Finland. The area of the lake is 103 km^2, the mean depth is 7.7 m, and the area of the drainage basin is

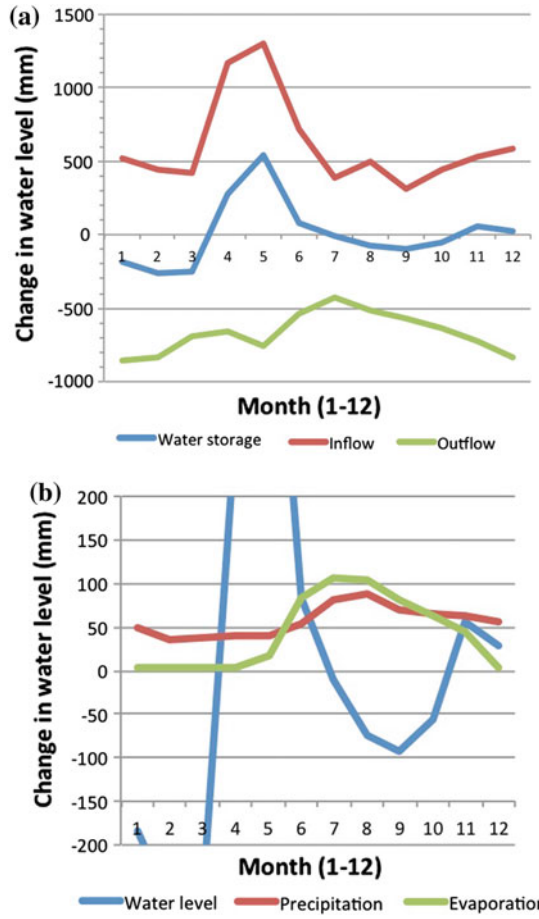

Fig. 2.11 Annual course of the water balance in Lake Vanajanselkä, southern Finland (Jokiniemi 2011): **a** Inflow and outflow; **b** Lake–atmosphere water exchange

2774 km^2. Due to the large size of the drainage basin, the inflow well dominates over precipitation as the source of water.

The flushing time or the water renewal time of a lake provides one fundamental time scale. This scale is defined as the ratio of volume to input or output: $t_R = S/(PA + I) = S/(EA + O)$. In this definition the volume and fluxes represent long-term averages, and to make sense we must have $dS/dt \approx 0$. Freezing and melting do not influence the overall water budget but the renewal of the water storage slows down (Fig. 2.12). Freezing of lake water just changes water molecules to the solid state but the water storage is unchanged. And as long as the ice is floating, liquid water level elevation is unchanged.

Example 2.8.

(a) Over the annual cycle the net change of water storage is normally close to zero and then $(P - E)\cdot A = I - O$. In dry regions, $P \approx 0$ and $O = 0$, and at equilibrium $AE \approx I$.

Fig. 2.12 The water budget of frozen lakes is reduced as compared with open water season. Precipitation is stored in the snow layer, and the ground over large regions is also frozen

(b) The change of the water storage can be written as

$$\frac{dS}{dt} = A\frac{dH}{dt} + H\frac{dA}{dt}$$

Consider a circular lake with a diameter L and a fixed shore slope β around the lake. Then

$$\frac{1}{A}\frac{dS}{dt} = \left(1 + \frac{H}{L}\cdot\frac{4}{\tan\beta}\right)\frac{dH}{dt}$$

If the shoreline slope is 4×10^{-3} and $H/L = 10^{-3}$, changes in the water storage are equally reflected both in the depth and surface area. The equation can be generalized by changing the factor 4/tan β into a general form $B = b/\tan\beta^*$, where β* is the characteristic slope around the lake and $b \sim 4$ is a parameter depending on the slope statistics around the lake.

2.3.2 Inflow and Outflow

Inflow and outflow consist of surface components and groundwater fluxes. The latter part, which is very difficult to measure directly, can be estimated as the residual of the water balance (Eq. 2.16) when the other terms have been measured. In springs, the inflow is predominantly from the groundwater storage. The source of the inflow is the precipitation over the drainage basin. Outflow is related to the water level elevation in the lake so that the outflow rate increases with increasing elevation.

In the Lake Vanajanselkä case (Fig. 2.11), the inflow and outflow average to 23.5–23.8 $m^3\ s^{-1}$, respectively. These correspond to monthly water layers of 610 and 671 mm spread over the lake surface. The flushing time-scale becomes about 12 months. The inflow shows an annual cycle with peak after snowmelt in April–May, about twice the mean inflow. About 90 % of the inflow comes from River Lepaanvirta, and the contribution of ground water flux is of the order of 1 % of the total. Two minima appear, in March and September. The outflow is much smoother with minimum in summer and maximum in winter largely due to the regulation of the water storage and the outflow is therefore controlled. The change in the water level elevation largely follows the inflow.

The surface inflow comes from the drainage basin along rivers and ditches and as runoff along the land surface. It is low during the ice season since the soil surface layer is usually frozen and precipitation over the drainage basin is mostly solid. Groundwater inflow and outflow also slow down during the cold season. At the time of melting of snow and ice, a major inflow peak follows. Closer to the climatological edge of freezing lakes, liquid precipitation events occur all winter. During the ice season the natural outflow decreases since the surface water level is lowered due to the slow renewal of water. In regulated lakes the water level may be even more depressed if the waters are used for hydropower plants. Water level variations caused by inflow–outflow imbalance have influence on the interaction between ice and shore and ice and lake bottom in the winter season.

2.3.3 Lake–Atmosphere Water Fluxes

The atmospheric contribution to the mass balance of lakes is due to precipitation and evaporation/sublimation or condensation/deposition. In general they both tend to decrease toward colder climate conditions since the saturation water vapour pressure in air does so (Fig. 2.7). The net exchange between lake and atmosphere equals $P - E$.

In Lake Vanajavesi (Fig. 2.11), the atmospheric fluxes show strong annual cycles but the rates are one order of magnitude less than the inflow and outflow. Precipitation is about 40 mm/month in winter and reaches the maximum of 88 mm/month in September. In winter it accumulates on top of the ice to be released at the time of ice melting. The level of evaporation/sublimation is about 5 mm/month in winter and more than 100 mm/month in August–September. Transfer of water to the atmosphere is lowered also because

sublimation needs more power than evaporation and because the surface temperature becomes closer to the air temperature when ice grows thicker that lowers the turbulent fluxes. The averages are 56.9 mm/month and 43.3 m/month for precipitation and evaporation/sublimation, respectively.

Evaporation and sublimation are strongly limited by the available heat fluxes. In practice, in cold climate conditions the mass loss per unit area is less than 10 mm liquid water equivalent per day, while the average level is 1 mm/day. Evaporation takes place in open water and melt ponds, while dry snow and ice surfaces lose mass by sublimation. Occasionally atmospheric water vapour deposits as hoar crystals or condenses into liquid water on the surface that also brings the phase change energy to the surface. Latent heat transfer Q_e for evaporation or sublimation, respectively, can be directly expressed as

$$\begin{aligned} Q_e &= -\rho_i L_S E \,(\text{ice}) \\ Q_e &= -\rho_w L_e E \,(\text{water}) \end{aligned} \tag{2.17}$$

where ρ_w is water density. The latent heat of vaporization of liquid water depends on the temperature, $L_e\left[\text{kJ kg}^{-1}\right] = 2{,}494 - 2.2 \cdot T[^\circ\text{C}]$, the latent heat of freezing is L_f = 333.5 kJ kg^{-1}, and the latent heat of sublimation is $L_S\left[\text{kJ kg}^{-1}\right] = 2{,}828 - 0.39 \cdot T\,[^\circ\text{C}]$ $(T \leq 0\,^\circ\text{C})$. Thus sublimation needs about 13.5 % more power than evaporation.

Example 2.9. For $Q_e \sim -30\,\text{W m}^{-2}$, we have $E \sim 1\,\text{mm day}^{-1}$. This energy flux can be estimated using turbulent transfer models. A common way is the bulk formula (Eq. 2.13c). For the relative humidity of air at 50 % and $U_a \sim 10\,\text{ms}^{-1}$, the latent heat loss is $Q_e \sim 100\,\text{W m}^{-2}\left(E = 3\,\text{mm day}^{-1}\right)$ at the temperature of 0 °C, but at −20 °C the energy would be reduced to $20\,\text{W m}^{-2}\left(E = 0.6\,\text{mm day}^{-1}\right)$.

2.3.4 Budgets of Impurities

Closely connected to the water budget are the budgets of impurities, which are received by atmospheric deposition and inflow from the drainage basin and lost of by outflow. Evaporation and sublimation remove only pure water. In addition to the water fluxes, concentrations of impurities are changed by sedimentation/resuspension and biochemical processes.

Consider the mass of a given chemical substance in a lake, $C = c \cdot S$, where c is the mean concentration as mass/volume. The balance is therefore

$$\frac{d}{dt}(cS) = c_i I - c_o O + APc_P + \int \phi dS \tag{2.18}$$

where c_i, c_o, c_P are the concentrations in inflow, outflow and precipitation, respectively, and ϕ is the influence of biochemical processes, resuspension and sedimentation. The renewal

time for each substance can be defined in a manner similar to the flushing time of the water mass. Freezing has no influence on the total budgets of impurities, but the concentrations of the impurities are different in ice and water. Therefore, freezing and melting influence on the concentration of impurities in the surface water layer beneath the ice.

2.4 Ice-Covered Lakes

2.4.1 Zonation of Freezing Lakes

In regards with ice, lakes can be divided into three main zones: ice-free zone, seasonal lake ice zone, and perennial lake ice zone. Years in these zones are qualitatively different. Between the perennial and seasonal zone there is a quasi-perennial zone, where lakes sometimes have ice-free summer, and between seasonal and ice-free zones there is an ephemeral zone, where ice occurs but some years are ice-free. The boundary between the seasonally and perennially ice-covered lakes is quite thin, since there are not many lakes, which are seasonal but occasionally possess multi-year ice. Proglacial lakes can be taken as a sub-category in the perennial lake ice zone, as there the water body is always in contact with land ice.

2.4.2 Seasonal Lake Ice Zone

The zone of seasonally freezing lakes covers large areas of the continents (Fig. 2.13). This zone is close to the diagram of Hutchinson and Löffler (1956), showing that lakes located between 40° and 80° latitudes may freeze in the seasonal cycle. Bates and Bilello (1966) estimated the southern boundary of seasonal ice cover in the Northern Hemisphere to follow approximately the latitude 45°N, higher in the Western Europe and lower in Asia and North America. In this latitude band there are also permanently ice-covered lakes in very high altitudes. Basically, where the mean air temperature in the coldest month is below the freezing point, shallow freshwater lakes are potential to freeze over (Fig. 2.2).

The seasonal ice zone can be further sub-classified into lakes with a stable ice or unstable ice cover. Lakes of the former class freeze over annually (Fig. 2.14), while in the latter class the ice cover breaks and full ice coverage is not necessarily achieved every year. This feature is lake-specific, since ice formation is strongly dependent on the regional climate conditions, as well as on the depth, size and morphology of the lake basin. For example, in the present climate in Europe, the whole Finland belongs to the stable ice zone, but two large lakes nearby, Ladoga (Prokacheva and Borodulin 1985) and Peipsi (Reinart and Pärn 2006), have unstable ice cover.

Apart from the ephemeral zone the mean annual maximum ice thickness in seasonally freezing lakes ranges within 20–200 cm. No reliable data exist on the maximum possible thickness of seasonal lake ice; based on the sea ice data from the Siberian shelf, it can be

Fig. 2.13 The zone of seasonally freezing lakes in the northern hemisphere (Bates and Bilello 1966) and the 0 °C climatological isotherm taken from Fig. 2.1. The contours 100 and 180 refer to the mean length of the ice season (days)

estimated that the seasonal ice in Siberian lakes can grow to approximately 2 m during one winter (Kirillin et al. 2012). As a theoretical upper limit, Kirillin et al. (2012) refer to 270 cm based on the freezing-degree-days in the coldest place in the northern hemisphere (Oymakon, East Siberia). In medium-size lakes (10 km scale), the thickness of ice needs to be more than 10 cm to span a solid, stable ice sheet across the lake.

The ephemeral zone can be several latitude degrees wide. In eastern Europe such lakes are found south from about 55°N, e.g., in Northern Germany and Hungary. In this zone the nature as well as the people need to adapt life for both ice and ice-free winters. Winter 1963 was the latest very cold winter in Central Europe, and at this extreme, even the deep Lake Constance (Bodensee) bordering Austria, Germany and Switzerland froze over (Fig. 2.15).

Fig. 2.14 Wuliangsuhai Lake in Inner Mongolia. In spite of the low latitude (40.5°), the lake freezes over annually and the ice thickness is about 1 m. *Photograph* Ms. Yang Fang, printed with permission

Fig. 2.15 Lake Constance (Bodensee) froze over in winter 1963, and the ice was thick enough for cars and for pressure ridges to form (Zintz et al. 2009). *Photograph* by Mr. Julius Pietruske, printed by permission

2.4.3 Lakes with Perennial Ice

There are two categories of lakes with perennial ice. In very cold climate it is possible that at least some of the ice grown in winter survives over summer and becomes multi-year ice. The second category, proglacial lakes, contains liquid water bodies at side, on top and beneath glaciers or ice sheets and therefore these lakes are always in contact with land ice.

If not all ice melts in summer, the ice cover consists of first-year ice and multi-year ice. Example in Nunavut there are such lakes (Veillette et al. 2010). Occurrence of multi-year lake ice was observed in Colour Lake, Axel Heiberg Island, Nunavut (Adams et al. 1989) but it is there a rare event. Another lake sometimes possessing multi-year ice is Teshekpuk Lake in Alaska (Arp and Jones 2011). But to the author's knowledge, in the present climate, the coldest place in the Northern Hemisphere—Siberia—contains only seasonally ice-covered lakes. In summer, lake ice melts mainly due to the radiation balance, which may account for up to 2–3 cm day^{-1} in ice thickness. Therefore, if the melting period is more than 100 days long, the melt volume will overcome the winter's ice growth. For a partial summer ice cover to survive, the conditions must be quite specific, since lakes have rather small dimensions. It may take place if a lake has bays sheltered from direct solar radiation etc. The partial ice cover state is something delicate between fully ice-covered state and seasonal ice cover (Fig. 2.16).

Perennially fully ice-covered lakes are found in very cold climate conditions, when the ice cover is snow-free and consists of clear ice, e.g., in the McMurdo Dry Valleys in Antarctica (Priscu 1998). Then the surface heat balance can be predominantly negative. Solar radiation heats the water body underneath, but the ice cover survives over summer. Due to the low thermal conductivity of ice, the absorbed heat does not escape easily, and accumulation of heat results in internal warming. This is similar to the so-called cool skin phenomenon in lakes and seas during calm and clear summer days. In the case of ice cover, the situation can be persistent, that leads to perennially ice-covered lakes. The ice cover in these lakes has been observed to be several meters thick, in Lake Vida the ice cover has been estimated as 20 m thick (Bar-Cohen et al. 2004).

There are three types of proglacial lakes connected to glaciers and ice sheets (e.g., Menzies 1995). *Epiglacial lakes* are found on the bare ground close to the boundary of the land ice mass (Kaup 1994); *subglacial* lakes are very old water bodies at the base of ice sheet (e.g., Siegert et al. 2001); and *supraglacial lakes* form in blue ice regions in the surface layer in summer (Winther et al. 1996; Bajracharya and Mool 2009; Leppäranta et al. 2013). Epiglacial lakes are as normal cold region lakes with a soil or rock bottom, fed mainly by glacial melt water inflow. They are an important habitat of life in the polar world. Normally these lakes have seasonal ice cover but blocks of glacial ice may be present.

Subglacial lakes are one of the most exciting geographical findings of the 20th century. The first evidence of their existence was from Soviet radio-echo soundings in the 1960s (see Priscu and Foreman 2009). Subglacial lakes are not yet well known but they form very specific physical and microbiological systems at the bottom of the Antarctic ice sheet. The water temperature is at the melting point corresponding to the ambient pressure,

Fig. 2.16 In Schirmacher oasis, Dronning Maud Land, Antarctica there are lakes where lake ice may survive over summer. The picture shows such lake at the Russian Novolazarevskaya Station (70°49.3′S 11°38.7′E) in late summer, February 4, 2005

at about –2.5 °C. The water body must be in balance between the geothermal heat flux from the ground and conduction of heat through the overlaying ice sheet. The largest subglacial lake is Lake Vostok, located close to the Russian Vostok station.

Supraglacial lakes form and grow from the penetration of solar radiation into the ice sheet. For sufficient penetration, the surface needs to be ice and therefore these lakes form in glacial *blue ice* regions. The depth of seasonal supraglacial lakes is of the order of 1 m. When the surface heat balance is negative, the lake has an ice cover. They are extremely low in biota (Keskitalo et al. 2013). Supraglacial lakes are found on the Antarctic and Greenland ice sheets and in many mountain glaciers. In Greenland they are much more developed and have a major impact on the ice mass balance (Hoffman et al. 2011; Liang et al. 2012). If a supraglacial lake can preserve some of its water in liquid state over the winter, it starts a year-by-year growing stage. This would accelerate local melting, lead to lake growth and eventually catastrophic formation of fractures taking the water in and ending in a major change in the local glacial environment.

2.5 Lake Ice Climatology

As written in Sect. 2.2.4, freezing lakes can be divided into the following three main zones: perennial zone, seasonal zone, and ephemeral zone (Table 2.8). Considering the climatology of these zones, two binary variables are introduced (see Jevrejeva 2004): *Ice occurrence I,* $I(n) = 1$ (0) if ice occurs (does not occur) in ice year n, and *Open lake occurrence O*, $O(n) = -1$ (0) if ice year n is ice-free (is not ice-free). In fully seasonal lakes, $I + O = 0$, while in ice-free and perennially ice-covered lakes $I + O$ equals -1 and 1, respectively. Note that in Sect. 2.1.1, the ice year was defined as the period between two consequent summer maxima of the lake heat content. There are long records of lakes freezing over in extreme years in relatively warm climate regions. Example Maurer (1924) reported of cases from southern Germany and Switzerland back to year 1400. In contrast, ice-free winters would provide information of extremely warm winters in the stable seasonal lake ice zone, but such records are not known to the author.[9]

Lake ice phenology studies the dates of freezing and ice breakup (Futter 2003). Their annual timing has been recorded for long periods in a large number of lakes due to practical reasons and due to general interest in nature phenomena (Magnusson et al. 2000). They are most eye-striking events with major impacts on the nature and society. Also lake ice phenology is a good climatic indicator due to its sensitivity to the climate conditions and the existence of long records (e.g., Robertson et al. 1992; Livingstone 2000; Duguay et al. 2006; Korhonen 2006; Karetnikov and Naumenko 2008; Bernhardt et al. 2011). To be precise, some basic definitions of ice phenology are first needed.

The *freezing date* is defined as the first day in an ice season when the observation area has frozen over. Often this date refers to the freeze-over of the whole lake, but in larger lakes observations do not necessarily cover the whole water body. The *freeze-up date*, also called ice-on date, is used for the first day of complete coverage of ice in a given season. The *ice break-up date*, also called ice-off date, in turn, is the last ice day in a given winter season. The *length of ice season* is the time between the freezing and breakup dates, while the *number of ice days* is the number of days when ice actually exists. Care should be taken in conducting a comparative analysis whether the freezing date or freeze-up date has been consistently used. Their difference can be appreciably long, especially in large and deep lakes.

An example of a phenomenological time series is given in Fig. 2.17 showing typical features in boreal lakes. In Lake Kallavesi (left) the variability of the freezing date is 2½ months, and for the breakup date it is 1 month. For the last 100 years most lake ice time series show slow trends toward milder winters with high random variability. Toward the climatological ice margin in Lake Stechlin (right) the variability of the freezing and breakup date increases and ice-free winters become more common.

Ice formation is generally governed by intense radiative and turbulent heat losses from the warmer lake surface to the colder atmosphere. The stratification in the atmospheric surface layer is unstable and turbulent losses can be large. When the water temperature is

[9] In Finland, all lakes have frozen over every year, except possibly some deep basins in 1930.

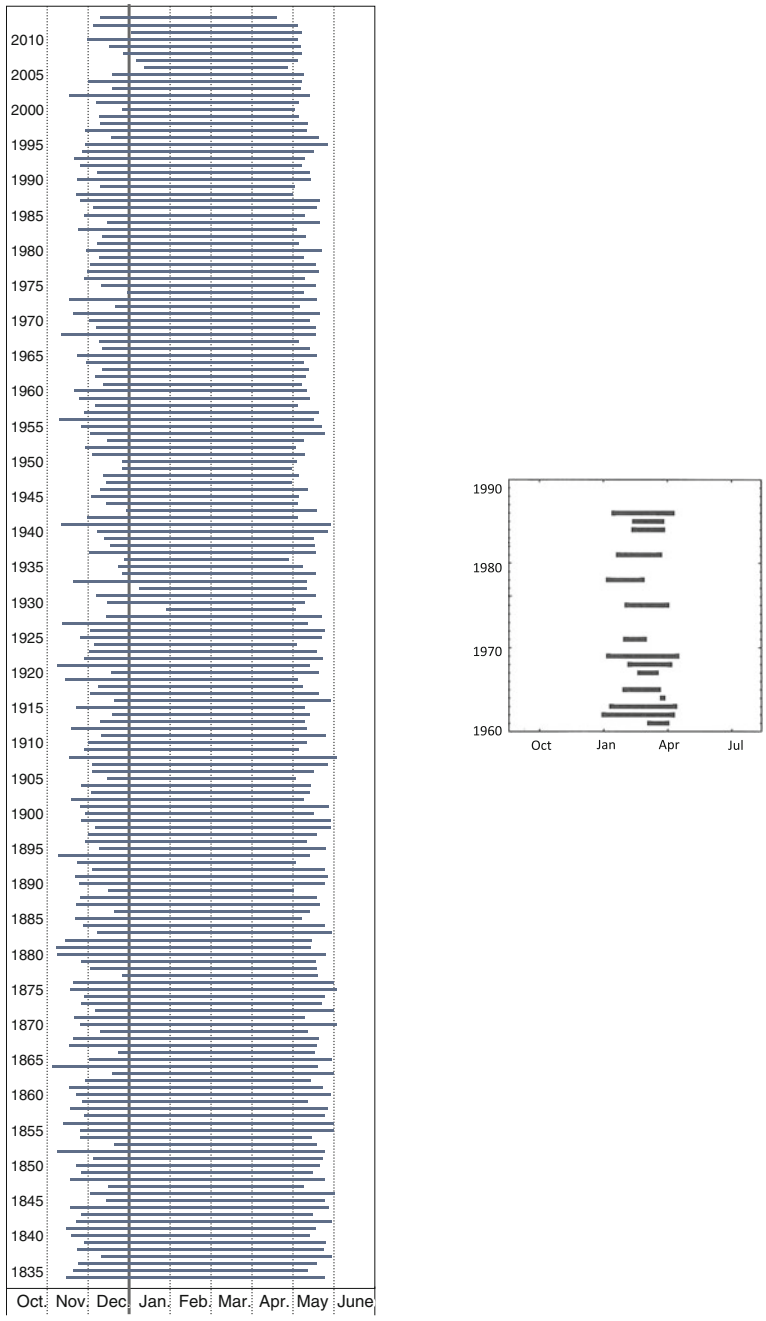

Fig. 2.17 Lake ice phenology time series for Lake Kallavesi, Finland (63°N 28°E), 1835–2013 and Lake Stechlin, Germany (53°N 13°E), 1960–1990; Lake Kallavesi data are from SYKE (Finnish Environment Institute) data base and Lake Stechlin data are from Kirillin et al. (2012) based on Bernhardt et al. (2011). The *thick lines* show the annual ice season from freezing to ice breakup

above the temperature of the maximum density (T_m), the lake water column is unstable in cooling, thermocline deepens and heat is removed from the deep water. Due to mechanically forced mixing, convection can continue at $T < T_m$. Finally, inverse stratification develops with surface layer close to the freezing point and a little warmer lower layer. Heat transport from the warm deeper layers to the lake surface is reduced, the surface cooling rate increases, and the surface temperature achieves the freezing point, followed by ice formation. Hence, the timing of freezing is strongly dependent on synoptic conditions—passages of cold air masses and strong winds—over the lake. In deep lakes, the convective phase can last long, even through the whole winter.

The heat balance during ice melting is fundamentally different from that during lake cooling and ice growth (Jakkila et al. 2009). Then the stable stratification of atmospheric surface layer strongly reduces the turbulent heat exchange at the lake–air interface. Solar radiation is the dominant source of heat for snow and ice melting, partly absorbed by the ice sheet and partly by the lake water below. This fact implies also that albedo and transparency of the ice sheet have a strong influence on melting. The key role of the solar radiation also explains the fact that ice breakup date is coherent at spatial scales of hundreds of kilometres (Magnuson et al. 2000). Other factors able to efficiently accelerate ice melting are liquid precipitation and strong and warm winds.

The sequence of an ice season, from the first freezing to the final break-up is not a simple cycle but there may be melt–refreeze events in between (Bernhardt et al. 2011; Kirillin et al. 2012). Ice formation and melting are not symmetric processes but ice is self-protecting. Once an ice cap has formed, it is difficult to melt it in since in winter solar radiation level is low and albedo feedback keeps the absorption of solar radiation low. Also the lake heat storage is largely isolated from the ice by weak mixing conditions. But still it is possible that ice cover disappears and forms again within one ice season, even several times. This is especially true in the vicinity of the climatological margin of freezing lakes. Then the freezing date and breakup date are still defined as the first and last ones in the ice season, and the presence of ice-free periods is seen in the difference between the length of ice season and the number of ice days. In the other extreme, in a cold year at high-latitudes or high-altitudes, it is possible that some ice survives over summer and becomes multi-year ice. The ice cover has then changed into perennial state.

Because of the heat budget, freeze-up of lakes depends on the lake depth and size, while melting is more up to the growth of ice and snow accumulation during winter. Therefore, ice breakup date follows closely the latitude, but individual lake characteristics show up in the freezing date (Fig. 2.18).

After ice cover formation, ice thickness increases as long as the released latent heat from freezing and the heat flux from the water body can be conducted through the ice to the atmosphere (e.g., Leppäranta 2009a). The main factors controlling the ice growth are the heat fluxes at the upper and lower boundaries of the ice cover together with the thermal properties of ice and snow. An early appearance of snow cover can play a crucial role in decelerating the ice growth due to the very low heat conductivity of snow. The total thickness of ice as well as the thicknesses of congelation ice and snow-ice layers is

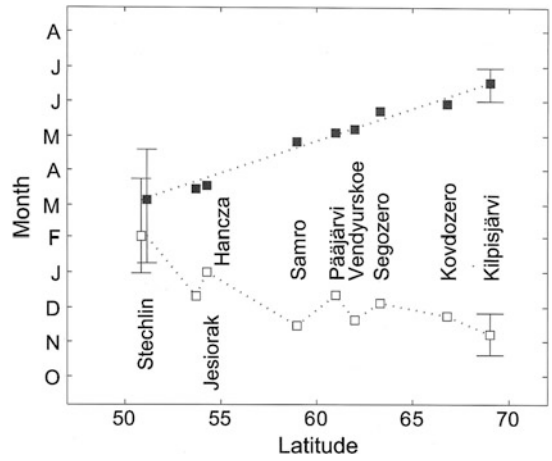

Fig. 2.18 Long-term averages of ice-on (*white squares*) and ice-off (*black squares*) in several European lakes (Kirillin et al. 2012). Data are from: Lake Stechlin, Germany, 1961–2002 (Bernhardt et al. 2011); Lakes Jesiorak and Hancza, Poland, 1961–2000 (Marszelewski and Skowron 2006); Lakes Samro, Segozero, and Kovdozero, Russia, 1936–1989 (Efremova and Palshin 2011); Lake Vendyurskoe, Russian Karelia, 1994–2000 and 2007–2011 (Terzhevik, unpublished); Lake Pääjärvi, Finland, 1910–1988 (Kärkäs 2000); and Lake Kilpisjärvi, Finland, 1964–2008 (Lei et al. 2012). The *error bars* for Lakes Stechlin and Kilpisjärvi show the earliest and the latest observed values

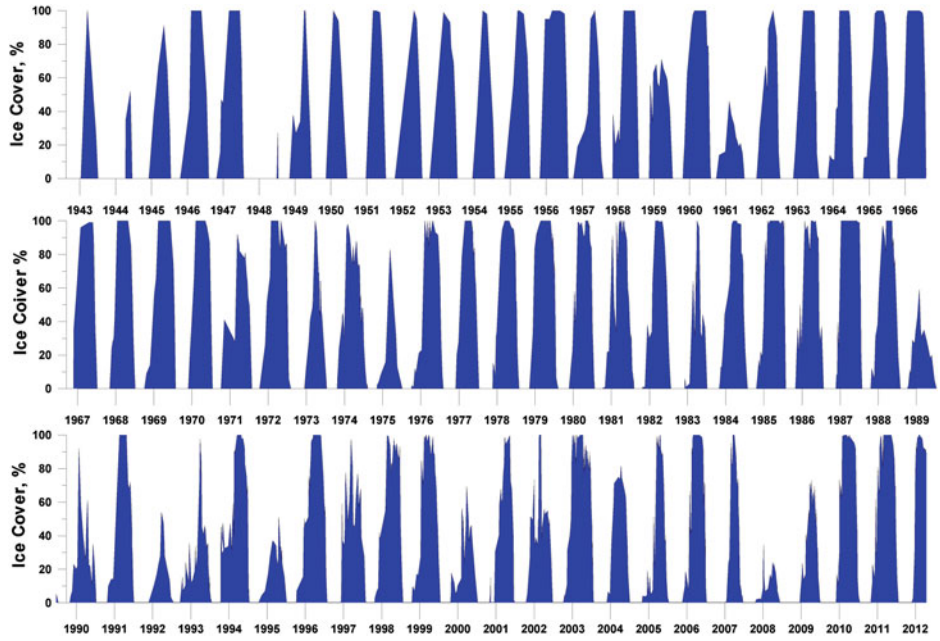

Fig. 2.19 Year-to-year variation of ice cover of Lake Ladoga from 1943 to 2010 (1944 and 1948 are missing) using various sensors from airplane and satellites (Karetnikov and Naumenko 2011; Karetnikov et al. 2015)

primarily controlled by the air temperature and snowfall time history. The general trend towards warmer winters in ice phenology may thus not be easy to detect in the ice thickness data (e.g., Leppäranta and Seinä 1985; Jevrejeva et al. 2004). Evolution of ice coverage is related to ice thickness in that thicker ice has more lateral strength and a thick enough ice cover does not break any more before the melting phase.

The severity of winters can be quantified with the *maximum annual ice thickness*. In large lakes, the period of lateral ice growth may be long, and therefore the quantity *ice coverage*, equal to the ice area divided by the total lake area, is another characteristic of the severity of the ice season. Example in Lake Ladoga the probability of complete ice coverage is about 50 %, although ice forms in the lake every year (Prokacheva and Borodulin 1985; Karetnikov and Naumenko 2008, 2011) (Fig. 2.19).

Structure and Properties of Lake Ice

3

Ice sampling work. Investigations of the structure of lake ice is based on ice samples. The ice stratigraphy and crystal structure is studied in a cold room from the samples and ice impurities are taken from the meltwater.

M. Leppäranta, *Freezing of Lakes and the Evolution of their Ice Cover*,
DOI 10.1007/978-3-642-29081-7_3

3.1 Ice Ih: The Solid Phase of Water on Earth

3.1.1 Ice Crystal Structure

In the Earth's nature, water is the only substance, which occurs in all three phases: gas, liquid, and solid. Phase transitions take place continuously. The water molecule consists of one oxygen atom and two hydrogen atoms connected to the oxygen atom by *covalent bonds* (Fig. 3.1a), which are strong and keep the water molecule stable. The hydrogen atoms are not symmetrically located but the bonds H–O–H form an angle of 104.5° that makes the water molecule an electric dipole. The center of each hydrogen atom is approximately 0.0957 nm from the center of the oxygen atom. The oxygen pole is negatively charged and the hydrogen pole is positively charged. The dipolar structure is the cause of several exceptional properties of water; e.g., liquid water is an excellent solvent.

Due to their dipolar structure, the water molecules are connected with each other by *hydrogen bonds* into linear chains in liquid water. The oxygen atom of a water molecule and a hydrogen atom of a neighbouring water molecule form the hydrogen bond, with the length of 0.117 nm. These bonds are much weaker than covalent bonds, and they form and break continuously. The hydrogen bonds are the reason of relatively high freezing and boiling points of water, as compared with similar substances.

There are several possible crystal lattice structures for the solid phase of water (Petrenko and Whitworth 1999). About ten are known. But in the natural pressure and temperature conditions within 10 km up or down from the Earth's surface, all ice has hexagonal crystal structure, named as *Ice Ih* (Fig. 3.1b). Cubic ice (Ice Ic) occasionally occurs in the upper atmosphere at low temperatures and low pressures. In this book only the hexagonal ice is considered.

The crystal lattice of Ice Ih (from now on, just '*ice*') is tetrahedral where each ice molecule is joined by hydrogen bonds to four other ice molecules. Then electron pairs are evenly spaced in their orbits and the covalent bonds H–O–H form an angle of 109.5°, which is very close to the angles in a perfect tetrahedron. The distance between neighbouring molecules is 0.2760 nm, and the distance between oxygen and hydrogen atoms in one molecyle is 0.095 nm. The lattice follows the Bernal–Fowler rules (e.g., Petrenko and Whitworth 1999): (1) There are two hydrogen bonds connected to each oxygen atom, and (2) There is only one hydrogen atom in a bond. Exceptions to these rules are defects in the crystal lattice and are concerned with ordering of the water molecules. The concentration of foreign molecules in ice crystal lattice is extremely small and can be ignored in lake ice investigations.

It is seen (Fig. 3.1b) that the ice crystal tetrahedra possess hexagonal symmetry, which is often visible, e.g., in the morphology of snow crystals and frost flowers. The arrangement of molecules is, however, anisotropic in the crystal lattice. They are concentrated in a series of parallel planes, which are called *basal planes*. Normal to the basal plane is the crystal *c-axis* or the optical axis. The basal plane is isotropic but there is

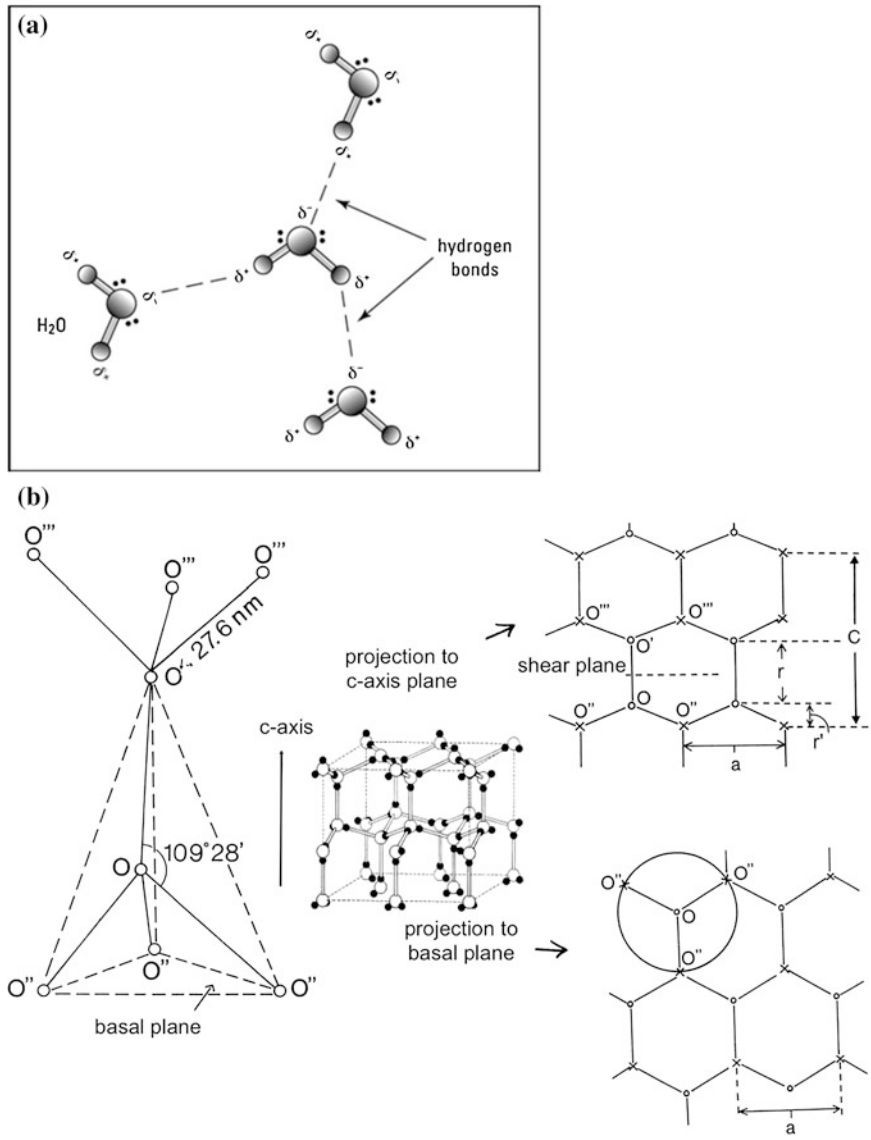

Fig. 3.1 **a** Water molecules in liquid state; **b** Ice Ih crystal lattice with projections to the basal plane and perpendicular to the basal plane. The lattice parameters are (0 °C): a = 0.4523 nm, c = 0.7367 nm (cell length along c-axis), r = 0.2760 nm (distance between neighbouring molecules), r' = 0.0923 nm. Modified from Pounder (1965)

anisotropy between the basal plane and the c-axis. In particular, there are more hydrogen bonds in the basal plane than perpendicular to it, and therefore many physical properties of ice show corresponding anisotropy.

The ice crystal lattice is an open structure, where molecules are more sparsely packed than in the liquid phase of water, and therefore ice is much less dense than liquid water. At the freezing point, the densities of liquid and solid phases are 999.84 and 916.7 kg m^{-3}, respectively, and therefore the density decreases by 8.3 % at freezing. This amount of density decrease at the phase change from liquid to solid is exceptional,[1] and actually water shows the largest decrease among all substances in the Earth's nature. Freshwater ice behaves as normal solid media with density decreasing with temperature. The thermal expansion coefficient is from 1.59×10^{-4} °C^{-1} at 0 °C to 1.43×10^{-4} °C^{-1} at −30 °C (volume expansion). The density of pure ice is 920.8 kg m^{-3} at −30 °C.

Example 3.1. *Ice density from the crystal lattice* (*Pounder 1965*). The density of ice can be evaluated as the mass/volume ratio of one mole of ice. The mass is obtained from the atomic weights of hydrogen and oxygen as 18.02 g, and the volume is obtained from the geometry of the crystal lattice, which has been determined by X-ray diffraction (see the right side of Fig. 3.1b). The geometric measures shown are at 0 °C. The length of one side (d) and width (a) of the hexagon are related as $a = \sqrt{3}d$, and consequently the area of the hexagon is $A = \frac{1}{2}\sqrt{3}a^2 = 0.1772\,\text{nm}^2$. The vertical separation between these double layers of oxygen atoms is $r + r' = 0.2760\,\text{nm} + 0.0923\,\text{nm} = 0.3683\,\text{nm}$. The prism volume is $A(r + r')$. This unit volume has six oxygen atoms, but each is shared between three hexagons. Thus the unit prism contains the mass of 6/3 = 2 oxygen atoms or two water molecules, and the volume of one mole is consequently $½\,N_A A(r + r') = 19.65\,\text{cm}^3$, N_A being Avogadros number. The ice density at 0 °C becomes then 917.0 kg m^{-3} (the direct measurement has given 916.7 kg m^{-3}).

The best method to determine the bulk density of ice is the direct way: measure the mass of a geometrically regular sample. The presence of pores in the ice gives biased estimates when the method of submersion of a sample in a liquid is employed.

Example 3.2. Ice density is a fundamental property of floating ice. According to the Archimedes law, the freeboard h_f is given by

$$h_f = \frac{\rho_w - \rho_i}{\rho_w} h$$

Thus for solid ice, the freeboard is 8.3 % of the thickness of the ice sheet, and an ice block of 1 m^3 volume can support the floating of a mass of 83 kg. The freeboard is 8.3 % of the total thickness. If the gas content of freshwater ice is 1 %, the freeboard would be 9.2 % of the ice thickness. The saying that 1/9 (11.1 %) of an iceberg is visible relates to icebergs floating on seawater, which has higher density than fresh water; with $\rho_w = 1{,}025$ kg m^{-3}, the freeboard would be 10.5 %, and adding 1 % gas content brings the freeboard to 11.4 %.

[1] Bismuth, gallium and germanium, for example, become less dense in the liquid–solid phase change. But the change is by far not so large than in water.

Ice is optically uniaxial with the *c*-axis as the optical axis. Light goes through unaffected in the direction of the optical axis, while in other directions birefringence (double refraction) takes place. Thermal conductivity is highest along the basal plane. Shear deformation is easiest parallel to the basal plane since then the number of bonds to be broken for shear is at minimum. Therefore this plane is also called slip plane or shear plane in ice mechanics.

3.1.2 Ice Nucleation

When liquid water is cooled, the nucleation temperature is always below the freezing point (Fig. 3.2). Certain amount of supercooling is needed to start nucleation, and thereafter the 'extra cold' is recovered and the temperature returns to the freezing point. Then, in the solid state, temperature decreases if heat removal continues. Homogeneous and heterogeneous nucleation modes exist in the *primary nucleation* (see Michel 1978). In the former case, very strong supercooling (down to −40 °C) would be required in pure fresh water, but this is not observed in natural lakes. Instead, heterogeneous nucleation takes place with suspended particles acting as the crystallization seeds, and supercooling remains small. Also snow or ice crystals falling on a supercooled lake surface may initiate nucleation. In the *secondary nucleation*, crystals grow on existing ice surfaces. The latent heat of freezing is large (333.5 kJ kg^{-1}) and severely limits the volume of ice produced in nature. For a heat loss of Q, an ice layer of thickness $h = Qt/(\rho_i L_f)$ is produced in time t; e.g., for Q = 100 W m^{-2} and t = 1 d, we have h = 28 mm (Fig. 3.3).

To build a crystal in a homogeneous fluid, work ΔG, called the Gibb's free energy, is required to form the surface and the bulk particle. This energy and the minimum radius of stable crystals are (Michel 1978), respectively,

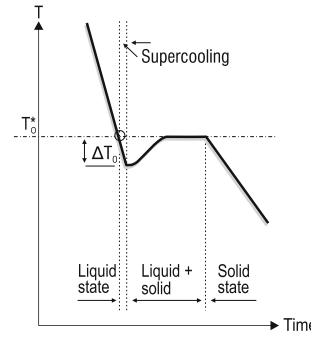

Fig. 3.2 Schematic cooling curve of a liquid with heat being removed at a constant rate; T is the temperature, T_0^* is the temperature of phase equilibrium, and ΔT_0 is the degree of supercooling. Modified from Michel (1978)

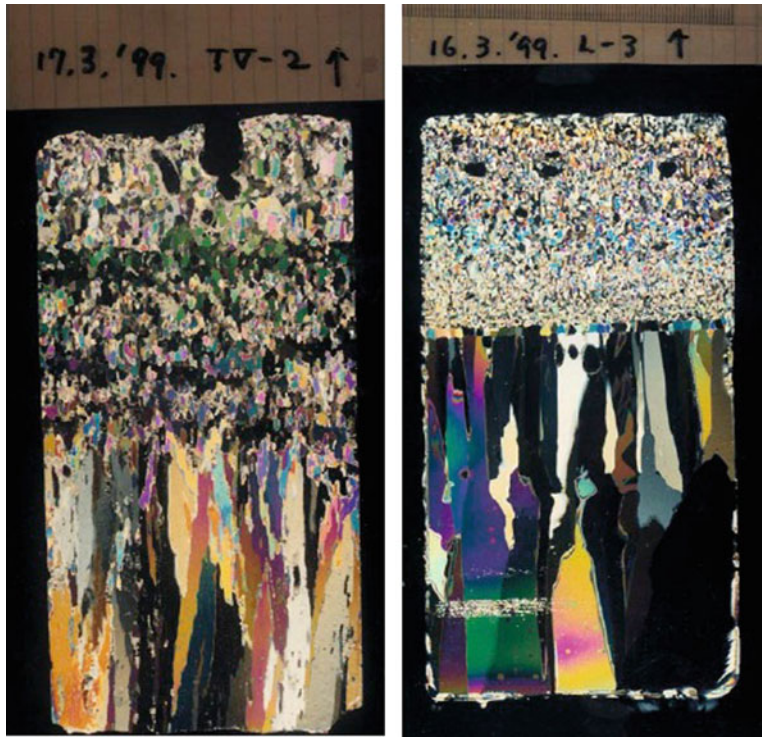

Fig. 3.3 Ice crystal structure Baltic Sea landfast ice (*left*) and lake ice (*right*). Each connected colour spot corresponds to one ice crystal; the scale on *top* is in millimeters. The *top* layer is fine-grained snow-ice, and the *lower* layer is columnar-grained congelation ice. According to Kawamura et al. (2002)

$$\Delta G = \frac{16\pi}{3}\sigma_{cl}\left(\frac{\sigma_{cl}T_0^*}{\rho_w L_f \Delta T_0}\right)^2 \tag{3.1a}$$

$$r_c = 2\frac{\sigma_{cl}T_0^*}{\rho_w L_f \Delta T_0} \tag{3.1b}$$

where σ_{cl} is the surface energy of the crystal in contact with the liquid, T_0^* is the solid-liquid equilibrium temperature (273.15 K at the standard atmospheric pressure), and $\Delta T_0 = T_0^* - T^*$ is the amount of supercooling. For pure water, σ_{cl} = 33 mJ m^{-2}, the amount of supercooling is 40 K, and r_c = 1.35 nm is the critical radius of a crystal, containing about 100 molecules.

In natural surface waters, with heterogeneous nucleation taking place on suspended particles, the amount of necessary supercooling is largely reduced from the homogeneous case. Assume that an *n*-faced prismatic ice crystal grows on a surface of a substrate.

The presence of the substrate brings the surface energies between the substrate and liquid (σ_{sl}) and substrate and crystal (σ_{sc}) into the problem (see Michel 1978). The nucleation temperature depends on the character of the substrate, and the key dimensionless parameter, γ, is defined by:

$$\cos\gamma = \frac{\sigma_{sl} - \sigma_{sc}}{\sigma_{cl}} \tag{3.2}$$

The parameter γ is usually taken as the angle of contact between ice and the nucleating material.

In heterogeneous nucleation, there is a critical crystal size after which the crystal grows freely, reducing the free energy of the system. The functional form of the critical radius is as in homogeneous nucleation, and the corresponding Gibb's free energy is

$$\Delta G = 4\pi\,(1 - \cos\gamma)\frac{\tan(\pi/n)}{\pi/n}\sigma_{cl}\left(\frac{\sigma_{cl}T_0^*}{\rho_w L_f \Delta T_0}\right)^2 \tag{3.3}$$

Thus the supercooling in the heterogeneous nucleation relative to the supercooling in homogeneous case equals

$$\frac{\Delta T_n}{\Delta T_0} = \sqrt{1 - \frac{\cos\gamma}{2}} \tag{3.4}$$

Ice as a substrate has $\gamma = 0$ and no supercooling is needed. Considering suspended particles, the best inorganic nucleators in nature have $\gamma = 10°$, and consequently the supercooling would be 3.5 K. This is, however, more than the observed supercooling in lakes. Field studies as well as laboratory experiments have shown that in calm fresh water crystallization starts at temperatures from −0.5 to −1.5 °C.

In turbulent flow conditions, the surface water layer is well mixed and supercooling takes place across the whole layer. It has been observed that the amount of supercooling is not more than about 0.1 K, which is much less than in spontaneous heterogeneous nucleation. Several theories have been proposed for the nucleation at such high temperatures. Michel (1978) suggested that near the lateral boundaries (shore or ice) turbulence is weaker, and steeper surface temperature gradient can be set up. Ice germs form at the surface, flow away to the turbulent flow, and serve for forced nucleation in the turbulent surface layer. The supercooling is in this situation

$$\Delta T = \frac{2\sigma_{cl}}{\rho_w L_f r_l} T_0^* \tag{3.5}$$

where r_l is the radius of the seed particle. For clay particles, $r_l \sim 1$ μm, and the supercooling in forced nucleation becomes 0.05 °C. The process of multiplication of crystals in this way is very fast. The border ice mechanism has been questioned, however. Osterkamp

(1977) suggested a mass exchange-mechanism to be responsible, with ice particles, cold soil particles, etc. falling on supercooled turbulent water initiating the nucleation. Splashing of water particles in cold air could freeze them and generate nucleus for secondary nucleation. With ice particles in the flow, secondary nucleation would cause them to multiply and produce high concentration of frazil[2] ice.

3.1.3 Ice Formation in Lakes

Ice crystal lattices are optically uniaxial. They start to grow on the lake surface into needle or platelet shapes with the *c*-axis perpendicular to the axis of the needle or to the plane of the platelet, as favoured by the anisotropic thermal conductivity of ice crystals. Overlain together the platelets form *macrocrystals*, which are optically like single crystals but structurally multiple crystals. In the geophysics of natural surface waters, the term *ice crystal* or *grain* refers to single crystals or macrocrystals equivalently. These crystals are classified in terms of their size, shape and *c*-axis orientation (e.g., Michel 1978) (Table 3.1).

The crystal size ranges from less than a millimetre to 1 m, and the common dimensions are 1 mm–10 cm. The size as well as the shape and orientation change in a continuous manner but they are absorbed into a few ideal classes. In general, the slower the ice grows the larger will the crystals be, and therefore the crystal size increases with depth. The main shape classes are granular and columnar, and in the beginning of ice formation there is a larger variability in shape with needle- and plate-like structures. The origin of the water

Table 3.1 Classification of ice crystals on the basis of size, shape and orientation

Crystal size	
Fine	<1 mm
Medium	1–5 mm
Large	5–20 mm
Extra large	>20 mm
Giant	meters
Crystal shape	
Needles, plates	
Granular (linear dimensions all of the same magnitude)	
Columnar: elongated vertically	
Crystal c-axis orientation	
Vertical	
Horizontal (random/aligned in 2D)	
Random in 3D	

[2] Frazil comes the French word fraisil, which refers to coal cinders.

molecules in ice crystals is the lake water body itself or precipitation. The latter case is also called *meteoric ice*.

The first ice layer on lake surface is called *primary ice*. Ice formation may initiate in three different modes of heterogeneous nucleation: nucleation on suspended particles at the surface in calm or laminar flow conditions, nucleation on suspended particles under the surface in turbulent conditions as *frazil ice*, or nucleation on snow or ice nuclei precipitating onto the water surface. In *frazil ice* formation, supercooling is limited to less than 0.1 °C. The physics of the primary nucleation is partly unclear (see above), but once the crystallization has started, secondary nucleation leads to a fast growth of the frazil ice volume. *Secondary ice* forms beneath the primary ice layer. In a lake ice sheet this is *congelation ice*, where crystallization takes place at the bottom of the ice sheet. Therefore no supercooling is needed any more. *Superimposed ice* forms on top of the primary ice. This includes snow-ice formation, freezing of surface ponds, and surface hoar formation. The source of the superimposed ice is slush,[3] liquid water ponds, or atmospheric moisture. Liquid water ponds originate from meltwater or liquid precipitation and they are thin, as surface hoar layers as well, both of the order of 1 cm. The main contribution to the superimposed ice layer is due to freezing of slush. Snow-ice crystals are small as in frazil ice but occasionally larger snow crystals or frozen water pockets are found.

In brackish or saline lakes, ice crystals are in size and shape much as freshwater ice crystals. No ice structure analyses are known to the present author for hypersaline lakes. Most of the investigations of saline ice are from the cold ocean—sea-ice—showing that there are two important differences caused by the large amount of dissolved substances in the parent water. In sea-ice the crystal boundaries are jagged, and between the single crystal platelets inside macrocrystals there are brine inclusions (Weeks 1998). Brackish ice has been examined from field data in the Baltic Sea (Palosuo 1961; Weeks et al. 1990; Kawamura et al. 2001), and the results show that the transition between freshwater ice type and sea ice type takes place when the salinity of the parent water is 1–2 ‰. It is anticipated that in brackish and saline lakes the situation is much as in seawater. Weeks and Lofgren (1967) have also shown that ice formed of sodium chloride solution (with salt concentration as in sea water) is similar to sea ice, when the salt concentrations are similar.

3.1.4 Physical Properties of Lake Ice

The properties of freshwater lake ice depend primarily on its crystal structure and gas content. The basic properties of this ice with the sensitivity to temperature are given in Table 3.2. More details are shown in Annex 1. For most properties the sensitivity to temperature is not very high (less than 5 % per 10 °C), and in many applications fixed values can be used. The bottom temperature of ice is at the freezing point while the surface temperature depends on the air temperature and the thicknesses of snow and ice. In the case

[3] Slush is water-saturated snow.

Table 3.2 Physical properties of freshwater lake ice at 0 °C and −20 °C temperature

Property	Value at 0 °C	Value at −20 °C	Liquid water at 0 °C
Density (kg m^{-3})	916.7	920.3	999.8
Latent heat of melting (kJ kg^{-1})	333.5	(333.5)[a]	
Latent heat of sublimation (MJ kg^{-1})	2.82	2.84	
Latent heat of evaporation (MJ kg^{-1})			2.49
Specific heat (kJ kg^{-1} $°C^{-1}$)	2.11	1.96	4.22
Thermal conductivity (W m^{-1} $°C^{-1}$)	2.14	1.88	0.561
Young's modulus (GPa)	8.7	10.0	
Poisson's ratio	0.33	0.33	
Speed of sound (km s^{-1})	3.08	3.30	1.45
Relative permittivity	91.6	97.5	87.90

[a]Melting takes place only at 0 °C

of saline ice, there are liquid brine inclusions within the ice sheet, and then the salt content together with the temperature become the dominant factors. Congelation ice with columnar crystals possesses anisotropy due to the geometry of ice crystals and alignment of *c*-axes.

Lake ice normally contains impurities, which influence its properties. In freshwater ice, the primary impurity is *gas bubbles*, which cover a volume of magnitude 1 % in congelation ice and 5 % in snow-ice. Lake ice also contains particles, which are in general called *ice sediments*. In brackish and saline lakes, the brine content of ice is the primary factor. Depending on the salinity of the parent water, liquid *brine* is captured by growing ice, and brine pockets are formed within the ice sheet (see Weeks 2010).

Example 3.3. The density of natural freshwater lake ice can be expressed as

$$\rho_i = (1 - v_a)\rho_0$$

where v_a is the gas content and ρ_0 is the density of pure ice. This equation can be used to estimate the gas content from the measured ice density. When $v_a = 1\,\%$, then (at 0 °C) ρ_i = 907.5 kg m^{-3}. Considering $v_a \sim 1\,\%$ as the scale in congelation ice, 910 kg m^{-3} serves as a convenient reference density.

3.2 Lake Ice Types and Stratigraphy

3.2.1 Ice Structure Analysis

Research on the crystal structure of ice is based on ice samples, which are usually taken by core drills with diameter 10–20 cm. Not much can be said about the ice structure without a manual sample processing. Ice samples are examined at the site for their visual features

Fig. 3.4 An ice sample has been taken and, the visible structure is recorded and temperature profile is measured

and immediate measurements (Fig. 3.4). *Thick sections* (1 cm) are prepared to examine the stratification and gas bubbles (Fig. 3.5). These sections are further processed in cold laboratory (at −10 °C or less); they are attached to glass plates and plained to less than 1 mm thickness, so-called *thin sections*. The crystal structure is revealed by examining thin sections in polarized light (Langway 1958). Crystals with *c*-axis perpendicular to the section appear black between crossed polarizers, but other crystals, due to birefringence, show different interference colours (see Fig. 3.3). The thin sections can be rotated in a universal stage to determine the zenith and azimuth angles of the *c*-axes (Langway 1958). The size and shape of ice crystals and their *c*-axis directions define the crystal structure for geophysical investigations.

3.2.2 Lake Ice Stratigraphy

The information about the ice growth history is stored in the layers and crystals and can be reconstructed from ice sample analyses. Table 3.3 shows the classification of lake ice sheets. There are three principal vertical layers in a static lake ice sheet: primary ice,

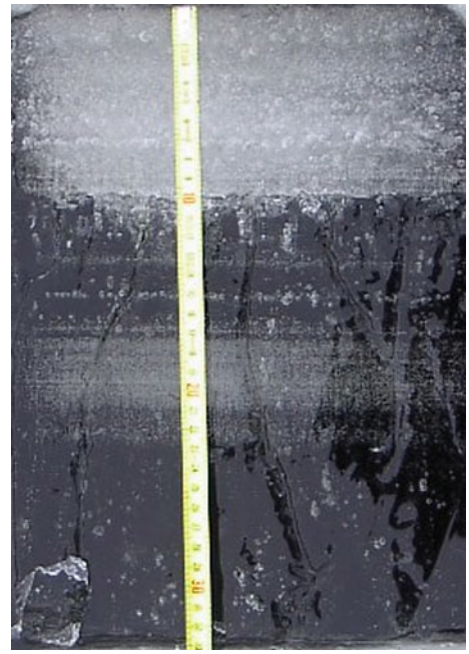

Fig. 3.5 A thick section of lake ice in normal light. The snow-ice and congelation ice layers are identified from the *grey* tone (*white* and *black*, respectively), and gas bubbles are clearly seen. The total thickness of ice is 30 cm

Table 3.3 Lake ice stratigraphy and forms of ice (Michel and Ramseier 1971)

		Grain size	C-axes	Conditions
Primary ice	P1	≥large	Vertical	Calm, slow growth
	P2	≥medium	Vertical/random	Calm, rapid growth
	P3	fine	Random	Turbulent
	P4	≤medium	Random	Snowfall
Secondary ice	S1	≥large[a]	Vertical	Beneath primary ice P1
	S2	≥large[a]	Horizontal	Beneath primary ice P2
	S3	≥large	Horizontal, aligned	Perennial lake ice
	S4	≤medium	Random	Frazil ice transport
	S5	≤medium	Random	Drained frazil slush
Superimposed ice	T1	≤medium	Random	Snow-ice
	T2	≤medium	Random	Drained snow-ice
	T3	As P and S	As P and S	Liquid water on ice[b]
Agglomerate ice	R	All size	All variants	General class for ice agglomeration of various ice types

[a]S1—granular grains, S2—columnar grains (Gow 1986)
[b]Ponds on ice may form own ice sheet as normal lake ice, may be layered

congelation ice, and superimposed ice (Fig. 3.5). The primary ice layer is often very thin and difficult to identify in vertical ice samples.

Primary ice forms the first layer of a lake ice sheet. Its texture depends on the prevailing weather conditions (Gow 1986). In calm or laminar flow conditions, the case called *quiet freezing* (Gow and Govoni 1983), a thin supercooled water layer forms at the surface and ice crystals appear when the nucleation temperature is reached. Supercooling is then 0.5–1.5 °C. Needle-shaped crystals form first on the surface with their main axis perpendicular to the *c*-axis, and the number of crystals depends on the number of crystallization seeds and the rate of cooling. The size of crystals varies largely depending on the concentration of nucleation seeds and the rate of the heat loss from the water. Ice skim grows horizontally in a supercooled surface layer. Smaller temperature gradient means slow crystallization, and the needles expand into plate shape aligned with the surface and with *c*-axis perpendicular to the surface. In the case of larger temperature gradient, the crystals grow fast and their number is larger. Then the plates do not float only horizontally, and the orientation of the *c*-axes becomes random.

In quiet freezing the primary ice layer is very thin (less than 1 mm), and it may be easily lost by melting or sublimation. This ice forms typically in a cold clear night with large thermal radiation losses from the water body. The freeze-up starts from the shoreline, where the lake is shallow and cools fast. The near-shore ice is called *border ice*. The ice cover extends further offshore on the surface if the conditions remain calm or laminar. Turbulent flow can break thin border ice to restart then in next calm phase. The crystal structure of primary ice depends on the rate of growth, and it will influence the crystal structure of the secondary ice, which will grow underneath (Gow 1986).

If freezing is initiated by ice or snow crystals falling onto water, the ice crystals remain small and randomly oriented. The solid precipitation may also come from the water body itself by frozen splashes or by evaporation–deposition mechanism. During heavy snowfall, the primary ice layer forms of congealed snow slush and can also be much thicker than what results from quiet freezing.

In turbulent conditions, frazil ice crystals form. These are circular disks, and they agglomerate into porous flocs. The *c*-axes are randomly oriented in three dimensions. The buoyancy of ice damps turbulence, and when the frazil volume is large enough, floating frazil aggregates appear, which will then freeze into solid layers of ice. Frazil flocs are effective in capturing impurities from the water column. Frazil ice formation can be fast since the surface temperature is kept at the freezing point and heat losses from the water body can be very large. Frazil ice formation is a common phenomenon in rivers, where the surface can be open in rapid stream sections throughout the winter (see, e.g., Ashton 1986). The thickness of the frazil layer can be several centimeters. Frazil crystals may join in the surface into plate aggregates, which collide with each other and become rounded. This is called *pancake ice* due to its visual appearance, the size of the pancakes being up to a few meters, often observed in large lakes (e.g., Nghiem and Leshkevich 2007).

Secondary ice grows down from the ice bottom into the water body as congelation ice (Shumskii 1956; Sokol'nikov 1957; Michel and Ramseier 1971; Gow and Govoni 1983;

Leppäranta and Kosloff 2000). The size of the ice crystals depends largely on the rate of growth so that the slower the growth the larger the crystals will be. Since thicker congelation ice grows slower, the crystal size increases with depth, and typically large or extra large crystals are found beneath a 10–20 cm thick *transition layer* (Gow and Govoni 1983). The orientation of the *c*-axes depends on the structure of the primary ice (Gow 1986). If the *c*-axes of primary ice are vertical, this alignment is inherited to the congelation ice below. However, if they are randomly oriented, the alignment turns horizontal with depth. This process is called geometric selection, illustrated in Fig. 3.6 (Kolmogorov 1949; see also Pounder 1965; Müller-Stoffels et al. 2009). Since a crystal grows faster perpendicular to the *c*-axis, the crystals with vertical *c*-axes are closed out during the growth process, and beneath the transition layer the *c*-axes are horizontal. In freshwater ice the directions of *c*-axes are usually random in the horizontal plane. In saline waters, preferred alignment in the direction of currents beneath the ice has been observed (Weeks and Gow 1978).

When the vertical *c*-axis orientation prevails, congelation ice crystals are giant macro grains (scale of 10 cm). Otherwise, when the *c*-axes turn horizontal, congelation ice layer has a columnar crystal structure, diameter 0.5–5 cm and height 5–50 cm. In both cases the crystal size increases with depth. The evolution is determined by external conditions, so that in a fixed lake either type of congelation may occur.

Another possible secondary ice type is frazil ice, but this has not been reported from lake ice field investigations. Frazil ice forms in open water areas. In large lakes semi-persistent open water spots are observed, and these would be potential sites for the generation of frazil ice. It is therefore likely that frazil ice layers exist in large lakes but available publications on lake ice crystal structure are too limited to confirm this. The crystals are small (1 mm or less), and they follow free with the water in turbulent flow and attach to the bottom of existing ice further downstream. If the spot remains open that may lead to fast production of ice due to the large air–lake temperature difference.

In turbulent, supercooled, shallow water, frazil ice can accumulate on the lake bottom leading to *anchor ice* formation. This phenomenon is often observed in rivers but has not been reported for freezing lakes. However, anchor ice is expected to occur where the given conditions exist. As a follow-up, anchor ice could rise to the surface when its buoyancy overcomes the binding forces at the bottom.

Superimposed ice forms on the top of the ice sheet, when liquid water or slush on ice freezes. In the former case, the source of water is melting or precipitation, and as far as it is known only a thin layer of ice is formed in this way on lake ice. Freezing of slush

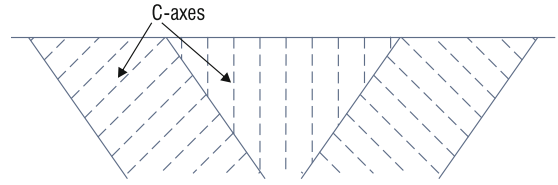

Fig. 3.6 Geometric selection in lake ice growth when the *c*-axes are randomly oriented in the primary ice layer Redrawn from Pounder (1965)

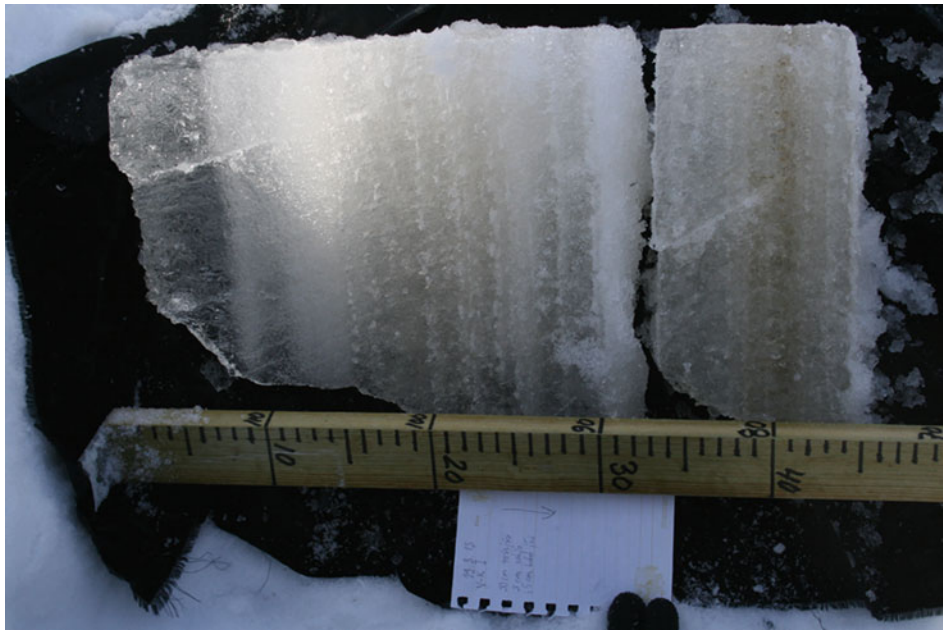

Fig. 3.7 Ice sample from Lake Valkea-kotinen, southern Finland, 19 March 2013. Ice bottom on the left side. Scale down in centimeters. Total thickness 45 cm with 5 cm of congelation ice shown by the clear layer. Within 30–35 cm from the *bottom* there was a 2-cm slush layer illustrated by the cut in the sample. *Photograph* by the author

produces *snow-ice*, which may form a thick layer, at extreme 90 % of the ice sheet in Finland (Fig. 3.7). The source slush is a mixture of snow and liquid water available from flooding, liquid precipitation or melting of snow. When the slush has formed by flooding, approximately half of it is liquid water and half of it is snow. This is because the snow layer experiences compression when it is mixed with lake water (Leppäranta and Kosloff 2000). If the liquid water is from precipitation, the proportions should be about the same but in the melt water case, the proportion depends on the daytime melt rate; however, at most the snow accounts for about 50 %.

Snow-ice grows from top of the slush down, and then pockets of slush can be captured inside the ice sheet (Leppäranta 2009a). In frozen slush, the crystals are fine or medium size, depending on the size of the snow crystals and voids between, and the orientation of the *c*-axes is random. Growth of snow-ice is limited by the presence of snow and availability of liquid water. Therefore, as has been observed (Leppäranta 2009a), it is possible that slush layers remain within the ice sheet and persist for several weeks. Snow-ice inherits air inclusions from the snow layer and has lower density than congelation ice

(860–890 kg m^{-3}, corresponding to 3–6 % gas content[4]; see Palosuo 1965). Because of the air inclusions, the thermal conductivity and strength are lower in snow-ice than in congelation ice, and snow-ice scatters light strongly and appears opaque.

For the flooding condition, the ice surface elevation from the water level, h_w, is given by the Archimedes' law as

$$h_w = \left(1 - \frac{\rho_i}{\rho_w}\right) h_i - \frac{\rho_s}{\rho_w} h_s \tag{3.6}$$

where h_i and h_s are the thicknesses of ice and snow, respectively. The ice surface sinks down as more snow accumulates. If the weight of the snow is enough, the ice is forced beneath the water surface level or $h_w < 0$. Cold freshwater ice is not permeable and can resist the pressure by the snow overload. It is often reported that under overload pressure, water flows up like a fountain when a hole has been drilled. This was well noted in Finnish Lake Päijänne, in winter 1999, when the ice surface was 12 cm beneath the water surface level at the instant of drilling (Leppäranta et al. 2003b). In saline lakes, the ice has better permeability and overload pressure is continuously released.

The flooding condition, from Eq. (3.6), can be expressed as $h_s > \gamma h_i$, where $\gamma = (\rho_w - \rho_i)/\rho_s$. Thus if $\rho_w - \rho_i = 90$ kg m^{-3} and $\rho_s = 250$ kg m^{-3}, the snow thickness must be at least about one-third of the ice thickness for the flooding to occur. Then, if cracks appear, water flows through them forming slush with the snow on ice and to freeze further into snow-ice. The theoretical upper limit of snow-ice formation by flooding is

$$h_{si} = \frac{h_s}{1 + 2\left[\left(\frac{\rho_w}{\rho_i}\right)^2 - 1\right]} \sim \frac{2}{3} h_s \tag{3.7a}$$

In this case only snow-ice forms, submerged snow is compressed, mixed with water and frozen, and according to the Archimedes law a fraction of the snow must stay above the water surface level. In winter 2013 snow accumulation was much more than average in southern Finland and the timing was favourable for snow-ice formation. As a result, in many lakes the ice thickness was about 50 cm with 90 % snow-ice, corresponding to close to 2/3 of the snow thickness on land. When there is a congelation ice layer, snow is first used to overcome its buoyancy and 'extra snow' is able to produce snow-ice.

In spring the day-and-night melting-freezing cycle produces snow-ice. Snow melts in daytime and the mixture of meltwater and snow freezes in nighttime. The resulting upper limit of snow-ice growth is

[4] In glaciology where snow transforms into ice by compression, the density is taken as 830 kg m^{-3} at the transition (e.g., Paterson 1999), corresponding to the gas content of 9.5 %.

$$h_{si} = \frac{\rho_s}{\rho_i} h_s \sim \frac{1}{3} h_s \tag{3.7b}$$

When liquid precipitation acts as the water source for slush formation, the snow-ice layer will be a half-and-half mixture of the snow on ice and the rainwater, with the upper limit of

$$h_{si} = 2\frac{\rho_s}{\rho_i} h_s \sim \frac{2}{3} h_s \tag{3.7c}$$

The thickness of snow-ice is usually below the theoretical limiting values (3.7a, b, c).

In large lakes, in the presence of a strong wind or current forcing the ice may break and the resulting blocks pile up into deformed or *agglomerate ice* (Fig. 3.8). The force is equal to the surface stress times the fetch, and with long fetches (length scale of the lake), wind can produce the highest forces to break the ice. In sea ice research this ice type is called (mechanically) deformed ice and divided into further sub-classes such as rafted ice and ridged ice (see WMO 1970, and later web updates).

Fig. 3.8 Agglomerate ice produce by ice pressure in the coastal zone in Lake Baikal. *Photograph* by Oleg Timoshkin, printed by permission

3.2.3 Snow Cover

In most lakes the ice is covered with snow, which differs from ice layers in many respects (Fig. 3.9). Observations and classification of snow on lake ice can be made following the methods in Fierz et al. (2009). Granberg (1998) has written a review of snow on sea ice, serving lake ice research as well. The snow cover has a major role in the physics of lake ice. The structure and properties of snow undergo evolution in metamorphic processes during the whole ice season. Snow on lake ice has two particular characteristics. First, since the ice is floating, the lower part of snow may become slush as shown in Sect. 3.2.2. Second, the presence of water at the freezing point temperature beneath the ice provides heat to cold snow and, consequently, influences snow metamorphosis. In particular, in cold conditions depth hoar may form in the lower snow layer.

In dry climate regions, the snow cover may be missing or is very thin, and, consequently, is rather a minor factor. Such areas are found, for example, in Tibet, Northeast China, and dry valleys of Antarctica. In very cold climate the adhesion between ice and snow is weak, and winds are able to clear the snow away if the snow accumulation keeps on a moderate level or less. This is the normal situation in Lake Baikal.

The basic properties of snow on lake ice are the thickness, density, grain size and shape, liquid water content, and impurities (Table 3.4). The density of seasonal snow ranges from 100 kg m^{-3} for new, loose snow to 400 kg m^{-3} for wind-packed tundra snow, while the grain size is within 1–10 mm. The liquid water content has a very large variability, from zero for cold snow to 50 % (volume) for water-soaked snow or slush and can be more for melting snow. The water holding capacity of snow is about 5 % (DeWalle and Rango 2008), and due to the relatively large particle (snow crystal) size, the hydraulic conductivity is good so that the water exceeding the holding capacity is filtrated down through the snow layer fast.

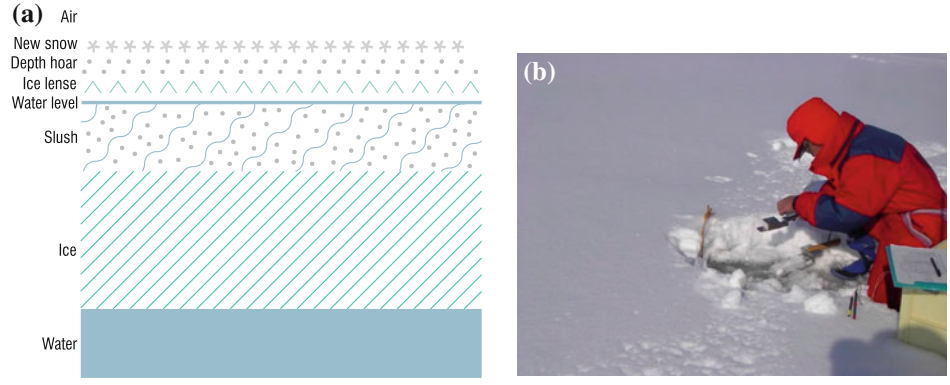

Fig. 3.9 **a** Schematic picture of snow on lake ice cover; **b** snow fieldwork on lake ice

Table 3.4 Physical properties of seasonal snow

Property	Value	Comments
Density	100–400 kg m^{-3}	Reference value 250 kg m^{-3}
Grain size	1–10 mm	Changes due to metamorphic processes
Liquid water content	0–100 %	Significant only at 0 °C; water holding capacity 5 %
Thermal conductivity	0.03–0.4 W m^{-1} $°C^{-1}$	Proportional to density squared
Albedo	0.5–0.9	Depends on liquid water content, grain size
Optical thickness	5–15 cm	Depends on liquid water content, grain size

The basic properties are used for the parameterization of other physical properties. The thermal conductivity of snow is very low due to the high air content. It has been taken proportional to the density squared (Abel's 1893); the widely-used formulae after Yen (1981) is $\kappa_s = 2.22362 \cdot \rho_s^{1.885}$, where κ_s is in W m^{-1} $°C^{-1}$ and ρ_s is in g cm^{-3}. Also the reflectance of snow is high and the optical thickness[5] is low compared with ice, so that in the presence of thick snow cover there is no sunlight in the ice or in the water body. The reflectance and transmissivity are highly sensitive to the liquid water content of snow. With these thermal and optical properties, the snow layer strengthens the isolation of the water body from the atmosphere.

3.2.4 Case Study

An example is given from a medium-size lake, Lake Pääjärvi in southern Finland (Ruuhijärvi 1974). The surface area of the lake is 13.4 km^2, and the mean depth is 15.3 m. The structure of the winter ice sheet has been monitored for 20 consecutive years in connection with field courses (Table 3.5). The ice cover was usually static but in one winter when the ice was relatively thin (33 cm), a minor mechanical shift was observed with a formation of a small ridge. The total thickness of ice as well as the thicknesses of congelation ice and snow-ice layers were primarily controlled by air temperature and snowfall time history.

The annual maximum ice thickness ranged from 24 to 80 cm, and the relative proportion of snow-ice ranged from a minimum of 5 % to a maximum of 64 % of the total ice thickness. The standard deviation of ice thickness was 12.5 cm, while for snow thickness it was 8.0 cm. Usually the ice formed in a cold calm night in late autumn and produced a vertical orientation of the crystal axes and extra large granular crystals in the congelation ice. The ice surface was within 5 cm from the water surface, and snow-ice formed mainly by flooding. In one winter out of four, a several centimetres thick, quasi-permanent slush

[5] The thickness where irradiance has decreased to the fraction e^{-1}, also called the e-folding thickness.

Table 3.5 Ice layers in Lake Pääjärvi in March

Year	Total ice	Congelation ice	Snow ice	Snow	Water level	Comments
1993	33	30	3	10	−0.1	Low ridge in the lake
1994	67	54	13	5	3.0	
1995	43	26	17	7	2.0	
1996	43	38	5	30	−5.0	
1997	35	21	14	1	3.0	Slush layer with algae in ice
1998	52	42	10	5	4.0	
1999	53	30	23	6	3.0	Slush 14–17 cm from top
2000	36	22	14	7	2.0	
2001	37	20	17	1	3.0	
2002	41	30	11	2	2.0	
2003	80	70	10	0	–	Freeboard estimated as 10 cm
2004	45	33	12	22	2.0	
2005	51	31	20	8	2.0	Slush layer with algae in ice
2006	48	44	4	16	2.0	
2007	37	26	11	0	2.0	
2008	28	28	0	0	1.0	
2009	33	25	8	19	−1.0	
2010	53	30	23	0	5.0	Slush layer with algae in ice
2011	50	26	24	11	2.0	
2012	42	17	25	3	3.0	
2013	44	16	28	9	2.0	
2014	24	23	1	3	2.0	Lowest thickness, mostly bare ice
Mean	44.3	31.0	13.3	7.5	2.5	
St. dev.	12.5	12.5	8.1	8.0	0.9	
Min	24	23	0	0	–5.0	
Max	80	70	28	30	5.0	

The thicknesses of congelation ice, snow-ice and snow, and water level elevation with respect to the ice surface (cm)

layer developed within the snow-ice layer, and the presence of algae could be visually observed. Leppäranta and Kosloff (2000) reported that the density of snow on Lake Pääjärvi is 0.23–0.33 g cm^{-3}.

3.3 Impurities in Lake Ice Cover

Lake ice sheet contains impurities, which originate from the water body, bottom sediments, or atmospheric deposition (Fig. 3.10). These impurities consist of gas bubbles, liquid inclusions, and particles, which are called *ice sediments*, and they influence on the physical properties of ice and biological processes inside the ice. The concentration of impurities is low, compared with river ice or sea ice. Freezing of lake water releases impurities from the growing ice to the liquid water body. Atmospheric deposition is stored in the ice sheet for the period of the ice cover. Flooding of a snow-covered ice by lake water forms slush, and when the slush freezes the impurities are kept in the ice sheet.

The size, shape and concentration of gas bubbles can be examined from thick sections using a microscope (e.g., Li et al. 2011). In congelation ice, gas bubbles appear sometimes as layers, and the bubbles may extend vertically into cylinders if there is continuous supply of gas during an ice growth episode. Lake ice liquid inclusions and sediments are examined from the meltwater of ice samples as usually water samples are treated (Leppäranta et al. 2003b). Ice cores are sectioned according to the stratigraphy, for a good resolution the slices are 5–10 cm thick. Gas bubbles are the most important impurities in freshwater lakes, while in saline ice liquid brine inclusions possess this role. Brine pockets can serve as habitats of biota, and they have been examined widely for sea-ice ecology.

The gas content (v_a) of congelation ice is usually small, magnitude 1 %, and in snow-ice it is 3–6 % (Palosuo 1965). Therefore the properties of freshwater congelation ice are close to the properties of pure ice, but in snow-ice the gas content is more significant. The size of the gas bubbles is in the range 0.1–10 mm (Fig. 3.11). In particular, the gas bubbles have a major influence on the backscattering of electromagnetic waves, and minor influences, e.g., on the thermal conductivity and strength of ice. In congelation ice the gas is derived from the water column or the lake bottom sediments, while snow-ice contains air inclusions from the parent snow. Gas exchange between lake water bodies and the atmosphere may take place through leads and fractures during the ice season.

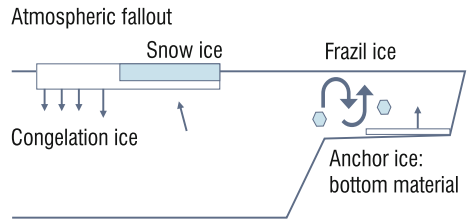

Fig. 3.10 The sources of impurities and their catchment processes in lake ice. Usually atmospheric fallout and flooding of lake water are the main sources, but where frazil ice and anchor ice forms the amount of impurities is at largest

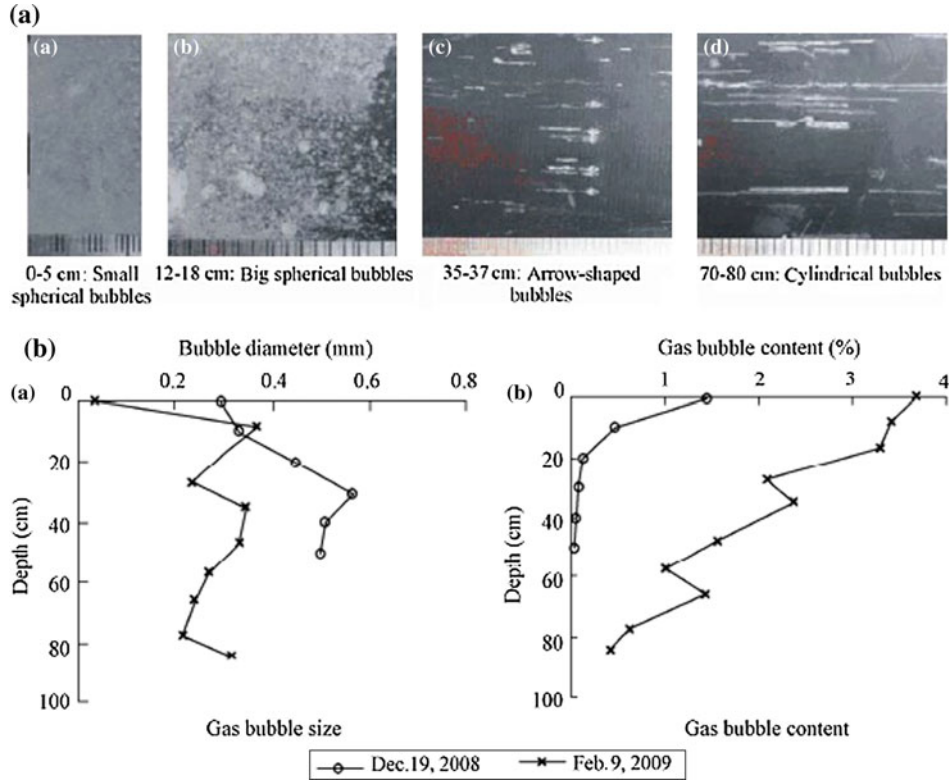

Fig. 3.11 Ice sample analysis for gas bubbles in winter 2008–2009. **a** Gas bubbles in lake ice sheet (top toward the right) in Hongipao Reservoir, Heilongjiang Province, China (February 9, 2009); **b** Bubble size and gas volume as functions of depth From Li et al. (2011)

A quantity proportional to ice volume scales as $(1 - v_a)$, as does the density (see Example 3.2), if the influence of gases can be ignored. A good reference density is for congelation ice 910 kg m^{-3} and for snow-ice 875 kg m^{-3}. Many properties of lake ice depend on areal cross-sections, e.g. ice strength and thermal conductivity; assuming gas inclusions as randomly spaced spheres, by dimensional analysis it is seen that these properties would be reduced by a factor of $1 - r_1 v_a^{2/3}$, where r_1 is a geometrical model parameter. If the inclusions were long vertical cylinders, the scaling factor would be $1 - r_2 v_a^{1/2}$, where r_2 is another geometrical model parameter (Assur 1958).

In brackish and saline lakes, liquid brine pockets may take a significant portion of the ice volume. They have been extensively examined for sea ice (Weeks 1998). When saline water freezes, ice crystals form of water molecules, i.e. freezing tends to separate

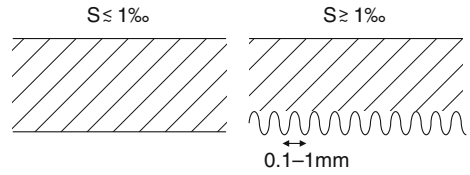

Fig. 3.12 Ice–water interface for freshwater ice and brackish/saline ice. *S* refers to the salinity of the water

dissolved substances out from the solid phase of water. However, due to constitutional supercooling in the molecular diffusion of salt and heat in the liquid phase, cellular ice–water interface forms (Fig. 3.12) and is able to close liquid brine pockets between crystal platelets (Weeks 1998). In fresh water, planar interface forms and separation is much more effective.

The surface water salinity, where the transition between fresh water ice type and saline ice type takes place, is within 1–2 ‰ according to observations in the Baltic Sea (Palosuo 1961; Weeks et al. 1990; Kawamura et al. 2001). Therefore brackish water ice is similar to saline ice rather than to fresh water ice. The salinity of new ice is a fraction κ of the salinity of the water: $S_i = \kappa S_w$, where κ is the segregation coefficient, $\kappa \approx 0.25$–0.5 for brackish and saline ice (Weeks 1998) and $\kappa \sim 0.1$ for freshwater ice (Leppäranta et al. 2003b). The segregation coefficient increases with growth rate of ice. The salinity of liquid brine within the ice must always correspond to the freezing point of the ambient temperature, $S_b^{-1}(T) = T_f$, and thus the brine salinity and consequently the brine volume change with the temperature. In addition, in very low temperature salts start to crystallize from the brine, each at its own eutectic temperature. The chemical composition of brine and formation of salt crystals can be studied from the phase diagram of the lake water. However, individual phase diagrams for particular freezing lakes are not known to the author. Since seawater is a chemically uniform solution throughout the oceans, one phase diagram is enough for all sea-ice (Assur 1958).

Brine volume is the primary factor to influence the properties of brackish and saline ice, since brine inclusions may reach 10 % and more of the ice volume when the ice is warm. Solid salt crystals scatter light and therefore influence on the optical properties of sea ice. Brine pockets serve as habitats of biota. They contain liquid water and nutrients, and with light penetration, sufficient conditions for primary production exist. The algae are captured into the ice in the freeze-up process, and their growth in the brine pockets is primarily light-limited, in oligotrophic lakes likely also by nutrients. In saline lakes, the most active layer is the bottom layer, so-called *skeleton layer*, which may become coloured brown-green by the algae.

In freshwater lakes, congelation ice does not provide an appropriate environment for living organisms, but algae can grow in a slush layer between snow-ice and congelation ice. The buoyancy of thinner ice is less, and therefore flooding events are more common. In very humic fresh water lakes, liquid humus layers have been found in the snow-ice

Fig. 3.13 Humus layers in snow-ice, scale in centimeters from the *top* surface (*top up*). Lake Valkea-kotinen, southern Finland

layer and humus pockets also in the congelation ice layer (Salonen et al. 2009) (Fig. 3.13). Humus absorbs light especially at short wavelengths and has therefore notable influence on the transparency and colour of the ice sheet.

Sediment particles originate from the water body, lake bottom and atmospheric deposition. In congelation ice their concentration is very low. They would be effectively harvested by frazil ice or anchor ice if these ice types were formed. Sediments may influence the properties of ice and they may also have a significant role in transporting matter if the ice drifts. In a normal congelation ice–snow-ice lake ice sheet, most of the impurities are due to the flooding of lake water on the ice and atmospheric deposition. In eutrophic or hypereutrophic lakes, floating vegetation is captured within the ice during the ice growth processes.

Example 3.4. Anchor ice has buoyancy of $(\rho_w - \rho_i)Vg$, where V is the volume. Therefore a cubic meter of anchor ice my lift a 90-kg stone from the bottom, or, if spread on a 10 m^2 area of bottom sediments, can overcome a cohesion of 10 Pa.

Meltwater samples have been examined for the presence of impurities in several lakes in southern Finland (Tables 3.6 and 3.7). In Lake Pääjärvi, the mean conductivity of the meltwater was 12 μS cm^{-1} (referenced to 25 °C), which represents 10 % of the conductivity of the lake water. The average dissolved matter content was 14 mg/l, and the concentration of suspended matter was 1.9 mg/l, which is also less than that recorded in

Table 3.6 Conductivity, concentration of dissolved matter and suspended matter in ice, snow and water in four Finnish lakes (Leppäranta et al. 2003b): oligotrophic Lake Päijänne, oligo-mesotrophic Lake Pääjärvi, eutrophic Lake Vesijärvi, and hypereutrophic Lake Tuusulanjärvi

Lake	Conductivity μS cm^{-1} (at 25 °C)	Dissolved matter mg l^{-1}	Suspended matter mg l^{-1} (organic fraction)	pH	Congelation ice fraction %
Päijänne					91.8
Ice	7.7	11.3	2.1 (23 %)	6.6	
Snow	19.0	20.0	17.0 (50 %)	×	
Water	78.7	31.3	1.4 (49 %)	7.0	
Pääjärvi					69.0
Ice	13.0	14.3	2.1 (36 %)	6.7	
Snow	16.5	15.0	4.2 (38 %)	×	
Water	108.0	64.0	3.7 (40 %)	6.6	
Vesijärvi					89.7
Ice	7.0	12.7	2.0 (33 %)	6.6	
Snow	28.0	23.5	9.9 (54 %)	×	
Water	128.3	52.3	1.1 (50 %)	7.0	
Tuusulanjärvi					77.8
Ice	15.0	17.3	12.6 (24 %)	6.6	
Snow	9.5	17.0	11.6 (58 %)	×	
Water	208.3	143.0	11.5 (22 %)	6.8	

The data show averages of the years 1997–1999

the liquid water. Congelation ice is typically much cleaner than the water from which it forms whilst snow-ice can include impurities from the lake water and the parent slush. When the ice melts, these impurities are released into the lake in a very short time. The meltwater of clean congelation ice may then be less dense than the underlying lake water due to its very low content of dissolved matter.

The concentration of a substance in lake ice can be formulated as

$$C = \gamma C_{ci} + (1 - \gamma)[vC_s + (1 - v)C_w] \tag{3.8}$$

where γ is the fraction of congelation ice, $v \sim 1/2$ is the fraction of snow in snow-ice, and the subscripts w, s and ci refer to lake water and snow in snow-ice, and congelation ice.

The vertical distribution of impurities shows usually an increase in the snow layer when snow ages, highest in old snow or snow ice, and congelation ice is clearly the cleanest layer (Fig. 3.14). The lake water shows much higher levels than snow or ice.

Table 3.7 Nutrient concentrations in ice, snow and water in four Finnish lakes in winter 1999 (Leppäranta et al. 2003b): oligotrophic Lake Päijänne, oligo-mesotrophic Lake Pääjärvi, eutrophic Lake Vesijärvi, and hypereutrophic Lake Tuusulanjärvi

Lake	Phosphorus (μg/L)		Nitrogen (μg/L)		Congelation ice fraction %
	$P–PO_4$	Total	$N–NO_3$	Total	
Päijänne					93.0
Ice	<2	2	11	102	
Snow	<2	4	390	590	
Water	<2	4	225	487	
Pääjärvi					56.6
Ice	2	3	95	260	
Snow	<2	3	592	987	
Water	5	14	867	1,257	
Vesijärvi					92.9
Ice	<2	<2	<5	204	
Snow	5	10	232	755	
Water	22	28	185	567	
Tuusulanjärvi					61.0
Ice	8	18	213	487	
Snow	5	6	130	318	
Water	40	85	3,216	4,799	

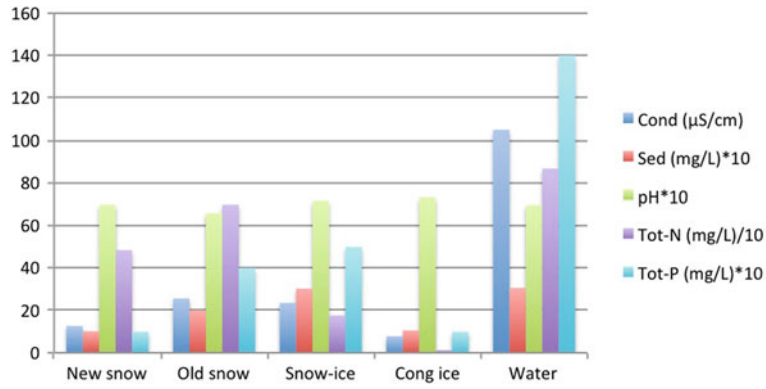

Fig. 3.14 Vertical distribution of the electric conductivity, concentration of suspended matter, pH, and concentration of total nitrogen and phosphorus across snow and ice layers in Lake Pääjärvi, winter 1999. Note that the scales have been adjusted so that the numbers fit into range of 1–100. *Data source* Leppäranta et al. (2003b)

3.4 Light Transfer Through Ice Cover

3.4.1 Solar Radiation

The Stefan–Boltzmann law for the total power of black body radiation was introduced in Sect. 2.2.5. It is based on the Planck's law, which provides the distribution of the radiational power with respect to the wavelength:

$$I(\lambda;T) = \frac{8\pi hc^2}{\lambda^5}\left[\exp\left(\frac{hc}{\lambda k_B T}\right) - 1\right]^{-1} \tag{3.9}$$

where λ is wavelength, h is Planck's constant, c is velocity of light in vacuum, and k_B is Boltzmann's constant. The distribution depends on the temperature of the body, with the level of radiation increasing with the temperature and the peak wavelength decreasing with the temperature. The Sun radiates almost as a black body at the temperature of its outer surface, 5,900 K (Fig. 3.15).

Example 3.5. The black body radiation is used as a reference to define the brightness temperature and the colour temperature. The *brightness temperature* T_B of a surface is equal to the temperature of the black body that would provide the same radiance at the given wavelength: $I(\lambda, T_B) = I'(\lambda, T)$, where I' is the spectral power density of the observed radiation from the given body. Black body radiates with the maximum power, and therefore always $T \geq T_B$. The *colour temperature* T_c is the temperature of an ideal black body radiator, which has the spectral energy distribution closest to the object in concern. It can be determined by measurement of power and absorbance A at two wavelengths:

$$\frac{1}{T} - \frac{1}{T_c} = \frac{k}{hc(\lambda_1^{-1} - \lambda_2^{-1})}\log\left[\frac{A(\lambda_1, T)}{A(\lambda_2, T)}\right] \tag{3.10}$$

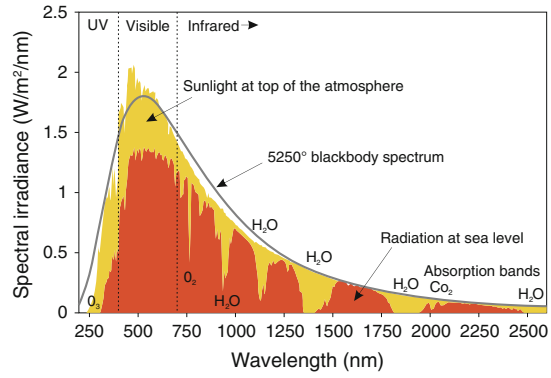

Fig. 3.15 Solar radiation spectrum at the *top* of the atmosphere and at the sea surface level. Atmospheric absorption bands due to ozone (O_3), oxygen (O_2), water vapour and carbon dioxide are illustrated in the solar radiation band

Table 3.8 The bands of the electromagnetic radiation referred in lake research

Ultraviolet	100–400 nm	UV-C	100–280 nm
		UV-B	280–315 nm
		UV-A	315–400 nm
Light[a]	380–750 nm	Violet	380–450 nm
		Blue	450–495 nm
		Green	495–570 nm
		Yellow	570–590 nm
		Orange	590–620 nm
		Red	620–750 nm
Infrared	750 nm–1 mm	Near IR (IR-A)	750–1,400 nm
		Short-wavelength IR (IR-B)	1.4–3 μm
		Thermal IR (IR-C)	3–15 μm
		Far IR	30–1,000 μm
Microwaves	1 mm–1 m	Millimeter waves (MMW)	1–10 mm
		Radar	1–30 cm

[a]Radiation visible to a human eye, also called 'visible light' and 'optical band'

In the derivation, it is assumed that $\lambda k_B T \ll hc$, which simplifies the Planck's law to derive the direct solution.

The wavelengths from ultraviolet to microwaves are divided into bands as shown in Table 3.8. The limits are not sharp, and the reference transition wavelengths of the bands show minor variability in literature. The solar spectrum peaks at 480 nm, has nearly all its energy in the ultraviolet, light, and infrared (IR-A and IR-B) bands (Fig. 3.15). Narrow Frauenhofer lines are seen in the short wave solar spectrum due to absorption by elements in the solar atmosphere.

At the Earth's surface, the visible light distribution shows yellow to our eye, and UV-C and most of UV-B are absent as absorbed by ozone in the upper atmosphere. According to observations, even though the level of solar radiation varies largely due to atmospheric conditions, the shape of the radiation spectrum is fairly stable. Atmospheric gases have absorption bands, which show up in the spectrum, while cloudiness decreases the level of radiation on the surface of the Earth. The radiation depends on the Earth–Sun distance r, solar zenith angle Z and the attenuation in the atmosphere. This distance depends on the time of year, and the solar zenith angle depends on the time of year and day and the latitude, obtained from astronomical formulae (see Annex).

Semi-empirical equations are available for the clear sky atmospheric transmittance T_{tr} and the influence of cloudiness N. A general form for the incident solar radiation on a horizontal unit area on the surface of the Earth is

$$Q_S(Z,e,N) = \cos Z \cdot Tr(Z,e) \cdot F(N,Z) \cdot (\tilde{r}/r)^2 \cdot Q_{sc} \tag{3.11}$$

where F gives the influence of cloudiness ($^1/_3 \le F \le 1$), and $\tilde{r}$ is the mean Earth–Sun distance, also known as the astronomical unit AU (see Annex 1). The solar constant is Q_{sc} = 1,367 W m^{-2}, and due to the ellipticity of the Earth's orbit, the Earth–Sun distance varies with time and causes the solar radiation above the Earth's atmosphere to range from 1,294 W m^{-2} (in June 20–22) to 1,483 W m^{-2} (in December 20–22).

The atmospheric transmittance is close to 0.9 except for very large solar zenith angles (Z > 80°). Zillman (1972) formula for the clear sky transmittance, found good in many applications (e.g., Curry and Webster 1999; Leppäranta and Myrberg 2009), is written as

$$T_{tr}(Z,e) = \frac{\cos Z}{1.085\cos Z + e \cdot (2.7 + \cos Z) \times 10^{-3} + 0.01} \tag{3.12}$$

where the water vapour pressure is given in millibars. The maximum of T_{tr} (Z = 0 and e = 0) is 0.913. In cold climate we can assume that e < 10 mbar. At this upper limit, for the direct radiation we have T_{tr} = 0.879 at Z = 30°, T_{tr} = 0.855 at Z = 60° and T_{tr} = 0.764 at Z = 80°. At the limit $Z \to 90°$, we have $T_{tr} \to 0$ that is not exactly true since the thickness of the atmosphere is finite.

For clear sky irradiance at the lake surface we have F = 0 in Eq. (3.11). By integration, it is seen that for horizontal planar irradiance, diffuse radiation corresponds to direct radiation at Z_D = 50.5°. Therefore, the total clear sky irradiance at the surface can be estimated as $Q_s(Z, e, 0) = vQ_s(Z, e, 0) + (1 - v)Q_s(Z_D, e, 0)$, where v is the fraction of direct solar radiation. For larger zenith angles the diffuse radiation becomes dominant.

Cloudiness can reduce the level of radiation at the Earth's surface to about one-third of the clear sky level. The cloudiness correction shows much more variability and uncertainty than the transmittance, since it depends on the quality of clouds. Lumb (1964) examined the hourly incoming radiation at different cloudiness levels and cloud types. However, usually only the total cloudiness data are available. From the results of Lumb (1964) we can formulate the cloud correction function as

$$F(N,Z) = 1 - (a - b\cos Z) \cdot N \tag{3.13a}$$

in the absence of precipitation. Here $a \approx 0.6$ and $b \approx 0.1$ are empirical parameters. Lumb (1964) also reported that the radiation reaching the Earth's surface is much smaller in the presence of rain. Several formulae have been designed for estimation of daily solar fluxes. A widely used one is by Reed (1977):

$$F(N,Z) = 1 - c_N \cdot N + 0.0019 \cdot (90° - Z°) \tag{3.13b}$$

where c_N = 0.62 is a cloudiness coefficient, and $Z°$ is the noon solar zenith angle in degrees. This is, however, inconsistent in that $F(0, 0)$ = 1.17 that would give $Q_s > Q_{sc}$. The

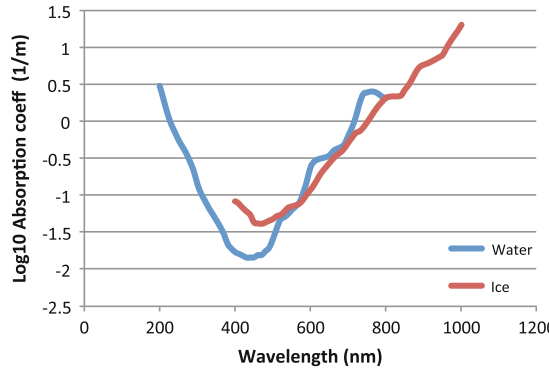

Fig. 3.16 Absorption spectrum of clearest natural waters (Smith and Baker 1981) and bubble-free polycrystalline ice (Grenfell and Perovich 1981)

coefficient c_N has been slightly modified in different applications. Curry and Webster (1999) noted that this equation tends to overestimate the solar radiation by as much as 6 % and should not be used for $N < 6$ %. Both forms (3.13a, b) are linear in cloudiness and the zenith angle makes a small modification (less than 0.05 in polar regions).

A narrow band of solar radiation travels through liquid or solid phase of water in lakes, about 300–1,200 nm (UV-A, light, and most of IR-A). Shorter wavelengths do not penetrate the atmosphere, and pure water (liquid or solid) itself absorbs longer wavelengths effectively (Fig. 3.16). In wavelengths longer than 1,200 nm the absorption coefficient is more than 1 cm^{-1} in pure water. Ultraviolet and near-infrared fractions attenuate fast, and only light is left from the solar radiation beneath 1 m layer of pure ice or water. In the light band the absorption coefficient is less than 0.03 cm^{-1}. Within the band 300–1,200 nm, ozone absorbs in UV-A, and oxygen (O_2) and water vapour absorption peaks occur at 760 and 1,100 nm, respectively (Fig. 3.15).

Transfer of sunlight is a key issue in lake ice research. Absorption of radiation in pure ice is much as in pure liquid water. In the absorption spectrum, due to hydrogen bonding the peaks are shifted toward lower energy in the ice.

3.4.2 Radiance and Irradiance

The basic quantity in the radiation transfer is *radiance*, defined as the light intensity (I) emitted in direction ξ by an infinitesimal small element of the source area dA through an infinitesimally small element of the solid angle $\Omega(\xi)$,

$$L(\xi) = \frac{dI(\xi)}{dA \cos\theta} \tag{3.14}$$

where θ is the angle between the normal to the surface and ξ (see, e.g., Dera 1990; Arst 2003 for a more complete treatment). Radiance can be spectral (W m^{-2} nm^{-1} sr^{-1}) or integrated over the wavelengths (W m^{-2} sr^{-1}).

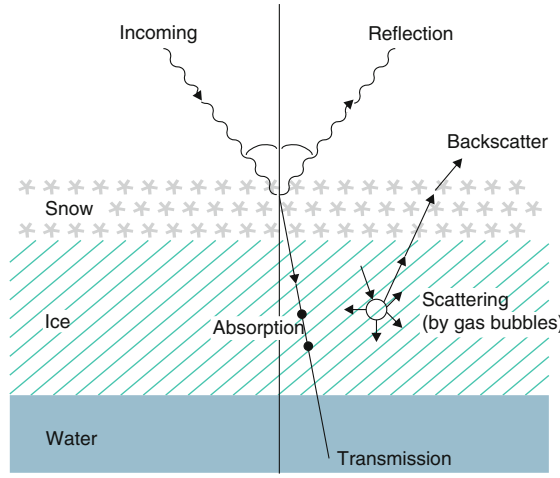

Fig. 3.17 Schematic picture of radiation concepts in the transfer through ice cover

Radiation is absorbed and scattered in ice and water, described with the absorption coefficient $a(\lambda)$ and scattering function, assuming isotropic medium, $\beta(\psi, \lambda)$, where ψ is the angle of the scattered beam from the unscattered beam ($0 \leq \psi \leq \pi$). The absorption coefficient and the scattering function are inherent[6] optical properties (Fig. 3.17). Absorption follows the Beer–Lambert law:

$$\frac{dL}{ds} = -aL \tag{3.15}$$

where s is the direction of light propagation. The scattering function is usually integrated over forward and backward hemispheres for forward scattering and backscattering coefficients $b_f(\lambda)$ and $b_b(\lambda)$, respectively. By diffusing the radiation, scattering reduces the radiance level in the direction of propagation, as specified by the total scattering coefficient $b(\lambda) = b_f(\lambda) + b_b(\lambda)$. For this reduction, an attenuation law similar to the Beer–-Lambert law is employed. Additivity is assumed for the influences of absorption and scattering, and the total beam attenuation coefficient becomes $c = a + b$.

Solar radiation comes to Earth's surface directly from the Sun and as diffuse radiation from the whole sky due to scattering in the atmosphere. The contributions of the direct and diffuse radiation depend on the solar zenith angle and cloudiness. To obtain the amount of incoming radiation at the surface and at different depths in ice-covered lakes, radiance needs to be integrated over all directions. This leads to the concept of *irradiance*. Take the vertical, z-coordinate zero at the lake surface and positive downward (the top surface may

[6] Inherent optical properties depend on the properties of the medium only, while apparent optical properties depend also on the directional distribution of the incoming light.

be snow, ice or water). Spectral downwelling and upwelling planar irradiances at the depth z are given, respectively, by:

$$E_d(z,\lambda) = \int_0^{2\pi} d\varphi \int_0^{\pi/2} L(z,Z,\varphi,\lambda)\cos Z \sin Z\, dZ \tag{3.16a}$$

$$E_u(z,\lambda) = -\int_0^{2\pi} d\varphi \int_{\pi/2}^{\pi} L(z,Z,\varphi,\lambda)\cos Z \sin Z\, dZ \tag{3.16b}$$

where (Z, φ) are the local spherical direction coordinates, the zenith angle ($-\pi/2 \le Z \le \pi/2$) and the azimuth φ ($0 \le \varphi \le 2\pi$). Integrating the solar irradiances with respect to the wavelength, the downwelling and upwelling solar energy fluxes are obtained. At the surface these are also called the incoming and outgoing solar radiation Q_s and Q_r, respectively.

The ratio of upwelling to downwelling irradiance is called *spectral reflectance* $r(z, \lambda)$, while *albedo* α, literally 'whiteness', is the ratio of these irradiances integrated over the wavelength at the surface,[7] respectively:

$$r(z,\lambda) = \frac{E_u(z,\lambda)}{E_d(z,\lambda)}, \alpha = \frac{Q_r}{Q_s} = \frac{\int_0^\infty E_u(0^-,\lambda)dz}{\int_0^\infty E_d(0^-,\lambda)dz} \tag{3.17}$$

where the notation 0^- stands for 'just above the surface'. Attenuation of irradiance is normally modelled with a first order equation analogous to the Beer-Lambert absorption law. For the downwelling irradiance, the transfer equation and the solution are:

$$\frac{dE_d(z,\lambda)}{dz} = -K(z,\lambda)\cdot E_d(z,\lambda) \tag{3.18}$$

where K is the *diffuse attenuation coefficient*. Sometimes (e.g., Warren 1982) K is termed as the 'extinction coefficient'. It is clear from Eq. (3.13a, b) that irradiance depends on the angular distribution of the incoming radiance, and therefore so do also optical properties defined from the irradiance. These optical properties, which include the albedo, reflectance and diffuse attenuation coefficient, are therefore *apparent optical properties* (see, e.g., Dera 1990; Arst 2003). The angular distribution of the incoming solar radiation depends primarily on the solar altitude and cloudiness.

Attenuation of irradiance tells how much solar power is available for heating and primary production. Upwelling irradiance just above the surface consists of the surface reflection and scattering and the volume backscatter from beneath the surface. In snow and

[7] Sometimes the expression *spectral albedo* is used instead of surface reflectance.

ice, scattering is strong and therefore also albedo is large, while in open water conditions the volume backscatter is at most 10 % of the surface reflection.

Since natural ice and snow are scattering media, a two-stream approach is often employed in modelling the irradiance. This model considers both downwelling and upwelling irradiance (Dunkie and Bevans 1956; Perovich 1990):

$$\frac{dE_d}{dz} = -aE_d - bE_d + bE_u \tag{3.19a}$$

$$\frac{dE_u}{dz} = aE_u + bE_u - bE_d \tag{3.19b}$$

This system has the general solution

$$E_d = A(1-\kappa)e^{\beta z} + B(1+\kappa)e^{-\beta z} \tag{3.20a}$$

$$E_u = A(1-\kappa)e^{\beta z} + B(1+\kappa)e^{-\beta z} \tag{3.20b}$$

where $\kappa = \sqrt{a/(a+2b)}$, $\beta = \sqrt{a(a+2b)}$, and A and B are constants determined by the boundary conditions.

3.4.3 Light Transfer in Ice-Covered Lakes

Snow and ice cover act as a diffusive filter for the solar radiation transfer from the atmosphere to the lake water body. The level of radiation decreases, but usually only small modifications are seen in the spectrum when passing through snow and ice layers (Fig. 3.18). Solar radiation provides heat and causes internal deterioration of the ice. It is the key factor in lake heat balance in the ice melting season. Also sunlight heats the water beneath the ice, triggers spring convection, and provides photons for primary production in snow, ice and water. Due to the strong scattering in ice and snow, radiation is diffuse beneath the ice (Leppäranta et al. 2003a; Arst et al. 2006). In clear sky, open water conditions, radiation becomes diffuse only at a distance from the surface.

Light transfer in ice and snow is influenced by the crystal structure of ice and *optically active substances* (OAS). Ice crystals are optically uniaxial, with c-axis as the optical axis. In extreme cases, in small ponds the crystals may grow with vertical c-axes and then it is possible to see through ice as through glass. Absorption of light in pure ice is much as in pure liquid water (Fig. 3.17), but there are no published results how much ice absorption depends on the crystal structure. Liquid water layers in the ice sheet reduce long wavelengths by absorption; in lake ice such layers may occur all winter in the ice–snow interface and across the whole sheet in the melting season.

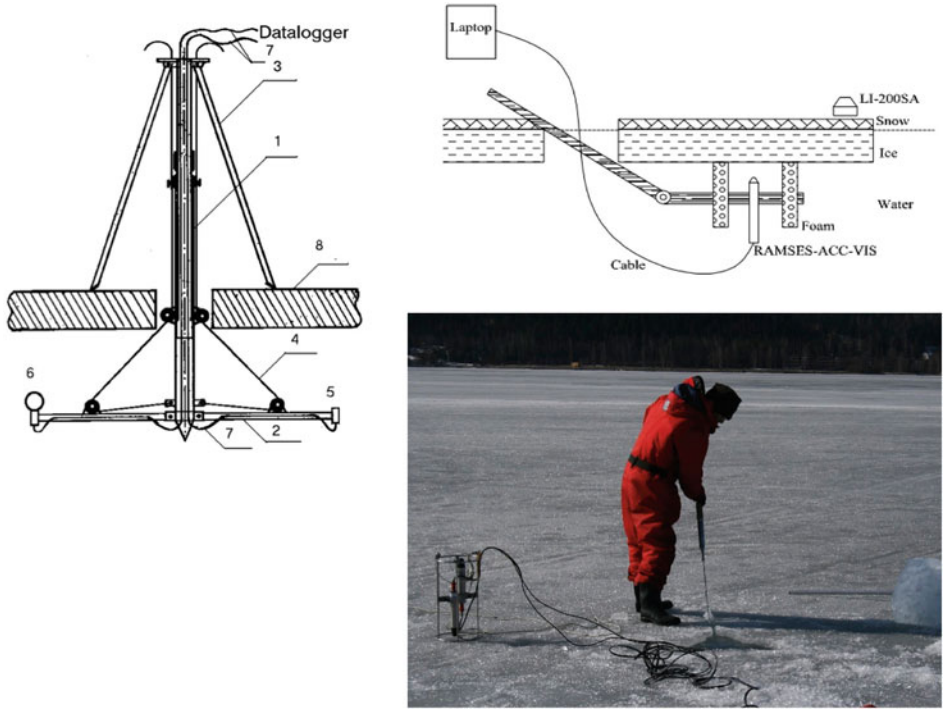

Fig. 3.18 Solar radiation is the key factor in the ice melting season. Measurements of solar radiation beneath ice are made using holes and specific techniques to push the light sensor away from the deployment hole (e.g., Arst et al. 2006; Lei et al. 2011)

In liquid natural waters, the OAS are classified into three groups: coloured dissolved organic matter[8] (CDOM), suspended matter, and chlorophyll *a* (e.g., Arst 2003). CDOM absorbs short wavelengths and turns the colour of the water toward brown, and chlorophyll *a* has two absorption peaks (430–440 nm and 660–690 nm). Humus is a common substance in the CDOM group in lake waters. Suspended particles show rather smooth light attenuation spectra, but lakes may show individual signatures depending on their geochemical balances.

The most important optically active substance in a lake ice cover is the gas content. Gas is contained in gas bubbles, which cause strong scattering, and since the size of the bubbles is much larger than the wavelengths of solar radiation, scattering is independent of the wavelength. The colour of lake ice appears black, blue or white, or something between. Congelation ice has been also called black ice, since with low gas content the ice is thinner than its optical thickness and backscattering from the ice and underlying water remains weak. When the ice is thicker and the volume of gas bubbles is small, the colour of pure ice appears blue due to the absorption of red wavelengths when the path lengths inside ice become long. This is seen clearly in icebergs. At the extreme, snow or even snow-ice is white.

[8] Also know as *yellow substance* in optical oceanography.

The OAS of liquid lake water can be also found in lake ice captured by growing ice (see Sect. 3.3; Leppäranta et al. 2003a, b). In freshwater congelation ice, the capture is not very effective, and the OAS levels are much lower in the ice than in the parent water (Fig. 3.8). Therefore bubble-free congelation ice is normally more transparent than the liquid water of the same lake. In the melting season, in particular, the presence of liquid water has major impact on the light transfer. Liquid solution in ice or snow influences on the light transfer: when it fills gas inclusions, scattering is reduced, and vice versa. In very humic lakes, liquid humus inclusions have been found from congelation ice resulting in stronger absorption of short wavelengths (Arst et al. 2006; Lei et al. 2011). Apart from the melting season, liquid water content of congelation ice is very small, and, consequently, chlorophyll is then practically absent.

Snow-ice formed by flooding has a contribution of about 50 % from the lake water with all its impurities (Leppäranta and Kosloff 2000). However, snow-ice has also a large gas content, which dominates the light transfer. Chlorophyll can be found in slush layers inside snow-ice when there is light available (Leppäranta 2009a). Frazil ice formation would be effective in capturing particles from the water body and would therefore influence the ice properties as in rivers. Atmospheric deposition adds to the impurities in the near-surface layer, whether congelation ice or snow-ice.

For light transfer in brackish and saline lakes, the presence of brine pockets makes a significant difference to freshwater lake ice (Weeks 1998). Brackish ice has been observed to be less transparent than freshwater ice in the same region (Arst et al. 2006). Primary production can become large in the brine pockets adding the chlorophyll *a* absorption spectrum to the light transfer (Arrigo 2003).

Because of the strong scattering, ice and snow surface have very high reflectances compared with open water surface. The variability of lake ice albedo is large depending primarily on the thickness of snow and presence of liquid water (e.g., Mullen and Warren 1988; Perovich 1998; Henneman and Stefan 1999; Arst et al. 2006). Table 3.9 shows references and ranges of the albedo for different surface types. These albedo values are similar to those observed in polar seas (Perovich 1998).

The albedo of snow depends on the liquid water content and grain size, impurities and cloudiness. Dry, fine-grained snow has an albedo as high as 0.9. With increasing grain size and especially increasing liquid water content, the albedo becomes lower, and for wet

Table 3.9 Typical level and range of albedo over lake surfaces

Surface	Albedo (%)		Sensitivity to surface material
	Reference	Range	
Dry snow	85	80–95	Grain size
Wet snow	50	40–70	Wetness
Dry ice	50	30–60	Gas content
Wet ice	30	20–40	Wetness, gas content
Open water	7	5–10	Water quality

snow it is typically around 0.5 (Sherstyankin 1975; Jakkila et al. 2009; Leppäranta et al. 2010). Bare, dry ice has an albedo of 0.5, and with increasing surface wetness and melt ponds, the albedo decreases to 0.2–0.3 during the melting season. When bare ice is thinner than 30 cm, albedo also depends on the thickness of ice, approaching open water albedo when thickness goes down to zero. This is due to much lower scattering of light in liquid water beneath the ice than in the ice itself. Thin (10 cm) and bare ice has an albedo of 0.2–0.3, but when the ice thickness is more than 30 cm and the surface is dry, the albedo is at the 0.5 reference level. In spring, when the snow on ice melts, the transparency of the ice increases and the light level beneath ice becomes high. In open water conditions, albedo is low (5–10 %) and stable.

Example 3.6. The solar energy flux to a lake ice sheet can be expressed as $(1 - \alpha_0)q_0$, where $q = Q_s/(\rho L_f)$. The dimension of q_0 is length/time and can be interpreted as the upper limit of the melt rate if other fluxes sum to zero.

(i) If the albedo is constant, the total melt in time t is $h_0 = (1 - \alpha)q_0 t$; for $t = 30$ d, $\alpha_0 = 0.5$ and $q_0 = 2$ cm d^{-1} we have $h_0 = 30$ cm.
(ii) If the albedo decreases with time, $\alpha = \alpha_0 - bt$, $b > 0$, the additional melt is $\frac{1}{2}\, bq_0 t^2$; for $b = 0.3$ month^{-1}, the melt increases to 39 cm.
(iii) If also melt rate increases with time, $q = q_0 + ct$, the additional melt to (ii) is $\frac{1}{2}\,(1 - \alpha_0)ct^2 + 1/3\; bct^3$; for $c = 2/30$ cm d^{-2} (this means increasing the solar heating from 2 to 4 cm d^{-1} in 1 month) the melt increases to 60 cm.

The attenuation law of irradiance (Eq. 3.18) integrates to

$$\begin{aligned} E_d(z,\lambda) &= E_d(0^+,\lambda)\exp\left[-\int_0^z K(z',\lambda)dz'\right] \\ &= [1 - r(0^-,\lambda)]E_d(0^-,\lambda)\exp\left[-\int_0^z K(z',\lambda)dz'\right] \end{aligned} \tag{3.21}$$

where the notation 0^+ and 0^- stand for just beneath and just above the surface, respectively. For a layer with K independent of depth, the inverse K^{-1} is its optical thickness. The influence of optically active substances on the attenuation is additive, i.e. we can write the attenuation coefficient as the sum of the contributions from pure water, gas bubbles, CDOM, particles and chlorophyll, respectively, as:

$$K = K_w + K_g + K_y + K_p + K_c. \tag{3.22}$$

Irradiance measurements at two levels provide the average diffuse attenuation coefficient of the layer between them. In congelation ice, $K \sim 1$ m^{-1}; Arst et al. (2008) reported values mainly between 0.5 and 2 m^{-1} in Finnish and Estonian lakes.

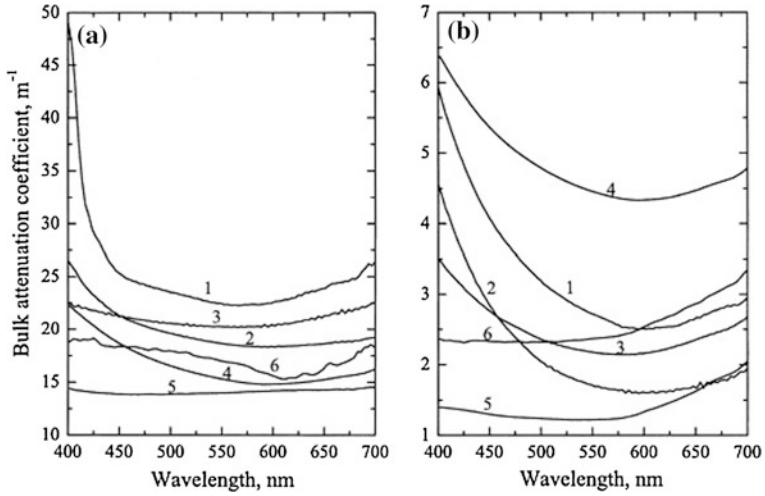

Fig. 3.19 Bulk attenuation coefficients of lake ice in winter 2009 in Estonia and Finland: Lakes *1* Lovojärvi, *2* Pääjärvi, *3* Iso Valkjärvi, *4* Peipsi, *5* Vanajavesi, and *6* Vesijärvi. **a** Natural conditions; **b** snow removed manually from the surface (Lei et al. 2011)

The attenuation coefficient depends on the wavelength, showing minimum at 500–600 nm and increasing strongly with increasing wavelength (Fig. 3.19). In humic lakes the attenuation coefficient of ice also increases toward shorter wavelengths due to absorption by CDOM. Consequently, it has become a custom to take the light band as the part of solar radiation that penetrates through the ice/snow/water surface, and the ultraviolet and near infrared parts are included in the surface absorption. This optically transparent 'surface' has finite thickness, several centimeters, and including it in the surface boundary condition is feasible for most physics research. However, in lake biology investigations the penetration of UV band into ice may be of concern.

Transmittance of an ice sheet is defined as the ratio of the radiation passed through the ice to the incoming radiation just above the ice:

$$\tau(\lambda) = \frac{E_d(h^+;\lambda)}{E_d(0^-;\lambda)} \tag{3.23}$$

where h is ice thickness. Thus the transmittance includes the influence of albedo. In general, the equation $\alpha + A + \tau = 1$ holds, where A is the total absorption of radiation by the ice sheet. In the case of a layered ice sheet, the attenuation coefficients for the individual layers determine the transmittance by

$$\tau(\lambda) = [1 - r(\lambda)] \exp\left[-\sum_{\ell} h_{i\ell} K_{d,\ell}(\lambda)\right] \tag{3.24}$$

where the subscript ℓ refers to the different layers, h_ℓ are the layer thicknesses, and $h = \Sigma_\ell h_\ell$ is the total thickness. This equation actually presents an inversion formula to estimate the attenuation coefficients of the individual layers by linear regression based on measurements of irradiance above and below the ice sheet and thicknesses of the layers (see Leppäranta et al. 2010). The number of layers to be included is limited by the number of degrees of freedom in the observational data set.

The transmittance of light is about the same for congelation ice and for liquid lake water but snow and snow-ice are much more opaque. The optical thickness of congelation ice and snow/snow-ice are 100–200 cm and 5–20 cm, respectively (e.g., Leppäranta et al. 2003a; Arst et al. 2006), while in lake waters it ranges from 10 to 500 cm depending on the water quality (Arst 2003; Arst et al. 2008). Thus the amount of snow and snow-ice is a critical factor for the light transfer. In spring, when the snow has melted, the solar radiation level is high and sunlight penetrates through the ice cover well. The optical properties of saline ice are influenced also by the salt content (Perovich 1998). The brine pockets absorb light and salt crystals scatter light, but the amount of salt crystals becomes significant only at very low temperatures. Especially in warm ice, chlorophyll in the brine pockets absorbs light strongly in the bands 430–440 nm and 660–690 nm.

3.5 Ice Mass Balance

The ice sheet consists of ice and snow layers. The mass per unit area, expressed in thickness of an equivalent water layer, is $h = (\rho_i h_i + \rho_s h_s)/\rho_w$. The density of ice can be taken as a constant ($\rho_i = 910$ kg m^{-3}) but snow density changes significantly in time and space. The mass of ice sheet changes at the lower boundary by freezing and melting, and at the upper boundary by precipitation (P) and sublimation (E). The mass balance is

$$\frac{dS_1}{dt} = \left(\frac{\rho_i}{\rho_w} \cdot \frac{dh_i}{dt} + f + P - E\right) A \tag{3.25}$$

where $S_1 = hA$ and f stands for the flooding of lake water onto the top of ice sheet. The growth rate of ice thickness, flooding and precipitation can be of the order of 1 cm per day, while submission is less than that. Precipitation is purely external factor, while sublimation depends on the difference between the absolute humidity in the lake surface and air (see Sect. 2.3). The mass budget is taken just as a vertical process, and the inflow and outflow of ice from the lake are ignored. In dry regions, the ice budget is simple since precipitation and slush are absent and $f = P = 0$ (Fig. 3.20).

The lake water storage can be expressed as $S = (h + H)A$, with $S_2 = HA$ as the liquid water part. Equation (3.25) represents the conservation of ice, and the conservation of liquid water is

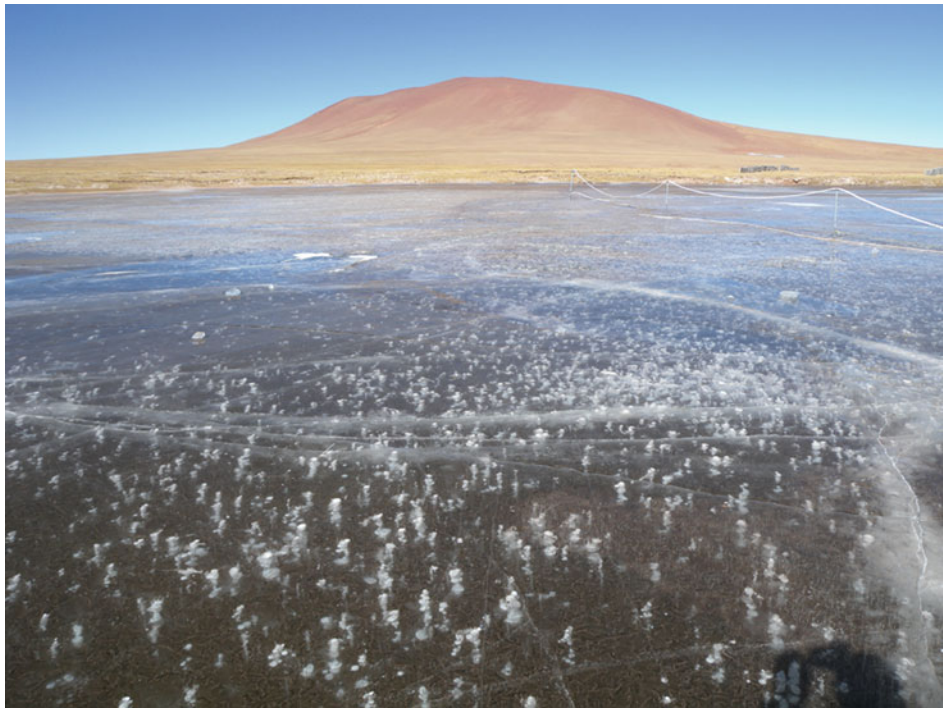

Fig. 3.20 Ice-covered lake in the Beiluhe Basin, Qinghai–Tibet Plateau at 4,000 m altitude. *Photograph* Zhijun Li

$$\frac{dS_2}{dt} = -\left(\frac{\rho_i}{\rho_w} \cdot \frac{dh_i}{dt} + f\right)A + I - O \tag{3.26}$$

An important dimensionless measure is the ratio of ice thickness to lake depth, $\upsilon = h/(H + h)$. Normally $\upsilon \ll 1$ and the ice cover has a minor influence on the lake volume, but as $\upsilon \rightarrow 1$, a significant portion of the water body freezes and at $\upsilon = 1$ the lake has frozen to the bottom.

In the system (3.25, 3.26) it is implicitly assumed that the whole lake is covered by ice. If this is not true, a quantity *ice coverage* needs to be introduced. Ice coverage, χ, is defined as the relative area of ice in the lake, $0 \leq \chi \leq 1$. Then $S_1 = \chi\, h\, A$, and the conservation laws are

$$\frac{dS_1}{dt} = \chi\left(\left.\frac{dh_i}{dt}\right|_{h_i > 0} + f + P - E\right)A + (1 - \chi)A\left.\frac{dh_i}{dt}\right|_{h_i = 0} \tag{3.27a}$$

$$\frac{dS_2}{dt} = \left[-\chi \left(\left. \frac{dh_i}{dt} \right|_{h_i > 0} + f \right) + (1 - \chi)(P - E) \right] A + I - O \tag{3.27b}$$

Budgets for impurities are constructed in similar fashion. Lake ice receives impurities from the atmosphere by precipitation and from the lake water by ice formation, and the water body receives impurities from ice, precipitation, and boundary fluxes.

Thermodynamics of Seasonal Lake Ice

4

The thermodynamics of the ice season in Lake Pääjärvi, southern Finland. Ice forms normally in December, snow accumulates on the ice and the ice thickness is at maximum on average half meter in March, and the ice melts in the latter half of April starting from the shore.

M. Leppäranta, *Freezing of Lakes and the Evolution of their Ice Cover*,
DOI 10.1007/978-3-642-29081-7_4

4.1 Heat Budget of Lakes

4.1.1 Total Heat Budget

The heat content of a lake consists of sensible and latent heat. It is convenient to take the reference level as the heat content of liquid water at the temperature of 0 °C. Thus the heat content per unit area can be expressed as $U = U_0 + E$, where U_0 is the heat content at the reference level and

$$E = \int_{h_B}^{h_b} \rho_w c_w T dz + \int_{h_b}^{h_0} \rho_i \left[-(1-v)L_f + c_i T \right] dz \tag{4.1}$$

Here h_0, h_b, and h_B are the altitudes of ice surface, ice bottom and lake bottom, ν is the liquid water content of ice, and the temperature is in degrees centigrade (Fig. 4.1). The integrals on the right-hand side represent the heat in the water body and ice sheet, respectively. Snow layer is considered as a part of the ice sheet. The evolution of the heat content is given by

$$\frac{dE}{dt} = Q_0 + \int_{h_B}^{h_0} \lambda Q_s dz - \kappa \left. \frac{\partial T}{\partial z} \right|_{z=h_B} + Q_A + Q_M \tag{4.2}$$

where Q_0 is the surface heat balance or the net surface heat flux, Q_s is solar radiation, κ is thermal conductivity, Q_A is the advective heat flux, and Q_M is the heat brought in by mass fluxes. The fluxes are defined positive into the lake. The surface heat balance is always important, while penetration of solar radiation has a key role in the melting season. Heat flux from the lake bottom is often significant in the early ice season. Solid precipitation decreases the heat content but liquid precipitation with temperature above 0 °C increases it. The distribution of heating between ice and water body depends on the internal properties of the system. At the ice–water interface, heat can be transferred from water to ice, and latent heat is released or taken when ice grows or melts, respectively.

The surface heat balance is written as

$$Q_0 = Q_{s0} + \varepsilon_0 Q_{La} + Q_{L0} + Q_H - \rho_w L_{ES} E + p(v,T)P \tag{4.3}$$

where Q_{s0} is the surface absorption of solar radiation, Q_{La} is the atmospheric thermal radiation, Q_{L0} is the thermal radiation from the surface, Q_H is the turbulent sensible heat flux, and p is the heat transfer function for precipitation. The last term depends on the liquid water content ν and temperature T, given as:

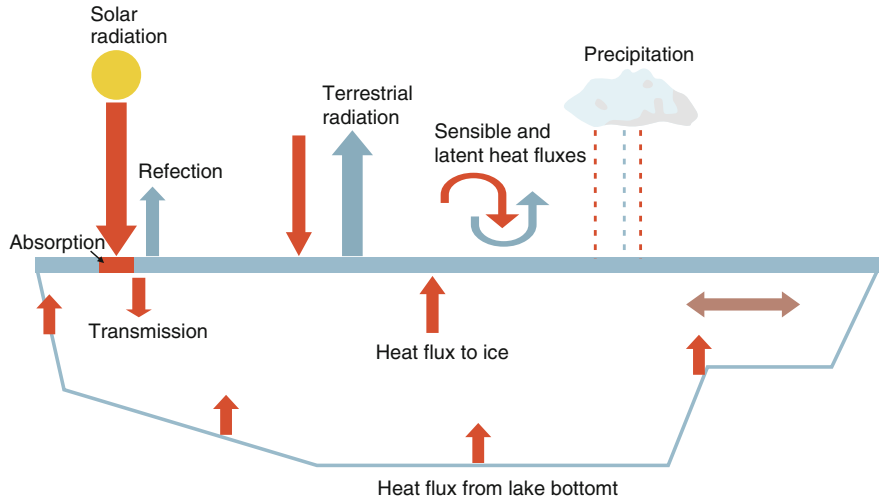

Fig. 4.1 Schematic picture of lake cross-section with the heat fluxes

$$p(v,T) = (1-v)\rho_i(-L_f + c_i(T-T_0)) + v\rho_w c_w(T-T_0) \tag{4.4}$$

To obtain the surface heat fluxes into lakes is a major issue. They can be measured directly, but for most situations they are parameterized from available weather and climate data. In the following sections these parameterizations are discussed in detail.

The radiation balance is the governing factor in the Earth's heat budget. The basis of the physics of radiation was introduced in Sect. 3.4 and serves here as the background for the heat transfer by solar and terrestrial radiation. Planck's law (Eq. 3.9) gives the radiation intensity as a function of temperature and wavelength. Solar radiation and terrestrial radiation are also called, respectively, as shortwave and long-wave radiation, because solar radiation comes mostly from the wavelength band 0.2–3 μm, while terrestrial radiation covers the band 5–15 μm. The turbulent transfer of sensible and latent heat is estimated using atmospheric boundary layer models of different degree of complexity.

Heat transfer from precipitation is a minor factor in general and contains sensible and latent heat. E.g., if P = 10 mm day^{-1} liquid water and T−T_0 = 5 °C, the sensible heat flux is ≈2 W m^{-2}. This is not much. But for the same rate of snowfall at –5 °C the heat flux is –30 W m^{-2}, which is comparable to the turbulent heat fluxes. Consequently, rainfall on snow or ice and snowfall on open water are important transient heat transfer mechanisms. Also snow cover is permeable to liquid water and therefore the latent heat of raindrops can be convected deeper. The time scale of precipitation events is of the order of 1 day. In the boreal zone the monthly average precipitation is around 50 mm covering a few events, and therefore in the climatological heat balance precipitation remains a small factor.

4.1.2 Solar Radiation

The level of solar radiation on the Earth's surface depends on time, latitude, clear sky atmospheric transparency T_{tr}, and cloudiness correction F (Eq. 3.11). At the lake surface, the incoming solar radiation is divided into three parts (Fig. 3.17): absorption at the surface Q_{s0}, transmission through the surface into the snow/ice/water medium Q_T, and outgoing back to atmosphere Q_r, $Q_s = Q_{s0} + Q_T + Q_r$. The outgoing radiation is expressed, using the albedo, as $Q_r = \alpha Q_s$ (see Eq. 3.17). The fraction of radiation transmitted through the surface is

$$\gamma = \frac{Q_T}{(1-\alpha)Q_s} \tag{4.5}$$

In thermodynamics, it means that the net solar radiation $(1 - \alpha)Q_s$ is decomposed to the fraction $1 - \gamma$, taken into the surface boundary conditions, and to the fraction γ taken as an internal source term. It has become custom to assume that light forms the transmitted part, while shorter and longer wavelengths are absorbed near the surface (within a few centimetres); then $\gamma \approx 0.45$–0.50. The fraction γ is fairly stable and not sensitive to cloudiness or solar zenith angle. Infrared radiation is strongly absorbed by pure ice or water, and ultraviolet is usually taken care by CDOM in lake waters (see Sect. 3.4). Ice and snow, as well as very clear lake water, however, are poor in CDOM and to add ultraviolet in the penetrating part the fraction γ should be higher by about 0.03.

Albedo is a critical factor in the heat budget. It varies widely (e.g., Arst et al. 2006), and its parameterization for modelling applications is an unsolved, tough question (see Sect. 3.4). Table 3.6 shows characteristic values of albedo over lake and lake ice surface. In open water conditions, albedo is low and stable, while in the ice season, scattering is strong that produces the high level of albedo. These variations are due to the surface type (snow or ice), presence of liquid water, and the thickness of snow and ice.

Especially in the melting season, the variability of albedo is large in space and time (Fig. 4.2). This is due to a positive feedback mechanism in the system. A disturbance in

Fig. 4.2 In the melting period, lake ice surface is patchy

albedo to decrease it leads to increased melting and further decrease of the albedo, and so on. Since the conduction of heat within the ice sheet is slow, the positive feedback system produces a patchy lake ice cover as can be well observed. This mechanism also increases the irradiance beneath the lake ice and can produce patchiness there as well.

Dry, fine-grained snow has albedo as high as 0.9, and for wet snow it is typically around 0.5 (see Sect. 3.4.3). Snow-ice has higher albedo than congelation ice due to scattering. Bare, dry ice has albedo of 0.5, and with increasing surface wetness and formation of melt ponds, the albedo decreases to 0.2–0.3. Thin (10 cm) bare ice has an albedo of 0.2–0.3. According to Perovich and Polashenski (2012), the albedo of Arctic Ocean seasonal sea ice is 0.85 in winter (dry snow-covered ice), and it decreases down to 0.2 in August. Most of the time the ponded ice cover has albedo within 0.4–0.6.

Albedo and the fraction γ are apparent optical properties, i.e., in addition to the properties of the medium, they depend on the directional distribution of the incoming radiation and, consequently, on the solar altitude and cloudiness. They also depend on the spectral distribution of solar radiation. On the surface of the Earth, the shape of solar radiation spectrum can be taken fixed (see Sect. 3.4) but inside snow, ice and water the spectral distribution changes. Snow and ice cover act as a diffusive filter for the solar radiation transfer but short and long wavelengths attenuate faster and the spectral band of radiation becomes narrower with depth.

To determine the distribution of solar power with depth, the attenuation should be determined from the spectral distribution since this influences the penetration depth. Attenuation of irradiance is modelled with a linear model shown by Eq. (3.18). The total power is obtained by integration:

$$Q_s(z) = \int_0^\infty (1-\alpha)E(0^-,\lambda)\cdot\exp\left[-\int_0^z K(z',\lambda)dz'\right]d\lambda \tag{4.6}$$

In practice, integration needs to take a few spectral bands only when using Eq. (4.6) for lakes. With the spectral approach also the division of solar radiation into the surface absorption and transmission can be properly treated and with desirable vertical resolution.

The mean light attenuation coefficient is $\kappa \sim 0.1$–$5\ \mathrm{m}^{-1}$ for lake water, $\kappa \sim 1\ \mathrm{m}^{-1}$ for congelation ice, $\kappa \sim 10\ \mathrm{m}^{-1}$ for snow and snow-ice. Thus snow accumulation has a major role in the light conditions in ice-covered lakes (see Sect. 3.4).

4.1.3 Terrestrial Radiation

Lake surface—whether liquid water, ice or snow—radiates as a grey body with emissivity very close to one ($0.96 < \varepsilon_0 < 0.98$):

$$Q_{L0} = \varepsilon_0 \sigma T_0^4 \tag{4.7a}$$

For the surface temperature between –30 and 0 °C, this radiation ranges between –200 and –300 W m^{-2}. The terrestrial radiation from the atmosphere is much more complicated. It comes from different altitudes, each altitude having its own temperature and emissivity, and usually such detailed information is not available. For standard weather data, a grey body analogical model is used with air temperature (at 2-m level) as the reference temperature and effective emissivity depending on the humidity and cloudiness N:

$$Q_{La} = \varepsilon_a(e, N)\sigma T_a^4 \tag{4.7b}$$

where e is the water vapour pressure (at 2-m height). The effective emissivity of atmosphere depends primarily on the water vapour pressure and cloudiness and its formulations vary widely. The air humidity also represents the altitude of 2 m. A common empirical approach has been to give the emissivity as the product of clear sky emissivity and cloud cover influence as $\varepsilon_a = \varepsilon_{\alpha 1}(e)\ \varepsilon_{\alpha 2}(N)$. Brunt (1932) introduced a widely used form for the clear sky emissivity:

$$\varepsilon_{a1} = A + B\sqrt{e} \tag{4.8a}$$

where A and B are the Brunt formula parameters, with typical values of A = 0.68 and B = 0.036 $mbar^{-½}$. The parameter A represents the dry atmosphere emissivity, while the square root term reflects the vertical distribution of water vapour. For the cloudiness factor there are several approaches. A common form is:

$$\varepsilon_{a2}(N) = 1 + CN^2 \tag{4.8b}$$

with a normal value of C = 0.18. As in the case of solar radiation, the influence of cloudiness is the most uncertain factor in the estimation of the atmospheric thermal radiation. The minimum atmospheric emissivity is A = 0.68, and at 0 °C the maximum is $(A + B \cdot (6.11\ mbar^{½}) \cdot (1 + C) \approx 0.91$; for the air temperature range from –30 to 0 °C the atmospheric thermal radiation is within 140–280 W m^{-2}. If the air temperature and surface temperature are equal, the terrestrial radiation loss is 20–90 W m^{-2} depending on the humidity and cloudiness.

Example 4.1. Solar radiation decreases with cloudiness (Eq. 3.13b) while net terrestrial radiation increases. Then we have a balance at

$$1 - \varepsilon_{a1}\left(1 + CN^2\right) = \frac{(1-\alpha)\cos(Z) \cdot Tr \cdot Q_{sc}}{\varepsilon_0 \sigma T_a^4}(1 - c_N \cdot N)$$

This equation has a solution for N, such that $0 \le N \le 1$, when the ratio on the right-hand side is about 0.35–0.45. Such case is feasible, and an equilibrium cloudiness exists but this equilibrium is not stable. A disturbance would not return, and if the disturbance is large enough no equilibrium can be reached.

4.1.4 Turbulent Heat Exchange with the Atmosphere

The atmospheric boundary layer is in turbulent state, and the exchange of heat between lakes and atmosphere can be modelled using the turbulent boundary layer theory. The first-order models are based on the analogy of laminar and turbulent flows and can be expressed as bulk exchange laws. Heat is transferred as sensible and latent heat, and together with the momentum transfer the bulk formulae read (see Sect. 2.2.4):

$$\tau_a = \rho_a C_{az} U_{az} U_{az} = \rho_a u_*^2 \tag{4.9a}$$

$$Q_c = \rho_a c_p C_{Hz} (T_{az} - T_0) U_{az} \tag{4.9b}$$

$$Q_e = \rho_a L_{ES} C_{ez} (q_{az} - q_0) U_{az} \tag{4.9c}$$

where u_* is the friction velocity, the subscript ES refers to evaporation or sublimation depending on the surface, and the lower index z has been added to indicate where the quantities depend on the altitude. The transfer coefficients C_{az}, C_{Hz}, C_{ez} in general depend on the surface roughness and stratification of the atmospheric surface layer.

In exact terms, the turbulent fluxes onto the surface are based on the cross-covariances of the given quantity with the vertical velocity. The direct formulae for the momentum, sensible heat and latent heat fluxes are, respectively (e.g., Tennekes and Lumley 1972):

$$\tau_a = -\rho_a \langle u' w' \rangle \tag{4.10a}$$

$$Q_c = -\rho_a c_p \langle \theta' w' \rangle \tag{4.10b}$$

$$Q_e = -\rho_a L_{ES} \langle q' w' \rangle \tag{4.10c}$$

where the quantities marked with ‘ are fluctuations and the brackets <·> stand for time averaging, e.g. $\theta = \langle \theta \rangle + \theta', \langle \theta' \rangle = 0, \langle \theta'(t)\theta'(s) \rangle = 0\,(t \neq s)$, and the x-axis has been aligned with the direction of the mean wind. These fluxes can be measured directly with eddy covariance measurement techniques or they can be estimated from the mean boundary-layer characteristics with methods of different degrees of complexity.

In the limit $U_{\mathrm{a}} \rightarrow 0$ this system gives zero fluxes. In such conditions, however, turbulent fluxes can arise from buoyant (free) convection. In the free convection limit, the sensible heat flux is (Louis 1979):

$$\langle w'\theta' \rangle_0 = 0.26 \sqrt{\frac{g z_0}{\theta_0}} \cdot (\theta - \theta_0)^{3/2} \tag{4.11}$$

Turbulent exchange of a property Q is proportional to its vertical gradient times the eddy diffusivity K, $F_{\mathrm{Q}} \sim K \partial Q / \partial z$ (see Tennekes and Lumley 1970); here the vertical

coordinate is positive upward. The coefficient K characterizes the turbulent flow, scaling as $K \sim u_* \ell$ where ℓ and u_* are the characteristic turbulent length and fluctuation scales. In the surface layer the fluxes are assumed constant. Therefore the flow can be simply aligned along the x-axis, and according to Prandtl's *mixing length hypothesis,*[1] the size of turbulent eddies scales with the distance from the boundary, $\ell \propto z$.

Neutral stratification provides the simplest case where the bulk transfer coefficients are fixed. Then the transfer coefficients and roughness lengths are related by

$$\sqrt{C_{az}} \log\left(\frac{z}{z_0}\right) = \sqrt{C_{Hz}} \log\left(\frac{z}{z_T}\right) = \sqrt{C_{ez}} \log\left(\frac{z}{z_q}\right) = \kappa \tag{4.12}$$

where $\kappa = 0.4$ is von Kármán constant, and the roughness lengths are z_0 for momentum, z_T for temperature, and z_q for humidity. For snow, ice and water surfaces typical values are C_D, C_H, $C_E \approx 1.2 \times 10^{-3}$ ($z = 10$ m), corresponding to the aerodynamic roughness length of 0.097 mm. These lengths result from the surface boundary conditions and they are related to the geometrical surface roughness but are not equivalent, and the aerodynamic roughness parameters in general also depend on the flow characteristics.

The temperature difference between lake surface and air may have any sign, and the sensible heat flux is usually within about ±50 W m^{-2}. The latent heat exchange takes place as evaporation and sublimation (heat loss) or condensation and deposition (heat gain) at the surface, and therefore it is also a part of the water budget (see Sects. 2.3.3 and 3.5). The latent heat flux is mostly negative and in magnitude close to the sensible heat flux; in general, in cold season it is weaker but it is stronger in warm season. Evaporation of 1 mm water or sublimation of 1 mm ice in 1 day corresponds to latent heat loss, respectively, by 28.8 or 30.0 W m^{-2}.

In the general case, when the stability of the stratification of the atmospheric surface layer is accounted for, the transfer coefficients are interdependent and the transfer equations must be simultaneously solved. The stability of the stratification can be expressed by the (gradient) Richardson number or the bulk Richardson number, respectively, as

$$Ri = \frac{g}{\theta_0} \cdot \frac{\partial\theta/\partial z}{(\partial u/\partial z)^2} \tag{4.13a}$$

$$Ri_B = \frac{g}{\theta_0} \cdot \frac{z(\theta_v - \theta_{v0})}{(u - u_0)^2} \tag{4.13b}$$

[1] According to Prandtl's mixing length hypothesis, turbulent transfer processes are described by a characteristic length-scale over which the turbulent eddies mix fluid properties.

where θ is potential temperature, θ_0 is a reference temperature, and θ_v is virtual temperature.[2] The stratification is stable (unstable) for $Ri > 0$ ($Ri < 0$). Richardson number provides the ratio between buoyancy and shear. The general problem is non-linear and cannot be solved in explicit form. However, approximate parameterized explicit formulations are available and they provide an insight of the role of stratification.

Curry and Webster (1999) used the bulk Richardson number parameterization for an approximate explicit solution. They assumed that $C_H = C_E$ and $z_0 = z_T$ ($\sim$0.1–1 mm), that implies $C_D = C_H = C_E$, and presented the forms

$$C_D = C_H = C_E = \left[\frac{\kappa}{\log\left(\frac{z}{z_0}\right)}\right] f(Ri_B) \tag{4.14a}$$

$$f(Ri_B) = \frac{1}{1 + 15\sqrt{1 + 5Ri_B}},\ Ri_B > 0 \tag{4.14b}$$

$$f(Ri_B) = 1 - \frac{15Ri_B}{1 + 75\left[\frac{\kappa}{\log\left(\frac{z}{z_0}\right)}\right]^2 \sqrt{1 + \frac{z}{z_0}|Ri_B|}},\ Ri_B < 0 \tag{4.14c}$$

where f is the stability parameter (Louis 1979). The exchange coefficients change quite fast in near-neutral conditions (Fig. 4.3). Taking z = 10 m and z_0 = 1 mm, their limiting values for $Ri \rightarrow 0$ are 0.12×10^{-3} from the right and 1.89×10^{-3} from the left. The neutral ($Ri = 0$) reference would be 1.00×10^{-3} as the average. Furthermore, $C_H(Ri_B = 0.1) = 0.097 \times 10^{-3}$ and $C_H(Ri_B = -0.1) = 2.61 \times 10^{-3}$.

Advanced methods for the vertical fluxes at the surface are based on the Monin–-Obukhov similarity theory (Tennekes and Lumley 1972; Kagan 1995). In addition to the Prandtl mixing length, in a stratified boundary-layer there is another length scale, the buoyant length scale or the Monin–Obukhov length, which is defined as

$$L = -\frac{\Theta_0 u_*^3}{\kappa g \langle w'\theta' \rangle} = -\frac{\rho_a c_p \Theta_0 u_*^3}{\kappa g Q_c} \tag{4.15}$$

where Θ_0 is the reference temperature. Monin–Obukhov length can be understood as the vertical length scale to where the role of the stratification is not significant. Since the mechanical mixing length is proportional to height z, the ratio z/L becomes a natural dimensionless length in a stratified boundary layer.

[2] An adjustment applied to the real air temperature to account for a reduction in air density due to the presence of water vapor, $\theta_v = \theta(1 + 0.6078q)$.

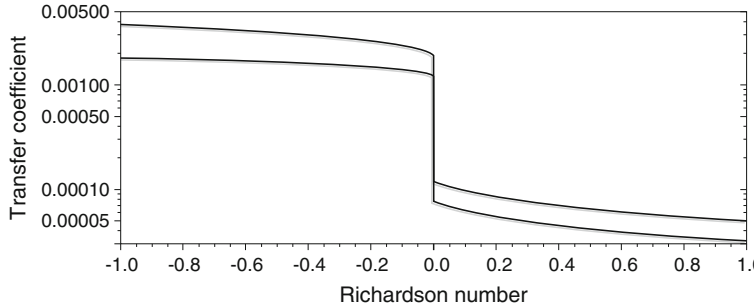

Fig. 4.3 The dependence of the transfer coefficient C_H on the stability of stratification. Surface roughness is 0.1 mm (lower curve) and 1 mm (upper curve), and the reference level is 10 m

In the general, stratified conditions, the distribution of velocity, potential temperature and specific humidity in the boundary layer can be expressed as functions of their characteristic scales, surface roughness, and the Monin–Obukhov length. The differential and integrated forms are:

$$\frac{\partial u}{\partial z} = \frac{u_*}{\kappa z}\phi_m\left(\frac{z}{L}\right) \quad u(z) = \frac{u_*}{\kappa}\left[\log\left(\frac{z}{z_0}\right) - \Psi_m\left(\frac{z}{L}\right)\right] \tag{4.16a}$$

$$\frac{\partial \theta}{\partial z} = \frac{\theta_*}{\kappa z}\phi_h\left(\frac{z}{L}\right) \quad \theta(z) = \theta_s + \frac{\theta_*}{\kappa}\left[\log\left(\frac{z}{T}\right) - \Psi_h\left(\frac{z}{L}\right)\right] \tag{4.16b}$$

$$\frac{\partial q}{\partial z} = \frac{q_*}{\kappa z}\phi_h\left(\frac{z}{L}\right) \quad q(z) = q_s + \frac{q_*}{\kappa}\left[\log\left(\frac{z}{z_q}\right) - \Psi_h\left(\frac{z}{L}\right)\right] \tag{4.16c}$$

where u_*, θ_* and q_* are the characteristic friction layer velocity, temperature and humidity scales, and ϕ_m, ϕ_h and Ψ_m, Ψ_h are the so-called universal functions of the boundary layer. It is quite common to use the same universal functions for temperature and humidity (see Andreas 1998). By direct integration, the integral and differential forms are related by

$$\Psi_m(\zeta) = \int_0^\zeta \frac{1-\phi_m(\zeta')}{\zeta'}d\zeta', \quad \Psi_h(\zeta) = \int_0^\zeta \frac{1-\phi_h(\zeta')}{\zeta'}d\zeta' \tag{4.17}$$

where $\zeta = z/L$. Common forms for the universal functions are (e.g., Vihma 1995; Andreas et al. 1998):

$$\text{Unstable } (\zeta<0): \quad \phi_m(\zeta) = \sqrt[4]{\frac{1}{1-16\zeta}} \text{ and } \phi_h(\zeta) = \sqrt{\frac{1}{1-16\zeta}} \tag{4.18a}$$

$$\text{Neutral } (\zeta = 0): \quad \phi_m(0) = \phi_h(0) = 1 \tag{4.18b}$$

$$\text{Stable } (\zeta > 0): \quad \phi_m(0) = \phi_h(0) = 1 + \gamma_s\zeta, \gamma_s = \text{constant } \sim 5 \tag{4.18c}$$

The unstable case is from Paulson (1970) and the stable case is from Webb (1970). In neutral stratification the potential temperature is constant, and, consequently, $L = \infty$. The universal functions are then ϕ_m, $\phi_h \equiv 1$ and Ψ_m, $\Psi_h \equiv 0$. The turbulent transfer coefficients are obtained as (e.g., Garrat 1992):

$$C_a = \frac{\kappa^2}{[\log(z/z_0) - \Psi_m(z/L)]^2} \tag{4.19a}$$

$$C_h = \frac{\kappa^2}{[\log(z/z_0) - \Psi_m(z/L)] \cdot [\log(z/z_T) - \Psi_m(z/L)]} \tag{4.19b}$$

$$C_e = \frac{\kappa^2}{[\log(z/z_0) - \Psi_m(z/L)] \cdot [\log(z/z_q) - \Psi_m(z/L)]} \tag{4.19c}$$

In the general case, the Monin–Obukhov boundary layer equations need to be simultaneously solved. The transfer coefficients depend on the Monin–Obukhov length, but in turn the Monin–Obukhov length depends on the transfer coefficients. We have a non-linear system of equations (Eqs. 4.9a–c, 4.15, 4.19a–c), which can be solved by iterative methods. Newton's iteration method would work for this but other formulations also exist (e.g., Launiainen and Vihma 1990).

4.1.5 Linearized Heat Flux

In analytic modelling and some other applications, a heat flux formula linear in the surface temperature is required. Such form can be expressed as

$$Q_0 + Q_T = k_o + k_1(T_a - T_o) \tag{4.20}$$

where the coefficients k_o and k_1 do not depend explicitly on T_o. Equation (4.20) contains the total solar and atmospheric heat flux into the lake, with k_0 dominated by the radiation balance and k_1 by the turbulent exchange. The formula has a simple interpretation: for $k_o \rightarrow 0$ the surface layer becomes a low pass filter for the atmospheric temperature, and for $k_1 \rightarrow 0$ the surface temperature becomes decoupled from the air temperature. The coefficients k_0 and k_1 have annual cycles (Table 4.1), especially the former, and in the first approximation we can take k_1 as a constant and $k_0 = k_0(t)$. In the equilibrium of $Q_0 + Q_T = 0$ we have $T_o = T_a + k_o/k_1$.

The linear approximation is obtained as follows. The solar radiation, the incoming terrestrial radiation from the atmosphere, and the heat flux from precipitation are purely external factors and are absorbed in k_o, while the sensible heat flux is as such proportional to $T_a - T_o$ and thus the proportionality coefficient simply goes to k_1. Outgoing terrestrial

Table 4.1 Linear heat flux coefficients in southern Finland. The contributions of solar radiation (Srad), terrestrial radiation (Trad), sensible heat flux (SH) and latent heat flux (LH) are shown separately, total refers the value of the coefficient

Month	k_0 (W m^{-2})				k_1 (W m^{-2} °C^{-1})			
	Srad	Trad	LH	Total	Trad	SH	LH	Total
September	90	–45	–16	29	5.0	5.2	10.5	20.7
October	38	–45	–9	–16	4.7	5.5	8.2	18.4
November	12	–43	–5	–36	4.5	5.8	6.2	16.5
December	3	–45	–4	–46	4.3	5.8	4.7	14.8
January	2	–46	–5	–49	4.2	5.6	4.0	13.8
February	8	–48	–5	–45	4.2	5.5	3.7	13.4
March	30	–56	–7	–33	4.4	5.5	5.0	14.9
April	76	–62	–10	4	4.7	5.5	7.7	17.9
May	193	–57	–36	100	5.0	5.5	11.0	21.5
June	209	–55	–40	114	5.2	5.2	13.3	23.7
July	203	–48	–41	114	5.4	4.9	14.6	24.9
August	151	–45	–29	77	5.3	4.9	13.3	23.5

radiation and latent heat flux contribute to both parameters k_o and k_1. The former is split into two parts[3] by $T_o^4 \approx T_a^4 - 4T_a^3(T_a - T_o)$. Then the net terrestrial radiation is

$$Q_{La} + Q_{Lo} \approx \varepsilon_0\sigma(\varepsilon_a T_a^4 - T_0^4) = -\varepsilon_0\sigma[(1-\varepsilon_a)T_a^4 + 4T_a^3(T_a - T_o)] \tag{4.21a}$$

where the truncated binomial formula gives accuracy of about 1 % when $|T_a - T_o| < 10$ °C and $T_a \sim 0$ °C. The latent heat exchange is split using the Clausius-Clapeyron equation (e.g., Gill 1982) for the saturation water vapour pressure e_s. Assuming that humidity is at the saturation level at the surface, $e_o = e_s(T_0)$, and writing $e_a = Re_s$, where R is the relative humidity, the latent heat flux can be expressed as

$$Q_e = -\rho_a L_E C_E \frac{0.622 e_s(T_a)}{p_a}\left[(1-R) - \frac{L_E}{R_v T_a^2}(T_a - T_o)\right]U_a \tag{4.21b}$$

where R_v is the gas constant of dry air. Finally, combining all together, the coefficients k_o and k_1 become

$$\begin{aligned} k_0 &= (1-\alpha)Q_s - \varepsilon_0(1-\varepsilon_a)\sigma T_a^4 - \rho_a L_{ES} C_E \frac{0.622 e_s(T_a)}{p_a}\cdot(1-R)U_a \\ k_1 &= 4\varepsilon_0\sigma T_a^3 + \rho_a c_p C_H U_a + \rho_a L_{ES} C_E \frac{0.622 e_s(T_a)}{p_a}\cdot\frac{L_{ES}}{R_v T_a^2}U_a \end{aligned} \tag{4.22}$$

[3] Write $T_o = [T_a + (T_o - T_a)]^4$, use the binomial formula and take the two leading terms.

The temperatures are taken in Kelvin-degrees in the calculations. These expressions look somewhat complicated but the resulting climatological values are rather smooth, with seasonal variation coming from the solar radiation and the latent heat flux (Table 4.1). In winter $k_0 \approx -45$ W m^{-2} and $k_1 \approx 15$ W m^{-2} °C^{-1}, while in the summer they are $k_0 \approx 100$ W m^{-2} and $k_1 \approx 25$ W m^{-2} °C^{-1}.

4.2 Ice Growth and Melting

4.2.1 Thermodynamic Principles

Whether the surface is snow, ice or liquid water makes a major difference to the albedo, and in the latent heat transfer sublimation (snow or ice) needs more energy than evaporation (water). Otherwise the same parameters can be used. But in the cold season, the thicker the ice the closer the surface temperature becomes to air temperature that reduces turbulent heat transfer.

When an ice cover forms and grows, the stratigraphy may contain three different types of layers: congelation ice, frazil ice, and superimposed ice (Fig. 4.4). On top of the ice sheet, there is often a snow layer. Each layer grows by its own specific mechanism, and the latent heat released needs to be conducted to the atmosphere, since the water body is warmer than the ice. The latent heat of freezing is large (333.5 kJ kg^{-1}), and therefore ice growth is slow process (order of 1–3 cm day^{-1}). The heat flux of 35 W m^{-2} is released when ice grows by 1 cm in 24 h. Ice sheet is primarily described by its thickness, which is defined as the distance between the upper and lower boundaries.

In the melting period, ice sheet is nearly isothermal. There is not much conduction of heat, and melting takes place at the top and bottom boundaries and by solar radiation also in the interior. Heat corresponding to the latent heat of freezing must be provided to melt the ice. Different layers melt by the same mechanisms but there are quantitative differences depending on the albedo and light attenuation coefficient. Therefore ice growth is first treated separately of different ice types, and thereafter melting is discussed together for all ice types.

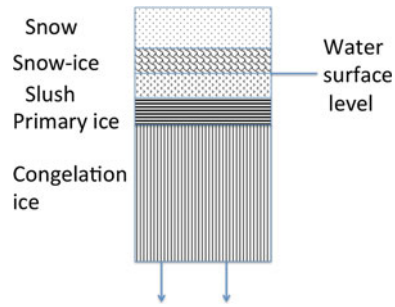

Fig. 4.4 A schematic picture of a vertical cross-section of a lake ice sheet

Internal melting is reflected in the porosity of the ice, defined as the relative volume of pores in the ice.

$$v = 1 - \frac{V_i}{V} \tag{4.23}$$

where V_i is the volume of ice in a volume element V. In growing ice the porosity equals the gas content and is very small, but in the melting season it can reach the limiting strength needed to keep the ice sheet together.

Lake ice may become thinner also by sublimation. In a dry environment, the ice is often snow-free, and if strong winds occur frequently, sublimation can become significant, to an order of 10 cm during one winter. There are such dry areas, e.g. northern China, Tibet and dry valleys in Antarctica, where snow cover is absent all winter (e.g., Priscu 1998; Huang et al. 2012). Then sublimation needs to be included into the ice thickness evolution models. In 24 h, heat loss by 30 W m^{-2} can sublimate a 1-mm layer of ice. Sublimation of snow also takes place but that is normally hidden behind snowdrift and the low accuracy of snow thickness data. Deposition of water vapour on ice and snow is a small and transient feature but appears as beautiful formations such as frost flowers on lake ice.

The surface heat budget of ice cover of Lake Pääjärvi, Finland was examined based on field data by Wang et al. (2005). The heat fluxes were derived from high-resolution measurements by Automatic Ice Station *Lotus* (Fig. 2.9). The radiation balance (solar plus terrestrial radiation) dominates the total heat flux (Fig. 4.5). In January the total heat loss was 50–70 W m^{-2} due to the strong outgoing terrestrial radiation, and at about mid-March the daytime solar radiation was high enough to turn the balance into a gain reaching 200 W m^{-2} at daily maximum. The level of the turbulent fluxes was high only for short periods and typically ranged between 20 and 30 W m^{-2} in January and from –10 to 10 W m^{-2} in March. In another study in the same lake, Jakkila et al. (2009) estimated the monthly average heat budgets. The surface balance was always negative, and in March internal melting of the ice was significant and heat flux from the water body also increased due to penetration of solar radiation through the ice (Table 4.2). The residual of the heat budget is due to errors in the estimation of the heat budget terms.

Thermodynamics of saline (or brackish) ice differs qualitatively from the fresh water ice case. The thermal properties change significantly as a function of temperature and salinity (Schwerdtfeger 1963; Yen 1981). Along with temperature evolution, the brine volume changes with associated phase changes at brine pocket boundaries. This brings an interesting viewpoint: saline ice has no definite melting point but always there is melting involved when ice warms in order to dilute the brine and vice versa (Assur 1958; Schwerdtfeger 1963). Thus brine pocket dynamics has a strong influence on the heat connected to temperature changes of saline ice, especially when the temperature is high.[4]

[4] High temperature refers here to vicinity of the freezing point of meltwater of the saline ice; in sea ice, with the freezing point of –1.8 °C, high temperatures are above –5 °C.

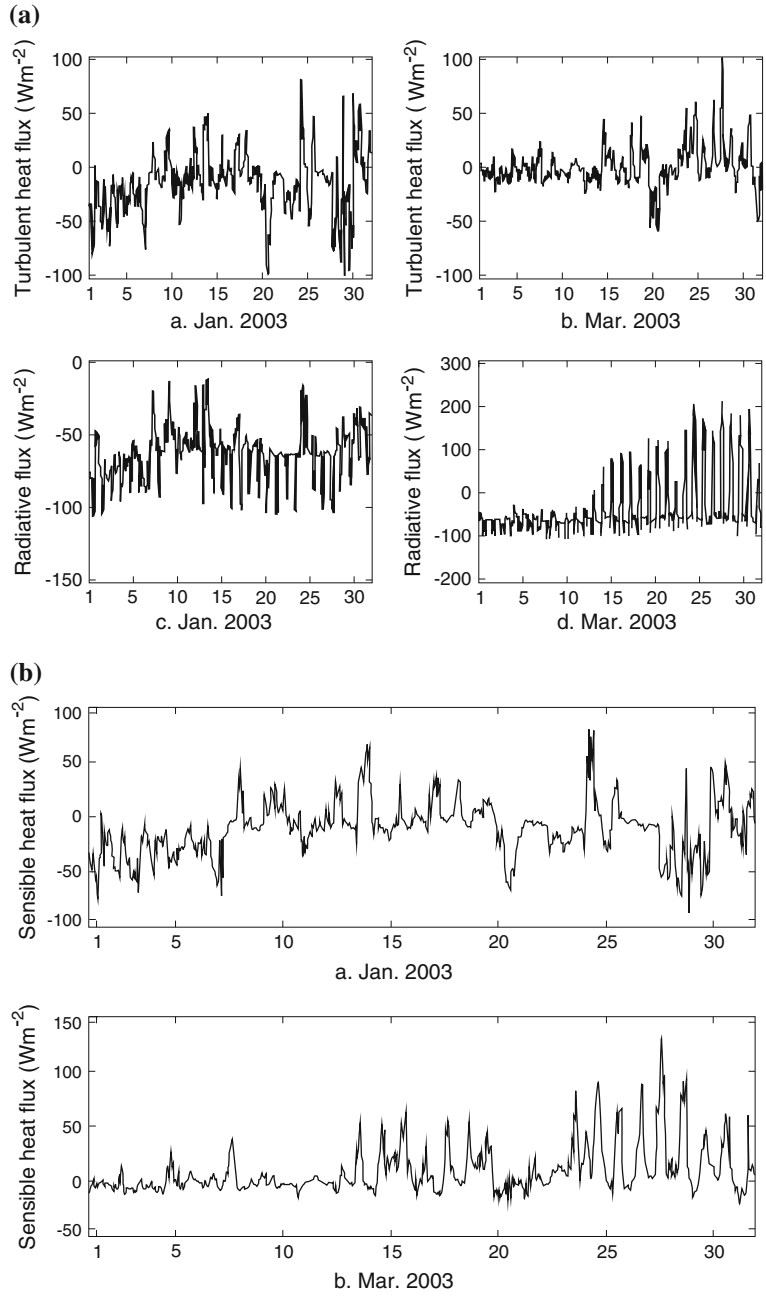

Fig. 4.5 Heat budget in Lake Pääjärvi, southern Finland in January and March 2003 (Wang et al. 2005). From *top down* total turbulent (sensible + latent) heat flux and radiation balance, sensible heat flux, and latent heat flux. The lake is frozen through December–April

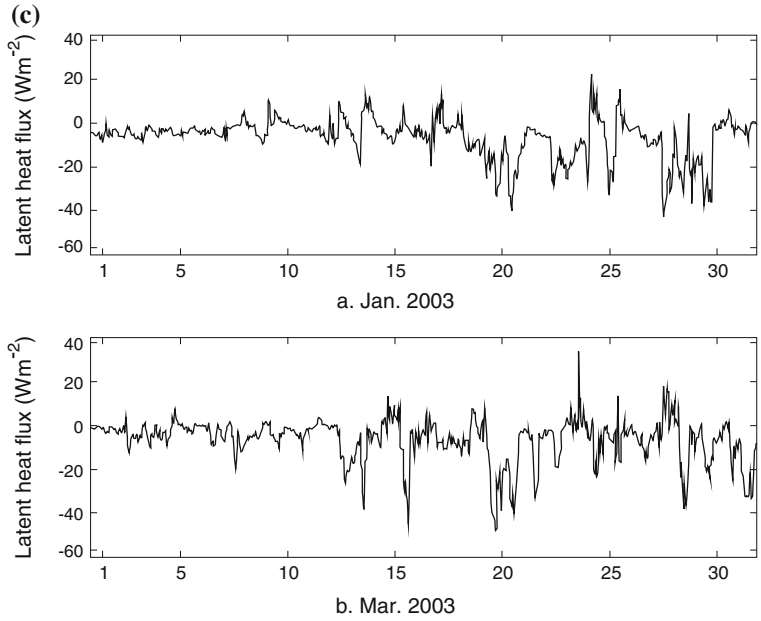

Fig. 4.5 (continued)

In addition, the thermal conductivity of brine is a little less than that of ice, and therefore the thermal conductivity of saline ice is slightly smaller than that of fresh water ice.

4.2.2 Congelation Ice Growth

In the growth of congelation ice, the latent heat of freezing released at the bottom of the ice sheet needs to be conducted through the ice to the atmosphere. This conduction is predominantly vertical. The growth of the ice sheet continues as long as the conductive heat flux through the ice is greater than the heat flux from the water body to the ice. The thicker the ice, the greater is the conduction distance and the slower is the subsequent rate of ice growth. We may say that congelation ice growth is 'self-isolative' (Stefan 1891; Barnes 1928).

The temperature of ice interior changes by conduction and solar heating. The equation of vertical heat transfer is written as:

$$\frac{\partial}{\partial t}(\rho c T) = \frac{\partial}{\partial z}\left(k\frac{\partial T}{\partial z} - Q_T e^{-Kz}\right), T \leq T_f \tag{4.24}$$

where c is the specific heat of ice, and k is the thermal conductivity of ice, and the vertical co-ordinate z is positive downward with zero at the ice surface. The thermal properties of

Table 4.2 The monthly mean heat fluxes (W m^{-2}) in Lake Pääjärvi in ice season 2003–2004 (19 December 2003–28 April 2004); only ice days have been included in the budget

Winter 2003–2004	December	January	February	March	April
Surface heat balance (S)					
Net solar radiation	0	0	3	10	38
Net terrestrial radiation	–19	–21	–25	–35	–47
Sensible heat flux	–10	–4	–4	–1	2
Latent heat flux	–8	–3	–4	–3	–2
Total	–37	–28	–30	–28	–8
Inside the ice sheet (I)					
Net solar radiation	0	1	3	11	39
Ice bottom (B)					
Heat flux from the water	5	5	5	5	12
Freezing	30	17	19	6	0
Melting	0	0	0	0	–41
Total	35	22	24	11	–29
Residual (error)					
Total (S + I + B)	–2	–5	–3	–6	2
Radiative heating of water	1	0	0	1	40

Budget residual is the sum of the heat fluxes from above and below and would be zero for a correct flux estimates (Jakkila et al. 2009)

freshwater ice depend on the temperature and gas content, but ρ = 910 kg m^{-3}, c = 2.1 kJ kg^{-1} °C^{-1} and k = 2.1 W m^{-1} °C^{-1} serve as convenient reference values. If they are constant, we obtain the heat diffusion equation with constant diffusion coefficient $D = k/(\rho c) = 1.1 \times 10^{-6}$ m^2 s^{-1} = 0.095 m^2 day^{-1}. This means that in one day the length scale of diffusion is $\sqrt{0.095}$ m $\approx$ 31 cm, e.g. one-day temperature cycle can penetrate 31 cm into the ice. In the yearly time-scale, the diffusion length scale becomes 5.9 m. The temperature must be below the freezing point; at there further heating leads to melting of ice.

The boundary conditions are determined by the heat fluxes into the system. These fluxes produce phase changes, i.e. growth and melting of ice, and consequently the boundaries of the ice sheet move:

$$z = 0 : T < T_f : \frac{dh}{dt} = -E, k\frac{\partial T}{\partial z} = -Q_0 \tag{4.25a}$$

$$T = T_f : \frac{dh}{dt} = -\frac{1}{\rho L_f}\mathrm{Max}(Q_0, 0) - E, k\frac{\partial T}{\partial z} = -\mathrm{Min}(Q_0, 0) \tag{4.25b}$$

$$z = h : \; T = T_f; \; \rho L_f \frac{dh}{dt} + Q_w = -k\frac{\partial T}{\partial z}. \tag{4.25c}$$

The upper boundary may lose ice due to melting ($Q_0 > 0$) or sublimation (E), while at the lower boundary both freezing and melting take place. Congelation ice growth is primarily a vertical process and a small-scale phenomenon, determined by the conduction of heat through the ice. In the full melting stage, the temperature of lake ice approaches the melting point and heat conduction. Then the boundary conditions (4.25a, b, c) give the melting at the top and bottom surfaces, while internal melting follows from Eq. (4.24). In the limiting case, at the absence of conduction, ice temperature equals the melting point, solar heating goes to latent heat of melting increasing the porosity:

$$\frac{\partial v}{\partial t} = \frac{Q_T}{\rho L} K e^{-Kz}. \tag{4.26}$$

However, due to the cool skin phenomenon, the surface temperature is mostly below the melting point, and a fraction of solar radiation absorbed near the surface is conducted back to the atmosphere. If $Q_T \sim 10$ W m^{-2} and $K \sim 1$ m^{-1}, we have $\partial v/\partial t \sim 0.28$ % day^{-1}.

Snow influences ice growth and decay due to isolation effects and snow-ice formation. The evolution of snow properties in snow metamorphic processes causes further complications. Next, the isolation is considered. For the mass and heat balance, a system of equations corresponding to the ice layer (Eqs. 4.24, 4.25a, b, c) can be constructed. The elevation of the snow surface ($z = -h_s$) changes due to precipitation, sublimation, melting and compression of snow, while at the snow-ice interface the continuity of heat flow is required. The heat conduction equation is formally the same, but the boundary conditions are for the snow layer:

$$z = -h_s : T < 0\,^\circ\mathrm{C} : \frac{dh_s}{dt} = \gamma h_s + \frac{\rho_s}{\rho_w}(P - E), k_s \frac{\partial T}{\partial z} = -Q_0 \tag{4.27a}$$

$$T = 0\,^\circ\mathrm{C} : \frac{dh_s}{dt} = \gamma h_s + \frac{\rho_s}{\rho_w}(P - E) - \frac{\mathrm{Max}(Q_0, 0)}{\rho_s L_f} \tag{4.27b}$$

$$\begin{aligned} k_s \frac{\partial T}{\partial z} &= -\mathrm{Min}(Q_0, 0) \\ z = 0 : \; k_s \left.\frac{\partial T}{\partial z}\right|_{z=0^-} &= k \left.\frac{\partial T}{\partial z}\right|_{z=0^+} \end{aligned} \tag{4.27c}$$

where γ is the snow compression coefficient, ρ_s is snow density, and k_s is the thermal conductivity of snow. Snow metamorphosis leads first of all to packing, i.e. decrease of thickness and increase of density. This has a major influence on the thermal conduction, since $k_s \propto \rho_s^2$ (see Sect. 3.2.3). Consequently, we need an equation for the snow density in ice models (Yen 1981; Leppäranta 1983; Saloranta 2000):

$$\frac{d\rho_s}{dt} = \Gamma(\rho_s, T_a, U_a); \rho_s' = \rho_{s0} \tag{4.28a}$$

where ρ_s' refers to new snow. The density of new snow is normally around 100 kg m^{-3}, while strong packing may lead to the level of 400 kg m^{-3} for old seasonal snow.

The temperature structure of the water column beneath the ice develops in the cooling season. The mixing conditions determine the deep-water temperature and the depth of the winter thermocline. In fresh and brackish waters, inverse stratification forms after the surface temperature has passed the temperature of maximum density. But long-lasting, strong mixing cools the deep water, in freshwater lakes down to 1–2 °C, and deepens the thermocline. After the ice cover has formed, the circulation slows down, heat exchange through the surface weakens remarkably, and the heat flux from the lake bottom becomes significant. The heat flux from water body to the ice bottom has been estimated as less than 5 W m^{-2} (e.g., Shirasawa et al. 2006; Kirillin et al. 2012; Yang et al. 2012).

Beneath a stable ice cover, heat flux from water to ice retards the growth rate or melts ice. This heat flux is expressed as

$$Q_w = k_w \left.\frac{\partial T}{\partial z}\right|_{z=h} \tag{4.28b}$$

where k_w is the heat conductivity in the water beneath the ice. In the case of laminar flow, the molecular heat conductivity k_w = 0.6 W m^{-1} °C^{-1} is employed. Then for $\partial T/\partial z \sim 1$ °C m^{-1}, we have $Q_w \sim$ ½ W m^{-2}. In turbulent conditions, the conductivity (due to eddy diffusion) is much larger, $k_w \sim 10^4$ W m^{-1} °C^{-1} (e.g., McPhee 2008). However, the water flow beneath a stable lake ice cover is often neither laminar nor turbulent but rather in the laminar–turbulent transition regime, where the value of conductivity is not well established. Petrov et al. (2006) employed an effective conductivity o f k_w = 20 W m^{-1} °C^{-1} in a medium-size, shallow lake in Russian Karelia.

In the presence of turbulent boundary layer under the ice, the exchange of momentum, heat and salts can be examined with the boundary layer theory similar to the atmospheric case (see Sect. 4.1). The heat transfer is then approximated by the bulk formula:

$$Q_w = \rho_w c_w C_{Hw}(z')\left[T_w(z') - T_f\right]U_w(z') \tag{4.29}$$

where $z' = z - h$ is the distance from ice bottom, C_{Hw} is the ice–water heat exchange coefficient, T_w is the water temperature, and U_w is the current speed (relative to the ice). This approach approximates the profile formula with effective heat conductivity represented by $\rho_w c_w C_{Hw} z' U_w$. Lake Pääjärvi station data gave the estimate of $C_{Hw} = 0.4 \times 10^{-3}$, corresponding to k_w = 16.8 W m^{-1} °C^{-1} for z = 1 m and U_w = 1 cm s^{-1}, and the heat flux magnitude of 2–5 W m^{-2} (Shirasawa et al. 2006).

The salinity balance in the boundary layer beneath the ice is important under a stable ice cover even in freshwater lakes. Growing ice rejects most of the impurities, but a small

fraction remains between crystals depending on the growth speed. As a result, the salinity of ice is an order of magnitude less than the salinity of the parent water (Leppäranta et al. 2003b). This may cause weak convection in the surface layer. More significant is the melt water, which is less saline, and therefore less dense, than the lake water, and which may form a thin stable layer under the ice.

4.2.3 Superimposed Ice Growth

Superimposed ice grows above the top surface of the ice sheet (see Sect. 3.2.2). The dominant type is freezing of slush, which is a mixture of snow and liquid water from the lake, rain or snowmelt (Fig. 4.7). But also rain water or melt water ponds on ice may freeze into superimposed ice. When the slush has formed, ice grows from its upper surface. The growth law is as in the case of snow-covered congelation ice, but the latent heat released is reduced since slush contains ice crystals. Also there is no heat flux from the slush to the bottom of the growing snow-ice. Consequently, the boundary condition (4.25c) is replaced by

$$\rho \nu L_f \frac{dh}{dt} = k \frac{\partial T}{\partial z} \tag{4.30}$$

where ν is the liquid water content of the slush. Observations suggest that typically ν ∼ ½ when slush forms by flooding (e.g., Leppäranta and Kosloff 2000), and then, with the same temperature gradient, snow-ice growth rate is twice the growth rate of congelation ice. Snow-ice growth is thus similar to snow-covered congelation ice, modified by the porosity influence.

If the underlying ice is very cold, the slush may also freeze at its bottom but this growth remains limited. Using the 'cold content of the ice' to place the latent heat of freezing, the growth of the slush layer at the ice–slush interface (Δh) is obtained from $-\rho c T h = \rho \nu L_f \Delta h$, where h is the thickness of congelation ice; if the mean temperature of ½ m thick ice is –5 °C, we have Δh = 3 cm.

The thickness of snow-ice is limited by the mass budget of snow (see Sect. 3.2.2). In the case of slush produced by flooding, there is always snow on top of the snow-ice

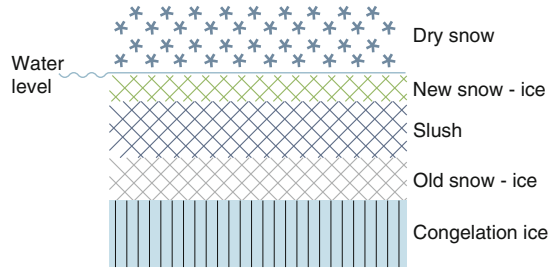

Fig. 4.6 Schematic cross-section of snow on lake ice: *top* layer is *above* the water surface level, and beneath snow is found in snow-ice and slush layers

providing weight to submerge the ice. The maximum snow-ice thickness is then $\sim 2/3\ h_s$. The insulation effect can be strong so that semi-permanent slush layers form inside the ice sheet. Furthermore, a new flooding event produces slush on top of the existing snow-ice, and thus it is possible that alternating slush and snow-ice layers exist. However, published data indicate only the existence of a single slush layer inside the ice sheet.

In melt–freeze metamorphosis, liquid water is provided by the snow layer itself. Meltwater may be convected down before freezing and will form snow-ice thereafter. The maximum thickness of snow-ice produced by this mechanism is $h_s/3$. When the volume of meltwater is small, hard crust layers or ice lenses may result from freeze-melt metamorphosis. In case liquid precipitation is the source of the water, in principle the maximum snow-ice thickness is $\sim 2/3\ h_s$. Data from the coastal landfast ice of Sakhalin has shown that the springtime snow-ice formation (melt–freeze cycles and liquid precipitation) may add up to 20 cm to the total ice thickness of about 100 cm (Shirasawa et al. 2005).

4.2.4 Frazil Ice Growth

Frazil ice forms in turbulent, supercooled open water (e.g., Michel 1978; Martin 1981). Ice crystals flow free in turbulent eddies and are transported by the mean current. They have buoyancy, which overcomes the turbulence when the frazil mass is large enough, and then a floating surface frazil ice layer forms. In lakes frazil ice may form the primary ice. In large lakes, there may be quasi-persistent open water areas to serve as frazil ice source areas. Because the surface water temperature is kept at 0 °C during frazil ice formation, the heat losses from the water body and consequently rate of frazil accumulation can be large.

Formulation of the physical law of frazil ice formation is straightforward, since the surface temperature must be at the freezing point and the surface heat loss changes the volume of frazil and compensates for the heat flux coming from the deeper water:

$$\rho L_f \frac{dh}{dt} + Q_w = -(Q_0 + Q_T) \tag{4.31}$$

where h represents the volume of frazil per unit area or the equivalent thickness of the frazil ice mass. The frazil may form a local ice cover or drift away, depending on the turbulence and circulation characteristics.

When the surface water has reached the freezing point, Eq. (4.31) shows that the water surface remains open as long as $Q_w + Q_T + Q_0 \geq 0$. When this is no more true, the surface layer cools, and after minor supercooling, frazil accumulation is commenced. Assuming that the heat flux from deeper waters is small, the volume of frazil can be directly integrated from Eq. (4.31), since the solar and atmospheric fluxes are independent of the frazil volume. Thus there is no self-insulating mechanism as in the case of congelation ice,

and because the surface temperature is held at the freezing point, the heat loss continues to be large. In the presence of strong turbulence in shallow waters, frazil crystals may be adhered into lake bottom to form anchor ice. Due to its buoyancy, anchor ice may rise to surface to join the ice cover. This is often observed in rivers and shallow coastal sea areas.

Frazil ice is not largely discussed in this book because of its likely unimportance in freezing lakes. For more information, the reader is referred to books and review papers in river ice and sea ice (Michel 1978; Martin 1981; Ashton 1986; Wadhams 2000; Weeks 2010).

4.2.5 Ice Melting

Ice melting is a similar process for all ice types. The main differences are due to optical properties of the ice. The melting season begins when the ice has warmed up to the melting point and the heat balance continues to be positive. This is largely determined by the net radiation balance. In winter the balance is negative, and the time it turns positive is a function of the latitude (ϕ). Due to the penetration of sunlight into the ice and thermal radiation losses at the surface, melting of ice begins in the ice interior some 10–20 cm from the top surface or at the ice bottom.

Snow-covered dry ice has a high albedo, around 0.9. When the solar radiation increases, at some time albedo begins to decrease that provides a positive feedback to the net radiation:

$$Q_R = (1-\alpha)Q_s + \varepsilon_0\sigma\left(\varepsilon_a T_a^4 - T_0^4\right) > 0 \tag{4.32}$$

As seen this balance is highly sensitive to albedo: $\delta Q_R = -\delta\alpha \cdot Q_R$. The net heat loss due to terrestrial radiation is $\sim$50 W m^{-2}, while solar radiation can be $\sim$500 W m^{-2} at daily maximum. If there is dry snow on ice, the albedo is $\sim$0.9, and it is difficult to reach positive radiation balance as is the case in the polar ice sheets (e.g., Leppäranta et al. 2013). To decrease the albedo, minor melting or recrystallization of snow layer at solar noon are essential factors. In the case on snow-free ice, the radiation balance becomes easily positive, and the transparency of the ice tells how the net solar energy is distributed with depth in the ice and underlying water body.

In the first approximation, the daily incoming solar radiation is proportional to cosine of the solar zenith angle at solar noon, which is obtained from the astronomical formulae as (see Appendix A.1):

$$\cos Z_0 = \cos(\phi + \delta) \tag{4.33a}$$

$$\sin\delta = \sin\varepsilon \sin(\vartheta - \vartheta_0) \tag{4.33b}$$

where δ is declination, ε = 23°27′ is the inclination of ecliptic, ϑ is year angle starting from January 1st ($0 \le \vartheta \le 2\pi$), and ϑ_0 is its value at the spring equinox. Assuming that the net terrestrial radiation is constant, zero upcrossing of net radiation takes place at a fixed solar zenith angle. The rate of change of declination is

$$\frac{d\delta}{dt} = \frac{2\pi}{365\text{d}} \cdot \frac{180^\circ}{\pi} \cdot \frac{d\delta}{d\vartheta} = \frac{360^\circ}{365\text{d}} \cdot \frac{\sin\varepsilon\cos(\vartheta - \vartheta_0)}{\sqrt{1 - [\sin\varepsilon\sin(\vartheta - \vartheta_0)]^2}} \tag{4.34}$$

This equation gives the change of declination in degrees per day.

Example 4.2. Assume that the zero upcrossing of the net radiation balance is at the time of spring equinox. Then $\vartheta - \vartheta_0 = 0$, and we have $d\delta/dt = 0.39^\circ\ \text{day}^{-1}$. When the latitude changes by 3.9°, Eqs. (4.33 and 4.34) show that the day of zero upcrossing of net radiation balance changes by 10 days. At $\vartheta - \vartheta_0 = 50$ days, May 10th, the change has decreased to $0.27^\circ\ \text{day}^{-1}$.

Melting takes place at the top and bottom boundaries and in the interior of the ice sheet. According to recent field data (Jakkila et al. 2009; Leppäranta et al. 2010), boundary melting and surface melting are of the same magnitude and the exact levels depend on the weather conditions during the melting season. Due to terrestrial radiation losses, i.e. the cool skin phenomenon, at the top surface, it is common to have $Q_o < 0 < Q_o + Q_T$ in the melting season. Solar radiation warms the water beneath the ice and a part of this will return to ice bottom to add on the bottom melting.

Typical to the melting season is the strong heterogeneity, which appears as a patchy surface with snow, bare ice and wet spots (Fig. 4.2). The patchiness develops due to positive feedback of melting to albedo: once albedo starts to decrease, melting further lowers the albedo and speeds up the decay process. Also, in shallow areas, the water beneath ice warms faster and melts ice from the bottom, as observed in melting starting from lake shorelines. Thus, melting of ice is a vertical–horizontal process.

Top and bottom melting decrease the thickness of ice, while internal melting increases the porosity of the ice. Therefore, a melting lake ice sheet needs to be described by the evolution of its thickness, temperature and porosity, $\{h = h(t),\ T = T(z, t),\ \nu = \nu(z, t)\}$. For freshwater ice, the melting of ice obtained from:

$$\rho L_f \frac{dh}{dt} = -Q_0' - \left(Q_w + k \left.\frac{\partial T}{\partial z}\right|_{z=h} \right) \tag{4.35a}$$

$$Q_0' = \max\left(Q_0 + k \left.\frac{\partial T}{\partial z}\right|_{z=0}, 0 \right), \quad \text{if } T_0 = 0\,^\circ\text{C}; Q_0' = 0, \quad \text{if } T_0 < 0\,^\circ\text{C} \tag{4.35b}$$

$$Q_I = \frac{\partial}{\partial z}\left(k\frac{\partial T}{\partial z} - Q_T e^{-Kz} \right) \tag{4.35c}$$

$$\rho L_f \frac{\partial v}{\partial t} = Q_I, \quad \text{if} \quad T = 0\,^\circ\text{C}\,(0 \le v \le 1); v = 0, \quad \text{if} \quad T < 0\,^\circ\text{C}; \tag{4.35d}$$

$$\frac{\partial}{\partial t}(\rho c T) = Q_I (T \le 0\,^\circ\text{C}) \tag{4.35e}$$

where $Q_\text{I} = Q_\text{I}(z, t)$ is the energy flux into the ice interior. Equations (4.35a, b) give the decrease of ice thickness, i.e. melting at the top and bottom surfaces. Equations (4.35c–e) are for the melting in the interior and present the evolution of the porosity and temperature, conditioned so that porosity can be nonzero only at $T = 0$ °C and temperature can be below 0 °C only if v = 0. Equations (4.35a, b) can be extended for brackish, saline or hypersaline ice but then porosity and temperature change together at all temperatures dictated by the phase diagram of the ice in question. Always when ice temperature increases, the volume of liquid brine increases. For sea ice case the problem has been largely investigated (see, e.g., Assur 1958; Cox and Weeks 1983; Leppäranta and Manninen 1988; Wadhams 2000; Weeks 2010).

Internal melting gives rise to structural defects. It starts from the crystal boundaries, and therefore the crystal structure is revealed by to human eye. Consequently, melting columnar-grained ice is called *candled ice* in common language. Once the porosity has reached 0.3–0.5, the ice cannot bear its own weight and breaks. Thereafter ice floes and blocks move with the wind, heat from the water body to ice increases strongly, and ice disappears rapidly. Breakage of ice increases the surface-to-volume ratio of the ice mass that also increases the melt rate. In the 1990s the author observed a 45-cm thick ice cover to disappear in 2 days in Lake Tuusulanjärvi, Finland; the ice was already porous to start with, risky to walk on. The very fast break-up of ice has been sometimes phrased as 'ice sinks overnight' (Humphreys 1934).

The physics of melting can be simplified assuming that the temperature is at the melting point across the ice sheet. Then there is no conduction through the ice but the ice melts at the boundaries by the surface fluxes and inside by the solar radiation. Melting of ice can be examined as a process with two characteristics, ice thickness h and mean porosity $\tilde{v}$:

$$\rho L_f (1 - \tilde{v}) \frac{dh}{dt} = -(Q_0 + Q_w) \le 0 \tag{4.36a}$$

$$\rho L_f h \frac{d\tilde{v}}{dt} = \left(1 - e^{-\kappa h}\right) Q_T \ge 0 \tag{4.36b}$$

The first equation stands for the thickness of ice (distance between top and bottom surfaces) and the second equation stands for internal melting; the net ice volume is $h(1 - \tilde{v})$. At the top surface the snow melts first, then the ice. Internal deterioration starts up only after snow has melted. Internal melting gives rise to structural defects and finally

the ice breaks into small blocks into the surface water. Then there is a rapid increase in the rate of melting.

Example 4.3. With the heat flux of 35 W m^{-2}, in 24 h we can decrease ice thickness by 1.0 cm or increase the mean porosity of 50 cm thick ice by 2.0 %.

4.3 Analytic Models

4.3.1 Basic Principles

The classical problem of modelling lake ice thermodynamics is the thickness cycle of congelation ice. Stefan (1891) derived the first ice growth model, which was based on a quasi-steady conduction of the latent heat released in freezing through the ice. He examined the ice in the Arctic Ocean, but in fact his model applies better for lake ice, since the thermal properties of sea ice vary largely depending on the brine volume. Stefan's model was further developed by Barnes (1928) for different kind of growth conditions in Canadian freshwater bodies. Since then these models have been applied for the first-order approximations for ice growth (e.g., Anderson 1961; Ashton 1986; Leppäranta 1993).

Analytic ice growth models are mostly quasi-steady. They are based on the solution of the steady-state heat conduction law with moving lower boundary of the ice sheet. Quasi-steady situation means that thermal inertia is ignored, or in other words there is no heat capacity. Also in the growth season the net solar radiation is low and either ignored or included in the surface boundary condition. The time scale of heat flux in the ice is $T \sim L^2 D^{-1}$, i.e. $T \sim 10\, L^2$ m^{-2} day. Thus when ice thickness is less than 20 cm, the daily temperature cycle can be resolved with quasi-steady models. In the polar winter, forcing changes slowly, and rather the synoptic time scale is the shortest one of interest. This can be resolved up to the ice thickness of 50 cm.

Modelling the decay of lake ice is in principle straightforward, since in the melting season ice loss is due to the net gain of energy from external fluxes and heat conduction is less significant. However, the space–time variability of the albedo and light attenuation coefficient of melting ice arise problems. Analytic melting models are simplified energy balance models, where changes in these ice properties can be parameterized.

Analytic models serve well lake ice research. They can be used to obtain the scale of ice thickness for different lakes and environmental conditions, and as well they are very good tools for sensitivity analysis and first-order evaluation of the climate change impact. The models also show how shallow lakes may freeze to the bottom providing information of the phenological event of *total freezing*.

4.3.2 Congelation Ice

Stefan's model considers a congelation ice sheet (Fig. 4.7). Latent heat released in the growth at the ice bottom is conducted away through the ice. The assumptions are the following: (i) Thermal inertia of ice is ignored, i.e., quasi-steady approach; (ii) Penetration of solar radiation into the ice is ignored, (iii) There is no heat flux from water to ice; and (iv) The surface temperature is a known function of time, $T_0 = T_0(t)$. The assumptions (i–ii) mean that the ice temperature profile is linear (see Eq. 4.24), and with the assumption (iii) ice growth is obtained from the bottom boundary condition (Eq. 4.25c) as a simple separable equation:

$$\rho L_f \frac{dh}{dt} = k \frac{T_f - T_0}{h} \tag{4.37}$$

In this quasi-steady model the heat conduction immediately adjusts to the surface temperature. With the assumption (iv), Eq. (4.37) integrates into (see also Fig. 4.8):

$$\begin{aligned} h(t) &= \sqrt{h^2(0) + a^2 S(t)} \\ a &= \sqrt{\frac{2k}{\rho L_f}}, S = \int_0^t \left[T_f - T_0(t')\right] dt' \end{aligned} \tag{4.38}$$

where a is a fixed coefficient, which depends on the thermal properties of ice, and S is the sum of freezing-degree-days. The theoretical value of a is 3.3 cm $°C^{-1/2}$ $day^{-1/2}$; this coefficient will be called Stefan's coefficient below.

The weakest point in Stefan's model is the assumption (iv), since the surface temperature is rarely known. Especially, when there is snow on the ice, the air temperature can be quite different from the ice surface temperature. In principle, monitoring the surface temperature would make it possible to produce a good estimator for the ice thickness evolution. Another weakness is that the assumptions (i)–(iii) all tend to bias the solution upward (Leppäranta 1993). Ignoring thermal inertia produces a little more growth compared with nature when the air temperature decreases toward middle winter. Solar radiation is weak in the ice growth season except in cold arid mid-latitude climate. The heat

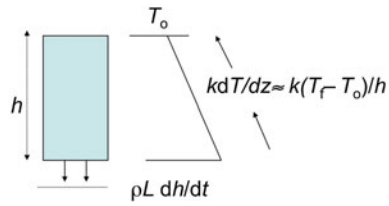

Fig. 4.7 A schematic picture of Stefan's model. Latent heat is released at the *bottom* in ice growth, and this heat is conducted through the ice to the atmosphere. For the conduction, the surface temperature must be below the freezing point

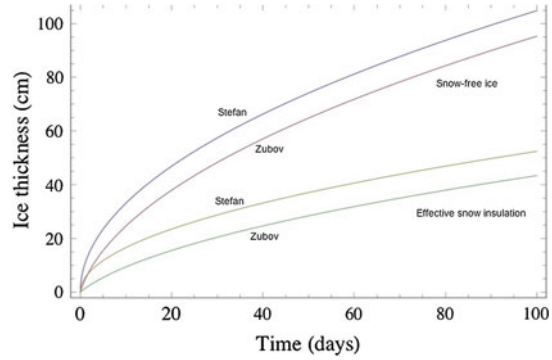

Fig. 4.8 Analytic solutions of the Stefan's model and Zubov's model, which accounts for the atmospheric surface layer buffering and snow cover. The cases of snow-free ice and effective snow insulation are shown

flux from water to the ice is small in lakes with weak winter circulation but in the presence of significant currents or heating from lake bottom the model can be badly biased.

In semi-empirical modifications of the model, the Stefan's coefficient is replaced with reduced coefficient a^*, $\frac{1}{2} \le a^*/a \le 1$. The ranges of the ratio a^*/a have been suggested as, e.g., 0.5–0.8 (Ashton 1989) or 0.6–0.85 (Nolan 2013). The surface temperature needs to be normally replaced by air temperature when it is below the freezing point, i.e. the freezing-degree-days are expressed as $S_a(t) = \int_0^t \max\left[0, T_f - T_a(t')\right]$.

Example 4.4.

(a) Using the air temperature data for Oymakon, East Siberia (the coldest location in the Northern Hemisphere) from the winter of 1981–1982 (the coldest one for this region in the period 1971–2000), Stefan's model provides the ice thickness of 2.7 m (Kirillin et al. 2012). This is an upper limit for the thickness of seasonal lake ice because the Stefan's model generally overestimates the ice growth rate.

(b) For a 100-day cold season with the mean air temperature –10 °C below the freezing point, we have S_a = 1000 °C d, and the Stefan's model gives the ice thickness of 105 cm, which can be reduced in empirical modification to 52.5 cm for $a^* = \frac{1}{2}\, a$.

(c) Ice growth can reach the bottom when $a\sqrt{S} \ge H$, where H is the lake depth. Assuming that the ice salinity is zero, the water salinity develops as $S_w(t)H(t) = S_w(0)H(0)$ that lowers the freezing point. Starting with $S_w(0)$ = 1 ‰ and $H(0)$ = 1 m, at $H(t)$ = 1 cm the salinity is 100 ‰ and the freezing point well below 0 °C (for sea-water, it would be –6.1°).

4.3.2.1 Atmospheric Surface Layer as a Buffer

A snow-free ice sheet is considered. In Stefan's model it is implicitly assumed that all heat conducted to the ice surface can be taken to the atmosphere. But this is not necessarily true. Therefore a more realistic approach is to add an atmospheric surface layer to the Stefan's model (Barnes 1928; Zubov 1945). Here the linear surface heat balance

$Q_0 = k_0 + k_1(T_0 - T_a)$ is used (see Sect. 4.1.5). The growth condition is that $Q_0 < 0$, and, by the continuity of the heat flow, we have

$$\rho L_f \frac{dh}{dt} = k\frac{T_f - T_0}{h} = -[k_0 + k_1(T_a - T_0)] \geq 0 \tag{4.39}$$

Elimination of the surface temperature from the latter equation gives

$$\rho L_f \frac{dh}{dt} = k\frac{T_f - T_a - b_0}{h + b_1}; b_0 = \frac{k_0}{k_1}, b_1 = \frac{k}{k_1} \tag{4.40}$$

There are two parameters in addition to the Stefan's coefficient: b_0 accounting mainly for the radiation losses and b_1 for the turbulent losses. By physics, $b_1 \geq 0$ that adds to the insulation of ice bottom from the atmosphere; and in practice, due to low solar radiation level, $b_0 \leq 0$ in the growth season that adds to the freezing-degree-days. The numerical values of these parameters are $b_0 \sim -3$ °C, $b_1 \sim 10$ cm. With k_0 and k_1 constants the solution is (see also Fig. 4.8):

$$h(t) = \sqrt{h^2(0) + a^2[S_a(t) - b_0 t] + b_1^2} - b_1 \tag{4.41}$$

Barnes (1928) and Zubov (1945) considered the situation $k_0 = 0$, where turbulence transfers the heat away from the ice surface. The relative difference between the Stefan's model and Eq. (4.40) is largest when ice thickness is small. When $k_1 \rightarrow \infty$, $T_0 \rightarrow T_a$ and the Stefan's growth law is obtained. This means that all heat conducted through the ice can be moved away. The coefficient k_1 becomes small at the limit of $U_a \rightarrow 0$, and ignoring solar radiation the ice growth is determined solely by the terrestrial radiation balance. Then $k_0 \approx 50$ W m^{-2} and $k_1 \approx 4$ W m^{-2} °C^{-1}, and, consequently, $b_0 \approx 12.5$ °C and $b_1 \approx 50$ cm.

4.3.2.2 Influence of Snow Cover on Congelation Ice Growth

The presence of snow cover gives a major impact on ice growth. The heat conduction law is as for ice (Eq. 4.24). Thermal inertia is ignored as in ice, and the temperature profile across snow and ice layers becomes piecewise linear. The system of Eq. (4.39) is expanded into

$$\rho L_f \frac{dh}{dt} = k\frac{T_f - T_s}{h} = k_s\frac{T_s - T_0}{h_s} = -[k_0 + k_1(T_a - T_0)] \geq 0 \tag{4.42}$$

where T_s is the temperature at the snow-ice interface, k_s is thermal conductivity of snow, and h_s is snow thickness. Here we have assumed that snow is not flooded by lake water: a sufficient condition is that $\rho_s h_s \leq (\rho_w - \rho_s)h$ or $h_s \lesssim \frac{1}{3}h$ (flooding leads to snow-ice formation treated in the following section). Eliminating the temperatures T_0 and T_s from the system (4.42), we can obtain the differential equation:

$$\rho L_f \frac{dh}{dt} = k\frac{T_f - T_a - b_0}{h + \beta h_s + b_1}; \beta = \frac{k}{k_s} \tag{4.43}$$

Compared with Eq. (4.40), the presence of snow cover has brought the term βh_s to the denominator. The parameter $\beta \sim 10$ describes the insulation efficiency of snow as compared with ice. If βh_s = constant, the solution (Eq. 4.41) applies with b_1 replaced by $b_1 + \beta h_s$. However, in general snow thickness depends on time, and Eq. (4.42) cannot be analytically solved; in fact, also the snow conductivity (and therefore β) depends on time determined by metamorphic processes in the snow cover. Since $\beta \gg 1$, even a thin snow cover dominates over the atmospheric surface layer buffering.

Example 4.5. Let us add a constant snow insulation thickness $h_s^* = \beta h_s$ to the Stefan's model. The snow-free Stefan solution is $h_0 = a\sqrt{S}$. It is easy to see that the ice thickness in the presence of snow is $h = h_0 - h_s^*$ for $h_s^* \ll h_0$, and $h \to ½\, h_0$ for $h_s^* \to h_0$.

A specific case of snow-covered ice is obtained by assuming that snow accumulation is proportional to the ice thickness. Snow and ice thickness are in general positively correlated, and although the proportionality is a quite limited assumption, it provides an overall view of the influence of snow cover during the whole ice growth season. The solution (4.41) can be utilized. Denoting $h_s = \lambda h$, the denominator in Eq. (4.43) becomes $(1 + \lambda\beta)h + b_1$, and, consequently, in the solution the coefficient a^2 is divided by $(1 + \lambda\beta)$:

$$h(t) = \sqrt{h^2(0) + \frac{a^2}{1 + \lambda\beta}[S_a(t) - b_0 t] + b_1^2} - b_1 \tag{4.44}$$

Requiring that only congelation ice forms, we must have $\lambda \lesssim 1/3$ (no flooding), and since $\beta \sim 10$, we have $1 + \lambda\beta \lesssim 4$. Therefore ice thickness evolution over the winter season is reduced by a factor of about ½ when the insulation of snow is most efficient (Fig. 4.8). This result also agrees with the fact that empirical modifications a^* of the growth law coefficient are at lowest about $a^* \sim a/2$.

4.3.2.3 Heat Flux from the Lake Body

The heat flux from the water body can be also examined using analytic tools (Barnes 1928; Leppäranta 1993). It is independent of the ice except that in the melting season, when the solar heating of the water depends on the snow and ice thickness. In analytic modelling, this flux is given as a prescribed function of time. The mean water–ice heat flux has been estimated as 1–5 W m^{-2}; e.g., 2–5 W m^{-2} in deep Lake Pääjärvi (Shirasawa et al. 2006) based on measurements and less than 1 W m^{-2} in shallow Lake Vanajavesi based on model tuning (Yang et al. 2012); both lakes are from southern Finland. The influence of the heat flux on the annual maximum ice thickness was up to about 5 cm. The source of the heat is in the water body itself, bottom sediments, or sun. The first and second sources are significant especially in the early ice season, while the third one can be large in spring and summer.

The heat flux from the water, Q_w, can be added to the Stefan's model (Eq. 4.37) as

$$\rho L_f \frac{dh}{dt} + Q_w = k\frac{T_f - T_0}{h} \tag{4.45}$$

Thus both the latent heat released in freezing and the heat flux from the water need to be conducted away through the ice. Both sides of this equation are nonnegative so that melting of ice is also allowed and takes place when the heat flux from water is larger than the heat conduction through the ice.

Assume that the surface temperature and the heat flux from water are constants. Then there is an equilibrium solution with dh/dt = 0:

$$h_e = k\frac{T_f - T_0}{Q_w} \tag{4.46}$$

Exactly the heat flux received from water is conducted through the ice to the atmosphere. Furthermore, with T_0 and Q_w constants, Eq. (4.45) can be solved analytically in an implicit form for $h = h(t)$:

$$\frac{\boldsymbol{h}}{\boldsymbol{h_e}} + \log\left(1 - \frac{\boldsymbol{h}}{\boldsymbol{h_e}}\right) = -\frac{t}{\tau}, \tau = \frac{\rho_w L h_e}{Q_w} = \frac{1}{2}\cdot\frac{a^2\left(T_f - T_0\right)}{\left[Q_w/(\rho_w L)\right]^2} \tag{4.47}$$

where τ is the time-scale of the system. The solution is illustrated in dimensionless form in Fig. 4.10. E.g., for $T_f - T_0$ = 10 °C and Q_w = 5 W m^{-2}, we have h_e = 40 cm and τ = 281 d. If the situation remains for, say, for 50 days, the solution is valid only to the time t/τ = 0.18. If the heat flux from the water is doubled, we have h_e = 20 cm and τ = 70 d. In the beginning ($h \ll h_e$), the left side is approximately −½ $(h/h_e)^2$ and the ice grows proportional to the square root of time. The thickness ½ h_e is reached at the time t = 0.19 · τ = 13 days.

In the Stefan's law, when the surface temperature is below the freezing point the ice grows without limit but any heat flux from the water body brings the asymptote h_e to the

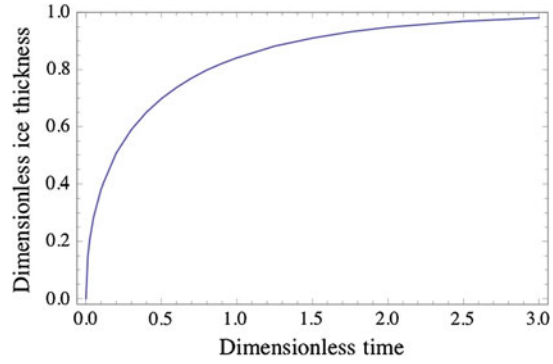

Fig. 4.9 Dimensionless ice thickness h/h_e as a function of dimensionless time in the presence of heat flux from the water body; ice thickness is scaled by the asymptotic equilibrium thickness h_e, and time is scaled by the rate of melting $\rho_w L h_e/Q_w$

thickness evolution. Since the flux from the water is fairly small in lakes, the equilibrium thickness is not reached but the growth rate of ice is reduced. However, in geothermal lakes, equilibrium thickness can be reached fast.

4.3.3 Snow-Ice

Snow-ice grows down from the top of the slush, and the growth model is similar to the case of snow-covered congelation ice (Eq. 4.42) (Leppäranta 1993). The only change in the heat conduction equation is that, since snow-ice grows into slush, in the moving lower boundary condition the latent heat of freezing is multiplied by the porosity of slush. The analytic model is thus

$$\rho L_f v \frac{dh_{si}}{dt} = k\frac{T_f - T_s}{h'_{si}} = k\frac{T_s - T_0}{h_s} = -[k_0 + k_1(T_a - T_0)] \tag{4.48a}$$

$$t = 0 : h_{si} = h_{si}(0) \tag{4.48b}$$

where h'_{si} is the thickness of snow-ice above the slush, and the time t refers to the beginning of the freezing of the present slush layer. With the initial condition (4.48b), the new growth from Eq. (4.48a) is added to the existing older snow-ice deeper down. Snow-ice layer is not necessarily continuous but there is a slush layer between old snow-ice and new snow-ice. After a slush formation event, h_s = constant, and the thickness of snow-ice is

$$h_{si}(t) = h_{si}(0) + \sqrt{v^{-1}a^2[S_a(t) - b_0 t] + (\beta h_s + b_1)^2} - (\beta h_s + b_1) \tag{4.49}$$

Here normally $\beta h_s \gg b_1$. Snow-ice layer grows faster by the factor of $\nu^{-1/2} \sim 3/2$ as compared with congelation ice.

The upper limit of snow-ice thickness is obtained assuming that new slush forms and freezes continuously. Then, if the slush is created by flooding, we have $h_s = \gamma h_{si}$, where $\gamma = (\rho_w - \rho_{si})/\rho_s$, and, consequently:

$$\frac{dh_{si}}{dt} = \frac{k}{\rho_w L_f} \cdot \frac{k_s}{k\gamma v} \cdot \frac{T_f - T_s}{h_s} = -[k_0 + k_1(T_a - T_s)] \tag{4.50}$$

This is similar to the growth law of congelation ice, except that the Stefan's coefficient is multiplied by the factor of $\sqrt{k_s/(k\nu\gamma)}$; since $k_s/k \sim 0.1$, $\nu \sim ½$, and $\gamma \sim 1/3$ (Leppäranta and Kosloff 2000), this factor is ~ 0.8. Thus, forming snow-ice with continuous snowfall and consequent flooding produces less ice than the growing snow-free congelation ice. This is because to produce slush with growing snow-ice, we need more snow freeboard that adds to insulation.

Snow-ice formation can also take place due to melt-freeze cycles and liquid precipitation. In both cases the question is that how much snow is available to form the slush. If a slush layer is formed in the lower part of the snow layer, it will freeze into snow-ice according to Eq. (4.49). Otherwise snow-ice formation is easier than by flooding since the insulating effect of snow becomes reduced when snow is consumed in snow-ice formation. However, these cases do not produce much snow-ice as compared with flooding.

Example 4.6. A special case is a heavy snowfall before freezing and in early ice season. The insulation effect of the snow cover is strong from the beginning, and the resulting ice sheet is snow-ice with variable ice thickness. Such situation occurred in winter 2013–2014 in Lake Kilpisjärvi, northern Lapland. Even though the winter was cold, there were even weak spots in the ice cover.

Example 4.7. It is easy to see that if lake water is pumped up to the snow layer, more ice will be produced than by keeping the surface bare to aid congelation ice growth. This is due to that by the pumping the insulation thickness of snow can be reduced and the ice grows much faster than natural snow-ice. Although snow-ice has low mechanical strength, the bearing capacity becomes large using the pumping method due to the large ice thickness. This method was used in Lake Katumajärvi, which served as the starting area in Finlandia Ski Marathon from Hämeenlinna to Lahti (Palosuo 1982). The bearing capacity question was not critical for the skiers but it was so for the trucks, which collected the skiers' bags to transport them to the goal area.

4.3.4 Frazil Ice

In open water conditions, frazil ice forms where the ice crystals move free in turbulent eddies (see Sect. 3.2.2). In this situation there is one important limitation in the surface energy balance: the surface temperature is at the freezing point. Therefore, in low air temperature conditions turbulent heat losses from the water surface can be quite large and, consequently, frazil ice production is fast. The mathematical model of frazil ice accumulation can be expressed as:

$$\frac{dh}{dt} = -\left[\frac{k_0 + k_1\left(T_a - T_f\right)}{\rho L_f}\right] - \frac{Q_w}{\rho L_f} = q \tag{4.51}$$

where h stands for the frazil ice volume per area. For frazil ice growth, we must have $q > 0$. Clearly $h = h_0 + qt$, where h_0 is the initial value. In winter conditions, $k_0 \sim -40$ W m^{-2} and $k_1 \sim 15$ W m^{-2} °C^{-1} (Table 4.1), and thus the k_1-term is strongly dominant when the air–surface temperature difference is more than 10 °C.

Figure 4.10 shows a comparison between the snow-free congelation ice and frazil ice. When the wind is strong, turbulent heat losses and frazil ice accumulation become much

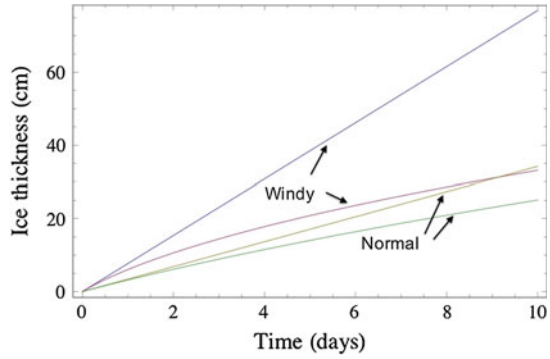

Fig. 4.10 Frazil ice accumulation and congelation ice growth at air temperature held constant at –15 °C. Normal case refers to climatological wind, and windy case refers to doubled wind speed. Frazil growth is stronger, especially at high wind

more than congelation ice growth. If the heat loss is 100 W m^{-2}, the resulting frazil ice production rate is 2.8 cm day^{-1}. Accumulation of frazil ice in a turbulent boundary-layer has been modelled by Omstedt and Svensson (1984) using a one-dimensional model. To solving the full frazil ice problem one needs to consider also advection and consequently take a two-dimensional modelling approach. Frazil ice models have been largely worked on in river ice research (Lal and Shen 1993).

Example 4.8. The model (4.51) can be extended to examine the open water question. For $q = 0$, the equilibrium solution between the heat loss to the atmosphere and the heat flux from the water body is

$$T_0 = T_a + \frac{Q_w + k_0}{k_1}$$

If $T_0 > T_f$, there is no frazil formation. The wintertime climatology shows that $k_0 \sim -40$ W m^{-2} and $k_1 \sim 15$ W m^{-2} $°C^{-1}$ (see Table 4.1). In the presence of strong geothermal heat flux, say, 190 W m^{-2}, we have $T_0 = T_a + 10$ °C, i.e. a freshwater lake may stay open down to the air temperature of –10 °C. In the case of a hypersaline lake, say, $T_f = -20$ °C, assuming $Q_w = 0$, we have $T_0 - T_a = -3$ °C. Thus the lake is open down to the temperature of –17 °C.

4.3.5 Melting

Analytic models of ice melting can be based on total absorption of heat by the ice changed to decrease the volume of ice; then 'ice thickness' represents the volume of ice per unit area. This approach corresponds to the physical picture where significant melting takes place at both boundaries and in the ice interior. In many applications, simple models are used where the rate of melting is proportional to the positive degree-days of air

temperature. Considering the linearized heat flux $k_0 + k_1(T_a - T_f)$, in April–May k_0 increases from 4 to 100 W m^{-2} and $k_1 \sim 20$ W m^{-2} °C^{-1} is rather stable (Table 4.1). Consequently, the direct physical link of melting to degree-day is weak, but it is clear that as the spring progresses, air temperature tends to increase and ice thickness tends to decrease, and the correlation between these two quantities follow.

As the first model, all melting can be included in the ice thickness defined as ice volume per unit area. We have, from Eq. (4.36a, b):

$$\frac{d}{dt}[(1-\tilde{\nu})h] = -\frac{1}{\rho L_f}\left[Q_0 + \left(1 - e^{-\kappa h}\right)Q_T + Q_w\right] \leq 0 \tag{4.52}$$

Since $Q_s \sim 200$ W m^{-2} and the other terms sum to ~ -50 W m^{-2}, albedo must fall below 0.75 for the melting season to begin. Using the linear approximation for the surface heat flux, we have the integrated form

$$h = h_0 - \frac{1}{\rho L_f}\int_0^t \left[k_0 + \left(1 - e^{-\kappa h}\right)Q_T + k_1\left(T_a - T_f\right) + Q_w\right]dt' \tag{4.53}$$

where h_0 is the ice thickness in the beginning of the melting period. In the melting season the net radiation is increasing strongly, and therefore k_0 and Q_T must be taken as functions of time. The first part is the integrated radiative energy, while the second part gives the positive-degree-day formula, which alone is often used for simple modelling of melting.

Example 4.9. Equation (4.53) can be simplified for an approximate model. If there are no significant heat sources in the water body or sediments, we can assume $Q_w \sim Q_T \exp(-\kappa h)$ and define $k_0^* = k_0^* + Q_T$. Also $T_f = 0$ °C can be assumed. Thus

$$h = h_0 - \frac{1}{\rho L_f}\int_0^t \left(k_0^* + k_1 T_a\right)dt'$$

It is seen that melting consists of two factors, one dominated by net radiation and one by degree-days. We can estimate that in the melting season (take April in southern Finland) $k_0 \sim 0$, $Q_T \sim 25$ W m^{-2} and $k_1 \sim 15$ W m^{-2} °C^{-1}. Taking $T_a \sim 3$ °C, we have $h_0 - h \sim 2.0$ cm day$^{-1} \times t$, and thus 50 cm thick ice would melt in ~25 days. However, in the melting season both net radiation and air temperature steadily increase. If this increase is nonlinear, the estimated length of the melting period will be affected. Non-linearity is particularly true in the case of solar radiation, since both incoming solar radiation and albedo increase with the time (see Leppäranta 2014). From the air temperature term we obtain the degree-day coefficient as 0.57 cm °C^{-1}. In high Arctic Canadian lakes, the degree-day coefficient is around 1.5 cm °C^{-1} (Mueller et al. 2009),

and therefore net radiation becomes stronger than the degree-days in the ice breakup. For comparison, river ice breakup is dominated by melting and erosion at the bottom of the ice (Shen and Yapa 1985).

A special case of ice decay is sublimation. Even though latent heat fluxes are usually small in cold environment, in arid cold climate the situation can be different (e.g., Huang et al. 2012). Ice decay due to sublimation is

$$\frac{dh}{dt} = \frac{Q_e}{\rho(L_f + L_e)} = \frac{\rho_a}{\rho} C_e(q_a - q_0)U_a \tag{4.54}$$

The saturation specific humidity at 0 °C is 3.8×10^{-3}. Thus for $C_e \sim 10^{-3}$, $U_a \sim 10$ m s^{-1} and relative humidity of 50 %, the sublimation rate is 2 mm d^{-1}. For 50 days, the loss of ice by sublimation would be $\sim$10 cm.

4.3.6 Multi-year Ice

The analytic growth and melting models can be combined for the equilibrium multiyear ice thickness. The classical Stefan's model is used for ice growth, and the summer melting is taken as $\Delta h = Q_0 + Q_T + Q_w t_s$, where t_s is the length of summer; 'summer' is defined as the period when the net heat flux is positive. Assuming that not all ice melts in summer, the thickness of ice after the nth summer is

$$h_n = \sqrt{h_{n-1}^2 + aS} - \Delta h,\ n \geq 1 \tag{4.55}$$

The growth of ice depends on ice thickness, but we may take $\Delta h \approx$ constant (independent of ice thickness). At equilibrium, $h_{n+1} = h_n = h_e$, where h_e is the equilibrium thickness,

$$h_e = \frac{h_1^2 - (\Delta h)^2}{2\Delta h} \tag{4.56}$$

The condition of multi-year ice is trivial: $h_1 > \Delta h$. When $h_1 - \Delta h$ is small, $h_e \approx h_1 - \Delta h$, and when $h_1 \gg \Delta h$, we have $h_e \approx h_1^2/(2\Delta h)$.

Example 4.10. For h_1 = 2 m and Δh = ½ m, we have h_e = 3.75 m, but changing the summer melt to 1 m gives us h_e = 1.5 m, illustrating the high sensitivity of the equilibrium thickness to summer melt. Dropping h_1 to 1 m would give h_e = 0.75. Net radiation can be easily increased by decreasing the summer albedo, while the sensitivity of the winter growth to freezing-degree-days is $\delta h = \frac{1}{2}(a^2/h_e)\delta S$. E.g., if $h_e \sim 3$ m, then $\delta h \sim 3.7$ cm for a change of 100 °C·day in the freezing-degree days, corresponding to a 0.5 °C

temperature change during 200 days. Thus we need a large change in the temperature or the winter length to get a significant reduction of the equilibrium thickness.

4.4 Numerical Models

4.4.1 Structure of Models

The analytic modelling approach to the growth and decay of lake ice has limitations. First of all, the snow cover cannot be properly considered. The insulating capacity of snow depends on snow accumulation and metamorphosis, which may also lead to slush and snow-ice formation. The resulting lake ice has then a multi-layer structure. Secondly, analytic models are coarse. High time-space resolution of temperature would give a more realistic heat conduction through ice and snow, and with more accurate surface temperature, the surface heat balance comes out much better (e.g., Cheng et al. 2003; Yang et al. 2012).

Numerical lake ice models are of two basic types: (1) Quasi-steady models, where the ice sheet is divided into layers with a quasi-steady heat flow through the system; and (2) Time-dependent models, where the vertical equation of heat conduction is directly integrated (Eqs. 4.24, 4.25a, b, c). In both cases the boundary conditions are properly treated. The present lake ice models are largely based on the sea ice models of Semtner (1976) and Maykut and Untersteiner (1971) for congelation ice representing the basic types (1) and (2), respectively. Later a snow-ice layer was added for subarctic seas (Saloranta 2000; Shirasawa et al. 2005). Turbulent air–ice heat transfer based on the Monin–Obukhov similarity theory was considered in Cheng (2002) and Cheng et al. 2003). Recent approach is a two-phase model, which includes porosity of ice for each grid cell and produces a realistic solution to ice deterioration in the melting season (Leppäranta 2009b).

Here we focus on the freshwater bodies. Saline lake ice models are similar apart from the salinity effects, which can be taken from the existing sea ice models. Since the length scale of heat diffusion in ice is less than 10 m in a year, lateral heat conduction is generally not an important issue, and numerical lake ice models are kept vertical. For freshwater lake ice, the thermal properties—density, specific heat and thermal conductivity—can be taken as constants for congelation ice and snow-ice layers. Optical properties—albedo and diffuse attenuation coefficient—however, undergo strong evolution in the melting season.

The first numerical models were based on the quasi-steady heat conduction law with time-dependent snow accumulation and heat flux from the water. Leppäranta (1983) employed a quasi-steady model to examine snow-ice formation and sensitivity of ice thickness and stratigraphy to thermal properties of snow. Later the quasi-steady approach was taken by Liston and Hall (1995) and Duguay et al. (2003).

Time-dependent models are a recent effort in lake ice modelling (Leppäranta and Uusikivi 2002; Yang et al. 2012, 2013), adapted from existing sea ice models (Maykut and Untersteiner 1971; Flato and Brown 1996; Saloranta 2000; Cheng et al. 2002, 2003).

These models solve the full time-dependent heat conduction equation. The advantages are that the temporal and vertical resolution can be taken in practice as high as desired, while in quasi-steady models they are limited by the time-scale of thermal diffusion.

The ice growth modelling problem possesses a negative feedback to errors. The background Stefan's law implies that the squared ice thickness is proportional to the freezing-degree-days S, and in the next step the sensitivity of model ice growth to temperature is

$$\delta h \sim \frac{a^2}{h}\delta S \tag{4.57a}$$

If the model ice thickness exceeds the observed level, the model ice grows then more slowly and returns towards the reality, and vice versa. Ice melting problem, on the other hand, possesses a positive feedback mechanism. In the next step, the sensitivity of ice melting to albedo is

$$\delta h \sim Q_s \delta \alpha \tag{4.57b}$$

When albedo begins to decrease the surface is transformed to absorb solar radiation better and produce more and more liquid water and consequently lower and lower albedo. Due to this reason the surface of a melting lake ice cover is patchy.

4.4.2 Quasi-steady Models

In the quasi-steady approach, the ice sheet is divided into n layers and the heat conduction is solved through all layers simultaneously. Whether we have cooling or warming depends on the boundary conditions, and the solution at each time step is iterated to satisfy the continuity of the heat flux. The system of equations is:

$$T_0 < T_f : \rho L_f \frac{dh}{dt} + Q_w = k\frac{T_f - T_{n-1}}{h_n} + q_{n-\frac{1}{2}} = \cdots = k\frac{T_1 - T_0}{h_1} + q_{\frac{1}{2}} \tag{4.58a}$$

$$T_0 = T_f : \rho L_f \frac{dh}{dt} = -(Q_w + Q_0 + Q_T) \tag{4.58b}$$

$$k\frac{T_1 - T_0}{h_1} = F(T_a, e_a, U_a, N, Q_s; T_0) \tag{4.58c}$$

where q_p's distribute the solar radiation penetrating into different ice layers. Equation (4.58c) gives the surface boundary condition in general form; the exact formulation is up to the modeller (see Sect. 4.1). The extremes are the full surface flux model or the linearized form with own parameters fixed for each time step.

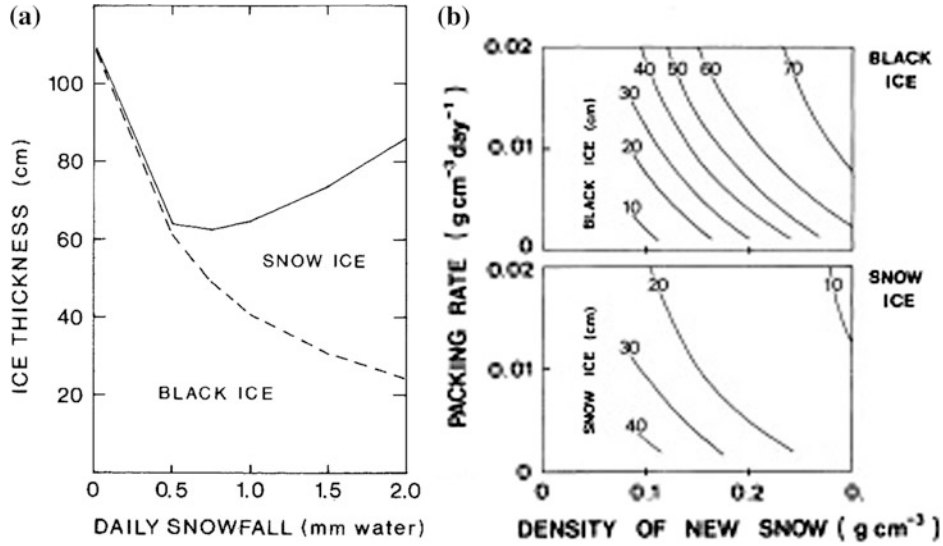

Fig. 4.11 **a** The thickness of congelation ice and snow-ice as a function of a fixed snow accumulation; **b** The thickness of congelation ice and snow-ice as a function of density of new snow and packing rate of snow. The air temperature corresponds to Oulu in the northern Finland (Leppäranta 1983)

When there is snow on the ice, its thickness and density need to be modelled. Snow accumulation is given in terms of water equivalent, and the thickness and density of new snow are obtained from $\rho_{s0} h_{s'} = \rho_w h_w$. The density of new snow is assumed or parameterized, the magnitude is $\rho_{s0} \sim 100$ kg m^{-3}. When the snow becomes older, its density increases due to snow metamorphosis, and old seasonal snow may reach densities of 400 kg m^{-3}. Thermal conductivity of snow is a sensitive function of density (see Sect. 3.2.3). The density change in snow due to compaction is formulated after Yen (1981) as

$$\frac{\partial \rho_s}{\partial t} = \rho_s C_1 V_s \exp\left[-\left(C_2 \rho_s + \frac{T_f - T_a}{12.5\,^{\circ}\mathrm{C}}\right)\right] \tag{4.59}$$

where $C_1 = 7.0$ m^{-1} h^{-1} and $C_2 = 21.0$ Mg^{-1} m^{-1} are empirical coefficients, and V_s is the volume of overlaying snow in equivalent thickness of water. A depth-dependent snow density profile due to snow compaction can be determined from this model.

Leppäranta (1983) used a three-layer (congelation ice, snow-ice and snow) model to examine the formation of snow-ice. A fixed packing rate with the upper limit of 450 kg m^{-3} for the snow density was assumed. Figure 4.11 shows the model outcome for the stratigraphy of the ice sheet and sensitivity of ice thickness to snow accumulation. The representative heat flux from the water was estimated from ice and atmosphere climatology.

4.4.3 Time-Dependent Models

Time-dependent models solve the heat conduction equation of the snow and ice layers for the evolution of temperature and thickness in a discrete grid or in a finite element system. Improvement as compared with quasi-steady models is the inclusion of thermal inertia that allows high vertical resolution in the simulations. Congelation ice models are based on the sea ice model of Maykut and Untersteiner (1971) and snow-ice models to Saloranta (2000). Numerical time-dependent lake ice models have been used mostly after the year 2000 (Leppäranta 2009). For Finnish lakes, the sea ice model of Saloranta (2000) was applied by Leppäranta and Uusikivi (2002), and the Baltic Sea model of Launiainen and Cheng (1998) and Cheng (2002) was applied by Yang et al. (2012).

The ice portion may have separate congelation ice and snow-ice layers, and the snow portion may have dry snow and slush layers (slush is understood as snow saturated with liquid water). At the upper boundary, the solar and terrestrial radiative fluxes and the turbulent heat fluxes are parameterized for weather data or taken from an atmospheric model. The surface temperature is solved from the surface energy balance that couples the ice sheet with the atmosphere (Eq. 4.58c). Snow thickness and density are modelled from precipitation, wind and temperature (see Eq. 4.57a, b). Formation of snow-ice is a source for the ice layer and sink for the snow layer. At the bottom of the ice sheet, the heat and mass balance are controlled by freezing and melting and heat flux from the water.

Time-dependent models have high vertical resolution (5–10 cm). 'High resolution' refers to the requirement that daily cycles in the temperature evolution can be resolved. The time scale of heat diffusion in ice is $\tau \sim L^2/D = 10\,(L/\mathrm{m})^2$ day, where D is the heat diffusion coefficient and L is the vertical length scale. For $L \sim 0.1$ m, we have $\tau \sim 0.1$ day, which is approximately the time-step needed for daily cycles in numerical modelling.

The full model simulates the development of four distinct layers: snow, slush, snow-ice and congelation ice. These layers interact in a dynamic way: snow accumulation creates slush and snow-ice depending on the total thickness of ice, while the growth and decay of congelation ice depend on the snow and slush conditions. Slush and snow-ice may form a multiple layer structure with alternating layers of snow-ice and slush. The thickness of snow decreases due to three different reasons: surface melting, compaction, and freezing of slush into snow-ice.

The core of time-dependent lake ice thermodynamics models consists of the classical 1-d heat conduction equation:

$$\frac{\partial}{\partial t}(\rho c T) = \frac{\partial}{\partial z}\left[\kappa \frac{\partial T}{\partial z} - Q_s(z)\right] \tag{4.60}$$

The thermal properties of ice vary in different layers in the ice sheet. For freshwater ice, this is a simple linear equation to solve numerically, and the main difficulties are in the treatment of the moving boundaries with mass and heat fluxes across. In saline ice,

however, care should be taken with parameterization of the thermal properties when the ice approaches the melting stage.

A typical grid size in numerical models has been 5 cm. Both the upper and lower surfaces move due to ice growth and melting that need to be considered in the top and bottom grid cells. The upper boundary is strongly dependent on the atmospheric conditions so that the surface temperature can be best solved with a coupled ice–atmospheric boundary layer model (Cheng 2002). For a strongly stable atmospheric surface layer, the heat transfer is tough to solve (Yang et al. 2013). The boundary conditions are given in general form as

$$z = h_0 : \frac{dh_0}{dt} = \frac{\rho_w}{\rho_{s0}} P - \frac{\rho_w}{\rho_0} E + \frac{1}{\rho L}\left(Q_0 + \kappa \frac{\partial T}{\partial z}\right); \kappa \frac{\partial T}{\partial z} = Q_0 \tag{4.61a}$$

$$z = h_b : \frac{dh_b}{dt} = \frac{1}{\rho L}\left(Q_w + \kappa \frac{\partial T}{\partial z}\right); \; T = T_f \tag{4.61b}$$

where ρ_{s0} is the density of new snow and ρ_0 is the density at the surface. The thickness of snow increases due to snowfall, given as the water equivalent into the model and changed to snow thickness using a fixed density of new snow, and decreases due to sublimation and melting. The threshold value between snow and no-snow conditions is a model parameter, e.g. 3 cm in Saloranta (2000).

Slush formation in the snow layer is technically straightforward to model. Flooding is assumed to follow from Archimedes law, i.e. lake water is let to penetrate the ice as soon as the ice surface level is beneath the lake water level. A threshold snow overload can be specified for a flooding event to begin. The proportion of snow crystals in water-saturated snow is assumed to rise to 50 %. When negative freeboard conditions appear, the amount of new slush is calculated from

$$\begin{aligned} \frac{\partial h_{sh}}{\partial t} &= \frac{1}{\rho_w + \rho_s - \rho_{sh}} \frac{\partial}{\partial t}(\rho_w V_s - B) \\ B &= h_{\mathrm{i}}(\rho_{\mathrm{w}} - \rho_{\mathrm{i}}) + h_{\mathrm{si}}(\rho_{\mathrm{w}} - \rho_{\mathrm{si}}) + h_{\mathrm{sh}}(\rho_{\mathrm{w}} - \rho_{\mathrm{sh}}) \end{aligned} \tag{4.62}$$

The product gB is the buoyancy of ice, snow-ice and old slush layers. Liquid precipitation is obtained from the forcing assuming that precipitation is liquid when the air temperature is above a given limit, e.g. $T_{\mathrm{a}} > 1°\mathrm{C}$. Melt water of snow comes from the model directly. This approach for snow-ice formation was taken by Saloranta (2000), used for lake ice by Leppäranta and Uusikivi (2002).

At the bottom of the ice sheet, the heat balance is determined by phase changes, conductive flux of heat into the ice sheet and the transfer of heat from the water column (see Sect. 4.2.2). The heat flux is formally written

$$Q_w = k_w \frac{\partial T}{\partial z} \tag{4.63}$$

In the case of laminar flow, molecular conductivity of water is used, k_w = 0.6 W/(m °C). If the flow is in the laminar—turbulent transition regime, molecular conductivity is replaced by effective thermal conductivity (Petrov et al. 2006; Shirasawa et al. 2006). An other way to express the heat flux is the bulk formula $Q_w = \rho_w c_w C_{Hw}(T_w - T_b)U_w$, where C_{Hw} is the heat exchange coefficient, and T_w and T_b are water temperature and ice bottom temperature.

As an example, a numerical modelling study of the ice cover in Lake Vanajavesi, southern Finland, is presented (Yang et al. 2012). The thermodynamics model HIGHTSI (Cheng 2002) was used for an individual ice season 2008–2009 and for the climatological period 1971–2000 with good calibration data. The novel model features were advanced treatment of superimposed ice and turbulent heat fluxes, coupling of snow and ice layers, and snow modelled from precipitation.

The model solves the surface temperature T_0 from a detailed surface heat balance. Solar radiation is strongly attenuated along the vertical depth immediately below the surface (Grenfell and Maykut 1977), and part of the radiation is taken to contribute to the surface heat balance. The level of this contribution depends on the quality of the surface layer, i.e. the first layer of snow or ice in model (Launiainen and Cheng 1998; Cheng 2002; Cheng et al. 2008). The albedo is critical for snow and ice heat balance. A parameterization suitable for the Baltic Sea coastal snow and land-fast ice was selected (Pirazzini et al. 2006):

$$\begin{aligned}
&\alpha = 0.15, h_i < 0.1 \text{ cm} \\
&\alpha = \min\left[\alpha_s, \frac{h_i}{0.1 \text{ cm}} \cdot (\alpha_i + \alpha_s)\right], h_i \geq 0.1 \text{ cm and } h_s \leq 10 \text{ cm} \\
&\alpha = \alpha_s, h_i \geq 0.1 \text{ cm and } h_s > 10 \text{ cm}
\end{aligned} \tag{4.64}$$

where α_s and α_i are the snow and ice albedo, respectively, taken as $\alpha_s = 0.75, \alpha_i = \min\left[0.55, 0.85 h_i^{1.5} \text{cm}^{-1.5} + 0.15\right]$. The surface turbulent heat fluxes were parameterized using the Monin–Obukhov similarity theory, and snow cover evolution was modelled as discussed above. The temperature criterion of T_a < 0.5 °C was set to decide when the precipitation is assumed solid.

The integral interpolation method was applied to build up the numerical scheme (Cheng 2002). A high spatial resolution (10 layers in snow and 20 layers in ice) ensures that the high frequency response of the snow and ice temperature to forcing and the distribution of the absorption of solar radiation near the surface are correctly resolved. The model parameters for this study are summarized in Table 4.3. The freezing date is provided as the initial condition by a thin ice layer (2 cm). The first day when the ice starts to grow successively is defined as the freezing date. This is a crude approximation, as the

Table 4.3 HIGHTSI model parameters

Parameter	Value	Source
Light attenuation coefficient of lake ice	1.5–17 m^{-1}	Heron et al. (1994), Arst et al. (2006), Lei et al. (2011)
Light attenuation coefficient of snow	6–20 m^{-1}	Patterson et al. (1988), Arst et al. (2006), Lei et al. (2011)
Lake ice density	910 kg m^{-3}	Corresponds to 1 % gas content
Initial snow density	330 kg m^{-3}	Assumed
Surface emissivity	0.97	Vihma (1995b)

model has no active water layer beneath the ice, but once the ice growth has started the model catches up well with the nature.

The results were good (Figs. 4.12 and 4.13). Modelled ice climatology showed growth by 0.5 cm day^{-1} in December–March and 2 cm day^{-1} melting in April. Tuned heat flux from the water to ice was 0.5 W m^{-2}. The diurnal weather cycle gave significant impact on the thickness of ice in spring. Ice climatology was highly sensitive to snow conditions, and surface temperature showed strong dependency on thickness of thin ice (<0.5 m). The lake ice season responded strongly to air temperature: a level increase by 1 or 5 °C decreased the mean length of the ice season by 13 or 78 days (from 152 days) and the thickness of ice by 6 or 22 cm (from 50 cm), respectively.

In fact, the fit of such model simulations largely depends on the quality of the forcing data and the sub-model for air–ice interaction. The annual cycle of the change in ice thickness is well represented by the model and demonstrates that the model can be used to simulate the evolution of the ice sheet under a range of meteorological conditions. The weakest components of the model appear to be snow formulation together with the onset of melting, which need further testing with winter seasons of varying snow conditions.

Internal melting is an important process in the melting season. The implications are that the physical properties of the ice sheet change, first of all the strength of the ice strongly decreases, and liquid water pockets form serving as habitats for biota. To properly treat the internal melting necessitates the inclusion of the ice porosity as a dependent model variable. This approach was taken by Leppäranta (2009b), who considered a two-phase approach with liquid phase and solid phase portions given for each grid cell in addition to the temperature (Fig. 4.14). When the temperature reaches the freezing point, additional heat adds on the porosity. At freezing point and zero porosity, heat loss takes the temperature below the freezing point. A realistic structural profile was obtained with locations of liquid water containing layers. In the case of brackish or saline ice, the same approach works but then the porosity changes at any temperature due to equilibrium requirement for the salinity of brine (see Maykut and Untersteiner 1971).

In the two-phase model the phase proportions are simulated for each grid cell in addition to the temperature. The melting season begins after the heat balance has turned positive. Once the temperature of the ice-sheet reaches the melting point, melting takes

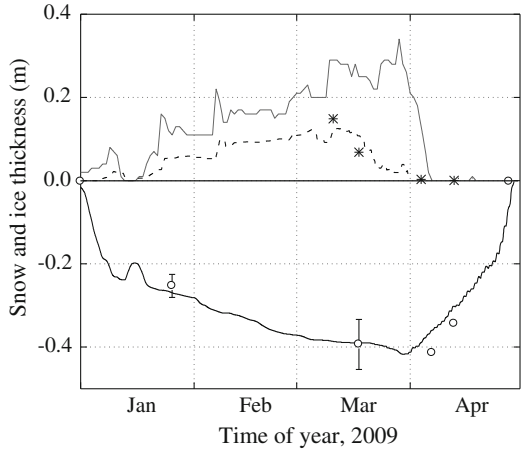

Fig. 4.12 Time series of observed and modelled snow (positive) and ice (negative) thickness in Lake Vanajavesi. The *dark grey line* and the *asterisk* are the observed snow thickness in Jokioinen and on Lake Vanajavesi, respectively. The *circles* are the observed average ice thickness and the spatial standard deviation is indicated by the *vertical* bar. Modelled snow thickness is the dashed line and modelled ice thickness is the black line. The heat flux from water is 0.5 W m^{-2} (Yang et al. 2012)

place at the boundaries by positive net surface fluxes and by the absorption of solar radiation inside the ice sheet. Internal melting gives rise to structural defects and once the porosity of the ice reaches 0.3–0.5, the ice cannot bear its own weight, breaks into smaller pieces into the water, and a rapid increase in the rate of decay follows. In warm ice and snow liquid water inclusions co-exist with the solid-state ice crystals. The ice and snow cover becomes a two-phase system, where the proportions of the solid and liquid phases change according to heat fluxes. The properties of this system also change with the phase proportions.

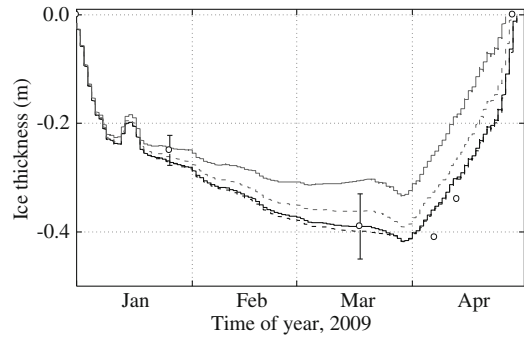

Fig. 4.13 Time series of observed and simulated ice thickness based on varying heat flux from water: 0 W m^{-2} (*black dashed*), 0.5 W m^{-2} (*black solid*), 2 W m^{-2} (*grey dashed*) and 5 W m^{-2} (*grey solid*). Measurements of ice thickness are shown as in Fig. 4.12 (Yang et al. 2012)

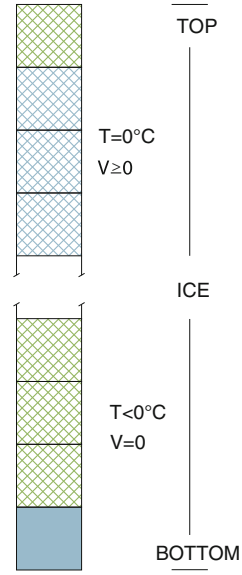

Fig. 4.14 A two-phase model grid for the freshwater lake ice model. In each grid cell the temperature (T) and porosity (v) are determined; if temperature is below the freezing point, the porosity is kept zero, and at the freezing point temperature is fixed but porosity changes

The model is based on the heat conduction law with solar radiation as the source term and ice growth and melting resulting from phase changes. In general, a volume element in ice sheet contains ice and liquid water. The differential heat content dE across a differential depth dz is

$$\mathrm{d}E = \rho L_{\mathrm{f}} v \mathrm{d}z + \rho c(1-v)T\mathrm{d}z \tag{4.65}$$

where v is the liquid water content (essentially the porosity of ice). We may assume the following. When the temperature is below the freezing point, the liquid water content is zero and heat gains and losses are reflected in the temperature; and when the temperature is at the freezing point, the liquid water content is positive and heat gains and losses are reflected in the porosity. Consequently, the model physics can be presented by:

$$T < T_f : \rho c \frac{\partial T}{\partial t} = q_I, v = 0 \tag{4.66a}$$

$$T = T_f \text{ and } v = 0 : \rho L_f \frac{dv}{dt} = \max(0, q_I), \rho c \frac{\partial T}{\partial t} = \min(0, q_I) \tag{4.66b}$$

$$T = T_f \text{ and } v > 0 : \rho L_f \frac{dv}{dt} = q_I \tag{4.66c}$$

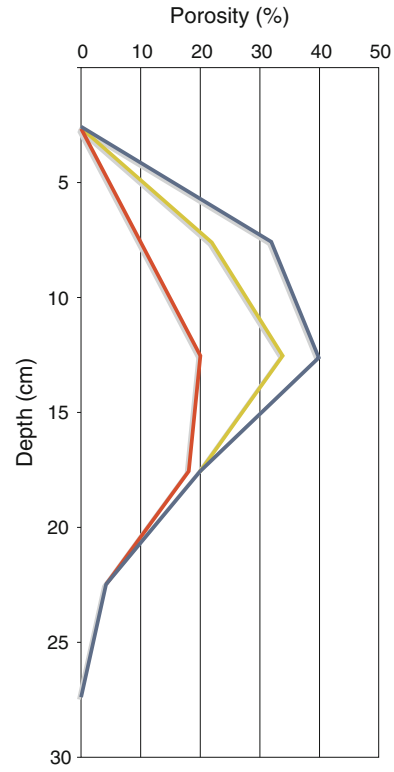

Fig. 4.15 A two-phase model outcome. The *lines* show evolution of ice porosity in the ice cover, peaking at 10–15 cm depth

$$q_I = \frac{\partial}{\partial z}\left(\kappa \frac{\partial T}{\partial z} - Q_s\right) \tag{4.66d}$$

The boundary conditions are similar to those in the classical models and positive boundary heating decreases the thickness of ice. Absorption of sunlight decreases with depth but surface heat balance tends to be negative due to terrestrial radiation losses and sublimation. As a result, the porosity will have a maximum beneath the surface, typically at 10–20 cm depth (Fig. 4.15).

In the two-phase model slush layers are well reproduced and the physical representation of melting ice is realistic. Also a mechanical model can be added to examine the breakage of ice, which is a critically important factor to the character of lake ice seasons. Mechanical problems have not been much discussed in the lake ice seasonal models, although mechanical events are thickness and ice quality dependent and therefore sensitive to climate variations. If the modelled ice structure evaluation is correct, better estimates for ice loads and bearing capacity are obtained, ice breakup comes correctly, and realistic locations of biological habitats are seen in the ice sheet.

Mechanics of Lake Ice

5

An ice road across Lake Pielinen in northeast Finland, between the villages Vuontislahti and Koli. This is one of the longest ice roads in Europe, about eight kilometres. Since the lake is 90 km long, the ice road makes a major shortcut to driving distances. Traffic rules give the maximum weight and speed of cars, and the minimum distances between cars, depending on the thickness of ice. Also cars are not allowed to pass or stop.

Photograph by Ms. Maritta Räsänen, Pohjois-Savo Centre for Economic Development, Transport and the Environment, Kuopio. Printed with permission.

M. Leppäranta, *Freezing of Lakes and the Evolution of their Ice Cover*,
DOI 10.1007/978-3-642-29081-7_5

5.1 Rheology

The science of *rheology* examines the relationships between the internal stress, mechanical deformation, and material properties of media. Material properties are such as density, temperature and porosity, while deformation is specified by strain and its time history.

The present chapter begins with a general introduction into rheology. There are two principal reasons for going to the basics. First, natural ice has quite complicated rheology, and, secondly, for students and scientists in lake physics or limnology, rheological questions are not so familiar, because lake water is a linear Newtonian fluid, and its mechanics obeys the well-established Navier–Stokes equation. Natural lake ice is a polycrystalline medium, and its mechanical behaviour depends on the time and space scales under consideration.

In mechanics, lake ice sheet is normally considered as a continuum. The basic rheology models—elastic, viscous, and plastic media—are all applicable in lake ice processes. For a continuous sheet of polycrystalline ice, the size, shape and orientation of ice crystals and the impurities between crystals influence on the mechanical properties. In the case of *broken ice*, i.e. the ice cover consists of ice blocks or floes (Fig. 5.1), the granular medium approach is taken where individual blocks or floes represent the individual 'grains'. When the number of grains is large, a continuum approximation can be taken for length scales much longer than the grain size. Important applications of granular models are mechanics of ridge formation from ice blocks and drifting of ice floes on a lake surface.

Mechanics is treated here in the three-dimensional space. The Cartesian co-ordinates are (x, y, z), with here x directed east, y directed north, and z directed up. The corresponding unit vectors are denoted by $\mathbf{i}$, $\mathbf{j}$ and $\mathbf{k}$. The gradient operator is in the Cartesian system $\nabla = \mathbf{i}\partial/\partial x + \mathbf{j}\partial/\partial y + \mathbf{k}\partial/\partial z$. Furthermore, we deal with three different mathematical quantities: *scalars* are numbers, *vectors* have magnitude and direction, and (*2nd order*) *tensors* have vector components on all the three coordinate planes. In the Cartesian system, tensors can be represented as matrixes.

Fig. 5.1 Solid ice sheet and broken ice on lakes

5.1.1 Stress

Consider a material sample of a continuum (Fig. 5.2). An internal stress field $\boldsymbol{\sigma}$ exists within the sample depending on the external loading and the mechanical properties of the medium. The stress provides the distribution of forcing on surfaces of infinitesimal volume elements in the sample; the dimension of stress is force per area. For an arbitrary unit surface with unit normal $\boldsymbol{n}$, the stress acts as a force vector $\boldsymbol{\sigma} \cdot \boldsymbol{n}$, which consists of the shear stress—the projection parallel to the surface—and the normal stress—the projection to the surface normal. Stress is thus a 2nd order tensor. In three-dimensional space, there are three independent surface orientations and three independent vector directions. Therefore, the stress tensor is given by $3 \times 3 = 9$ components (Fig. 5.2). In Cartesian form:

$$\sigma = \begin{bmatrix} \sigma_{xx} & \sigma_{xy} & \sigma_{xz} \\ \sigma_{yx} & \sigma_{yy} & \sigma_{yz} \\ \sigma_{zx} & \sigma_{zy} & \sigma_{zz} \end{bmatrix} \tag{5.1}$$

The diagonal components are the *normal* (*compressive or tensile*) *stresses* and the off-diagonal components are the *shear stresses*. The component σ_{xx} gives the normal stress in x-direction, the component σ_{yx} gives the shear stress across y-axis in the x-direction, etc. The stress tensor is necessarily *symmetric*, since otherwise there would be net internal torques, which would not disappear when the particle size approaches zero (e.g., Hunter 1976). Thus $\sigma_{xy} = \sigma_{yx}$, $\sigma_{xz} = \sigma_{zx}$ and $\sigma_{yz} = \sigma_{zy}$ that reduces the number of independent stress components to six.

The stress tensor can be uniquely decomposed into spherical and deviatoric parts σ_S and σ', respectively, by

$$\boldsymbol{\sigma} = \sigma_S \mathbf{I} + \boldsymbol{\sigma}'; \ \sigma_S = \frac{1}{3}\mathrm{tr}\boldsymbol{\sigma} \tag{5.2}$$

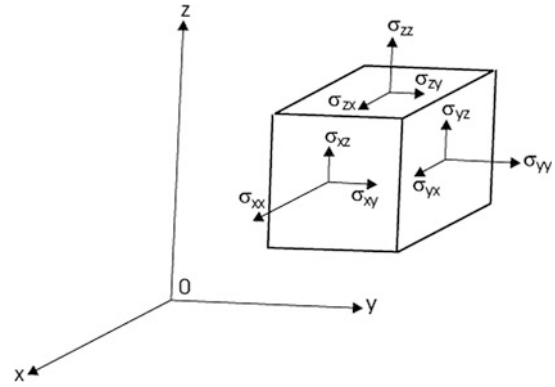

Fig. 5.2 Stress $\boldsymbol{\sigma}$ on material element

where $\mathbf{I}$ is the unit tensor, I_{pq} = 1 (0) for p = q (p ≠ q), and tr is the trace operator. For a matrix $\boldsymbol{A} = (A_{pq})$, $\mathrm{tr}\boldsymbol{A} = A_{xx} + A_{yy} + A_{zz}$. In Eq. (5.2), the factor 1/3 comes from the three-dimensionality; in two-dimensional theory the factor is ½. The eigenvalues of $\boldsymbol{A}$ are the solutions (λ) of the eigenvalue equation $\det(\boldsymbol{A} - \lambda\mathbf{I}) = 0$, and the corresponding eigenvectors $\boldsymbol{\Lambda}$ are the solutions of $(\boldsymbol{A} - \lambda\mathrm{I})\boldsymbol{\Lambda} = \mathbf{0}$. The eigenvalues of the stress tensor are called the principal stresses, and the eigenvectors give the directions of these stresses.

Example 5.1. Hydrostatic pressure is a stress $\boldsymbol{\sigma} = -p\mathbf{I}$, where $p > 0$ is scalar pressure. It is spherical with $\sigma_S = -p$, compressive (i.e. $\sigma_S < 0$), and in any direction, $\boldsymbol{\sigma} \cdot \mathbf{n} = -p\mathbf{n}$. In lake water, $p = p_a + \rho_w g D$, where p_a is the surface atmospheric pressure and D is the depth. At D = 10 m, $p = 2p_a$, i.e. each 10 m of water adds the pressure equivalent to one atmosphere to the total.

5.1.2 Strain and Rotation

The techniques to describe deformation are given in books on continuum mechanics (e.g., Mase 1970; Hunter 1976). A brief summary is presented here. Let $\boldsymbol{x}$ stand for the reference configuration of a material body, and consider a change of the body to $\boldsymbol{X}$, represented by a mapping $\boldsymbol{x} \rightarrow \boldsymbol{X}$. The *displacement* $\boldsymbol{d} = \boldsymbol{X} - \boldsymbol{x}$ consists of translation, rotation and strain. Translation and rotation correspond to rigid body motion, while strain corresponds to physical deformation of the body. Strain and rotation are included in the *displacement gradient* $\nabla\boldsymbol{d}$. For small deformations ($|\nabla\boldsymbol{d}| \ll 1$), the linear theory is employed. Then the strain $\boldsymbol{\varepsilon}$ and the rotation $\boldsymbol{\omega}$ are given by the symmetric and anti-symmetric parts, respectively, of the displacement gradient:

$$\boldsymbol{\varepsilon} = 1/2[\nabla\boldsymbol{d} + (\nabla\boldsymbol{d})^{\mathrm{T}}] \tag{5.3a}$$

$$\boldsymbol{\omega} = 1/2[\nabla\boldsymbol{d} - (\nabla\boldsymbol{d})^{\mathrm{T}}] \tag{5.3b}$$

where the superscript T stands for the transpose. Rotation has three independent components, which give the rotations of the body around the co-ordinate axes (Fig. 5.3). Strain is symmetric and possesses six independent components, three representing the normal strains and three representing the shear strains analogous with the stress components.

A rotation of 1 % corresponds to turning of the body by 0.01 rad ≈ 0.573°. There are two modes of strain: normal strain and shear strain (Fig. 5.3). Inversely, any physical deformation of a body can be decomposed into normal and shear strains. Normal strain is extensive (positive) or contractive (negative), while shear strain changes the shape of particles. A tensile/compressive strain of 1 % means that the corresponding material dimension has lengthened/shortened by 1 %, and a shear strain of 1 % means that a right angle in the material configuration has changed by 0.01 rad ≈ 0.573º.

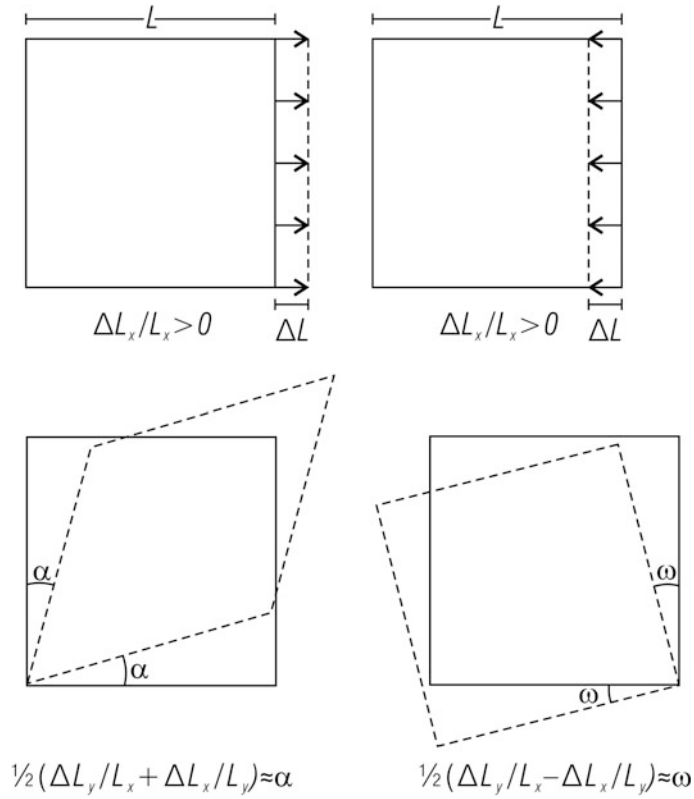

Fig. 5.3 Strain modes and rotation, and their measures: *upper graphs*, extension and contraction; *lower graphs*, shear and rotation. Note that shear and rotation are drawn for positive signs

Example 5.2. *Simple shear* is given by $\frac{\partial d_x}{\partial y} \neq 0$, with other displacement derivatives equal to zero. Then the *xy* shear strain is $\frac{1}{2}\frac{\partial d_x}{\partial y}$ and the rotation around *z*-axis is $-\frac{1}{2}\frac{\partial d_x}{\partial y}$. In *pure shear*, we have $\frac{\partial d_x}{\partial y} = \frac{\partial d_y}{\partial x} \neq 0$, with other displacement derivatives equal to zero. Then the *xy* shear strain is $\frac{\partial d_x}{\partial y}$ and the rotation is zero. In both cases the spherical strain is zero ($\mathrm{tr}\boldsymbol{\varepsilon} = 0$).

Velocity equals the rate of displacement, and consequently the strain-rate and the rotation rate or the vorticity are obtained from the velocity gradient just as strain and rotation were obtained from the displacement gradient.

5.1.3 Rheological Models

The basic models are *linear elastic* or *Hooke's medium*, *linear viscous* or *Newton's medium*, and *ideal plastic* or *St. Venant's medium* (e.g., Mase 1970; Hunter 1976). One-

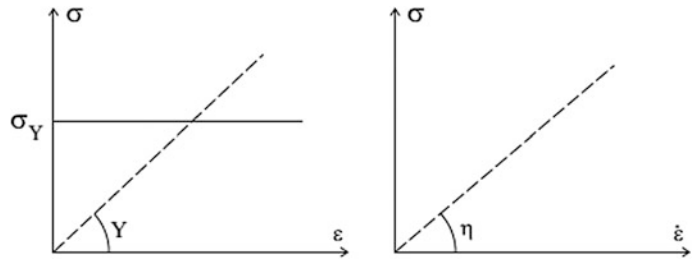

Fig. 5.4 The basic rheology models (in one dimension) for the stress σ as a function of the strain ε and the strain-rate $\dot{\varepsilon}$; E is elastic modulus, η is viscosity, and σ_Y is yield strength

dimensional cases are illustrated in Fig. 5.4. The linear elastic model assumes that stress is proportional to strain, while in the linear viscous model stress is proportional to the strain-rate; the proportionality coefficients are, respectively, the elastic modulus (or Young's modulus) and viscosity. Rubber and water[1] are good material examples of linear elastic and viscous media. An ideal plastic medium collapses once the stress achieves yield strength (children's modelling wax serves as an example of a plastic medium). Mechanical analogues for these models include spring balance for linear elasticity, dashpot[2] for linear viscosity, and static friction for plasticity.

The behaviour of a one-dimensional linear elastic beam is determined by Young's modulus E:

$$\sigma = E\varepsilon \tag{5.4}$$

Thus Young's modulus appears as the slope angle in Fig. 5.5. For an isotropic three- (or two-) dimensional case, one additional parameter is required for shear. Usually this is treated using the Poisson's ratio μ. For a beam in uniaxial (x) tension, tensile strain ε_{xx} is seen in the loading direction but contraction appears in the perpendicular directions, and the Poisson's ratio is:

$$\mu = -\frac{\varepsilon_{yy}}{\varepsilon_{xx}} = -\frac{\varepsilon_{zz}}{\varepsilon_{xx}} \tag{5.5}$$

Once Young's modulus and Poisson's ratio are known, the bulk modulus K and the shear modulus G are obtained as:

$$K = \frac{E}{3(1-2\mu)},\ G = \frac{E}{2(1+\mu)} \tag{5.6}$$

Linear elastic rheology is written in three-dimensional form as

[1] In laminar flow; in turbulent flow stresses are properties of the flow, not properties of the medium.

[2] Such as a door stroke compressor, which dampens or softens the movements of a door.

$$\boldsymbol{\sigma} = \frac{E}{1+\mu}\left[\boldsymbol{\varepsilon} + \frac{\mu}{1-2\mu}(\mathrm{tr}\boldsymbol{\varepsilon})\mathbf{I}\right] = K(\mathrm{tr}\boldsymbol{\varepsilon})\mathbf{I} + 2G\left[\boldsymbol{\varepsilon} - \frac{1}{3}(\mathrm{tr}\boldsymbol{\varepsilon})\mathbf{I}\right] \tag{5.7}$$

In isotropic media, the principal axes of the stress and strain tensors are parallel. In two-dimensional case, in the last term $^1/_2$ is taken instead of $^1/_2$.

In a viscous medium, the stress depends on the rate of strain, and the linear viscous rheology is as Eq. (5.7) with $\boldsymbol{\varepsilon}$ replaced by the strain-rate $\dot{\boldsymbol{\varepsilon}}$. The basic case is the simple shear flow $\boldsymbol{u} = u(y)$, where the viscous stress is proportional to the rate of shear strain, and the proportionality coefficient is the viscosity η:

$$\sigma_{xy} = 2\eta\dot{\varepsilon}_{xy} = \eta\frac{du}{dy} \tag{5.8}$$

For compressible fluids, a second viscosity or bulk viscosity (ζ) is added to account for spherical stresses:

$$\boldsymbol{\sigma} = \zeta(tr\dot{\boldsymbol{\varepsilon}})\boldsymbol{I} + 2\eta\left[\dot{\boldsymbol{\varepsilon}} - \frac{1}{3}(tr\dot{\boldsymbol{\varepsilon}})\boldsymbol{I}\right] \tag{5.9}$$

In ice applications, non-linear viscous rheologies are used, obtained from Eq. (5.9) by allowing the viscosities to depend on the invariants of the strain-rate tensor.

An ideal plastic medium fails at yield stress. In one dimension,

$$\varepsilon = 0, \sigma < \sigma_Y; \varepsilon \neq 0, \sigma = \sigma_Y \tag{5.10}$$

where σ_Y is the yield stress. In two (three) dimensions, the yield point is replaced by a yield curve (yield surface), which describes the yield stress as a function of strain invariants. At yield, the actual strain evolution depends on inertia and external forces acting on the system. In stable plastic medium strain hardening takes place. The yield strength increases under strain, and more stress is needed for further deformation. To continue the modelling wax example, more and more force would be needed to make a wax ball smaller, and therefore for a constant load a stationary steady state results. In unstable plastic medium strain softening takes place, and even if forcing is lowered the strain may continue.

Basic rheological models can be expanded for more complex ones (e.g., Mellor 1986). First, linearities can be changed to general non-linear laws in the elastic and viscous models. Second, models can be combined. E.g., linear elastic and linear viscous models in series give the Maxwell medium, while combining them parallel gives the Kelvin–Voigt medium. For a constant load, Maxwell medium has an immediate elastic response followed by linear viscous flow, while a Kelvin–Voigt medium flows in a viscous manner toward an asymptotic determined by the elastic part.

The strength is defined as the maximum stress a test specimen can support, and it depends on the mode of deformation and the mode of failure. In brittle failure the specimen breaks but in ductile failure the strain increases in the specimen with no increase in the stress. Usually the former deals with fast loading cases when the response is elastic, while the latter concerns long-term viscous or plastic flow. The general equation of motion of a continuum is the Cauchy equation (Hunter 1976):

$$\rho \frac{D\boldsymbol{u}}{Dt} = \nabla \cdot \sigma + \sum\nolimits_l \boldsymbol{F}^{(l)} \tag{5.11}$$

where $\frac{D}{Dt} = \frac{\partial}{\partial t} + \boldsymbol{u} \cdot \nabla$ is the material time derivative consisting of the local change and advection, and $\boldsymbol{F}^{(l)}$'s are the external forces. In a static situation, the left hand side is zero.

In the next section the mechanical properties of lake ice are briefly presented. The discussion is limited to the general level, without details of experimental techniques, which are well covered in engineering literature (e.g., Michel 1978; Ashton 1986). The goal is to provide the essential information of the mechanical properties of lake ice and their variability. The information is based on laboratory experiments with ice samples, in situ field tests, rheological models, and semi-empirical equations for the ice properties. In the recent decades there has been more work done on the mechanical properties of sea ice that also can be utilized for lake ice applications (e.g., Mellor 1986; Sanderson 1988; Palmer and Croasdale 2012).

Lake ice sheet is considered as a polycrystalline continuum, and the relatively large variability of its mechanical properties comes from large crystal size, high homologous temperature, and impurities. In addition, test arrangements and the sizes of ice specimens have caused artificial variability. Isotropy is normally assumed, although columnar ice, which is a common ice type in lakes, has strong anisotropy between vertical and horizontal in the crystal structure (see Sect. 3.2). Granular ice is isotropic. Lake ice lies on water foundation, where the water pressure at the ice bottom is ρgh, which is balanced by the weight of ice. For small vertical displacements (ice is neither submerged nor raised out of water), the response of the foundation is proportional to the displacement. This behaviour is analogous to elasticity, and therefore the theory of plate on elastic foundation can be utilized for the mechanics of floating ice. In situ field tests have the great advantage that ice can be loaded in natural conditions with the bottom at the melting point.

5.2 Ice Cover as a Plate on Water Foundation

5.2.1 Elastic Lake Ice Cover

In short-term loading, ice shows elastic behaviour (Michel 1978; Ashton 1986). Short term refers here to the time scales of the order 100 s or less. In very short time scale (seconds) ice is perfectly elastic–brittle material, where it cracks once the strength limit

has been reached. Longer-term response is elastic-plastic, where the ice yields after having reached the strength level.

The elastic parameters of lake ice depend on the temperature, gas content, size and shape of crystals, and impurities. Based on experimental data, the standard references for isotropic lake ice are Young's modulus $E = 9.0$ GPa and Poisson's ratio $\mu = 0.33$ (Ashton 1986). The bulk modulus and shear modulus are then $K = 0.98\ E$ and $G = 0.38\ E$. Assumption for isotropy is widely used, and experimental data show that the variations in Young's modulus and Poisson's ratio are within 0.5 GPa and 0.015 or 5 % from the standard values. The elastic model is valid up to the strength of the ice.

The strength is the fundamental quantity to evaluate ice loads, bearing capacity of ice, and the stability of ice cover. In the elastic regime, the brittle strength of ice is of the order of 1–10 MPa, depending on the mode of loading (Table 5.1).

Table 5.1 Elastic modulus and strength of freshwater ice

	Modulus (GPa)	Strength (MPa)	Strain at breakage
Compression	9.0	10	1.1×10^{-3}
Tension	9.0	1.5	0.17×10^{-3}
Shear	3.4	1.0	0.29×10^{-3}

The maximum strain at failure is strength/modulus $\sim 10^{-3}$. The flexural strength of lake ice is 1.5 MPa (e.g., Weeks 1998). Flexural strength can be measured in situ and therefore it is a good reference for the strength of floating ice.

The brittle compressive strength of lake ice is about 10 MPa at the temperature of –10 °C (Ashton 1986). This holds for all congelation ice, snow ice and frazil ice. Ductile strength is less than the brittle strength and decreases with strain-rate, reaching 1 MPa at the strain-rate of $10^{-7}\ \mathrm{s}^{-1} \sim 10^{-3}\ (3\ \mathrm{h})^{-1}$. Strength increases with decreasing temperature, and the brittle compressive strength is 20 MPa at temperatures of about –30 °C. In various tests, at a fixed temperature and strain-rate, the strength has varied by a factor of two. For compressive strength borehole tests have been made with a cylindrical pressure meter.

Michel (1978b) has presented a semi-empirical model for the uniaxial compressive brittle strength of lake ice:

$$\sigma_c[\mathrm{Pa}] = 9.4 \times 10^4 (d[\mathrm{m}]^{-1/2} + 3|T[^\circ\mathrm{C}]|^{0.78}) \tag{5.12}$$

where d is grain size and the units of the quantities are given in brackets. The compressive strength ranges then within about 1–10 MPa. Multi-axial tests have indicated higher strength values.

Tensile strength depends primarily on the grain size and less on the temperature (Ashton 1986). Also it is not sensitive to the strain-rate. The level of brittle tensile strength has been 1–2 MPa in experimental data. Shear is a special case of multi-axial loading

(two principal stresses have equal magnitude and opposite signs). Shear strength depends primarily on the loading rate and not much on the temperature, and the test results are mostly in the range 0.5–1.5 MPa.

A convenient reference of strength of floating ice is the flexural strength, because in situ tests can be easily performed in the specific natural temperature conditions (Weeks 1998). The bottom temperature of ice is at the freezing point of the lake water, while the surface temperature can be much lower, and therefore a steep temperature gradient would be present. In laboratory tests such conditions cannot be reproduced. The flexural strength is about 1.5 MPa. In comparison with fresh water ice, Young's modulus and compressive strength are one order of magnitude larger for wood and two orders of magnitude larger for steel. There is not much data available on the strength of porous lake ice, but we can gain understanding on this from the results of sea ice investigations. As shown by Weeks (1998), the strength drops by one order of magnitude when the brine volume (ν_b) increases from $\nu_b = 0$ to $\nu_b = 0.15$ (Fig. 5.5). The brine content is highly sensitive to temperature in warm ice.

5.2.2 Viscous Behaviour of Lake Ice

When the time scale of loading is more than the order of 100 s and the stresses are below the brittle strength of ice, viscous behaviour results. This can be observed in the flow of glaciers and ice sheets (e.g., Paterson 1999). The viscous regime is much more complicated than the elastic regime. Experiments of viscous ice flow are usually made by monitoring the deformation of the test specimen at a constant load. The strain history undergoes three consecutive regimes (Fig. 5.6). In primary creep (I) the ice is hardening, while in tertiary creep (III) the ice start to fail into an accelerating strain. Between them there is a linear regime (II). The strain inflection point is at about 1 %-strain level in the secondary creep stage (Ashton 1986; Mellor 1986). The viscosities and the time scales of the regions depend strongly on the ice temperature (Table 5.2).

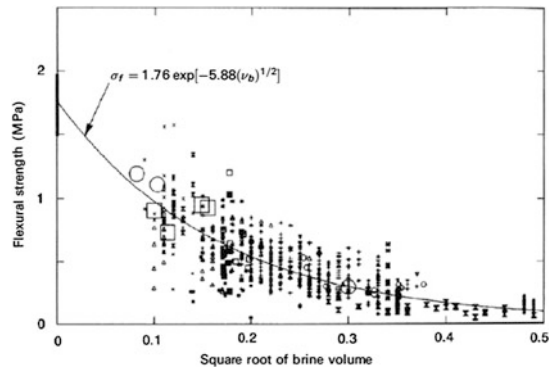

Fig. 5.5 Flexural strength of sea ice as a function of brine content (ν_b). Reproduced from Weeks (1998)

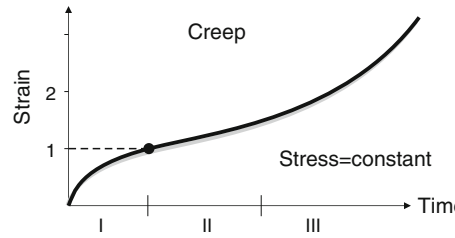

Fig. 5.6 Creep of ice under a constant load. The primary, secondary and tertiary regimes are shown

Table 5.2 Creep regimes in viscous deformation of ice under constant load

Regime	Name	Viscous law
I	Primary creep	Sub-linear
II	Secondary creep	Linear
III	Tertiary creep	Super-linear

Law $y(x) = cx^a$ is sub-linear for $a < 1$, linear for $a = 1$, and super-linear for $a > 1$

Modelling these creep regimes is discussed in Schulson and Duval (2009) for glacier ice. The primary creep is modelled as (Glen 1955).

$$\varepsilon_p = \varepsilon_0 + \beta\sqrt[3]{t} + \dot{\varepsilon}_{\min} t \tag{5.13}$$

where ε_0 is the instantaneous strain, and the transient strain $\varepsilon_t = \beta\sqrt[3]{t}$ is made of recoverable delayed elastic strain ε_d and irreversible viscous strain (see Schulson and Duval 2009). Delayed elastic strain can be an order of magnitude larger than immediate elastic strain, while transient creep can be two orders of magnitude larger than the elastic strain. The secondary creep is well described by the Glen's (1955) law (see Paterson 1999)

$$\dot{\varepsilon} = A\sigma^n \tag{5.14}$$

where A and n are the flow law parameters. Data for the stresses in the range 0.2–2 MPa support the value $n = 3$, and for lower stresses the power is less than 3 (Schulson and Duval 2009). The parameter A depends primarily on the temperature. In tertiary creep the strain-rate increases from the minimum achieved in the secondary creep.

The Maxwell medium, where elastic and viscous models are connected in series, serves as the basic model for ductile behaviour of ice. The viscous part is taken as a nonlinear law, which is far preferable to the linear form. For a fixed temperature the model can be written in the form (see Glen 1955; Ramseier 1971; Ashton 1986)

$$\varepsilon = \frac{1}{E}\sigma + M \cdot D \cdot \left(\frac{\sigma}{E}\right)^n \tag{5.15}$$

where M and n are in general functions of strain, strain-rate and stress, and D is the self-diffusion coefficient for the water molecules in ice. The parameter M shows a very large variability in experimental data, and the coefficient D is given by

$$D = D_0 \exp\left(-\frac{Q_s}{RT}\right) \tag{5.16}$$

where $D_0 \approx 9.1 \times 10^{-4}$ m^2 s^{-1}, Q_s = 59.8 kJ mol^{-1} is the activation energy for self-diffusion, R = 8.31 J mol^{-1} K^{-1} is the universal gas constant, and T is the absolute temperature.

5.2.3 Thermal Cracking and Expansion

The thermal expansion coefficient of ice depends weakly on temperature. The linear coefficient is 5.0×10^{-5} °C^{-1}, i.e. 5.0 cm across 1 km distance for each one-degree temperature change. It is clear that the strongest temperature variations take place near the ice surface.

When the temperature changes fast, the elastic response dominates. In a cooling situation the surface ice contracts and tensile cracks are formed, while in warming the ice cover expands. When the pressure is released by cracking, wave motion takes place in the ice sheet and the crack propagation can also be heard. However, contraction and expansion are not symmetric, since in the case of cracking, water comes up to fill the cracks and freezes in. Then there is net expansion to spread the ice sheet further. In the absence of snow, ice surface layer cools fast, and thermal cracking can be intensive (Fig. 5.7). The temperature change is fast and large, so that the ice has not time enough for viscous adjustment to the forcing.

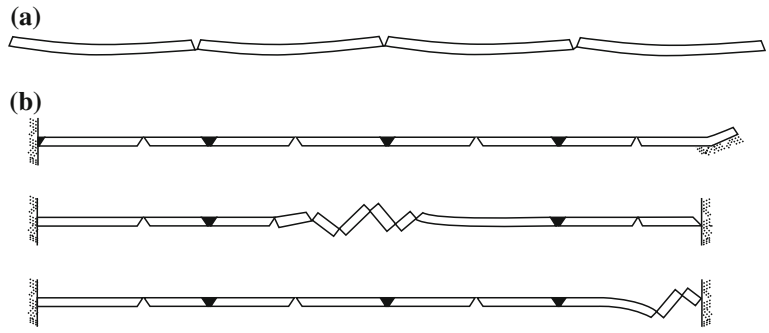

Fig. 5.7 Schematic picture of thermal expansion (modified from Bergdahl 2002). **a** *Right* after a rapid decrease in air temperature; and **b** Expansion of ice on a sloping shore, in mid-lake, and at a *straight shoreline*

Metge (1976) classifies thermal cracks into dry, narrow and wide categories (see also Ashton 1976). *Dry cracks*, which are the most common ones, do not penetrate the ice sheet and act as bellows with temperature changes. *Narrow wet cracks* can freeze rapidly and consequently add material to the ice sheet. Most of the contraction of an ice sheet is concentrated at 1–2 *wide cracks*, which often form between two tensile stress risers, e.g. between two headlands. They can be up to 20 cm wide (Metge 1976). In a long channel they form at regular intervals, while other cracks skirt the shore from headland to headland. Wide cracks do not freeze through in one night but a thin ice bridge forms, and if the daytime temperature is higher the bridges will break. This breakage is usually along shear of inclined plane, and one side of the crack slips over the other that may initiate a pressure ridge.

The rate of strain can be obtained from the temperature change as

$$\dot{\varepsilon} = \alpha \dot{T} \tag{5.17}$$

where α is the coefficient of linear thermal expansion. On the other hand, the relation between strain-rate and stress can be taken as (Bergdahl and Wernersson 1978; Cox 1984)

$$\dot{\varepsilon} = \frac{1}{E}\dot{\sigma} + A\sigma^n \tag{5.18}$$

Actual measurements of thermal pressure show magnitudes of 100 kN m^{-1}.

5.2.4 Displacements in the Ice Cover

Occasionally shifts are observed in lake ice cover. They result from mechanical effects by wind, water currents or gravity (lake surface tilt). Small displacements are also caused by thermal expansion or contraction. These shifts can be detected by surface measurements, and satellite SAR interferometry can be utilized to map two-dimensional small displacements (see Dammert et al. 1998; Vincent et al. 2012).

The main forcing to break a lake ice cover comes from the wind. This is because a strong wind blows in nearly the same direction across the lake, and wind stress τ_a integrated over a long fetch L grows into high level of forcing on the windward side of the lake. There, at the shoreline the wind force is $\tau_a L$. The strength of the ice sheet is modelled as $P = P(h; l)$, where l is the length scale of ice stress. The strength represents the integrated strength through the thickness of ice, and therefore its dimension is force/length. The ice cover is stable as long as

$$\tau_a L < P(h; l) \tag{5.19}$$

A simple approach of $P = P^* h$, $P^* \sim$ 10–100 kPa, has been used widely in sea ice modelling (Hibler 1979). Then it is seen that at the limit of stability we have

$$\frac{\tau_a}{P*} = \frac{h}{L} \tag{5.20}$$

Wind stress depends quadratically on the wind speed U_a, $\tau_a = \rho_a C_a U_a^2$ (see Eq. 4.9a), where $C_a \approx 1.5 \times 10^{-3}$ is the drag coefficient. At the wind speed of 15 m s^{-1}, wind stress is $\tau_a \sim$ ½ Pa. With $P^* = 50$ kPa, we have $\tau_a/P^* \sim 10^{-5}$; then, if $L = 10$ km, the lake ice is stable as soon as $h > 10$ cm.

In general, the dependence of ice strength on ice thickness and length scale is formulated as

$$P(h;\ l) = P^*(l)\left(\frac{h}{h^*}\right)^n \tag{5.21}$$

where h^* is the scaling thickness and n, ½ ≤ n ≤ 2, is the power of the thickness dependence (Coon 1974; Hibler 1979). The power depends on the mode of breakage. The length scale dependence scales as $l^{-1/2}$ (Sanderson 1988; Leppäranta 2011). In coastal landfast ice basins, where the size corresponds to medium-size lakes, the power $n = 2$ has given a good fit (Leppäranta 2013). The compressive strength in engineering experiments is 1–10 MPa ($l \sim$ 1–10 m), and thus at the length scale of 10–100 km the strength magnitude is 50 kPa.

The plastic strength of drift ice depends on the mode of deformation. In compressive failure the ice breaks by crushing and $n = 1$, i.e.

$$P = \sigma_c h \tag{5.22a}$$

where σ_c is the three-dimensional compressive strength of ice. Using the theory of plate on elastic foundation, bending failure (Coon 1974) is obtained as

$$\sigma_B = \frac{\pi^2}{192}\sqrt{\frac{\rho_w g E h}{3(1-\mu^2)}} = 10.8 \cdot \sqrt{\frac{h}{\mathrm{m}}}\mathrm{kPa} \tag{5.22b}$$

Thus the crushing strength is by one order of magnitude larger than the bending strength. In the case of buckling failure (see Ashton 1986), the limiting buckling force per unit width is $F_b = \rho_w g \lambda^2$, where λ is the characteristic length of ice beam on water foundation. The stability condition is

$$\frac{\tau_a}{\sigma_c} = \frac{\tau_a}{\rho_w g \lambda^2 h^{-1}} = \sqrt{\frac{3(1-\mu^2)}{\rho_w g \cdot Eh}}\tau_a < \frac{h}{L} \tag{5.22c}$$

$$\lambda = \sqrt{4}\frac{Eh^3}{\rho_w g \cdot 3(1-\mu^2)} \tag{5.22d}$$

resulting in $n = 3/2$. The stability condition depends on ice thickness. The crushing and buckling failure criteria become equal at $h \approx 20$ cm; for thinner ice buckling is more likely while for thicker ice it is crushing. In sea ice dynamics, potential energy created in overriding of ice sheets is proportional to the square of the ice thickness (Coon et al. 1974). This is a minor term but, however, it has been found that frictional losses in pressure ridge follow the square law (Hopkins 1994), and therefore the power $n = 2$ represents small-scale sea ice dynamics.

When thin ice fractures, it is also possible that the fractured sheets are overridden into a double ice layer. This phenomenon is called *rafting*. A specific, eye-striking case of rafting is *finger rafting*, where the interacting ice sheets fracture along lines perpendicular to the direction of the fracture and form an interlocked structure with alternate overthrust and underthrust fingers.

A model for simple rafting was presented by Parmerter (1975). Two floating ice sheets of thickness h are forced together, and if the edges are not exactly vertical, overriding takes place and develops into rafting. The ice sheets can be treated as plates on elastic foundation except where a plate is submerged (or lifted up) with respect to the water surface level. The solution depends on the parameter $\xi = (\rho_w - \rho_i)/\rho_w$, which determines where the lower plate submerges, as well as on the elastic properties of ice. The problem can be formulated using a dimensionless force N and stress Σ:

$$N = \frac{F}{\rho_w g \lambda^2}; \quad \Sigma = \frac{\sigma_t h}{\rho_w g \lambda^2} \tag{5.23}$$

where σ_t is the tensile strength of ice. The limiting value $N \sim 0.4$ is reached when the submerged plate buckles. This is about 40 % of the force required in normal case of buckling of an ice sheet on water foundation. Bending of the ice sheets during rafting creates tensile stresses. Simple rafting can take place when the stresses are beneath the fracture levels, but otherwise, blocks break off from the ice sheet to form a rubble field or a ridge. The largest stress is experienced by the submerged ice sheet is obtained from an asymptotic limit $\Sigma_0 = 0.46$ (see Parmerter 1975). Then we can obtain an estimate for the maximum thickness of rafting ice as

$$h_{max} = \left(\frac{1}{\Sigma_0}\right)^2 \frac{3(1-\mu^2)\sigma_t^2}{\rho_w g E} \tag{5.24}$$

Inserting freshwater ice parameters, we have $h_{max} = 32$ cm. Parmerter examined sea ice, and due to the lower tensile strength his estimate was 17 cm which corresponded well with observations. In the case of freshwater ice there is not much data about rafted ice to confirm to thicker limit.

If the ice breaks and starts to drift, the next question is that how large lead is formed. Also the persistence and recurrence of leads is of interest. The location of leads is often at the lee side of lake basins but also across lakes guided by the lake geometry. If leads open

up, there will be compression zones elsewhere in the ice cover. In large lakes the unpredictability of sudden displacements in the ice cover endanger ice fishermen. Sometimes in good fishing days a large number of fishermen are driven out by the ice and need to be rescued by hydrofoils or helicopters. E.g., on February 9th, 2009, in all 150–300 fishermen experienced this event together in Lake Erie,[3] North America.

When the ice breakage becomes more regular, the ice cover appears as *broken ice* as usually called in the research of lake ice and river ice. It is a granular medium, where the 'grains' are ice floes. Interactions between ice floes contain the stress generating mechanisms, and variations in smaller scale properties become less important. When the scale of interest is much more than the size of floes, continuum models are employed. This is the regime of drift ice (Leppäranta 2011), to be treated in Sect. 5.5.

5.3 Bearing Capacity of Ice

One of the fundamental problems in the research of floating ice is the bearing capacity (see overview by Goldstein et al. 2014). Ice cover has been used for travel and transportation as long as cold regions have been inhabited. In his map and booklet of northern Europe, Olaus Magnus Gothus (1539) described ice crossing by skiing, skating (metal and bone blades) and riding, and also showed fishing from ice-covered lakes. A dramatic case in the 1200s was a battle between Novgorod and Livonian Knights on the ice of Lake Peipsi, located at the border between the present Estonia and Russia. According to historical sources, the ice broke under the Livonian troops and the battle was then done.[4] The world's first railway ice crossings were built in the late 19th century in Russia. For the first time the track was laid on the ice cover of the Volga River near the town Kazan. The successful experience contributed to the creation of similar crossings in other regions, in particular, on the Volga River near Saratov (1895) and Lake Baikal (1904).

Substantial progress on the use of floating ice cover for support and transportation of heavy loads has been made in North America in the 1970s and 1980s in connection with the development of mineral deposits in Northern Quebec, the Canadian Arctic and Northern Alaska (Masterson 2009; Mesher 2008). The longest winter ice road is 568 km long connecting Tibbitt Lake and Contwoyto Lake and crossing 65 smaller lakes in the Canadian Arctic (Mesher 2008). This road was operated annually from 1979 to 1998 and it provided transportation of cargo to the mines and minerals extracted in the opposite direction. In this road the first attempt was made to use a mobile radar to monitor the thickness of ice. In recent years, interests in ice crossings, roads and islands to support

[3] This case was reported in many Canadian and U.S. news sites on February 10, 2009; the number of fishermen varied in different sources.

[4] The scale of this event is not clear but it is thought to have a true basis. This battle on ice is a scene in the film Alexander Nevsky by Sergey Eisenstein (1938), one of the most famous scenes in the film history.

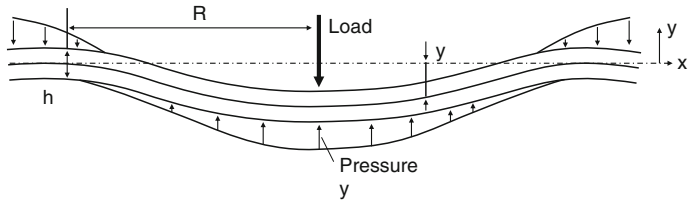

Fig. 5.8 Schematic picture of the bending of ice sheet under load; h is ice thickness and R is the characteristic length (Goldstein et al. 2014)

drilling rigs have risen again in connection with the planned development of oil and gas resources on the shelf of Russian Arctic.

The physical basis of the bearing capacity problem was presented by Hertz (1884). Among the first practical results was a special issue of the Proceedings of the Scientific and Technical Committee of the People's Commissariat of Transport of the USSR (see Goldstein et al. 2014), where there were also links to the papers by Sergeev (1929) and Bernshteyn (1929). The formulation of the theory by Wyman (1950) has been widely used in the western literature. For a point load, the ice is forced down, while it is supported by water pressure (Fig. 5.8). The supporting pressure is $\rho_w g w$, where w is the deflection, and thus a liquid water body acts mathematically in the same way as an elastic foundation (i.e., the response of the foundation is proportional to the deflection). The general theory gives the equation of deflection as (e.g., Michel 1978):

$$\nabla^4 w = \rho_w g w \tag{5.25}$$

The load acts in the origin and is accounted for in the boundary conditions. Under a static point load, the solution for the deflection shows an exponentially damping flexural sine wave with maximum under the load. The wavelength is $2\pi\lambda$, where

$$\lambda = \left(\frac{Eh^3}{12\rho_w g(1-\mu^2)} \right)^{1/4} \tag{5.26}$$

is the characteristic length of ice plate on water foundation.[5] Equation (5.25) can be reduced to the Bessel equation (see Goldstein 2014). For an infinite plate, centrally symmetric solution has the form

$$f(r) = \frac{P}{4\rho_w g L^2} \mathrm{Re} H_0\left(\frac{r}{L}\right) \tag{5.27}$$

[5] Note that, in one-dimensional case, the characteristic length is defined for beams and that is larger than the plate value by a factor of $\sqrt{2}$, see Eqs. (5.22d) and (5.26).

where $H_0(r/L)$ is the Hankel function of zero order, $L = \lambda\mu^{1/2}$, and r is the distance from the point of the load application. The maximum deflection occurs at the point $r = 0$:

$$f(0) = \frac{P}{8\rho_w g\lambda^2} \tag{5.28}$$

In the case of a centrally loaded ice plate, the characteristic length is taken as the size of the deflection bowl or action radius. The stresses at $r \to 0$ are equal to

$$\sigma_r = \sigma_\varphi = \frac{3(1+\mu)}{2\pi}\frac{P}{h^2}\log\left[\left(2\frac{\lambda}{r}\right) - c\right] \tag{5.29}$$

where c is Euler's constant ($c = 0.577216$).

The deflection of the plate and its elastic surface curvature changes sign, and at $r >$ two to three times λ it is practically invisible. At greater distances an ice plate can be considered infinite with respect to the vertical load. The maximum tensile stress acts on the lower ice plate surface under the point of the force application. Within the region $r < \lambda$ the upper surface of the ice is compressed. For practical evaluation of the bowl deflection for freshwater ice at short-term loading, it is convenient to use a simple relation (Gold 1971): $\lambda \approx 16\, h^{3/4}\ \mathrm{m}^{1/4}$. The analytical solution shows that the maximum concentrated load at the edge of the half-infinite ice plate or a semi-infinite crack, is half of that for an infinite plate, while the deflection is increased by four times.

Equation (5.25) admits centrally symmetric solutions, also with several axes of symmetry. Radial cracks occur initially at the lower surface directly under the ice load. Solutions for vertical loads of other distributions may be obtained by integration of the problem on the action of the concentrated load. Calculations show a small effect of a distribution of uniform loads on the maximum values of the ice plate deformation parameters. Increasing the radius of the loaded area to 10 m reduces the deflection at the center on 12 %.

The limit load can be written as

$$P_{cr} = \left[3(1+\mu)C_1\left(\frac{b}{\lambda}\right)\right]^{-1}\sigma_f h^2 \tag{5.30a}$$

where b is the characteristic size of the loaded area, and $C_1(b/\lambda)$ is a coefficient (Fig. 5.9).

Existing solutions for the evaluation of the limit load comprise coefficients determined by complicated functions, while obtainable dependences of the limit load until crack formation, in the most sought interval of the parameter (b/λ) from 0.07 to 1.0, can be represented more simply as (Panfilov 1960)

$$P_{cr} = A\left(1 + B\frac{b}{\lambda}\right)\sigma_t h^2 \tag{5.30b}$$

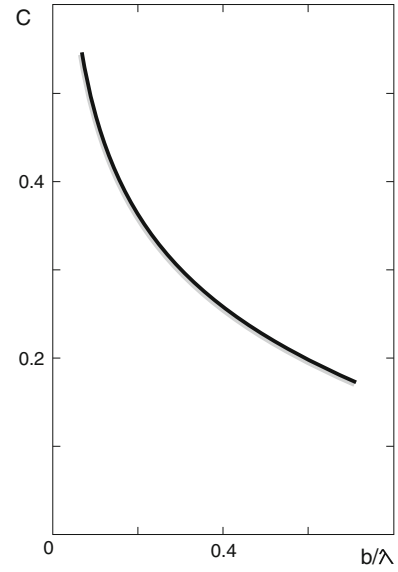

Fig. 5.9 The dependence of coefficient C_1 on b/λ

where the coefficients A and B for an infinite plate are equal to 0.38 and 2.3, respectively, while for a semi-infinite plate they are 0.16 and 2.3.

First-order approximation is obtained from the first term of the series solution shown by Eq. (5.27): the ice can bear mass $M < ah^2$, where $a = a(\sigma_t, \lambda)$ is the model parameter, $a \sim 5$ kg cm^{-2}. The radius of influence of a point load is 2λ and, consequently, this is the safe distance between loads if the ice thickness is close to the critical level.

Interest in the dynamical loads originates from practical problems, in particular the problems on loads (cargo, vehicle) motion along an ice route. The possibility of dangerous resonance phenomena has been expressed in the book by Zubov (1942). The conclusion that there is a certain speed, the excess of which can lead to the fracture of ice cover, was formulated in Bregman and Proskuryakov (1943) on the basis of the data analysis of the ice cover oscillations in Lake Ladoga.

When the speed of a motor vehicle is below the critical value, disturbances are propagated along the ice cover at a speed of the vehicle and they disappear behind practically with the same velocity. But when the speed becomes close to the critical level, i.e. the speed of the shallow water wave $c = \sqrt{gH}$ in the water body, due to resonance in bending of the ice the bearing capacity becomes in practice less than half of that for static loads. When the speed is much more, the resonance disappears but then the high speed must be kept the whole way across the lake.

In deep water, the deflections are always smaller than in shallow depths (the effect of shallow water for surface waves in fluids). At subcritical speeds, maximal bending moments occur under load. In the case of supercritical speeds, the moment peak is located in front of the load. Motion of a load on an ice cover is accompanied by only bending vibration, or just gravity vibration or both types of vibration, depending on the speed.

If the flexural wave in the plate accompanies the gravitational wave in the water, the sequence is called flexural-gravitational wave.

Example 5.3. Assume that there is a large number of people on lake ice, evenly spaced at distances of d, and denote ice thickness by h and mass of one person by M. First, to prevent ice from sinking, the buoyancy conditions requires that $M \leq (\rho_w - \rho_i)hd^2$. Second, to prevent ice from breaking, we must have $nMg \lesssim 0.4\left(1 + 2.3\frac{d\sqrt{n}}{\lambda}\right)\sigma_t h^2$. Take $d \sim 1$ m and $d\sqrt{n} \sim \lambda$. For $h = 0.1$ m, the buoyancy criterion gives $M \leq 9$ kg, and, since $\lambda \sim 10$ m and consequently $n \sim 100$, the strength criterion gives $M \leq 20$ kg. The buoyancy condition is more limiting. For $h = 1$ m, the buoyancy criterion gives $M \leq 90$ kg while the strength criterion gives $M \leq 660$ kg. The buoyancy condition is more limiting factor.

5.4 Ice Forces

5.4.1 Ice Load Problems

Forces due to ice have been investigated for a long time in ice engineering because of practical applications. The maximum loading takes place when the ice fails at a structure, then depending on the failure mode. In lake ice environment the ice loading cases are concerned with harbour structures and piers, ships, coastal constructions, and the natural coastline itself (Fig. 5.10). The failure of ice is not necessarily ever achieved due to short fetches, and therefore the forces are generally lower than in marine environment. On the other hand the strength of freshwater ice is higher than the strength of sea ice, and in non-fetch-limited situations loads can be higher in lakes.

Two examples of ice loading situations are given first.

Example 5.4 'Ice quakes'. In the beginning of January 2009, a rare 'ice quake' was experienced on the shore of Lake Vesijärvi, Lahti, Finland (Fig. 5.10). The lake ice thickness was about 10 cm. Residents in new, high buildings located about 40 cm from the shoreline were alarmed by vibrations of the buildings. Recording of these vibrations were started in three buildings on January 8th. The frequencies of the floors were then 2–10 Hz, around the lowest expected natural frequency of the houses in the so-called pendel vibration mode (Makkonen et al. 2010). All the houses, which felt the vibrations, have been supported by using vertical concrete piles on stiff moraine. The building site itself has been filled in the lake with a 6 m thick filling resting on original quite soft 15 m thick clay/silt layer above the moraine. The in-lake building site is probably the main reason why the vibrations due to cracking of the lake ice can be transported into the buildings via the soil. When the melting of ice began in spring, vibrations started again after a 2 months quiet period. The highest measured velocities were 1.2 mm s^{-1}, exceeding the comfort limit of people, but at that level no structural damages are expected and indeed they were not observed.

Fig. 5.10 'Ice quakes' were felt in the houses close to the shore due to pressure by strong wind

Example 5.5. Thermal pressure. In Lake Mälaren, Sweden thermal pressure has caused damage in the past (Bergdahl and Wernersson 1978). In winter 1953 a swing bridge was partly damaged. Air temperature rose by 14 °C in 12 h and 22 cm thick ice expanded and pressed toward the bridge. The forcing was estimated as 270 kN m^{-1}. In winter 1976 four beacons mounted on pile groups were destroyed by thermal expansion, with pressures estimated as 100–270 kN m^{-1}.

5.4.2 Estimation of Ice Loads

The load of ice on structures depends on the mode of loading, strength of the structure, and form of the structure. The fundamental method to evaluate ice loads is the Korzhavin (1962) equation for vertical structures:

$$F = Ik_1k_2\sigma Dh \tag{5.31}$$

where I is the indentation factor, k_1, k_2 and D are the contact factor, shape factor and width of the structure, and σ and h are the strength and thickness of ice. The indentation factor I accounts for the 3D nature of the stress in ice representing the stress-strain field around the structure and accounting for the difference between the real and the unconfined stress

distribution, k_1 takes into account incomplete contact between the ice edge and structure while k_2 is responsible for the structure cross- section form, $k_1 \geq 1/2, k_2 \leq 1$. In case of non-vertical structures, inclination of the loaded surface has also influence. The indentation factor depends on the aspect ratio D/h, and $I \approx 1$ for narrow structures and $I \approx 2.5$ for wide structures.

On the basis of the Korzhavin (1962) model, further simplifications can be derived. The force on a pier-type structure can be estimated by

$$F = K\sigma_c Dh \tag{5.32}$$

where K is a scaling coefficient, and σ_c is the compressive strength. The coefficient K depends on the mechanical properties of ice and the geometry of the pier structure (Ashton 1986). For a narrow structure the ratio $\delta = D/h$ is an important parameter, $K = 2.5$ for $\delta = 1$ and $K \longrightarrow 1$ for $\delta \gg 1$. For wide structures and wedge-shaped piers, $K = 1$ can be taken. For inclined structures $K < 1$ depending on the slope angle of the structure and ice-structure friction.

Example 5.6. For a 1-m pier, the maximum force is 10 MN for thin ice (10 cm) and for thick ice (1 m) it would be 25 MN.

When ice has frozen to structures, changes in water level elevation cause vertical forces. The largest forces result when the change in the elevation is fast, since the ice then behaves in elastic manner. Kerr (1975) examined vertical loads on a cylindrical pile. The load increases with the thickness of ice and with ratio b/h. When the ice thickness is 0.5 m, the load magnitude per water level change is 5×10^5 N cm^{-1}. According to Gamayunov (1960) the ice fails in bending at the cylinder surface with an effective moment $M = h^2\sigma_f/6$.

If the ice cover is frozen to vertical walls, uplifting and downdragging forces also result from vertical movement of the water level (Ashton 1986). Based on the theory of beam on semi-infinite elastic foundation, the load is

$$\frac{P}{b} = \frac{\rho_w g}{\lambda}\Delta\xi \tag{5.33}$$

where $\Delta\xi$ is the change in water level elevation and λ is the characteristic length of ice plate on water foundation (Eq. 5.26).

5.5 Drift Ice in Large Lakes

5.5.1 Drift Ice Material

The horizontal structure of ice cover in large lakes is well revealed by optical satellite images (Fig. 5.11). The ice sheet is occasionally broken into floes by wind forcing, water level variations and thermal cracking, and the floes may be forced to move. This field of

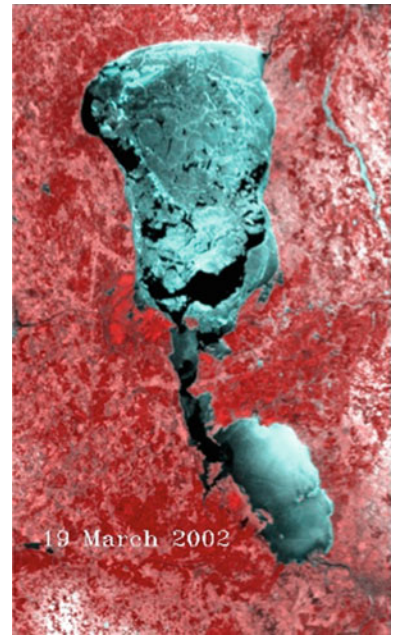

Fig. 5.11 Ice situation in Lake Peipsi according to MODIS imagery, 19 March 2002. The dark elongated zones on the western and central coasts indicate major leads, and small leads and fractures can also be seen far from the coast

broken ice is a granular medium called *drift ice*, and here, as usual, a continuum approximation is employed for this medium. The motion of drift ice takes place in the three-dimensional world, but it can be treated as a *two-dimensional* phenomenon on the lake surface. In sea ice basins, ice drift is a common phenomenon with major short-term and climatological impacts, and the theory and models of sea ice dynamics are now well-developed and applicable to lake ice covers (e.g., Leppäranta 2011).

From the point of view of ice mechanics, 'large lakes' are those, in which wind-driven mechanical displacements are common. In small and medium-size lakes the ice cover is static, apart from fractures and thermal cracks. Fetch is the critical factor for the ice displacements, and therefore islands can limit the mobility of ice in large lakes such as Lake Saimaa in Finland. A linear dimension of 100 km can be taken as a convenient magnitude for lakes where ice displacements occur regularly.

In Europe there are five large lakes, where major ice displacements are common: the Caspian Sea, Ladoga, Onega, Peipsi, and Vänern (see Burda 1999; Wang et al. 2006). Ice forms annually in the northern part of the Caspian Sea, where it is mostly drift ice. As an example, Fig. 5.11 shows the ice conditions in Lake Peipsi for March 19, 2002. In Asia, wind-driven ice is observed in the Aral Sea (Kouraev et al. 2004) and in Lake Baikal. Drift ice is also common in the Great Lakes of North America. In between large and medium-size lakes, there is a grey area: the ice cover is static in cold winters and may be mobile in mild winters. An example is Lake Lappajärvi (63°12′N 23°42′E), a medium-size lake in Finland. Its surface area is 148 km^2 and its mean and maximum depths are 7.4 m and 36 m, respectively. The lake basin depression is a wide meteorite impact crater. It is

annually covered by ice, and the maximum annual ice thickness is 50–70 cm. Mechanical ice breakage, displacements and formation of small ridges is a common phenomenon, but the length scale of lateral displacements is limited (Alestalo 1980).

Drift ice physics is conveniently presented in right-hand co-ordinate system (x, y, z) with positive directions east, north and up, respectively. The drift ice medium is described by the state variables, which contain the properties needed to model the internal stress. The first approximation is a two-level ice state $J = \{A, h\}$, where A is ice compactness and h is mean ice thickness (Doronin 1970). If necessary, this can be refined by using the ice thickness distribution for the ice state with several thickness categories (Thorndike et al. 1975). For a region Ω, the distribution function is defined by

$$\Pi(h) = \frac{1}{\Pi(\infty)} \int_{\Omega} H[h - \zeta(\omega)] d\Omega \tag{5.34}$$

where h and ζ denote the thickness of ice so that h is the thickness distribution argument and ζ is the actual thickness in points $\omega \in \Omega$, and H is the Heaviside function $H(x) = 0$ (1) for $x \leq 0$ ($x > 0$); $\Pi(h)$ is simply the normalized area of ice with thickness less than or equal to h in a region Ω. Ice state is specified as a histogram by the set of classes $J = \{\Pi(0), \Pi(h_1) - \Pi(0), \Pi(h_2) - \Pi(h_1), \ldots, 1 - \Pi(h_n)\}$, where h_k's are n + 1 fixed thickness levels.

For a two-dimensional medium, the stress σ is obtained from the three-dimensional stress $\underline{\sigma}$ by integration: $\sigma = \int_{-h''}^{h'} \underline{\sigma} dz$, where h' and h'' are the freeboard and draft of the ice sheet, respectively. Drift ice rheology investigations have been made for sea ice and river ice but the results are applicable for lake ice as well, provided the broken structure of the ice cover prevails (see Leppäranta 2011). The rheological law of drift ice is in general form

$$\boldsymbol{\sigma} = \boldsymbol{\sigma}(J,\ \boldsymbol{\varepsilon},\ \dot{\boldsymbol{\varepsilon}}) \tag{5.35}$$

The simplest rheology is the no-stress case ($\boldsymbol{\sigma} \equiv 0$) known as the *free drift*. The main drawback of this model is that mechanical ice accumulation is not limited by any resisting force, and unrealistic ice thickness fields may result. Nevertheless, free drift is applicable for $A < 0.8$, when stress levels are very small and convergence/divergence in ice drift just arranges distances between ice floes.

Realistic rheologies of compact drift ice ($A > 0.8$) have the following general properties: (1) The strength is sensitive to ice compactness in $0.8 \leq A \leq 1$, (2) Yield strength $\gg 0$ for $A \approx 1$, (3) Compressive strength > shear strength $\gg 0$, (4) Tensile strength is small, and (5) No memory. The two-dimensional ice stress is the three-dimensional stress integrated through the thickness of ice; its dimension is therefore force per length. The low tensile strength is due to that not much force is needed to drive ice floes further away from each other. At high ice compactness, a plastic flow results with yield strength increasing with ice thickness (Coon et al. 1974). The plasticity is not perfect but the ice

shows elastic or viscous behaviour when the stress is below the yield level depending on the time scale (see Sect. 5.1).

The original plastic drift ice rheology was the elastic-plastic model developed in the AIDJEX (Arctic Ice Dynamics Joint Experiment) -programme for Arctic sea ice (Coon et al. 1974; Pritchard 1975). A few years later, Hibler (1979) introduced a viscous-plastic rheology, which is more feasible for long-term sea ice simulations. These rheologies have served the basis of later plastic models, where the main concern has been the shape of the yield curve. Because of computational reasons, ideal plastic models have not been used but the stress inside yield curve has been taken either as a linear elastic (Coon et al. 1974) or linear viscous law (Hibler 1979).

The strength of the ice is taken as a function of thickness and compactness as

$$P = P_n^* h^n \exp[-C(1-A)] \tag{5.36}$$

where P_n and n are the compressive strength parameters, and C is the strength reduction for lead opening. In the original version n was equal to one, but in general we can allow the power to vary between ½ and 2 (see Sect. 5.2.1). Physically C^{-1} is the e-folding value of strength for changes in compactness, and, due to the high sensitivity, $C \gg 1$. The normal parameter values are $P_\mathrm{n} h^\mathrm{n} = 25$ kPa for $h = 1$ m and $C = 20$. In a research effort of landfast ice in the Baltic Sea, Leppäranta (2013) found $n = 2$ as a good representative value.

Two-dimensional plastic yielding is specified with a yield curve $F(\sigma_1, \sigma_2) = 0$, where σ_1 and σ_2 are the principal stresses. Drucker's postulate for stable materials states that the yield curve serves as the plastic potential, and consequently the failure strain is directed perpendicular to the yield curve, known as the normal, or associated flow rule (e.g., Davis and Selvadurai 2002). Consequently, we have

$$\varepsilon_k = \Lambda \frac{\partial F}{\partial \sigma_k} \tag{5.37}$$

where Λ is a parameter to be obtained as a part of the solution. Drift ice is strain hardening in compression, and therefore pressure ice formation may proceed only to a certain limit. Inside the yield curve, $F < 0$ and stresses are elastic or viscous, while $F > 0$ would go outside the yield curve and is not allowed. The plastic failure criterion tells when the ice fails, and when it does, the plastic flow is obtained from the equation of motion.

The stability of ice cover was treated in Sect. 5.2.1. Then, once the ice cover has become broken into a system of floes, it does not resist tensile stresses, and the yield curve must be located in the quadrant where $\sigma_1, \sigma_2 < 0$. Different shapes have been used (Fig. 5.12). In the elastic-plastic model, a diamond, triangle (Coulomb) and a teardrop shape yield curves have been employed. The Hibler viscous-plastic model has an elliptic yield curve, which has good computational properties.

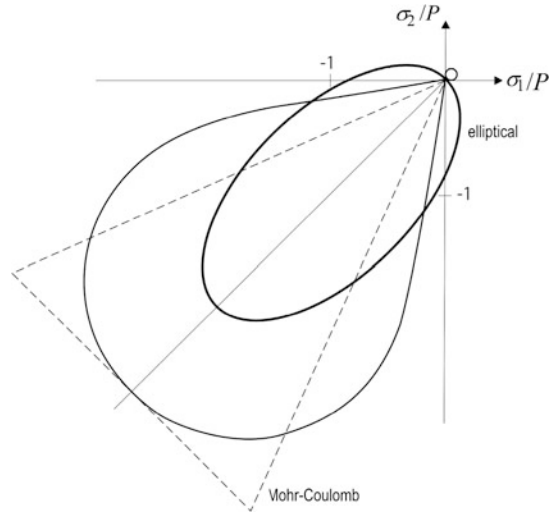

Fig. 5.12 Drift ice yield curves: Coulomb or triangular (Coon et al. 1974), teardrop (Coon et al. 1974), and elliptic (Hibler 1979)

Example 5.7. The elliptic yield curve has the advantage that the failure yield can be expressed in closed form. The yield curve is defined as (see Fig. 5.12):

$$F(\sigma_1, \sigma_2) = \left(\frac{\sigma_1 + \frac{1}{2}P}{\frac{1}{2}P}\right)^2 + \left(\frac{\sigma_2 + \frac{1}{2}P}{\frac{1}{2e}P}\right)^2 - 1$$

where P is the compressive strength of ice and e is the ratio of compressive strength to shear strength. Using the associated flow rule (Eq. 5.37) we can get the solution

$$\sigma = \frac{P}{2\sqrt{\varepsilon_I^2 + e^{-2}\varepsilon_{II}^2}}\left[\varepsilon_I \boldsymbol{I} + e^{-2}(\varepsilon - \varepsilon_I \boldsymbol{I})\right] - \frac{P}{2}\boldsymbol{I}$$

where ε_I and ε_{II} are the strain invariants equal to the sum and difference of the principal strains. Clearly the stress is independent of the absolute level of the strain. For spherical compressive strain, $\varepsilon_I < 0$ and $\varepsilon_{II} = 0$, we have, $\sigma = -P\boldsymbol{I}$. In the case of pure shear, $\varepsilon_I = 0$, we have $\sigma_{xx} = \sigma_{yy} = -1/2P$ and $\sigma_{xy} = \sigma_{yx} = (\boldsymbol{\varepsilon}/\varepsilon_{II})\ 1/2eP$. Since it is considered that shear strength is significant but less than the compressive strength, we must have $1 < e << \infty$; normally $e = 2$ is chosen.

Inside the yield curve, the ice may be assumed to behave in a rigid, elastic or viscous manner. The linear elastic model gives the stress proportional to the strain:

$$\boldsymbol{\sigma} = \boldsymbol{\sigma}(\boldsymbol{\varepsilon};\ K,\ G) = K(\mathrm{tr}\boldsymbol{\varepsilon})\mathbf{I} + 2G\boldsymbol{\varepsilon}',\ F(\sigma_1,\ \sigma_2) < 0 \tag{5.38}$$

where $\boldsymbol{\varepsilon}' = \boldsymbol{\varepsilon} - \varepsilon_I \mathbf{I}$ is the deviatoric strain. The dimension of two-dimensional stress and the moduli K and G is force/length. The magnitude of the drift ice elastic moduli is

10–100 MN m^{-1}, and they tell how the ice deforms up to the yield stress. The original bulk and shear moduli were given as K/h = 100 MN m^{-2}, $G \approx ½ K$ in the AIDJEX model by Coon et al. (1974). The corresponding Poisson's ratio is 0.29. From physical basis the ratio between compressive strength and bulk modulus of ice should be of the order of 10^{-3}, and therefore elastic strains remain below 10^{-3} (i.e., less than 10 m across 10 km distances). Pritchard (1980) chose the ratio as 2×10^{-3}. The elastic moduli and brittle strength are lower than in small-scale mechanics, since the amount of faults increases with length scale. The strength of ice (σ) scales with the length scale L as $\sigma \propto L^{-1/2}$ (Sanderson 1988).

In compressive deformation, if there are cracks ice floes may override each other resulting in rafting. Rafting may extend to long distances or end due to bending failure, which starts piling up of ice floes if rafting and breaking continue. However, if the floe edges are vertical in cracks, there is no overriding but the ice breaks in compression. In the drift ice scale, the compressive elastic strength is $\sigma_c/h \approx 0.1$ MN m^{-2} (Pritchard 1980). Rafting or piling up of ice blocks may also take place on the windward shore. Then the amount of shore ice accumulation depends on the thickness of ice and shoreline morphology.

Drift ice models have mostly taken a viscous approach, largely due to computational reasons. The linear viscous option is given analogously with the elastic model, with strain replaced by strain-rate and the elastic moduli replaced by bulk and shear viscosities ζ and η, respectively:

$$\sigma = \sigma(\dot{\varepsilon}, \zeta, \eta) = \zeta(\mathrm{tr}\dot{\varepsilon})\boldsymbol{I} + 2\eta\dot{\varepsilon}' - \frac{1}{2}P, F(\sigma_1, \sigma_2) < 0 \tag{5.39}$$

These viscosities have been kept large ($\sim 10^{12}$ kg s^{-1}, $\eta \sim ½ \zeta$) to limit viscous deformation and have a good approximation for the plastic flow. Therefore, plastic yield level is reached at the strain-rate of the order of 10^{-7} s^{-1}. Glacier flow obeys a nonlinear viscous law (Paterson 1999), linearized viscosity would be $\sim 10^{13}$ kg s^{-1} at the strain-rate of 10^{-8} s^{-1}. An anisotropic extension was developed by Hibler and Schulson (2000) to examine the dynamics of oriented lead and crack systems.

The original viscous-plastic drift ice model Hibler (1979) included an inconsistency of having non-zero stress for an ice field at rest, with $\boldsymbol{\sigma} = -½P\mathbf{I}$ for $\dot{\varepsilon} = 0$. This inconsistency was later removed (Hibler 2001). Also in the case of low, long-term forcing, the viscous case has an unrealistic feature for lake applications in leading to continuous creep. The length of an ice beam would be changed by a factor of $\exp(\dot{\varepsilon}t)$ due to creep, and this would account for 2.5 % in 1 month for a creep of 10^{-8} s^{-1}. The viscous strain-rates should be much smaller than allowed in the model but it is not exactly known how much. In sea ice fields, however, the ice is mostly dynamically active that keeps the creep within the noise.

Lake ice cover is loaded by the tangential air–ice and water–ice stresses (e.g., Andreas 1998; McPhee 2008) and the surface pressure gradient, which is due to tilting of the water

surface. The forcing is resisted by the strength of the ice as specified by the rheology model. The external forces are in general given by

$$\tau_a = \rho_a C_a U_a \boldsymbol{U}_a \tag{5.40a}$$

$$\tau_w = \rho_w C_w |\boldsymbol{U}_w - \boldsymbol{u}| [\cos\theta_w (\boldsymbol{U}_w - \boldsymbol{u}) + \sin\theta_w \boldsymbol{k} \times (\boldsymbol{U}_w - \boldsymbol{u})] \tag{5.40b}$$

$$\boldsymbol{G} = -\rho g h \nabla \xi \tag{5.40c}$$

where C_a and C_w are air and water drag coefficients, θ_w is the boundary layer angle in water, $\boldsymbol{U}_a$ and $\boldsymbol{U}_w$ are the surface wind and current velocities, and ξ is the water level elevation. The reference depth of the current velocity can be taken at the vertical mid-level or bottom (zero current) in shallow lakes, while in deep lakes a convenient depth is the bottom of the layer of frictional influence of the ice. Representative values of the parameters are $C_a = 1.4 \times 10^{-3}$ for the wind speed at 10-m altitude (Andreas 1998), $C_w = 1 \times 10^{-3}$ for shallow reference depth (Shirasawa et al. 2006), and $\theta_w \to 0$ in shallow lakes, $\theta_w \to -25°$ (northern hemisphere) or $\theta_w \to 25°$ (southern hemisphere) in deep lakes. In a stratified fluid the drag parameters depend also on the stability of the stratification (see Sect. 4.1).

When the forcing is strong enough, the ice fails and the flow goes into the plastic regime. The wind stress is $\tau_a \sim 0.5$ N m^{-2} for a wind speed of 15 m s^{-1} over a lake ice cover. If the fetch L becomes 10 km, the stress integrates to a force of $\tau_a L \sim 5$ kN m^{-1} at the windward side of the lake, enough to break 10-cm thick ice by compression. This is the correct magnitude according to observations in ice-covered lakes. Since water circulation is weak and has changing direction under the ice, the integrated forcing by the ice–water stress never gets close to the wind forcing. On a sloping lake surface, gravity produces a force of $\rho_i g h \Delta\xi$, where $\Delta\xi$ is the water level difference across the lake, at the shallow end. Thus to obtain lake surface slope more than 10^{-4} would be needed to break the ice in a 10-km size lake but such slope is most unlikely to occur.

5.5.2 Equations of Drift Ice Mechanics

Even very large lakes are small enough to allow a local Cartesian co-ordinate system. The liquid water surface serves as the zero reference level. A *drift ice* field is described with the fields of ice thickness $h = h(x, y; t)$ and velocity $\boldsymbol{u} = \boldsymbol{u}(x, y; t)$, $\boldsymbol{u} = u\mathbf{i} + v\mathbf{j}$. A 'point' in the drift ice field is a finite cell, where the velocity is represented by the average value while the *drift ice state* is represented by the thickness distribution of ice (Thorndike et al. 1975).

Displacements in floating lake ice are two-dimensional, horizontal. The equation of motion can be derived by integrating, *across* the thickness of the ice, the three-dimensional continuum law the (see Leppäranta 2011):

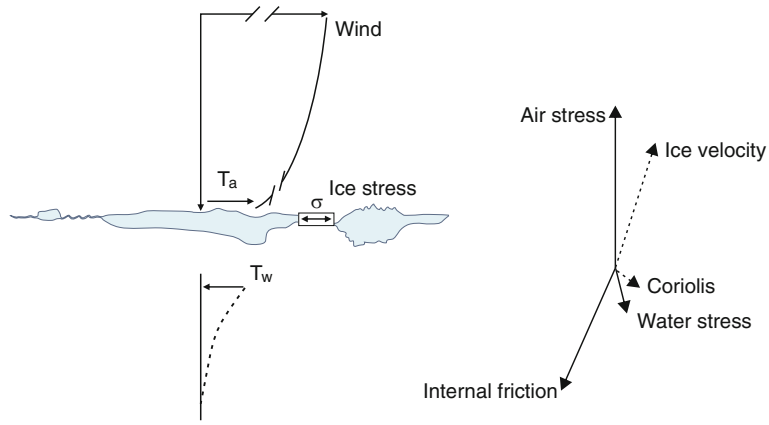

Fig. 5.13 Lake ice drift and the physical problem. Ice is driven by forcing from the atmosphere and lake water body, and the ice responds to forcing through its internal stress field. A typical force diagram is also illustrated

$$\rho\left(\frac{D\boldsymbol{u}}{Dt}+2\boldsymbol{\Omega}\times\boldsymbol{u}\right)=\nabla\cdot\boldsymbol{\sigma}+\sum_{k}\boldsymbol{F_k} \tag{5.41}$$

where D/Dt is the material time derivative, $\boldsymbol{\Omega}$ ($\Omega = 7.292 \times 10^{-5}$ s^{-1}) is the angular velocity of the Earth, and $\boldsymbol{F}_k$'s are the external forces. In the integration, the inertia, advection and Coriolis acceleration are just multiplied by ice thickness. Vertical component results in the Archimedes law, i.e. how the ice floats, while the horizontal component gives the motion on the lake surface plane. The horizontal component of Coriolis acceleration is further simplified to $hf\mathbf{k}\times\boldsymbol{u}$, where $f = 2\,\Omega\sin\phi$ is the *Coriolis parameter* and ϕ is the latitude.[6] Integration of the internal ice stress gives the internal friction and wind and water stresses at the top and bottom boundaries. If the lake water surface is tilting, a pressure gradient force results from the hydrostatic water pressure on ice floes. Finally, the general form of the equation of motion of ice on the lake surface plane is (Fig. 5.13):

$$\rho h\frac{\partial\boldsymbol{u}}{\partial t}+\boldsymbol{u}\cdot\nabla\boldsymbol{u}+f\boldsymbol{k}\times\boldsymbol{u}=\nabla\cdot\boldsymbol{\sigma}+\boldsymbol{\tau_a}+\boldsymbol{\tau}_w-\rho gh\nabla\xi \tag{5.42}$$

In very large lakes the Coriolis acceleration becomes significant in ice drift (the derivation is shown, e.g., in Cushman-Roisin 1994).

Figure 5.13 also shows a schematic force diagram of ice drift. Usually, wind is the driving force, balanced by the ice–water drag and the internal friction of the ice. Coriolis

[6] Latitude is taken positive in the northern hemisphere and negative in the southern hemisphere.

acceleration is smaller than the three major forces and is always perpendicular to the ice motion, directed to the right (left) in the northern (southern) hemisphere. The other terms are smaller still. In rivers, the water current provides the main transport mechanism. For a surface slope of 10^{-5} and ice thickness of ½ m, the magnitude of the surface pressure gradient force is 0.05 Pa. Compared with vertically integrated lake circulation models, the following points can be noted: ice thickness corresponds to lake depth; ice–water friction corresponds to bottom friction; and the internal friction of ice corresponds to horizontal viscous or turbulent friction. Hydrostatic pressure, which is a major factor in lake water circulation, is not important in ice dynamics.

The lateral boundary of a lake ice field can be simply taken as the shoreline, where the ice velocity is zero. In case a lake is partly ice-covered for a longer period, ice and open water areas define an open water boundary (Ovsienko 1976). At the open water boundary the ice does not support normal stresses and the motion of ice changes the boundary configuration. At the land boundary, the ice is allowed to stay or move away into the drift ice basin, but it is not allowed to override the solid boundary out from the basin. As soon as the ice has moved out and lost contact with the shore, the boundary changes to an open water boundary. The boundary conditions are often replaced by a simplified form: open water is defined as 'ice with zero thickness' and then the open water boundary question is removed.

To close the system, an ice conservation law is needed for the ice state. Since we can take here ice density as a constant, conservation laws are needed for the classes of the ice thickness distribution only. Taking $J = \{A, h\}$, where h represents the mean thickness and A is ice compactness, we have

$$\frac{\partial h}{\partial t} + \boldsymbol{u} \cdot \nabla h = -h\nabla \cdot \boldsymbol{u} + \phi_h \tag{5.43a}$$

$$\frac{\partial A}{\partial t} + \boldsymbol{u} \cdot \nabla A = -A\chi(\dot{\varepsilon}_I, \dot{\varepsilon}_{II}) + \phi_A (0 \le A \le 1) \tag{5.43b}$$

where ϕ_h and ϕ_A are the thermal growth rate of ice thickness and compactness, respectively, and the function χ provides the opening and closing of the ice field. These equations are the conservation laws of ice mass compactness. The formulation using χ is needed, since open water may also be created in pure shear. When the mean ice thickness and compactness are known, the thickness of ice floes is obtained from $h_\mathrm{i} = h/A$.

Thermal change of ice thickness is given with a growth rate depending on the present thickness and energy budget as shown in Chap. 4, while thermal change of ice compactness is given by

$$\phi_\mathrm{A} = \frac{\phi(h_\mathrm{o})}{h_\mathrm{o}}(1 - A) \tag{5.44}$$

Here ice thinner than h_0 is accounted as 'open water'. When $A < 1$, lateral melting may take place via absorption of solar radiation in open water patches. This can be added to Eq. (5.44) in straightforward way by distributing the heat evenly to vertical floe surfaces (see Rothrock 1986).

5.5.3 Static Ice Cover

Static ice cover is also termed as landfast ice. Stability was considered in Sect. 5.2.4 above. Now the question can be revisited based on the equation of motion. In the static conditions, $u \equiv 0$, and, consequently,

$$\nabla \cdot \sigma + \tau_a + \tau_w - \rho h g \nabla \xi = 0 \tag{5.45}$$

Stationarity is satisfied as long as the internal ice stress is beneath the yield level. Consider the one-dimensional (x-axis) case, the lake located between $x = 0$ and $x = L$. Integrating the static equation across the lake, we have

$$\Delta\sigma + F = 0, F = (\tilde{\tau}_a + \tilde{\tau}_w)L - \rho h g \Delta\xi = 0 \tag{5.46}$$

where Δ refers to difference across the lake from $x = L$ to origin, and the symbol '$\sim$' stands for spatial averaging. In this case the ice cover can be viewed as an elastic-plastic medium (Coon et al. 1974; Leppäranta and Wang 2008; Leppäranta 2011). To break the ice, the integrated external forcing must reach the compressive strength $P_n h^n$ (Eq. 5.36) at the windward side (Fig. 5.14). Equation (5.46) provides also a first approximation to two-dimensional cases when L represents the fetch in the wind direction.

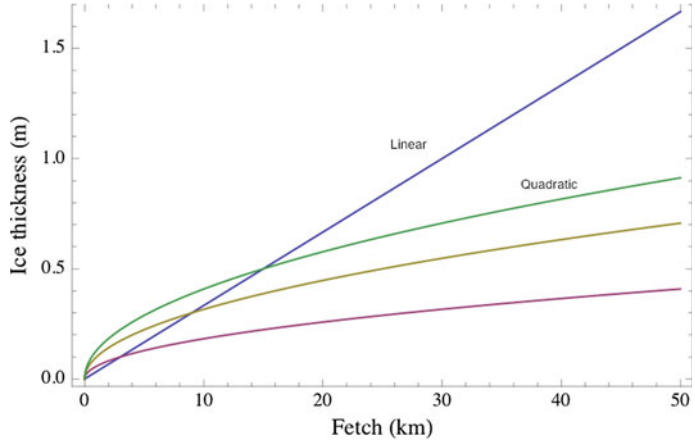

Fig. 5.14 Stability of lake ice at very strong winds. The *lines* show the breakage limit of ice thickness as a function of fetch for ice strength linear and quadratic in ice thickness. The three quadratic lines are set to agree with the linear case at ice thicknesses of 0.1, 0.3 and 0.5 m

Assume that $n = 1$. Then the aspect ratio h/L is the key dimensionless quantity of the ice cover. For the ice cover to break, we must have $\tau_a/P_1 > h/L$. E.g., take $P_1 \sim 30$ kPa. Wind stress for wind speed $U_a = 10$ m s^{-1} is $\tau_a \approx 0.3$ Pa, and then, $\tau_a/P_1 \approx 1 \times 10^{-5}$. In Lake Peipsi, $L \sim 50$ km and when $h \sim 30$ cm, $h/L \sim 0.6 \times 10^{-5}$ and the ice is mobile. In a medium-size lake in southern Finland, $L \sim 10$ km and $h \sim 40$ cm, and the ice cover is stationary. But with a major decrease in ice thickness and/or increase in wind speed the ice cover can become mobile; very rare observations of modest ridging exist from the past in mild winters but in general the ice cover is static. In spring, the ice cover rottens and the strength decreases. Then ice cover may be displaced as sometimes seen as on-shore ride-up or pile-up. However, the period of potential mobility is short and a considerable wind speed is needed for displacements. It is known by experience in Finland that in some years stable rottening takes place and in some years breakage and drift results.

In the ice strength law (Eq. 5.36), it seems that the power n should be more than 1. In a study of landfast ice in the Baltic Sea, Leppäranta (2013) concluded that in the scales of coastal basins $n = 2$ corresponded well to observations. Thus, if $h \sim 0.3$ m is the critical thickness for lake size $L \sim 50$ km, then for $h \sim 0.1$ m and 1.0 it would be $L \sim 5$ km and $L \sim 500$ km, respectively.

5.5.4 Models of Drift Ice Dynamics

When a lake ice-cover tends to break and the ice drifts, the ice appears as drift ice, and the full dynamics equation (Eq. 5.42) provides the ice velocity solution. In spite of the important role of ice mechanics in large lakes, very little research has been done in respect of full thermal–mechanical modelling. Continuum models were originally developed for oceanic drift ice in the 1960s, but for lake ice they followed later. The first efforts were made in Soviet Union for the Caspian Sea (Ovsienko 1976) and in North America for the Great Lakes (e.g. Wake and Rumer 1983). Thereafter, not much more was done in lake ice

Table 5.3 Scaling of the equation of motion of drift ice in lakes

Term	Scale	Value	Comments
Local acceleration	$\rho HU/T$	<0.001	0.05 for rapid changes ($T = 10^3$ s)
Advective acceleration	$\rho HU^2/L$	<0.001	Long-term effects may be significant
Coriolis term	ρHfU	0.005	Mostly <0.025
Internal friction	PH/L	0–0.5	0—open ice field, 0.5—compact ice field
Air stress	$\rho_a C_a U_{ag}{}^2$	0.2	Mostly significant
Water stress	$\rho_w C_w U^2$	0.01	May become 0.2 for open drift ice
Pressure gradient	$\rho Hg\nabla\xi$	0.005	Surface slopes limited in ice-covered basins

The representative elementary scales are: ice thickness $H = ½$ m, ice velocity $U = 10$ cm s^{-1}, ice strength $P = 50$ kPa, wind velocity $U_a = 10$ m s^{-1}, water velocity $U_w = 0$, lake surface slope $\nabla\xi = 10^{-6}$, time $T = 1$ day, and horizontal length $L = 50$ km. The unit of "Value" column is Pa

dynamics before the year 2000. But much work was done for small marine basins, and these models can be easily employed for lake research (e.g., Wang et al. 2003, 2006b; Kubat et al. 2010). Recently, in Europe lake ice dynamics modelling work has continued in Lake Peipsi (Wang et al. 2006a; Leppäranta and Wang 2008), and in North America this work was restarted for the Great Lakes (Wang et al. 2010).

Table 5.3 shows the result of magnitude analysis of the terms of the equation of motion based on the typical scales in lakes. Wind stress is the main driving force, largely compensated by the internal friction of ice. Internal friction is strong due to the limited size of lake basins with the presence of land boundary felt all over. The ice–water stress, surface pressure gradient and Coriolis acceleration have secondary influences. In free drift of ice, internal friction is zero and the wind stress must be compensated by ice–water stress and surface pressure gradient. The inertia can become significant for very rapid changes in the forcing. Advective acceleration is very small and will remain smaller than the ice–water stress term as long as $H/L < C_w$, condition that is valid except for extremely exceptional cases.

In the lake ice drift problem there are two principal time scales: local acceleration $T_I = U/(C_w H)$, and advection $T_D = L/U$. Where Coriolis acceleration is significant, the Coriolis period f^{-1} also needs to be considered. These time scales are well separated, $T_I << f^{-1} << T_D$.

In *free drift*, by definition, we have $\nabla \cdot \boldsymbol{\sigma} \equiv 0$. Since the momentum advection is very small and $T_I < 1$ h, an algebraic steady state equation results as a very good approximation. There are two specific classes of solutions (see Leppäranta 2011). If the Coriolis acceleration is significant, we have

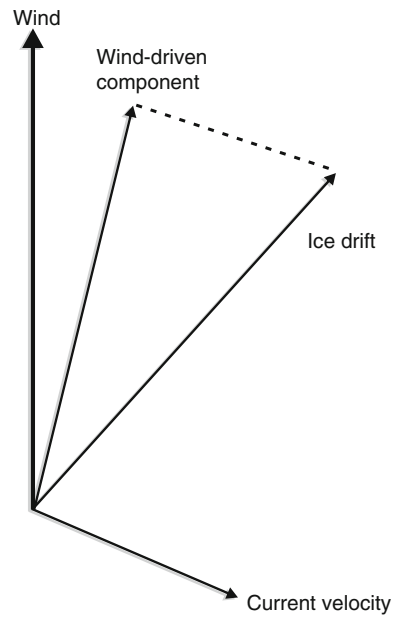

Fig. 5.15 The free drift solution as the vector sum of wind-driven ice drift and geostrophic current (when the Coriolis acceleration is significant)

$$\boldsymbol{u} = \boldsymbol{u}_{\mathrm{a}} + \boldsymbol{U}_{\mathrm{wg}} \tag{5.45a}$$

where $\boldsymbol{u}_{\mathrm{a}}$ is the wind-driven velocity and $\boldsymbol{U}_{\mathrm{wg}}$ is geostrophic current velocity: The wind-driven part is given by the wind factor $u_{\mathrm{a}}/U_{\mathrm{a}} \approx 2.5$ % and the deviation angle, which tells that the direction of ice drift is about 10–30° to the right (northern hemisphere) or left (southern hemisphere) from the wind (Fig. 5.15). When the Coriolis acceleration is not significant, we have

$$u = \sqrt{\frac{\rho_a C_a}{\rho_w C_w}|\boldsymbol{W}|}, \boldsymbol{W} = U_a \boldsymbol{U}_a - \frac{\rho}{\rho_a C_a} gh\nabla\xi \tag{5.45b}$$

and the direction of ice drift follows the direction of the vector $\boldsymbol{W}$.

In compact ice, the forcing needs to be strong enough to break the yield criterion. The ice starts motion, and the importance of the internal friction is then described by the friction number

$$X = \frac{P(H)}{FL} \tag{5.46}$$

The ice rheology has a distinct asymmetry: during closing the stress may be very high but during opening it is nearly zero. In a channel with closed end the full steady state solution is a stationary ice field with a very sharp ice edge. In the spin-down the ice flows as long as the forcing overcomes the yield level ($X < 1$).

In general, in the presence of internal friction the ice drift problem is solved using numerical models. The one-dimensional channel case can be treated semi-analytically, and the solution provides a good insight into the role of internal friction. The channel is aligned along the x-axis and closed at $x = L$ (Fig. 5.16). The boundary conditions are $u = 0$ at $x = L$ and $\sigma = 0$ at the free ice edge. The channel flow is examined using the quasi-steady-state momentum equation and the two-level ice state $J = \{h, A\}$. The system of equations is then written as:

$$\frac{\partial\sigma}{\partial x} + \tau_a + \rho_w C_w |U_w - u|(U_w - u) - \rho g h \nabla\xi = 0 \tag{5.47a}$$

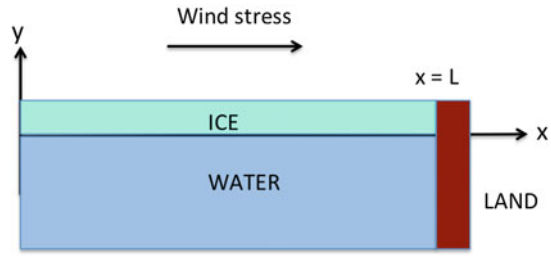

Fig. 5.16 The geometry of the channel flow problem

$$\frac{\partial h}{\partial t}+\frac{\partial}{\partial x}(uh)=0,\frac{\partial A}{\partial t}+\frac{\partial}{\partial x}(uA)=0(0\le A\le 1) \tag{5.47b}$$

If the landfast ice condition is broken, ice drift commences. Without loss of generality we can assume that the forcing is toward the positive x-axis, $\tau_a-\rho hg\nabla\xi>0$. The free drift solution is directly obtained as:

$$u_F=\sqrt{\frac{\tau_a-\rho hg\nabla\xi}{\rho_w C_w}}+U_w \tag{5.48}$$

If the ice velocity were negative, the ice would flow free toward left in the channel. Therefore it is assumed that ice velocity is positive and thus directed toward the rigid boundary at the channel end. The steady-state solution of Eq. (5.47a, b) shows that uA and uh are constant across the ice field, and thus, if the ice field is in contact with a rigid boundary, the steady state velocity is $u\equiv 0$.

For the remainder of this section, we assume that the ice field is in contact with the rigid boundary and vertical average water velocity is zero. If the ice is moving, it will drag surface water with it, but then there is a return flow at a deeper layer because of the continuity; a zero reference current for ice–water stress is therefore a reasonable assumption. The solution of the quasi-steady-state momentum equation is formally:

$$u=\sqrt{\frac{1}{\rho_w C_w}\left(\tau_a+\frac{d\sigma}{dx}\right)} \tag{5.49}$$

where the expression under square root must be positive, $\tau_a\ge -d\sigma/dx$. At the end of the channel the ice must stop and there $\tau_a=-d\sigma/dx$. In plastic flow, the stress is given by the yield level $\sigma=\sigma(A,h)$. The surface pressure gradient is zero as shown in the next paragraph.

The steady-state solution of the one-dimensional coupled lake ice–water body model for constant forcing is straightforward. In the channel of depth H, closed at one end, the coupled system is

$$\frac{\partial\sigma}{\partial x}+\tau_a+\rho_w C_w|U_w-u|(U_w-u)-\rho hg\nabla\xi=0 \tag{5.50a}$$

$$-\rho_w C_w|U_w-u|(U_w-u)-\rho_w C_b|U_w|U_w-\rho_w Hg\nabla\xi=0 \tag{5.50b}$$

where U_w is chosen as the vertical average mean current. The wind stress on the system is balanced by the internal friction of ice, sea surface tilt, and bottom friction. At the steady state for the ice thickness and water level elevation, $u\equiv 0$ and $U_w\equiv 0$, and then we must have $\nabla\xi=0$. In the absence of ice, the equilibrium condition would be $\tau_a=\rho Hg\nabla\xi$. Thus, in the steady state internal ice stress totally removes the surface pressure gradient, and the

solution is the same as in the ice-only channel model. However, to reach the equilibrium may take a long time.

5.5.5 Ice Thickness and Compactness Profiles

Let us start with an ice field that ranges from $x = 0$ to $x = L$, with $h = h_o$ = constant and $A = 1$. Let us further assume that $\sigma = -P_n\, h^n\, q(A)$, where q is the influence of ice compactness, $q(0) = 0$ and $q(1) = 1$. Wind stress is taken as a constant $\tau_a > 0$. The solution to the landfast ice problem shows that motion starts when $\tau_a L > \sigma(L)$. Plastic rheology allows a steady-state solution $u \equiv 0$ with a finite ice field.

It is known that q is highly sensitive to compactness. Ice stress goes down one order of magnitude when compactness drops from about 1 to 0.8–0.9 and furthermore thereafter. This means that a very sharp ice edge, less than 1 km wide, forms at on-ice forcing (see Leppäranta and Hibler 1985). Beyond this edge zone, $A \approx 1$, and we have two conditions to solve for the ice thickness profile. The thickness increases with distance from the ice edge due to the increasing fetch, and the conservation of ice must be satisfied:

$$\frac{dP_n h^n}{dx} = \tau_a \tag{5.51a}$$

$$\int_{x_o}^{L} h dx = h_0 L \tag{5.51b}$$

where x_o is location of the ice edge. In the steady state, wind force must exactly balance the ice strength at the channel end: $\tau_a(L–x_o) = P_n h^n$. For the linear form $n = 1$, the ice thickness in the channel end, the location of the ice edge, and the friction number are:

$$\begin{aligned} h(L) &= h(x_0)\left(\sqrt{\frac{1}{4} + 2X_0} - \frac{1}{2}\right), X_0 = \frac{\tau_a L}{P_1 h} \\ x_0 &= L\left[1 - X_0 \frac{h(L)}{h(x_0)}\right] \end{aligned} \tag{5.52}$$

For $X_0 \to 1$, $h_L \to h_0$ and $x_0 \to 0$ or, in words, the landfast ice condition results from the initial conditions. The excess of X_0 above 1 states how much deformation will take place during the adjustment process. For $\tau_a \sim 0.1$ Pa and $P_1 \sim 10^4$ Pa, $dh/dx \sim 10^{-5}$ or, in words, ice thickness increases by 1 m over 100 km. In the adjustment process, the motion of ice starts to change at the boundaries. At the free boundary the ice edge zone develops by outward opening (i.e., the compactness of ice decreases to satisfy the no-stress condition). Then the edge zone remains static and the deformation zone spreads out from the boundary, with compactness equal to 1 and thickness gradient approaching τ_a/P_1 throughout the ice field (see also Leppäranta and Hibler 1985).

The steady-state solution can be generalized to spatially variable winds and other types of yield strength formulations. The steady-state compactness and thickness profile is obtained from:

$$\sigma(x;A,h) = -\int_{x_0}^{x} \tau_a(x')dx' \tag{5.53}$$

which is valid as long as the wind stress integral is negative. Thus, the ice compactness and thickness profiles adjust to the forcing distribution. In places where the stress integral vanishes, new free boundaries form and establish drifting zones free from the channel end. In general, the steady-state profiles provide the functional form of the ice strength.

Example 5.8. Consider ice formation in an open lake with fetch L in the wind direction (Fig. 5.17). Assume that the wind stress τ_a is constant across the lake. Due to wind-driven turbulence, frazil ice forms and accumulates into a thickness profile corresponding to ice strength. In equilibrium, the ice is stationary and covers the lake, and the thickness profile is obtained from $P(h) = \tau_a x$, where x is the distance from the lee side in the wind direction. In particular, if $P = -Ph$, then the thickness profile is linear, $h = (\tau_a/P_1)x$. For $P_1 \sim 10$ kPa, $\tau_a \sim 0.1$ Pa and $L \sim 10$ km, the thickness at the windward side of the lake is 10 cm.

5.5.6 Numerical Modelling

A full lake ice model consists of four basic elements: ice state, rheology, equation of motion, and conservation of ice. Any proper ice state has at least two levels, ice compactness and thickness. The primary geophysical parameters are the drag coefficients and

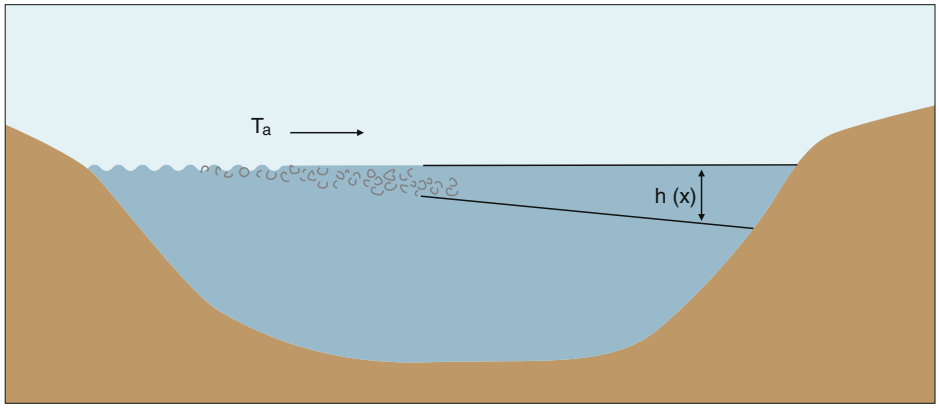

Fig. 5.17 Accumulation of wind-driven frazil ice in an open lake. Typical scale is L = 10 km for the fetch and h = 10 cm for the thickness of the accumulated frazil

the compressive strength of ice. The former tune the free drift velocity, while the compressive strength tunes the length scale and the mobility in the presence of internal friction. There are also other rheology parameters, for the dependence of the ice strength on the ice state and for the shear strength. When the plastic flow is approximated by an elastic-plastic (Coon et al. 1974) or a viscous-plastic (Hibler 1979) rheology, there is an additional rheological formulation for the stresses below the yield level. The numerical design includes the choice of the grid and, since the system is highly non-linear, the stability of the solution may require smoothing techniques. Since the minimum continuum particle size D is fairly large, the grid size can be taken as $\Delta x \sim D$. The grid size can be down to less than 1 km in basins with small floe size and in the melting season when floes break into smaller pieces.

As an example, the numerical values of the Hibler (1979) sea ice model parameters are shown in Table 5.4 based on field data and model experiments in lakes. Almost twice as large air and water drag coefficients were used in the Lake Erie model (Wang et al. 2010) than in Lake Peipsi model (Wang et al. 2006). The free drift wind factor has been about 2 %, as supported by observations. In the Lake Erie model, the standard plastic strength constant was used (compressive strength of ice of unit thickness equal to 25 kPa). The ice was quite thin, less than 10 cm, and the standard strength may have resulted in a too stiff ice cover. The transition between viscous and plastic regimes must be very low to avoid production of unrealistic creep of ice; here has been taken as 10^{-10} s^{-1}, much lower than strain-rates in major deformation events.

Table 5.4 The parameterisation of the viscous-plastic lake ice models

	Parameter	Value	Comments
I	Air–ice drag coefficient, C_a	$1.4–2.3 \times 10^{-3}$	Surface wind
	Ice–water drag coefficient, C_w	$1–2 \times 10^{-3}$	Shirasawa et al. (2006)
	Ice–water Ekman angle, θ_w	[0, 25°]	Depth dependent
II	Compressive strength $P_b h^b$	25 kPa	At h = 1 m, $½ \leq b \leq 2$
	Shear strength	12.5 kPa	Half of the compressive strength
	e-folding scale for opening	0.05	Change of strength by e^{-1} due to ΔA
	Maximum viscous creep rate, Δ_o	$<10^{-10}$ s^{-1}	Viscous–plastic transition
III	Demarcation thickness, h_o	5–10 cm	Open water—ice cover transition
IV	Spatial grid size, $\Delta x = \Delta y$	$\Delta x \gg d$	1–5 km, much more than floe size d
	Time step, Δt	3 h–1 d	Stability requirement
	Smoothing	Diffusion	Harmonic and bi-harmonic

The parameter groups are *I* atmospheric and oceanic drag parameters, *II* rheology parameters (Hibler's 1979 viscous–plastic rheology, *III* ice state redistribution parameters, and *IV* numerical design parameters

Drift ice dynamics is lateral scale dependent in two aspects. The resolution is limited by the floe size, and the forcing is limited by the size of the basin. These models have been also used for large-scale simulations in the polar oceans, semi-enclosed mesoscale marine basins such as the Baltic Sea and Gulf of St. Lawrence, and down to the scale of the Niagara river in North America (Shen et al. 1993).

In short-term modelling, the time scale of ice cover evolution is 1 h–10 days. Because the inertial time scale of drift ice is quite small (less than 1 h), the initial ice velocity can be taken as zero. In large lakes the scale of the basin size is close to the length scale of ice motion, and therefore a proper treatment of the boundary configuration is critical.

An alternative to viscous–plastic models is elastic–plastic approach provided by the AIDJEX model, which was produced in the extensive AIDJEX programme in the 1970s (Coon 1980). The elastic part necessitates the tracking of the change from the reference configuration, and the basis seems to be preferable for lake ice covers, because often the drift episodes are short events between static situations. However, applications of AIDJEX models to lake ice are not known to the author.

The objectives of ice drift modelling are basic research of the dynamics of drift ice, ice–land interaction, ice forecasting, and applications for ice engineering. Leads may open

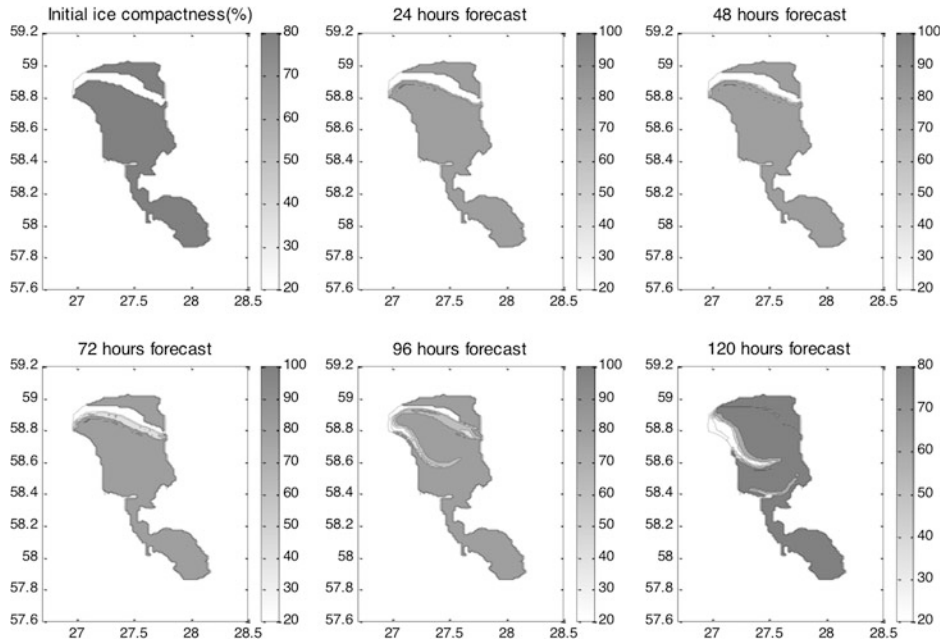

Fig. 5.18 Maps showing the results of the mechanical model simulation that showed the day-today variation in the compactness field for ice on Lake Peipsi between March 14 and 19, 2002 (Wang et al. 2006)

and close and pressure ridges may build up in one-day time scale. The key area of short-term modelling research is the scaling problem, in particular the downscaling of the stress from geophysical to local scale. In long-term modelling, ice dynamics is often neglected. First, only thermodynamic models were available for the times of freezing and ice break-up and for the evolution of ice thickness. But realistic ice dynamics are needed for the ice evolution in large lakes and, in particular, ice cover deterioration in the melting season. Ice drift has a strong influence on operations on lakes, and changes in ice conditions in large lakes or lake districts are important for weather forecasting over a few days (Yang et al. 2013) or for climate scenarios.

The Lake Peipsi ice dynamics model (Wang et al. 2006) employed a viscous-plastic rheology with the compressive strength linear in ice thickness. The model was validated by comparing the model outcome with a series of MODIS images acquired by the Aqua/Terra satellite (Fig. 5.18). The first image shows that there was an open lead in the northern part of the lake on the 15th of March. The ice then drifted towards the northeast gradually closing the lead as more open water appeared in the southern and western parts. Another lead opened in the middle of the lake on the March 18 before the ice drifted towards the northwest.

In the model simulation, the initial ice thickness and compactness were taken as 40 cm and 99 %, respectively, for the ice areas. The winds were taken from the NCAR reanalysis data at 10 m altitude. Northern winds were dominant before 17th of March and southern winds thereafter. The highest wind speed was less than 7 m s^{-1}. The model output (Fig. 5.18) follows the same pattern as the satellite images (see example in Fig. 5.11). In the first 2 days, the ice cover was immobile forced by the northern wind but a lead appeared in the middle part of the lake on March 18. The simulation for the following day shows the ice cover opening towards the south. The openings clearly result from wind forcing and the geometry of the lakeshore. Thus, as the mechanical forcing reaches the yield strength of the ice cover, the ice season changes from stable to unstable regime.

Mechanical movements of this kind are very rare in small or medium-size lakes. If the climate warms and lake ice becomes thinner, the ice cover is more likely to break in lakes smaller than before. The mobility of the ice cover is given by the criterion $\tau_a \ell > P_n h^n$. In southern Finland, the thickness of lake ice is currently 30–60 cm, and even with long fetches $\ell \sim 10$ km the climatological minimum thickness >25 cm still results in stable ice cover. With this fetch and a wind speed of 15 m s^{-1}, the ice would have to be about 15 cm thick for any significant breakage to occur. Since 1 °C climate warming would reduce the ice thickness by 5–10 cm, ice breakage would become common in Finnish lakes and in lakes as soon as the winter air temperature has increased by 2–3 °C.

In the Lake Erie model of Wang et al. (2010) validation was made against ice compactness and ice velocity histograms. There was in general a reasonable agreement. The whole ice season was simulated, and at times the ice velocities were large, 20–60 cm s^{-1} suggesting that the drift of the ice has an important role in the seasonal ice climatology of the lake.

Proglacial Lakes

6

Epiglacial lake in New Zealand. Glacial margins can sometimes be easily reached. As such glaciers and epiglacial lakes are beautiful and exciting nature objects, and the exposed land areas at retarding glaciers provide a real-time view into glacial processes creating a new landscape. Here tourists are taken to boat excursion in an epiglacial lake in the New Zealand Alps.

M. Leppäranta, *Freezing of Lakes and the Evolution of their Ice Cover*,
DOI 10.1007/978-3-642-29081-7_6

6.1 Ice Sheets and Glaciers

Ice sheets and glaciers form during long periods from annual snow accumulation exceeding ablation (see Paterson 1999). Ice sheets are large (area more than 50,000 km^2) continental ice masses, and in the present Earth such are only the Antarctic and Greenland ice massifs. Smaller long-term accumulations of ice on land are counted as glaciers. The largest of them is the Southern Patagonia ice field in Argentina and Chile, covering an area of 13,000 km^2 (Rignot et al. 2003), which is just 0.75 % of the area of Greenland ice sheet. In Europe the largest glaciers are Austfonna, Svalbard (8,500 km^2), and Vatnajökull, Iceland (8,100 km^2) (Fig. 6.1). In high-polar regions, glaciers exist at all altitudes but only in mountains in lower latitudes. At the Arctic Circle in northern Europe the glaciation level is close to 1 km altitude, and in tropical regions this altitude is 4–5 km.

The areal distribution of the surface mass balance of ice sheets and glaciers is

$$\frac{dM}{dt} = P - E - R + Y \tag{6.1}$$

where $M = M(x, y; t)$ is the ice mass per unit area, P is the precipitation, E is the evaporation, R is runoff, and Y is the net transport due to snowdrift. Each ice sheet and glacier possesses an accumulation and an ablation zone, where the annual surface mass

Fig. 6.1 Landscape photograph showing Vatnajökull in summer

Fig. 6.2 An epiglacial lake at the Russian Novolazarevskaya Station, eastern Dronning Maud Land

balance is positive and negative, respectively. In ice massif equilibrium, ice flows from the accumulation zone to the ablation zone to balance the budget.

Ice sheets and glaciers are very cold environments but even there three kinds of lakes are found (e.g., Hodgson 2012). Glacial meltwater forms seasonal or perennial lakes, which are called *proglacial lakes*.[1] Their common characteristic is that the water balance is dominated by glacial meltwater available in the ablation regions, and therefore they are located mainly close to the warm boundary of land ice massifs. But also within the accumulation zones there are two kind of isolated ablation regions. Nunataks are warm spots within the ice sheets and their surface is largely bare ground, which absorbs solar heat well (Leppäranta et al. 2013a). The surface of nunataks is kept bare by sublimation, snowdrift, and melting of snow and ice. The lakes, which form of the glacial runoff water at the edge of the ice massifs and in nunataks are *epiglacial lakes* (Fig. 6.2).

In places, on ice massifs, sublimation and net snowdrift exceed snow accumulation by precipitation, and therefore the surface is bare ice, as a distinction to the snow surface in the accumulation zone. Because of their visual appearance, these ablation regions are called *blue ice*. Due to the low albedo, blue ice absorbs much solar heat resulting in melting in the surface layer and, consequently, formation of *supraglacial lakes* (Fig. 6.3). The most exotic class of proglacial lakes is *subglacial lakes*. Such lake forms at the base of an ice massif due to the heat flux from ground and high pressure.

[1] The concept of *glacial lakes* includes all lakes with basins formed by glacial erosion.

Fig. 6.3 Supraglacial lake Suvivesi at Basen nunatak is used for the household water source in the Finnish station Aboa in the western Dronning Maud Land. Water is pumped from the lake water body to the Finnish Sisu NA-110 bandwagon

Cryoconite holes (MacDonell and Fitzimons 2008) are the extreme lower boundary of supraglacial liquid water bodies (Fig. 6.4). They are small cylindrical holes in the ice surface layer, likely formed by windblown material including mineral sediments and dry microbial mats that absorb solar heat to melt their way down into the ice. The subsequent growth of microbial mats can enhance this process and form a self-maintaining ecosystem in these holes. They have been proposed as one of the refugia for the eukaryotic biota in the controversial Snowball Earth hypothesis, when the Earth is thought to have undergone extreme freezing-drying events between 750 and 580 million years ago.

Proglacial lakes are found at polar ice sheets and as well at mountain glaciers in lower latitudes. All these lake types exist in Antarctica, where the continent and sub-antarctic islands form one of the most diverse lake districts on Earth. There has been an ongoing debate on the origin of life in the Antarctica (e.g., Gibson et al. 2006). The key question is whether the biota are primarily postglacial, or whether they are vicariant and have survived glacial advances in lacustrine refuges. The latter model would allow for a greater degree of endemism, and it could be possible that Antarctic lakes contain species that are relicts of Gondwana. There is evidence of zooplankton that has survived an entire glacial cycle, and there is also evidence that species have dispersed to the Antarctic in the present interglacial from the sub-Antarctic islands and from other higher latitude continents of the southern hemisphere.

Fig. 6.4 A cryoconite hole in the western Dronning Maud Land, initiated by windblown sediment from the Basen nunatak. The *vertical* meter stick is 2 cm wide with 10 cm long *white*- and *red* sections

6.2 Epiglacial Lakes

6.2.1 Occurrence of Epiglacial Lakes

Epiglacial lakes are found along the grounded edges of glaciers and ice sheets, and, in nunataks, on the surface or at the foot (Fig. 6.2). The presence of a depression in the ground at the glacial edge is a necessary condition for their formation. A drainage system is also needed for the glacial meltwater to take care of the water renewal. On the surface of nunataks there are seasonal snow patches and small glaciers to act as water sources. The size of epiglacial lakes varies from small ponds to large lakes. After the Last Glacial Maximum, about 10,000 years ago, the present Baltic Sea was a large, epiglacial lake of the Weichselian Ice Sheet, called the Baltic Ice Lake (e.g., Leppäranta and Myrberg 2009).

Epiglacial lakes form parts of glacial drainage systems and are common in glaciated regions. In Antarctica, this is the most common lake type and these lakes are found even deep in the interior of the continent. Precipitation also contributes to their water budgets.

Epiglacial lakes can be seasonal or perennial, and in the course of years frequent changes occur in the water storage and morphology on account of glacial movements and changing meltwater inputs.

Example 6.1. The characteristic dimensions are area A, thickness h, and renewal time-scale T for a glacier or a lake. Clearly, for epiglacial lakes we have the approximate relation

$$\frac{A_L h_L}{T_L} \approx \frac{A_G h_G}{T_G}$$

where the subscripts L and G refer to glacier and lake, respectively, Thus, if $A_G \sim 10$ km^2, $h_G \sim 200$ m, and $T_G \sim 10^3$ a, the runoff from glacier becomes 2×10^6 m^3 a^{-1}. This flux of water is able to keep a lake with, e.g., $A_L \sim 2$ km^2, $h_L \sim 10$ m, and $T_L \sim 10$ a. Using the volume of glacier or lake, $V = Ah$, we have $V_G{:}V_L = T_G{:}T_L$.

Epiglacial lakes are often perennially ice-covered, with occasional open water spots forming as a result of advected heat on the landward sides melting the lake ice during warm summers. The glacial meltwater can also occasionally flood the surface and refreeze restoring the "flat" surface of the lake, as seen, e.g., at Edge Lake in Davis Valley.

In Antarctica, the exposed areas include coastal oases (e.g., Kaup et al. 1988; Priscu 1998; Sokratova 2011). The largest oasis is the McMurdo Dry Valleys situated near the coast of the Ross Sea. Other large oases are found in the eastern Antarctica (Vestfold Hills, Larsemann Hills, Bunger Hills, Schirmacher Oasis and Syowa Oasis), and at the Ablation Point (Punta Ablación), on the east coast of Alexander Island at the Antarctic Peninsula. In Schirmacher Oasis, epiglacial lakes are ice-free in summer (Kaup 1994; Fedorova et al. 2010). Also in the Antarctic Peninsula and on the sub-antarctic islands the lakes are often ice-free in summer. In the western Dronning Maud Land, East Antarctica both ice-free and ice-covered epiglacial lakes are found at nunataks (Keskitalo et al. 2013; Leppäranta et al. 2013b). Lake Untersee in the central Dronning Maud Land is one of the largest epiglacial lakes in Antarctica, with area of 11.4 km^2 and mean depth of 169 m (Kaup et al. 1988; Wand et al. 1997). It is permanently covered by ice, which is 2–6 m thick, and it is thought to have been such at least 100,000 years. Some of the largest epiglacial lakes (Lake Fryxell and Lake Hoare) are found at glacier fronts in the McMurdo Dry Valleys.

6.2.2 Physics of Epiglacial Lakes

The size of epiglacial lakes ranges from small ponds (Fig. 6.5) to large lakes, and their depth is up to more than 300 m. The time scale of the lakes may vary from seasonal to full glacial cycles, and they may have seasonal or perennial ice cover. Epiglacial lakes can be locally important fresh water resources. Example, this is true in northern Italy, where glacial meltwater from the Alps is critically important for the agriculture. Outbursts of

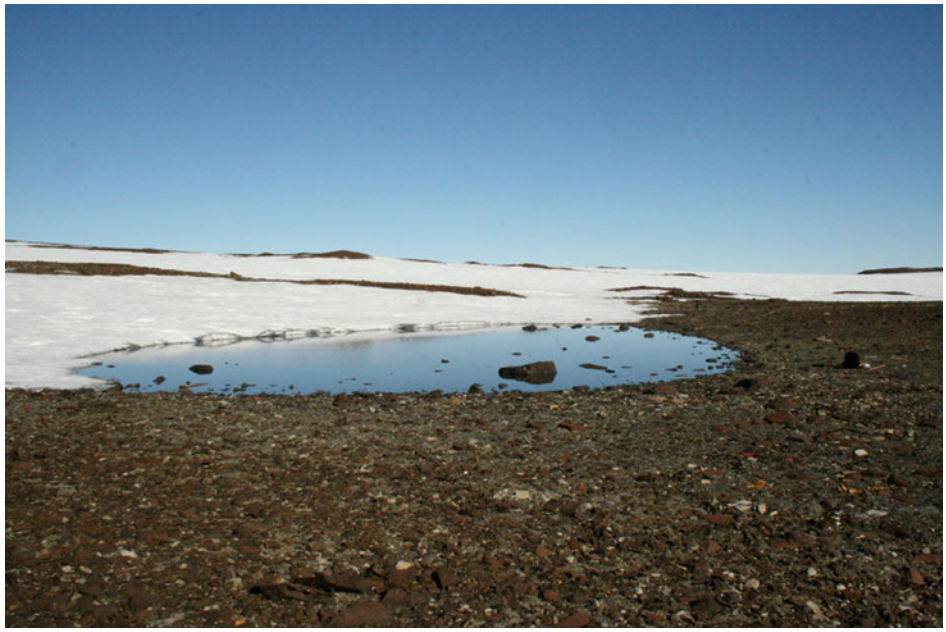

Fig. 6.5 An epiglacial pond on *top* of Basen nunatak, Dronning Maud Land

alpine epiglacial lakes have caused losses of human life and economical damages (e.g., Huss et al. 2007). Melting of Himalayan glaciers is also producing new lakes (Raj 2014) that will have impacts on the water resources in Southern Central Asia.

In Antarctica, when the ice sheet withdrew after the Last Glacial Maximum depressions were exposed in the landscape. These depressions were filled with water, the lakes were colonized by a range of organisms, and they began to accumulate the sediments that today reveal their history. In some rare areas lakes survived intact through the Last Glacial Maximum, for example, the Larsemann Hills and the Schirmacher Oasis, and in the McMurdo Dry Valleys, lakes have lifetimes for over 300,000 years. Lakes on the sub-antarctic and peri-antarctic islands are often of Holocene[2] age, formed during the retreat of local ice masses and cirque glaciers.

The physics of epiglacial lakes is not much different from 'normal' lakes. Characteristic to epiglacial lakes is that the water balance and water quality are governed by glacial meltwater. Consequently, the inflow has a remarkable seasonal variability, and the temperature of the inflow water is always low. If part of the lake shoreline is ice, it makes a strong boundary condition controlling the temperature of the lake, possibly also creating thermohaline circulation. It makes a big difference whether an epiglacial lake is perennially or seasonally covered by ice, as in the case of the normal lakes.

[2] The geological epoch, which started about 12,000 years ago and continues at present.

Epishelf lakes are formed in marine embayments or fjords, dammed by advancing glaciers and ice shelves. The marine water is replaced by fresh melt water from glaciers and snow. In some cases a hydraulic connection to the sea persists under the ice shelf or glacier, sometimes more than 100 m below sea level. Then the epishelf lake becomes meromictic.

Many of the lakes at lower altitudes in ice-free areas are below the Holocene marine limit (below 40 m in the Antarctic Peninsula, below 8 m in the Larsemann Hills) and have formed in depressions emerging from the sea as a result of postglacial isostatic rebound. Where the lakes have no surface outflow they are referred to as closed (or endorheic) lakes. Some of these closed lakes have subsequently experienced an excess of evaporation over precipitation and have gradually become saline. Examples of these are found in the McMurdo Dry Valleys. Some saline lakes become stratified for part of the year (monomictic) and others are permanently stratified (meromictic). Lakes that have outflow streams are classified as open lakes; these typically contain fresh water and do not accumulate salts to the same degree as closed lakes do. Both types of lake are common in Antarctic oases and maritime Antarctic islands.

When the main water source is glacial meltwater, the heat budget provides a limitation to the discharge. The heat provided for melt is $Q_{\mathrm{n}}A_{\mathrm{n}}T_{\mathrm{n}}$, where Q_{n} is the mean net heat flux, A_{n} is the ablation area, and T_{n} is the length of the ablation period. The volume of lake water becomes

$$V = \frac{Q_n A_n T_n}{\rho L_f} \tag{6.2}$$

This is the maximum volume for the annual water inflow and can be considered as the scale of the lakes with 1-year renewal time. In the cold season, the ice cover of epiglacial lakes grows due to heat loss from the lake to the atmosphere as presented in Chap. 4. The water body becomes perennial if the depth is more than the thickness of ice, i.e.

$$H = \frac{V}{A} > h_{\max} \tag{6.3}$$

where A is the lake area and $h_{\max}$ is the maximum annual ice thickness. In case the ice cover is seasonal, $h_{\max} \sim 2$ m serves as a good estimate for very cold climate conditions (see Sect. 4.3). There are polar lakes with a perennial ice cover, e.g. in McMurdo Dry Valleys in Antarctica. There Lake Vida has the thickest ice cover, about 20 m (Doran et al. 2004; Mosier et al. 2007). To achieve such large thickness is possible when the summer melting remains small (see Eq. 4.56).

Example 6.2. For $Q_{\mathrm{n}} \sim 100$ W m^{-2}, $A_{\mathrm{n}} \sim 100$ km^2 and $T_{\mathrm{n}} \sim 100$ days, we have $V \sim 0.28$ km^3. For $h_{\max} > 10$ m, the water body is perennial, and the horizontal scale is $\sqrt{V/h_{max}} < 170$ m. But for $h_{\max} < 1$ m, the water body is seasonal, and the horizontal scale is $\sqrt{V/h_{max}} > 530$ m.

Chemically, the lakes range from some of the freshest lakes in the world to hypersaline lakes, which do not freeze over, even in winter when their temperature can drop below −10 °C.

Epishelf lakes such as Kakapon Bay in the Bunger Hills can exhibit full marine conditions together with a marine flora and fauna including seal populations. Depending on the degree of chemical influence from the sea, versus interior climate regimes, lakes are often classified as coastal maritime lakes or coastal continental lakes. The nutrient status of Antarctic lakes is typically oligotrophic, with eutrophy usually restricted to those, which are directly influenced by visiting marine mammals, birds or people. Table 6.1 shows characteristics of the water quality in several epiglacial lakes in the western Dronning Maud Land.

Epiglacial lakes are an important habitat of life in the polar world (Kaup 1994). They contain phytoplankton, few zooplankton but no fish. Mosses are the highest forms of aquatic plant life on the continent, while higher plants are present in lakes on the peri-antarctic and sub-Antarctic islands (e.g., in South Georgia). However, the bulk of the biomass and primary productivity is benthic, consisting of cyanobacteria, diatoms and green algae, often in luxuriant mats several meters thick (Vincent 2000; Ellis-Evans 1996). The mats can be grazed by communities of rotifers, ciliates and crustacea, though

Table 6.1 Basic geochemistry of epiglacial lakes in austral summer 2010–2011 based on in situ sounding with YSI handheld multiparameter instrument (Keskitalo et al. 2013)

Date	Site	Cond (25 °C) (S cm^{-1})	Diss O_2 (mg l^{-1})	pH	Tot-N (mg m^{-3})	Tot-P (mg m^{-3})
Dec 22	Top pond	11.5	12.11	7.88	149	3
Dec 30		59.5	10.84	6.91	x	x
Jan 23		45.8	10.16	6.14	x	x
Jan 10	Top pond 2	249.0	8.48	8.19	82	4
Jan 23		253.8	9.73	8.42	85	3
Dec 29	Ring pond	26.3	12.15	9.64	x	x
Jan 08		27.2	12.50	7.6	180	15
Jan 17		35.3	11.72	8.54	149	3
Dec 29	Velodrome	162.8	10.54	7.83	x	x
Jan 08	Centre	93.0	11.94	7.8	717	4
Jan 17	Centre	82.6	12.12	7.70	205	2
Jan 08	Shore	163.7	19.62	10.82	253	15
Jan 17	Shore	93.1	15.05	9.94	800	34
Jan 13	Fossilryggen					
	Centre	63.6	12.37	9.78	220	3
	Shore	61.0	12.68	8.96	284	3

Top pond and Top pond 2 are located on top of Basen nunatak, Ring pond and Velodrome pond are located at the foot of Basen, and Fossilryggen on the top of Fossilryggen nunatak

usually these zooplankton are present at low densities. Benthic microbial mats are less common in saline lakes, but even the most saline ones contain some biota. Other biological habitats include pockets within the lake ice, the under surface of the lake ice, and the micro-stratified chemoclines of meromictic lakes where gradients of conductivity, oxygen, pH, and sulfur provide numerous niches for photosynthetic sulfur bacteria, other anoxic bacteria, and methanogenic Archaea. With many higher organisms unable to survive there, the Antarctic continent could be seen as a microbial world with the lakes being its principal bastion.

6.3 Supraglacial Lakes

6.3.1 Occurrence of Supraglacial Lakes

Supraglacial lakes form and grow from the penetration of solar radiation into an ice massif (Figs. 2.17 and 6.3). Within the ice, the heating comes from the balance between solar radiation and conduction, while at the surface there are also strong terrestrial radiation losses. Therefore, the water body may grow in the presence of an ice cover. Figure 6.3 shows a situation when the ice thickness must have been more than 30 cm to carry the 5-ton bandwagon in a water pumping operation.

Supraglacial lakes are found on the Antarctic and Greenland ice sheets and in many mountain glaciers. In Greenland they are much more developed than in Antarctica and have a major impact on the ice mass balance (Hoffman et al. 2011; Liang et al. 2012). Lake water masses may also transport latent heat deeper into the ice sheet by convection across the lake water body and penetration of lake water into fractures (Chikita et al. 1999; Joughin et al. 2008; Hoffman et al. 2011). Lake outflows may form moulins into the ice advecting heat across the ice sheet and reducing the sliding friction at the base of the ice sheet. Supraglacial lakes in mountain glaciers possess potential to create floods in the nearby environment (Bajracharya and Mool 2009). They are extremely low in biota (Keskitalo et al. 2013).

Supraglacial lakes form in blue ice regions in the surface layer of ice sheets and glaciers. The condition for the existence of the bare, blue ice surface is negative mass balance. The albedo is low due to the bare ice or open water surface (around 0.4–0.6 for ice cover and 0.1 for open water). Therefore these lakes absorb solar energy about 5–10 times more effectively than the snow-covered ice (albedo around 0.9). Solar heat is distributed across the optical thickness of the ice, which for clean blue ice is 1–2 m. On the other hand, conduction of heat in the ice is slow, and as a result the solar heat is trapped, blue ice surface layer warms, and melting of ice may start beneath the surface and grow into water bodies (Figs. 1.2 and 6.3). In summer the surface radiation balance is close to zero but the radiation transmitted through the surface (Q_T) is typically 50–100 W m^{-2} (Leppäranta et al. 2013b).

The size of supraglacial lakes ranges from small ponds to medium-size shallow lakes of several square kilometres in area. They are mainly seasonal. In the Dronning Maud Land, Antarctica they are recurrent summer lakes with the depth scale of 1 m (Winther et al. 1996; Leppäranta et al. 2013b). In Greenland they are much more developed and have a major impact on the ice mass balance (Hoffman et al. 2011; Liang et al. 2012). Since the main water source is the glacial ice, the water quality depends on the state of the surface layer.

The depth of seasonal supraglacial lakes is of the order of 1 m and their surface area can be up to several square kilometres. The thermodynamics of their formation is governed by the summer radiation balance and conduction of heat: penetration of solar radiation provides heat for subsurface melting of ice, and the low thermal conductivity of ice prevents fast heat leakage. This is one kind of a greenhouse phenomenon. The surface must be essentially snow-free to allow the penetration of sunlight.

Example 6.3. There are two vertical length scales associated with supraglacial lakes. The light attenuation distance $\kappa^{-1} \sim 1$ m and heat conduction distance $d = \sqrt{Dt}$, where $D \sim 0.10$ m^2 day^{-1} is the heat diffusion coefficient. If the consequent heat gain and loss at the depth z are equal, the temperature difference ΔT between the surface and depth z is

$$\Delta T = \frac{(1-\alpha)e^{-\kappa z}\gamma Q_s}{\rho c D} z = \frac{e^{-\kappa z} Q_T}{\rho c D} z$$

For $z \sim 1$ m and $Q_\mathrm{T} \sim 100$ W m^{-2}, we have $\Delta T \sim 10$ °C. If the temperature difference is larger, absorbed solar heat is leaked out and vice versa.

The life cycle of supraglacial lakes is a reverse process to the freezing cycle of seasonally ice-covered lakes. Their formation begins well beneath the surface, and when the ice layer on top becomes thinner, albedo decreases providing a positive feedback to the lake growth. A supraglacial lake has an ice cover, if the surface heat balance is negative. In fall, supraglacial lakes start to freeze down from the upper surface, as lakes usually do (e.g., Leppäranta 2009a), and up from the bottom. In principle, it is possible that pockets of liquid water could survive over the winter resulting in multiyear supraglacial lakes.

Lake water masses may also transport latent heat deeper into the ice sheet by convection across the lake water body and penetration of lake water into fractures (Chikita et al. 1999; Joughin et al. 2008; Hoffman et al. 2011). In particular, multiyear supraglacial lakes are not stable but grow year-by-year. This will accelerate local melting and eventually lead to catastrophic formation of fractures that ends up in a major change in the local glacial environment. Fracturing of the ice may even empty a whole lake in a short time. Meltwater convection is therefore a very important mechanism in the warming and deterioration of ice sheets and glaciers.

6.3.2 Structure of Supraglacial Lakes

Supraglacial lakes were investigated in two summers in the western Dronning Maud Land by Leppäranta et al. (2013b). The surface area of the main study lake, Lake Suvivesi (73°S 13.5°W, altitude 200 m), was about 7 km^2 at maximum, and the evolution of its vertical extent can be summarized as follows (Fig. 6.6). The lake starts to form in the solid ice sheet in the beginning of December. From about the 10th of December the lake could be utilized for liquid water supply in the nearby Aboa research station (the water usage was about 1 m^3/day, pumped from one hole in 15 min). The timing of the birth of the lake has a very small interannual variability, less than 10 days.

At the initial stage, Lake Suvivesi appears patchy. Due to the positive albedo feedback mechanism, the patches expand laterally and vertically, and thereby the lake achieves more integrity. In the peak of the summer, mid-January, there is a 0–10 cm thick ice cover on top, and the lake body extends down to about 200 cm depth consisting of two layers (Fig. 6.6). The main, upper layer is mostly liquid water and extends down to the depth of ½–1 m. The lower layer is stratified and contains slush and hard ice layers. The deepest layer is a slush layer with gravel and soil sediments. The source of this sediment is most likely the neighbouring nunatak. The lake is thus not a continuous body of liquid water but an ice–water mixture, which can be described by porosity ν equal to the relative volume of liquid water in a volume element. When $\nu > \nu_0$, the ice loses its integrity and the element turns into slush. Therefore, the lake boundaries can be defined by $\nu > \nu_0$ (Leppäranta et al. 2013b). The boundaries appear as an 'ice bog' zone from the lake main body to the solid ice sheet.

After the summer peak, the surface ice layer starts to strengthen but the radiation balance is still positive and the main body of the lake continues to grow. The field data did not cover beyond February 1st, and it is not exactly known when the lake shrinking by freezing

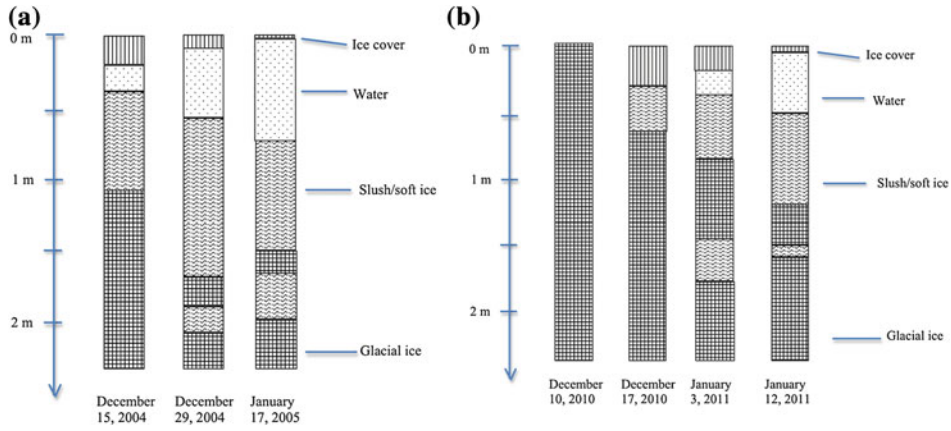

Fig. 6.6 The *vertical* profile of Lake Suvivesi in **a** December 2004–January 2005 and **b** December 2010–January 2011 (Leppäranta et al. 2013b)

begins. In the closing period of the lake, the growth of ice is expected to be 1–2 cm/day, based on experience of lake ice growth in general (see Sect. 4.3). This means that the lake would be completely frozen by April–May. Thus, the inferred age of the lake is 4–6 months, 1–2 months for growth and 3–4 months for close-up. Observations from two other lakes at Plogen and Fossilryggen nunataks within 50 km from Aboa showed similar summer evolution but the exact timing depends on the location. Further south, there is also a small, seasonal supraglacial lake at Svea Research Station (74°35′S, 11°13′W, altitude 1,245 m).

The surface of a supraglacial lake may be liquid water or ice depending on the heat fluxes and surface heat balance. The continuity of heat flux through the surface tells that in equilibrium,

$$-Q_0(T_0) = k\frac{T_f - T_0}{h} = Q_T[1 - \exp(-\kappa h)] \tag{6.4}$$

These two equations provide the solution for the surface temperature T_0 and ice thickness h. If a physically realizable solution ($T_0 \leq T_f$, $h > 0$) does not exist; then, $h = 0$ and the surface temperature is obtained from the balance between the first and third terms in Eq. (6.4).

In Greenland there are open water lakes (Liang et al. 2012), but in the western Dronning Maud Land the lakes have ice cover (Leppäranta et al. 2013b). The surface ice layer exists because the surface heat balance in this region is negative. Much of the incoming solar radiation penetrates into the ice (and liquid water beneath), and the surface absorption does not compensate for the thermal radiation loss. Only in the peak of the summer, a few days in mid-January, melting surfaced in some spots and the ice bearing capacity was below the level needed for on-ice walking or skiing. The thin ice cover corresponds to the 'cold skin phenomenon' observed in lower latitude lake and sea surfaces in daytime calm summer conditions.

The presence of hard and soft sub-layers in the lower layer is most likely due to the variability of the absorption coefficient of solar radiation with depth caused by sediments and ice crystal structure. The absorption coefficient of the sediment-rich ice is much larger than that of the clear ice, and this enables more intensive heating deeper even though the level of radiation is less. Example, if there is a strongly absorbing layer at (z, $z + \Delta z$), absorption of light in this layer relative to the previous Δz thick clear layer is (see Sect. 3.5):

$$\frac{\int_z^{z+\Delta z} a\exp(-az)dz'}{\int_{z-\Delta z}^{z} a\exp(-az)dz'} \approx \frac{a^*\exp(-a^*\Delta z)}{a_0} \tag{6.5}$$

where a_0 and a^* are the absorption coefficients in the clear ice and sediment-rich ice, respectively, If $\Delta z \sim 10$ cm and ½ $a^* \sim a_0 \sim 1\ \mathrm{m}^{-1}$, the ratio becomes 1.64. In summers sediments have melted their way down. The presence of the concentrated sediment layer below 200 cm reflects the maximum depth of the lake in recent history. The bottom of

Lake Suvivesi was quite uneven. Superposed on smoother geometry, there were holes due to condensed sediment accumulations, which had melted their way deeper.

The annual cycle of seasonal supraglacial lakes is a stationary process. Summer growth of the lake is forced by the solar radiation, which is primarily dependent on the cloudiness, while winter close-up is primarily dependent on the air temperature. But if the liquid water volume becomes large enough, the water pressure may crack the ice sheet, and the lake water would disappear into the interior of the ice sheet, slowly or catastrophically into moulins. This has been observed in the Greenland ice sheet (Joughin et al. 2008; Hoffman et al. 2011). Ice growth in winter would decrease in a warming climate, and after a certain limit the lake would turn perennial. This would further accelerate the long-term growth of the lake. In the Dronning Maud Land field study, however, no deep-water layer was found in the beginning of summer and it was therefore concluded that those lakes were seasonal.

6.3.3 Thermodynamics of Supraglacial Lakes

The heat flow in the glacier surface layer follows the heat conduction law with solar radiation as the source term (as discussed for lake ice in Sect. 4.1):

$$\frac{\partial}{\partial t}(\rho c T) = \frac{\partial}{\partial z}\left(k\frac{\partial T}{\partial z}\right) + Q_T \kappa e^{-\kappa z} \tag{6.6}$$

Two boundary conditions are needed, to be chosen from the set of fixed temperature or flux conditions:

$$z = 0: \quad T = T_0; \quad k\frac{\partial T}{\partial z} = Q_0 \tag{6.7a}$$

$$z = H: \quad T = \tilde{T}; \quad k\frac{\partial T}{\partial z} = Q_b \tag{6.7b}$$

where $\tilde{T}$ = constant is the deep ($H > 10$ m) temperature in the ice sheet. As shown in Example 6.3, the key length scales here are the light attenuation distance κ^{-1} and heat conduction distance $d = \sqrt{Dt}$, $D \sim 0.10$ m^2 day^{-1}; thus $d \sim 30$ cm in 1 day.

In the spring warming of solid blue ice, we have $\Delta T \sim 10$ °C, depth scale of the thermally active layer is $L \sim 10$ m, and the absorption of solar radiation is normally 50–100 W m^{-2}. Equation (6.6) shows then that in the active layer the mean ice temperature may change due to diffusion by $D\Delta T/L^2 \sim 0.01$ °C day^{-1}, while the vertical mean radiative heating is 0.45 °C day^{-1}. Then the radiative heating overcomes diffusion down to the depth of 5 $\kappa^{-1} \sim 4$ m. The diffusive length scale equals 2.5 m in 2 months. Thus, solar radiation rapidly warms the lake with little diffusive losses and, once the melting has begun, the solar radiation melts the ice by 2.8 cm day^{-1}. Also surface losses are small in summer compared to the heating of the lake body. Melting starts in the

interior at depth depending on the light attenuation distance and heat conduction, and then there is, due to a positive feedback in that diffusion is slower in water than in ice, drop in the daily conduction distance to 11 cm.

Consider the heat content of the upper layer of depth $H \sim 2(\kappa^{-1} + d)$, taken as the representative depth of supraglacial lakes. In the beginning of the summer, the heat content above 0 °C liquid water reference is $U = \rho(cT - L_f)H$, where T represents the mean temperature (see Eq. 4.1). The heat content changes as

$$\frac{dU}{dx} = Q_0 + Q_T + k\frac{\partial T}{\partial z}\bigg|_{z=H} \tag{6.8}$$

where the last term is the bottom heat flux, denoted below by Q_b. The summer energy gain is used for increasing the temperature and eventual melting. The main part of the heat gain is due to the penetration of solar radiation into the ice. The surface absorption of solar radiation is to a large degree compensated by heat loss due to net terrestrial radiation and sublimation; the bottom heat flux is small and stable, $Q_b \sim -2$ W m^{-2}, corresponding to a temperature gradient of –1 °C m^{-1}.

During the time period t, the vertically integrated melt becomes

$$\tilde{H} = \frac{(\overline{Q}_0 + \overline{Q}_b + \overline{Q}_T)t}{\rho L_f} + \frac{cTH}{L_f} \tag{6.9}$$

where the overbar stands for time averaging. The criterion whether a supraglacial lake forms is thus $\tilde{H} > 0$, or, since $|\overline{Q}_0 + \overline{Q}_b| \ll \overline{Q}_T$, we have an approximate criterion

$$T_{\min} > -\frac{Q_T t}{\rho c H} \tag{6.10}$$

where T_{min} is the minimum monthly mean winter temperature. With $Q_T \sim 100$ W m^{-2}, $t \sim 60$ days and $\kappa^{-1} \sim 1$ m, we have $H \sim 7$ m and $T_{\min} > -38.8$ °C.

Example 6.4. In the Aboa station, western Dronning Maud Land, the winter temperature of the surface layer of the ice sheet is –20 °C. Taking $H = 7$ m, solar heating by 100 W m^{-2} in 60 days gives melt water equivalent of $\tilde{H} = 0.83$ m. This is approximately as observed in the vicinity of the station. Further south 200 km, in the Svea Research Station, the annual mean air temperature is about –20 °C (Isaksson and Karlén 1994), and assuming that the amplitude of the annual cycle is there similar to that in Aboa, $T_{\min}$ would lie in the range from –30 to –25 °C in Svea, high enough to satisfy the criterion $\tilde{H} > 0$.

Next, consider the depth scale of the lake in more detail. The distribution of solar energy with respect to depth depends on the transparency of the medium. At depth z, the solar power absorption is $Q_T\kappa \exp(-\kappa z)$, which suggests $\tilde{H} \sim \kappa^{-1}$, i.e. the optical thickness, as one natural depth scale. Furthermore, in time t the porosity profile $\nu = \nu(z)$ can be

easily obtained from Eq. (6.6), if heat diffusion is ignored and a constant attenuation coefficient is assumed. Then, defining the lake water body by $\nu(z) > \nu_o$, the lake depth scale becomes

$$\tilde{H} = \frac{1}{\kappa}\log\left(\frac{Q_T t\kappa}{\nu_0 \rho L_f}\right) = \frac{1}{\kappa}\log\left(\frac{h'\kappa}{\nu_0}\right) \tag{6.11}$$

where h' is the meltwater production by the available radiation. For $\kappa \sim 1\ \mathrm{m}^{-1}$, $Q_T \sim 100\ \mathrm{W\ m}^{-2}$, $t \sim 60$ days, and $\nu_o \sim 1/3$, we have $\tilde{H} \sim 1.65$ m. At $\nu > \nu_o$, the strength of the ice becomes low and disappears, and the ice matrix changes into slush as observed. Thus the lake depth in the present study region scales as the inverse of the light attenuation coefficient.

Light attenuation in ice is described by a linear law as shown in Sect. 3.4 (Eq. 3.18), and the solution can be written as

$$Q_s(z) = Q_T(0)\exp\left(-\int_0^z \kappa dz'\right) = Q_T(0)\exp(-\tilde{\kappa}z) \tag{6.12}$$

where $\tilde{\kappa}$ is the mean attenuation coefficient in the surface layer of depth z. The optical thickness of the lake body is $\kappa^{-1} \approx 1$ m. According to observations (Leppäranta et al. 2013b), warming of ice is strongest ½–1 m beneath the surface in the beginning of summer when the melting of ice initiates. In the hard ice beneath the lake body, the attenuation is expected to be larger for ice rich in sediments or gas bubbles but smaller for clear ice. Since the attenuation of light in ice and water is wavelength-dependent (Sect. 3.4), for a more accurate solution of the light transfer the spectral distribution should be accounted for. However, for simplicity, in the scaling analysis we can take a constant, representative attenuation coefficient across the PAR band and depth.

The original diffusion equation can be examined in more detail for the warm-up of the glacial surface layer and initialization of melting. For this, a steady state solution is obtained for Eq. (6.6). Taking the both boundary conditions at the surface (6.7a), we have the solution:

$$T(z) = T_0 - \frac{Q_0}{k}z - \frac{Q_T}{k}\left[z - \frac{1}{\kappa}(1 - e^{-\kappa z})\right] \tag{6.13}$$

This consists of a linear profile from the surface heating plus a modification by the depth-distributed solar heating. The scale of validity of this solution is up to the length of the steady state conditions; the longer the boundary conditions hold, the deeper the solution goes. For $\kappa \to \infty$, sunlight is absorbed at the surface and linear temperature profile results. For a finite κ, the temperature profile is nonlinear in the surface layer, and when $Q_0 < 0$, a temperature maximum is obtained beneath the surface at the depth

$$z_{max} = \frac{1}{\kappa} \log \frac{Q_T}{Q_T + Q_0} \tag{6.14}$$

The temperature increase from the surface to the depth $z_{\max}$ scales with $(Q_0 + Q_T)/(k\kappa)$. Lower conductivity gives higher temperature, since the heat does not escape easily out of the ice. Example, if $Q_T \sim 50$ W m^{-2}, $Q_0 \sim -25$ W m^{-2} and $\kappa = 1$ m^{-1}, we have $z_{\max} \sim 0.69$ m and $T(z_{\max}) - T_0 \sim 20$ °C. Thus, when the melting stage is achieved inside the surface layer, the surface temperature is still quite low. According to observations in Lake Suvivesi, the surface temperature was less than –10 °C in this instant.

When the surface heat balance is negative ($Q_0 < 0$), the lake has an ice cover. This is clear in the early stages of lake development, since ice formation starts well beneath the surface. Heat flux through the ice cover equals kT_0/h, and at equilibrium it equals the heat flux from the lake body to the bottom of the ice cover. The surface ice layer also becomes thinner by sublimation, which is significant in dry climate regions. Convective mixing keeps the water temperature at the freezing point. In case conditions become favourable for the cold skin development ($z_{\max} > 0$), a thin ice sheet will form at the surface.

Recurrent supraglacial lakes close up in winter. They start to freeze down from the upper surface, as lakes usually do (see Chap. 4), but also up from the bottom. The surface heat losses are of the order of ∼–50 W m^{-2}, while the bottom loss is much smaller ∼–2 W m^{-2}. These losses correspond to ice growth rates of 14 or 0.6 mm d^{-1}, respectively.

In the closure season, the net solar plus atmospheric heat flux is negative, and the air temperature is below the freezing point. Then the ice growth is obtained from Zubov's formula (see Eq. 4.41):

$$h = \sqrt{a^2 S + b^2} - b \tag{6.15}$$

The parameter a depends on the physical properties of ice and varies very little, and in snow-free conditions, as here, also b can be fixed to represent typical atmospheric conditions (see Sect. 4.3): we can take $a \approx 3.3$ cm (°C day)$^{-1/2}$ and $b \approx 10$ cm. If air temperature is continuously below 0 °C and the average is –15 °C, the freezing-degree-days sum to $S = 2{,}250$ °C day in 5 months, then we have $h = 1.48$ m; in 10 months, the figures would be $S = 4{,}500$ °C day and $h = 2.13$ m. In addition, the lake also loses heat to the deeper ice sheet. The bottom heat loss adds a little to the growth of ice. If the temperature decreases downward by 1 °C m^{-1}, the resulting heat loss is 2 W m^{-2} and in 5 months this gives 9 cm ice growth. The thickness of ice is not very sensitive to air temperature variations. In the present case, ±3 °C overall change in the air temperature would change the ice thickness from 1.48 m by less than 20 cm, to 1.31 m or 1.63 m. The exchange of heat with the underlying ice sheet is quite stable.

The summer and winter evolution of the lake would change in a changing climate, toward a pure blue ice layer or a perennial lake. The lake growth and closing scales are shown by Eqs. (6.11) and (6.15), respectively. For no lake formation, the summer heat

gain should be less than heat needed the raise the surface layer temperature to the melting point. If a lake forms, the summer melt and winter ice growth become equal when:

$$\sqrt{\frac{2k}{\rho L_f}(-T_{a-}t_-) + b^2} - b = \frac{(\overline{Q}_0 + \overline{Q}_T)t_+}{\rho L_f} \tag{6.16}$$

where T_{a-} represents the winter mean air temperature, and $t_- + t_+ = 1$ year. The heat taken out to cool the ice compensates for the heat added for warming the ice in the annual heat balance. These factors are small, since the energy needed to raise the temperature of ice from –15 to 0 °C is only 10 % of the energy to melt the ice. With ">" or "<" inequality in Eq. (6.16), we have seasonal or perennial lakes, respectively. The balance between summer and winter to determine the survival of the lake over summer is delicate. But since ice thickness is proportional to the square root of the winter air temperature, how summer climate changes in future is more critical to assess whether these presently seasonal lakes can change to perennial.

Example 6.5. Take $T_{a-} \sim -10$ °C, $t_+ = 90$ days and $Q_0 + Q_T \sim 100$ W m^{-2}. The summer melt is 2.55 m, and the winter growth is less, 1.63 m, resulting in a perennial, growing lake. Decreasing the temperature to –15 °C and length of summer to 60 days, the summer melt becomes 1.71 m and the winter growth is (in theory) more, 2.13 m, turning the lake into a seasonal lake.

If the lake survives one summer, there will be a liquid pocket as the initial condition in the following summer, and therefore perennial lake is not stable but growing year by year. Changing of a supraglacial lake from seasonal to perennial accelerates local melting, leads to lake growth and eventually to formation of fractures taking the water in and ending in a major change in the local glacial environment.

6.3.4 Case Study

A case study of summertime thermodynamics of Lake Suvivesi, western Dronning Maud Land, was presented by Leppäranta et al. (2013b). The radiation balance, based on field measurements, is shown in Fig. 6.7. The net radiation as well as the radiation penetrating into the lake (i.e. sunlight) varied within 50–150 W m^{-2}, while the surface balance was between –50 and +20 W m^{-2}. Solar radiation is relatively high in the study region during summer since the sky is mostly clear. In January 3–20 the surface balance was slightly positive for a longer time, indicating the thinning of the surface ice layer. Turbulent fluxes were not continuously measured. The sensible heat flux was low in summer in the study region but evaporation was up to 1–2 mm/day in windy conditions, corresponding to latent heat loss of 30–60 W m^{-2}. These losses are transient but reflected in the thickness of the surface ice layer. The loss of ice by sublimation accounts to the total of 2–4 cm during summer.

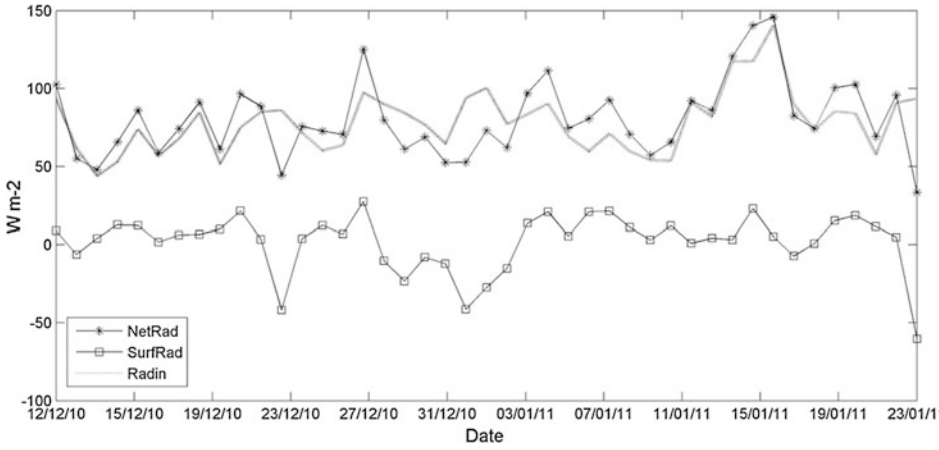

Fig. 6.7 Radiation balance from December 12, 2010 to January 22, 2011 in Lake Suvivesi. *Netrad* net radiation, *Surfrad* surface radiation balance, and *Radin* solar radiation penetrating into the lake body (Leppäranta et al. 2013b)

The lake body has a good transparency. Figure 6.8 shows the quantum scalar irradiance recorded with a spherical PAR sensor at a depth of 60 cm at 10-min intervals. The numerical values can be converted to energy flux (in W m^{-2}) approximately by dividing by 5.0 (see Sect. 2.2) and, assuming diffuse irradiance conditions, they need to be further divided by 4 to obtain the planar downwelling irradiance. The peak values in the first half of the record are about 2,500 μmol m^{-2} s^{-1} and in the latter part 2,000 μmol m^{-2} s^{-1}. Daily averages were about 900–1,200 μmol m^{-2} s^{-1}. Using the albedometer measurements, the estimated attenuation coefficient was $\kappa = 0.5–0.7$ m^{-1} (Leppäranta et al. 2013b). This corresponds to the transparency of the surface ice and the mixture of liquid water and slush. In the hard ice beneath the lake, the attenuation is expected to be larger if there are sediments or gas bubbles, but smaller for clear ice.

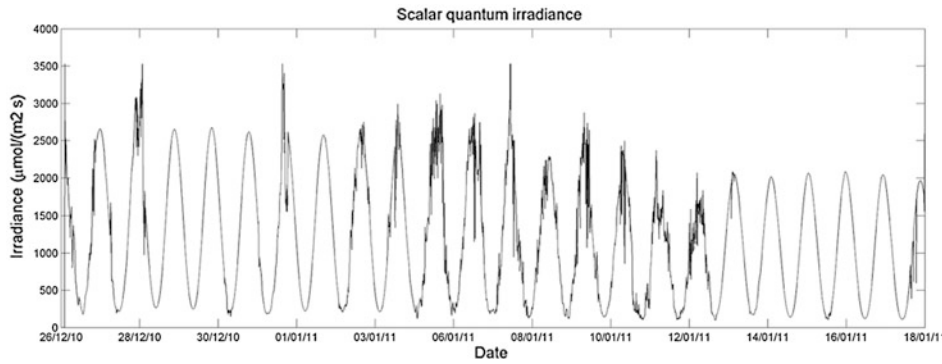

Fig. 6.8 Quantum scalar irradiance at a depth of 60 cm in Lake Suvivesi in austral summer 2010–2011. Date is given as day/month/year (Leppäranta et al. 2013b)

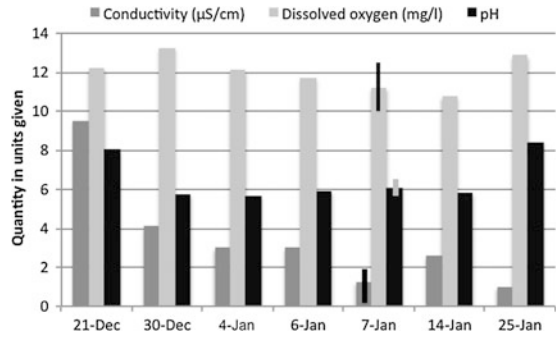

Fig. 6.9 Conductivity (25 °C), dissolved oxygen and pH in Lake Suvivesi, December 2010–January 2011. For January 7th, ± standard deviations are shown by the *narrow columns* (Leppäranta et al. 2013b)

The water was very clean in the lake (Fig. 6.9). The electric conductivity (at 25 °C reference) was 1–10 µS m^{-1} and limnologically it was classified as ultra-oligotrophic. The water was nearly saturated by oxygen, and pH varied between 6 and 8. Higher values were due to transport from the nearby nunatak. The lake was extremely low in biota (Keskitalo et al. 2012).

6.4 Subglacial Lakes

Subglacial lakes, rivers and wetlands are very old water bodies at the base of ice sheet (e.g. Siegert et al. 2001; Priscu and Foreman 2009). They are very specific physical and microbiological systems at the bottom of the Antarctic ice sheet (Fig. 6.10), not yet well known. They were first found by airborne radio echo sounding. These lakes lie up to 4,200 m under the ice sheet surface, and their length dimension ranges from 1 to 241 km. The best known is Lake Vostok. Other lakes are found in the Dome C and Ridge B

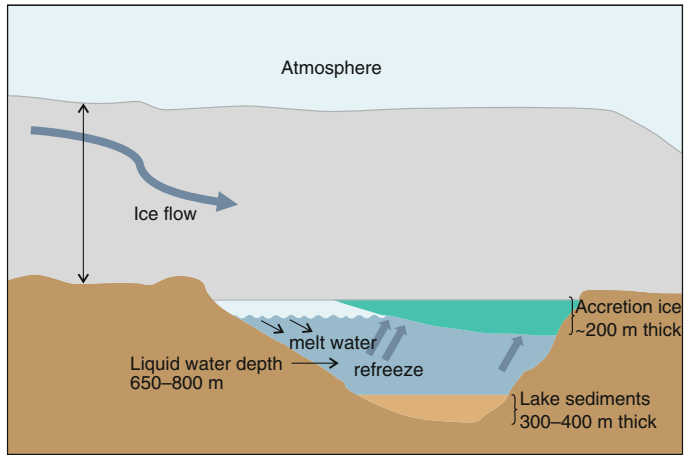

Fig. 6.10 Schematic picture of a subglacial lake

regions of eastern Antarctica (Siegert et al. 2001). Recently subglacial lakes have been found also in Greenland (Palmer et al. 2013) and European Alps (Vincent et al. 2012). There is evidence that subglacial Lake McGregor existed under the Laurentide ice sheet in North America in the last glacial maximum (Munro-Stasiuk 2003).

The earliest evidence of Antarctic subglacial lakes was from Russian aircraft pilots flying missions over the Antarctic continent. The presence of the lakes was subsequently verified by seismic investigations and airborne radio–echo sounding during the 1960s and 1970s (Masolov et al. 2006). We now know that more than 150 lakes exist beneath the Antarctic ice sheet, many of which may be connected by large subglacial rivers. The largest of them is Lake Vostok (Zotikov 2006). Approximately 81 % of the detected lakes lie at elevations less than 200 m above the mean sea level, while the majority of the remaining lakes are 'perched' at higher elevations. Sixty-six percent of the lakes lie within 50 km of a local ice divide. The high density of lakes in the Dome-C region implies that they may be hydrologically connected within the same watershed and would be an important system to study from the standpoint of subglacial hydrology and biological and geochemical diversity.

6.4.1 Formation and Diversity

Subglacial lake environments rest at the intersection of continental ice sheets and the underlying lithosphere. This unique location sets the stage for generating a spectrum of subglacial environments reflective of the complex interplay of ice sheets and the lithosphere. The association of subglacial lakes with local ice divides leads to a fundamental question concerning the evolution of the lake environments. Is the location determined by the ice sheet or by characteristics of the lithosphere (e.g., basal morphology, geothermal flux, sub-ice aquifers)? With the exception of central West Antarctica, where only few lakes exist, we know little about either the lithospheric character along these catchment boundaries or the history of their migration, given by layering within the ice sheet.

There are two factors that lead to the formation of subglacial lakes: the presence of geothermal heat flux (Q_g) at the base of the ice sheet and the good insulation capacity of the ice sheet. At the lake surface, the phase equilibrium and the continuity of the heat flow require that

$$T(H;t) = T_f(p,S) \tag{6.17a}$$

$$\rho_w L \frac{dH}{dt} = k_i \left.\frac{\partial T}{\partial z}\right|_{z=H} + Q_g \tag{6.17b}$$

where H is the depth of the lake surface from the top of the ice sheet. Considering a long-term balance, we can assume a linear temperature gradient across the ice sheet. At the steady state, $H =$ constant and the geothermal heat flux is fully conducted through the ice

to the atmosphere. Then the left-hand side of Eq. (6.17b) is zero, and we can solve this equation for the depth H:

$$H = \frac{k(T_f - T_0)}{Q_g} \tag{6.18}$$

Here T_0 is the surface temperature of the ice sheet. The freezing point decreases with pressure by $p \times 7.53 \times 10^{-3}$ °C bar^{-1} (see Eq. 2.7b). Beneath 4 km of ice, the pressure is about 350 bar and the freezing point of fresh water is –2.7 °C. If $Q_g \sim 50$ mW m^{-2} and $T_f - T_0 \sim 50$ °C, we have $H \sim 2$ km. The result is quite sensitive to the geothermal heat flux. For a physically realizable subglacial lake, the solution for H must be less than the thickness of land ice in the considered location. As discussed in Sect. 4.4, the time-scale of thermal diffusion is L^2/D, where L is the length scale and D is the diffusion coefficient, $D \sim 0.1$ m^2 day^{-1} for ice. Thus, for $L = 1$ km the time-scale is 30,000 years.

Antarctic subglacial lakes have been categorized into three main types: (1) lakes in subglacial basins in the ice-sheet interior; (2) lakes perched on the flanks of subglacial mountains; and (3) lakes close to the onset of enhanced ice flow. The bedrock topography of the ice-sheet interior involves large subglacial basins separated by mountain ranges. The lakes in the first category are found mostly in and on the margins of subglacial basins. These lakes can be divided into two subgroups in regards with their location: (a) Sites where the subglacial topography is relatively subdued, often toward the center of subglacial basins; and (b) Sites where significant topographic depressions exist, often closer to subglacial basin margins, but still near the slow-flowing center of the Antarctic Ice Sheet. Where bed topography is very subdued, deep subglacial lakes are unlikely to develop. The subglacial lakes in Antarctica have remained unexplored except by using remote sensing technology. There are no bottom sediment samples to tell about the history of the ice sheet.

Theoretical models reveal that the subglacial environment may hold about 10 % of all surface lake water on Earth, enough to cover the whole continent with a uniform water layer with a thickness of about 1 m (see Priscu and Foreman 2009). These models further reveal that the average water residence time in the subglacial zone is 1,000 years. The biology of subglacial lakes is largely an open question. The evidence to date suggests that communities of microorganisms may exist in these lakes. Recently, attention has been focused on the possibility that subglacial environments of Antarctica may harbour microbial ecosystems isolated from the atmosphere for as long as the continent has been glaciated (20–25 million years).

6.4.2 Lake Vostok

Lake Vostok (Zotikov 2006) is the largest known subglacial lake. Its surface area is about 14,000 km^2 or about the same size as Lake Ladoga, Russia. The mean depth of Lake

Vostok is 150 m, the maximum depth is about 800 m, and the volume is about 5,400 km^3. The water residence time has been estimated to be around 50,000 years. It is the only lake that occupies an entire section of a large subglacial trough.

An ice core extracted from above Lake Vostok has revealed a diversity of yeasts, Actinomycetes, algae, and spore-forming bacteria. Some of these organisms have remained viable in the ice for 36,000 years. Since the ice above Lake Vostok is over 500,000 years old, the lake could contain microbial genomes, which have been isolated from the rest of the biological world for that period. The prospect of analysing these subglacial communities, their genetics and physiology might open up a wide variety of questions concerning Antarctic biogeography and microbial evolution (Doran et al. 2004).

Ice cores comprised of water from Lake Vostok frozen to the overlying ice sheet have shown the presence, diversity, and metabolic potential of bacteria within the accreted ice overlying the lake water (see Priscu and Foreman 2009). Estimates of bacterial abundance in the surface waters range from 150 to 460 cells ml^{-1} and small subunit rDNA gene sequences show low diversity. The sequence data indicate that bacteria in the surface waters of Lake Vostok are similar to present day organisms. This similarity implies that the seed populations for the lake were incorporated into the glacial ice from the atmosphere and were released into the lake water following the downward transport and subsequent melting from the bottom of the ice sheet. Subglacial lakes present a new paradigm for limnology, and once sampled, will produce exciting information on lakes that have been isolated from the atmosphere for more than 10 million years.

Lake Water Body in the Ice Season

7

Seasonally freezing lakes cool in the autumn and start to freeze from the shore areas. The period of freeze-up is short in small or shallow lakes, but in large or deep lakes the freeze-up can take a long time and full ice coverage is not necessarily reached. Melting of ice begins from the near-shore areas. The presence of ice introduces major changes into the lake–atmosphere interaction as compared with the open water season.

M. Leppäranta, *Freezing of Lakes and the Evolution of their Ice Cover*,
DOI 10.1007/978-3-642-29081-7_7

7.1 Ice Formation

7.1.1 Cooling Process

The annual cycle of cold region lakes is influenced by the ice formation. Seasonal ice cover is typical in the boreal zone, while a perennial lake ice cover occurs in some high polar or high mountain lakes. The ice cover buffers the surface water temperature to the freezing point and largely decouples the water body from the atmosphere. The circulation changes from wind-driven to thermohaline (Kirillin et al. 2012b). Processes beneath the ice are slowed down, and lake memory effects extend over the winter. In the ice season, the inflow and outflow also normally decrease. The heat storage of the bottom sediments becomes an important source (Falkenmark 1973), and heat leakage is only by molecular conduction through the ice cover. Oxygen is consumed especially in the bottom waters of eutrophic lakes, and the primary production becomes light-limited in snow-covered frozen lakes.

The first phase of the winter season in seasonally freezing lakes can be taken as the period when the lake is open and the surface temperature T_0 is beneath the temperature of maximum density, $T_0 \leq T_m$. This period, called as 'pre-winter' by Kirillin et al. (2012), can be long in freshwater and brackish lakes but the lake has then the potential to freeze rapidly. It needs only a short, calm and cold event to establish a stable stratification in a thin surface layer resulting in ice formation. Example for a 1-m water layer, cooling by 50 W m^{-2} lowers the temperature by 1 °C in 1 day, easily reached by net terrestrial radiation loss.

The quality of the cooling process in seasonally freezing lakes can be classified in terms of the water salinity (Table 7.1). In brackish and saline lakes, the seawater formulae (see Eqs. 7.2–7.7) can be used for the temperatures of the freezing point and maximum density, but in hypersaline lakes the exact chemical constitution of the liquid water becomes significant and these temperatures need to be determined individually for each lake. In saline and hypersaline lakes, free convection to the halocline continues until ice formation, and the pre-winter does not exist in the sense it does in freshwater and brackish lakes. In brackish lakes, the strength of the stratification at temperatures $T < T_m$ decreases with salinity (Fig. 2.5).

During the pre-winter, stratification and mixing events come and go until freezing. Since the thermal expansion coefficient drops to zero at T_m, near T_m the influence of temperature on density is small. Then small differences in salinity may overcome the temperature effects on the water density (see Example 2.4).

Table 7.1 Characteristics of cooling process in seasonally freezing lakes

	Salinity S (‰)	Freezing point T_f° (C)	Cooling	Turnover
Fresh water	$S < 0.5$	≈0	$T_f < T_m$	Full
Brackish	$0.5 \leq S < 24.7$	0 to −1.3	$T_f < T_m$	To halocline
Saline	$24.7 \leq S < 40$	−1.3 to −2.5	$T_f \geq T_m$	To halocline
Hypersaline	$S \geq 40$	<−2.5	$T_f \geq T_m$	To halocline

Vertical stratification of a lake has a major role in the cooling process. The quality of the stratification is given by the vertical temperature profile: in stable, neutral or unstable situation, the temperature gradient toward increasing depth is positive, zero or negative, respectively.[1] In very deep lakes, such as Lake Baikal, the compressibility of water needs to be also considered. Unstable situations are very short living and lead to vertical convection to the depth across where a neutral or stable stratification is recovered. The density of lake water depends in general on the temperature, salinity, and pressure, given by the equation of state (see Sect. 2.12).

The strength of the stable stratification can be expressed by the vertical density gradient, which scales to the Väisälä frequency N by

$$N = \sqrt{\frac{g}{\rho_0} \cdot \frac{\partial \rho}{\partial z}} \tag{7.1}$$

where ρ_0 is reference density and z is the vertical co-ordinate positive downward. The quantity N gives the highest frequency of free oscillation of a water particle in a stratified fluid. In pre-winter conditions, $N \sim 10^{-2}$ s^{-1}. In turbulent boundary layers, the stability of the stratification is the ratio of buoyant production to shear production of turbulence, given by the Richardson number

$$Ri = \frac{g}{\rho_0} \cdot \frac{\frac{\partial \rho}{\partial z}}{\left(\frac{\partial u}{\partial z}\right)^2} = \frac{N^2}{\left(\frac{\partial u}{\partial z}\right)^2} \tag{7.2}$$

In stable (unstable) situation, $Ri > 0$ ($Ri < 0$). According to observations, for $Ri > 0.2$ turbulence would be damped by the buoyancy.

Example 7.1. For fresh water, the density at 0 °C is 0.13 kg m^{-3} lower than at 4 °C. For temperature change from 0 to 4 °C across a 10-m water layer, Väisälä frequency is $N = 0.011$ s^{-1} and to damp the turbulence, the vertical shear needs to be less than 0.025 s^{-1}. This is valid for very weak winds over open lakes or beneath a full ice cover. In brackish water with salinity 10 ‰, the density difference $T_m - T_f = 0.045$ kg m^{-3}, and the limiting shear is half of that in the fresh water case.

Thus, in pre-winter, strong winds can easily destroy the inverse stratification, which then returns in weak wind periods. Several mixing–restratification phases may occur. This process determines the distribution of temperature in the water–sediment system of a lake at the time of freezing and also controls the oxygen storage for the winter, since the oxygen saturation level depends on the temperature (Fig. 7.1) (Terzhevik et al. 2009). Mechanically forced mixing can extend over a large temperature range, from T_m down to

[1] Strictly speaking, stable stratification means that a water parcel returns to its original position after a vertical disturbance, while in unstable stratification a disturbed parcel goes further away.

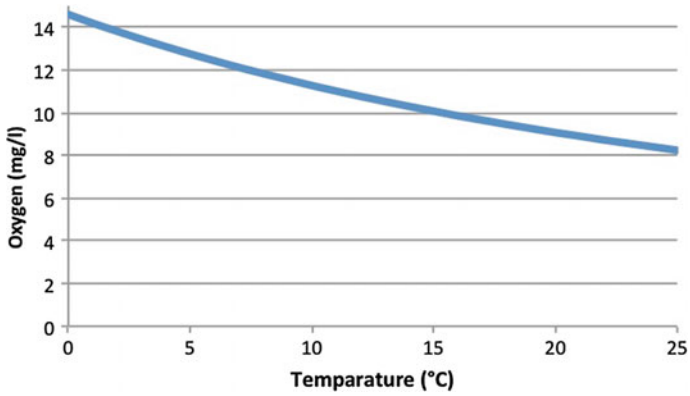

Fig. 7.1 Oxygen saturation as a function of temperature

the freezing point (Homén 1903). Example in the large lake Päijänne in Finland, maximum depth 95 m, in windy autumn the turnover continues down to 1–2 °C (Pulkkanen and Salonen 2013). Eventually, a persistent inverse winter thermocline develops, and then freezing state can be reached fast. At freeze-over of freshwater lakes, initial winter stratification is set up.

Also in pre-winter conditions, factors having usually secondary effects on the stratification dominate the stability of the water column, in particular hydrostatic pressure variations in very deep lakes. The temperature of maximum density decreases with increasing pressure, $T_m = T_m(p)$, at the rate of 0.020 °C bar^{-1} (or about 0.2 °C/100 m water depth). Therefore, with the isothermal water column held at the temperature $T_m = T_m(p_0)$, a transition depth exists where the local temperature equals $T = T_m(p)$. Deeper down, a temperature increase produces gravitational instability, called *thermobaric instability*. Hence, downward movement of initially stable water may turn into free convection, if the wind mixing is strong enough to penetrate below the transition depth (Farmer and Carmack 1981; Carmack and Weiss 1991). Once created, thermobaric convection penetrates deep into a neutrally stratified water column and contributes significantly to the ventilation of deep lakes such as Lake Baikal (Shimaraev and Granin 1991; Shimaraev et al. 2011).

Lake waters cool together with the ambient atmosphere (Fig. 7.2). Convection takes place deeper and deeper as the temperature of maximum density is approached from above. Therefore in deeper lakes the timing of potential ice formation is later than in shallow lakes. Freshwater lakes mix through at their temperature of maximum density $T_m = 3.98$ °C, and after some further cooling stable winter stratification is set up. Surface water experiences a minor supercooling, depending on the particular weather conditions (usually $\sim$0.1 °C but may be up to 1 °C).

Brackish, saline and hypersaline lakes, unless very shallow, are stratified in salinity, and mixing does not need to reach the bottom but only the halocline, which thus represents the maximum mixing depth in fall. In limnology such lakes are called meromictic. In

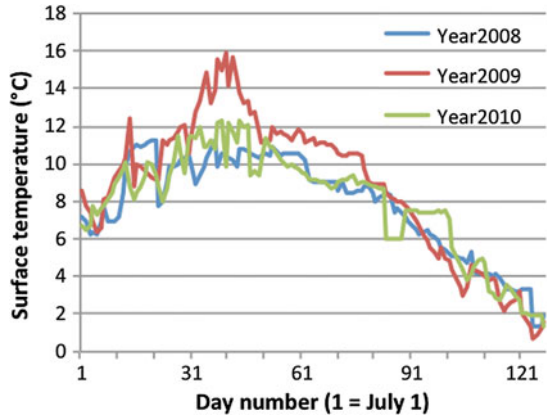

Fig. 7.2 Cooling of surface layer water in a tundra lake, Lake Kilpisjärvi in years 2008–2010. The data are from the data base *Hertta* of the Finnish Environment Centre

brackish lakes the $T_m > T_f$ but the difference $T_m - T_f$ decreases with salinity and the density maximum at $T = T_m$ weakens. In saline and hypersaline lakes, $T_m < T_f$ so that convection continues down to the halocline until freezing. In saline lakes the freezing point is still above −2 °C, but in hypersaline lakes the freezing point can become very low, at extreme around −50 °C in Don Juan Pond in Victoria Land, Antarctica. In brackish lakes, $\rho(T_m, S) - \rho(T_f, S) < 0.1$ kg m^{-3}, which corresponds to the influence of increase of 0.1 ‰ salinity unit to density. Since the salinity influence to density is to first order independent of the absolute salinity level, it is seen that quite weak halocline is able to stop convection in cooling of cold lakes.

Heat is transferred into/out of lakes by fluxes at the boundaries and by solar radiation in the interior. In three-dimensional analyses it is convenient to fix the zero level of the vertical co-ordinate (z) beneath the lake bottom. The lake bottom and surface are then $b = b(x, y)$ and $\xi = \xi(x, y)$, respectively. The heat conservation law for a lake is expressed as

$$\frac{\partial}{\partial t}(\rho cT) + \boldsymbol{u} \cdot \nabla(\rho cT) = \nabla \cdot (\boldsymbol{\kappa} \nabla T) + \exp[-k(\xi - z)]Q_T \tag{7.3}$$

where c is specific heat, and $\boldsymbol{\kappa}$ is thermal conductivity tensor.[2] We can approximate the volumetric heat content as $\rho cT \approx \rho_0 c_0 T$, where $\rho_0 c_0 = 4.20$ MJ m^{-3} °C^{-1} is a fixed reference heat capacity. In turbulent flow, the thermal conductivity is anisotropic with $\kappa = \kappa_H$ in the horizontal plane and $\kappa = \kappa_V$ in the vertical direction, $\kappa_H \gg \kappa_V$; thus $\kappa_{xx} = \kappa_{yy} = \kappa_H$, $\kappa_{zz} = \kappa_V$ and $\kappa_{pq} = 0$ ($p \neq q$).

[2] It is assumed here that lakes with open water surface are turbulent. For laminar conditions, the heat conductivity would be replaced by the isotropic molecular heat conductivity κ.

Denoting $\boldsymbol{K} = \boldsymbol{\kappa}/(\rho_0 c_0)$, $\boldsymbol{K}$ being then the thermal diffusivity, we have:

$$\frac{\partial T}{\partial t} + \boldsymbol{u} \cdot \nabla T = \underline{\nabla} \cdot (K_H \underline{\nabla} T) + \frac{\partial}{\partial z}\left(K_V \frac{\partial T}{\partial z}\right) + \left[1 - \mathrm{e}^{-k(\xi - z)}\right] \frac{Q_{si}}{\rho_0 c_0} \tag{7.4}$$

where the underlined quantities refer to the horizontal plane. The left-hand side gives the material rate of change of temperature (local change plus advection), and the right-hand side terms are horizontal diffusion, vertical diffusion and penetration of solar radiation into the lake. This equation can be solved with prescribed velocity field or simultaneously with a 3-dimensional circulation model. If $\xi - b \gg k^{-1}$, solar radiation does not reach the lake bottom and the bottom heat storage remains passive. The surface boundary conditions of Eq. (7.4) read:

$$\left.\frac{\partial T}{\partial z}\right|_{z=\xi} = \frac{Q_0}{\rho_0 c_0} \tag{7.5}$$

The vertical temperature gradient at the surface closes the surface heat balance. The bottom boundary condition can be based on the temperature or the heat flux. Inflow and outflow introduce also open boundary conditions.

Since cooling is primarily a vertical process, one-dimensional (vertical) models can tell much of its physics. These vertical models are classified into analytical models, mixed-layer models, and turbulence models.

Integration of Eq. (7.4) from the level d to the surface gives

$$\begin{aligned}(\xi - d)\frac{d\tilde{T}}{dt} = & K_V \left.\frac{\partial T}{\partial z}\right|_{z=d}^{z=\xi} + \left[1 - \mathrm{e}^{-k(\xi - d)}\right] \frac{Q_T}{\rho_0 c_0} \\ & + \int_d^\xi \left\{ -w\frac{\partial T}{\partial z} - \left[\underline{\boldsymbol{u}} \cdot \underline{\nabla} T + \underline{\nabla} \cdot (K_H \underline{\nabla} T)\right] \right\} dz\end{aligned} \tag{7.6}$$

where $\tilde{T}$ is the mean temperature across the integrated layer. The horizontal advection and diffusion terms have been moved together into the brackets $[\cdot]$ in the integral, and they need to be parameterized in vertical models. Vertical advection cannot be integrated in general form and it is usually neglected as a small term. The depth of lake is $H = \xi - d$.

Assuming that d = constant and water level variations to be small compared to the depth, $\xi \ll d$, we can take $H \approx$ constant. Then, also assuming that the lake depth is much larger than the optical thickness of lake water, $H \gg \kappa^{-1}$, Eq. (7.6) can be written as

$$\frac{d\tilde{T}}{dt} = \frac{Q_0 + Q_T + Q_b}{\rho_0 c_0 H} + \Gamma_H \tag{7.7}$$

where Q_b is the heat flux from lake bottom, and Γ_H is the influence of horizontal advection and diffusion.

7.1.2 Two-Dimensional Features in Pre-winter

The progress of the pre-winter also contains two-dimensional features, apart from the influence of general circulation. Cooling of water is naturally fastest in shallow areas, in particular in the near-shore zone, and extends offshore. At $T_0 > T_m$, cooling nearshore waters become denser, sink, and flow toward deeper parts along the sloping bottom. Central basin surface waters flow laterally toward shore to close the loop. Even in medium-size lakes the deep basin may freeze several weeks later depending on the weather conditions. In deep lakes, mixing with no freeze-up may continue through the winter; in limnology they are called warm monomictic lakes (Hutchinson 1957).

The situation $T_0 < T_m$ is first reached near the shoreline. Then the thermohaline circulation system becomes blocked at the shore, and the 4 °C isotherm is shifted further offshore (Fig. 7.3), and as a result the freezing of the central lake is delayed. The blocking 4 °C isotherm is called *thermal bar* (Zilitinkievich et al. 1992). In principle it is present in all lakes but in large lakes the time scale of the thermal bar lifetime becomes long. Example thermal bar is regularly observed in Lake Ladoga, the largest lake in Europe, where it persists for several weeks (e.g., Rumyantsev et al. 1999).

7.1.3 Analytic Slab Models

Analytical modelling of the cooling process is based on Eq. (7.7). Approximating the water temperature to be vertically uniform, we have a one-layer equation, called the slab model. The linearized form (Eq. 4.20) is employed for the atmospheric and solar heat flux to the lake. Then Eq. (7.7) becomes:

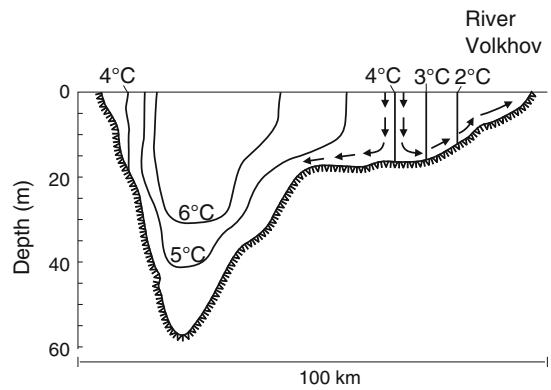

Fig. 7.3 Thermal bar in Lake Ladoga (redrawn from Melentyev et al. 1997). The 4 °C isotherm separates the circulation from coastal and central parts of the lake for longer periods

$$\frac{dT}{dt} = \lambda(T_a - T) + r + q_b + \Gamma_H; \quad \lambda = \frac{k_1}{\rho_0 c_0 H}, \quad r = \frac{k_0}{\rho_0 c_0 H}, \quad q_b = \frac{Q_b}{\rho_0 c_0 H} \tag{7.8}$$

Here λ is the inverse response time of the water layer to thermal forcing, and r represents the part of the surface boundary condition explicitly independent of the water temperature. The bottom heat flux q_b and horizontal heat flow Γ_H may be prescribed or may depend on the water temperature T; in the latter case they introduce own time scales to the system. The solution can be written as

$$T(t) = T(0)e^{-\lambda t} + \int_0^t e^{-\lambda(t-\tau)}(\lambda T_a + r + q_b + \Gamma_H)d\tau \tag{7.9}$$

where the integral on the right side is taken independent of T. Assume that $q_b = \Gamma_H = 0$. The memory time scale of the system is λ^{-1}; its magnitude is $\lambda^{-1} \sim 3$ day m$^{-1} \times H$ (Leppäranta 2014). Then, if T_a and r are constants, we have $T(t) = T(0)e^{-\lambda t} + (T_a + \Delta T)(1 - e^{-\lambda t})$, where $\Delta T = \lambda^{-1} r = k_0/k_1 \sim -2$ °C. After the time of $\sim 3\lambda^{-1}$, the equilibrium $T = T_a + \Delta T$ is nearly obtained ($e^{-3} = 5$ %).

In case $Q_b \neq 0$ or $\Gamma_H \neq 0$, the term can be absorbed into r if it is independent on T; then the level of water temperature evolution is shifted. Otherwise, if expressed analogous to the term $\lambda(T_a - T)$, $Q_b = \lambda_b(T_b - T)$ or $\Gamma_H = \lambda_H(T_H - T)$, the term can be absorbed there. In the cooling season, the heat flux from the sediments is much smaller than the surface heat flux, except in geothermal lakes. Horizontal advection may be significant in lakes with through flow or in connection with circulation bringing water from the central basin to the littoral zone.

Example 7.2. Take the bottom heat flux as 5 W m^{-2}, which represents an upper limit according to observations. If $k_1 > 10$ W m^{-2} °C^{-1}, the water temperature will be raised by less than 0.5 °C in the steady state. This is indeed a small factor in the cooling process. But after freeze-over of the lake it becomes important.

The analytic model provides a view whether a lake is ice-free or freezes over, i.e. the fundamental question of ice occurrence in ice phenology. Consider (for simplicity) a freshwater lake, and take a parabolic form of the winter temperature evaluation, expressed as $T_a(t) = 4T_{am}t(\tau_f - t)/\tau_f^2$, where $T_{am} < 0$ °C is the minimum air temperature in winter and τ_f is the length of the period when the air temperature is below 0 °C. Integrating Eq. (7.9) we have the condition:

$$t_C > \frac{2}{\lambda}\sqrt{\frac{\lambda T_{am}}{\lambda T_{am} + r}}, \quad r < -\lambda T_{am} \tag{7.10}$$

In the cooling season normally $r < 0$ so that the latter condition is not a severe restriction. Thus very shallow lakes freeze if the air temperature falls below zero, but deep lakes may survive unfrozen throughout the winter (Fig. 7.3). When turbulent heat losses

dominate, $\lambda T_{am} + r \approx \lambda T_{am}$, and the lake freezes if the cold period is at least twice the lake response time, $t_C > 2\lambda^{-1}$; when radiational losses dominate, the condition is asymptotically $t_C > 2\lambda^{-1}\sqrt{\lambda T_{am}/r}$. Equation (7.10) works more generally when the temperature reference is changed to the freezing point instead of 0 °C.

Next, consider the fall cooling process. In linear atmospheric cooling by the rate α, $T_a = -\alpha t$, the water temperature is

$$T(t) = T_a(t) + \left(1 - e^{-\lambda t}\right)\left(\lambda^{-1}\alpha + \Delta T\right) + e^{-\lambda t}T(0) \tag{7.11}$$

The water temperature is thus the air temperature plus a weighted average of the surface heat balance effect and the initial temperature. The inverse of the parameter λ represents the thermal response time scale of the lake system. The asymptotic solution for $\lambda t \gg 1$ is that the water temperature is above the air temperature by $\lambda^{-1}\alpha + \Delta T$, where the first term represents the lag and the second term represents the shift. In Finland autumn, $\alpha \sim 5$ °C month^{-1} and then for $H \sim 10$ m we have $\lambda^{-1}\ \alpha \sim 5$ °C; and as shown above, $\Delta T \sim -2$ °C.

In deep lakes the linear atmospheric cooling assumption is not good, since the cooling period is long. Periodic air temperature forcing $T_a = \bar{T}_a + \Delta T_a \sin(\omega t)$, where $\bar{T}_a$ is the mean air temperature, ΔT is the air temperature amplitude and ω is the frequency, gives the solution

$$T = \bar{T}_a + \Delta T + \frac{\lambda}{\sqrt{\lambda^2 + \omega^2}}\Delta T_a \sin(\omega t - \varphi), \quad \varphi = \arctan\left(\frac{\omega}{\lambda}\right) \tag{7.12}$$

For the annual air temperature cycle, $\omega = 2\pi$ year^{-1}, and thus $\omega = \lambda$ when the mixed layer depth is $H = 20$ m. The amplitude of the air temperature sine wave ΔT_a is damped in the mixed layer as shown by the formula. In deep lakes, $\omega \gg \lambda$, the forcing cycles are damped proportional to ω^{-1} and phase shift is asymptotically a quarter cycle, while in shallow lakes, $\omega \ll \lambda$, the surface water temperature follows the air temperature with a shift ΔT and with an asymptotically vanishing lag. Equation (7.12) also gives the freezing condition $T = 0$ °C:

$$\frac{\Delta T_a}{\sqrt{1 + \left(\frac{\omega}{\lambda}\right)^2}} > -(\bar{T}_a - \Delta T) \tag{7.13}$$

Thus, if $\bar{T}_a > 0\,^\circ\mathrm{C}$ and $\Delta T_a > \bar{T}_a$, shallow lakes freeze but deep enough lakes do not. Lake Shikotsu, close to Sapporo in Hokkaido has the mean depth of 265 m and does not freeze. The mean air temperature is about 5 °C and the amplitude is 14 °C, and for $H = 265$ m the left-hand side is 1.02 °C not satisfying the condition (7.13).

Example 7.3. Autumn cooling model (Rodhe 1952). The slab model was used in the past for forecasting the autumn cooling. Rodhe (1952) considered just the λ-term in Eq. (7.8),

and took the air temperature piecewise as daily means. Knowing the actual/predicted air temperatures in days 1, …, n, the prediction for the surface temperature at the time $t = n\Delta t$, or on the nth day, is

$$T(t) = T(0)e^{-\lambda t} + (1 - e^{-\lambda t}) \sum_{i=1}^{n} T(i\Delta t)e^{-\lambda(n-i)\Delta t}$$

This is known as the method of the weighted air temperature sum. It is easy to see that the solution is a weighted average of initial temperature and predicted daily mean air temperatures with exponentially decaying weights. In other words, the air temperature is low pass filtered for the mixed layer temperature, and the filter weights depend on the depth of the water layer. For $r \neq 0$, the term $[1 - \exp(-\lambda t)]\ \lambda^{-1} r$ is added to the solution.

Example 7.4. Freezing date delay (Simojoki 1940). Simojoki (1940) examined the freezing date of lakes in Finland (Fig. 7.4). Taking a linear atmospheric cooling rate, $T_a = -\alpha t$ and r = constant, the slab model can be directly integrated as shown by Eq. (7.11). Leaving the transient terms out, the solution is $T(t) = T_a(t) + \lambda^{-1}\alpha + \Delta T$. The freezing date t_F is then obtained from $T(t_F) = T_f$, where $T_f = 0$ °C is the freezing point temperature. We have

$$t_F \approx \lambda^{-1} + \alpha^{-1}\Delta T$$

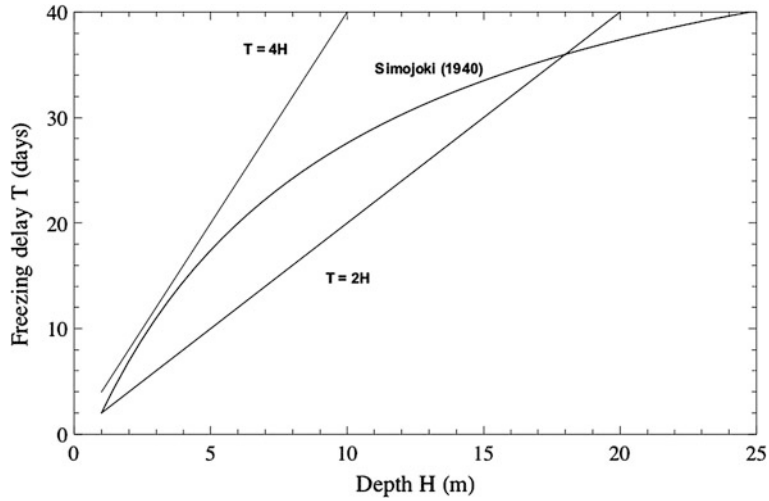

Fig. 7.4 Freezing date delay after 0 °C downcrossing of air temperature as the function of lake depth. Simojoki (1940) shows data from Finnish lakes, and the lines T = 2H and T = 4H refer to delays of 2 and 4 days/m, respectively

Thus, if $\Delta T \approx 0$, the freezing date is delayed by λ^{-1} days from the air temperature zero downcrossing. Shallow lakes ($H \approx 5$ m) freeze after a 1–2 week cold period but deeper lakes need more than 1 month.

Heat flux from bottom sediments is important in shallow lakes. Falkenmark (1973) reported that the sediment heat storage of a shallow Lake Velen (17 m mean depth) in Sweden was at maximum 110 MJ m^{-2}. This would mean winter heat fluxes of the order of 5 W m^{-2} from the bottom sediments. Falkenmark (1973) regarded the sediment heat flux as a very significant factor for heating and also due to triggering slow density currents along the sloping bottom.

Taking the bottom temperature as a constant, a new forcing term $K_b(T_b - T)$ is added to the one-layer model, and the solution becomes easy. For a more complete treatment, an equation is needed for the bottom temperature also:

$$\frac{dT_b}{dt} = e^{-\kappa H} Q_{si} + \frac{K_V}{H_b} \cdot \left. \frac{\partial T}{\partial z} \right|_{z=-H} \tag{7.14}$$

where H_b is a representative thickness of the active bottom sediment layer.

7.1.4 Mixed Layer Models

Extending slab models to have the depth of the mixed layer as a dependent model variable takes us to mixed layer models, $H = H(t)$ (see Niiler and Kraus 1977). For a deepening mixed layer, the rate $w_e = dH/dt$ is called the entrainment[3] rate. These models do not include horizontal effects. To determine the evolution of the mixed layer depth brings the mechanical energy budget to the model and then also the water velocity needs to be solved. The model equations are:

$$\frac{dT}{dt} = \frac{Q_0 + (1 - e^{-\kappa H}) Q_T}{\rho_0 c_0 H} - w_e \frac{\Delta T}{H} \tag{7.15a}$$

$$\frac{d\boldsymbol{U}}{dt} = -f\boldsymbol{k} \times \boldsymbol{U} + \frac{\boldsymbol{\tau}_a - \boldsymbol{\tau}_H}{\rho_0 H} \tag{7.15b}$$

$$w_e \left(c_i^2 - sU^2 \right) = 2mu_*^3 + \frac{H}{2} \left[(1+n) B_0 - (1-n) |B_0| \right] + \left(H - \frac{2}{\kappa} \right) Q_s \tag{7.15c}$$

The first two equations are straightforward. There ΔT is the temperature difference across the pycnocline at the bottom of the mixed layer, f is the Coriolis parameter, $\boldsymbol{U}$ is the horizontal water velocity, and $\boldsymbol{\tau}_a$ and $\boldsymbol{\tau}_H$ are the surface and mixed layer bottom stresses.

[3] Erosion of the underlying water layer by the mixed layer turbulence.

The third equation presents an equilibrium condition for the entrainment rate: the left-hand side has the energy consumption consisting of radiation by internal waves and entraining of deep water, and the right-hand side has the energy production due to wind stress, buoyancy and solar radiation. There c_i is the internal wave speed, u_* is the friction velocity of wind, B_o is the buoyancy flux at the surface, and the factors s, m and n represent the corresponding fractions of the kinetic energy of the mixed layer, wind stress and buoyancy flux taking part in the entrainment (see Niiler and Kraus 1977 for more details).

A specific mixed layer model—*Flake*, see http://www.flake.igb-berlin.de/—with parameterized vertical temperature distribution has been widely used in recent years (Mironov et al. 1991, 2004; Kourzeneva et al. 2008; Golosov and Kirillin 2010; Kirillin 2010). The model is based on similarity theory approach for the vertical structure of the thermocline and variable mixed layer depth. Flake has been used in numerical weather prediction and climate models to provide better estimate for the surface temperature and as well it has been used in several other applications.

7.1.5 Turbulence Models

For a more detailed description of the vertical temperature–velocity structure, advanced turbulence models are needed. In Nordic lakes a $k-\varepsilon$ type 2nd order closure model has been widely used (Svensson 1979), known better as the general equations solver 'PROBE' (Svensson 1998; Omstedt 2011). The quantities k and ε are the turbulent kinetic energy and the dissipation rate of turbulent kinetic energy, respectively. The system of equations for the average (averaged over turbulent fluctuations) temperature and velocity is

$$\frac{\partial T}{\partial t} = \frac{\partial}{\partial z}\left(K_T \frac{\partial T}{\partial z}\right) + \kappa Q_s e^{-\kappa z} \tag{7.16a}$$

$$\frac{\partial \boldsymbol{U}}{\partial t} = f\boldsymbol{k} \times \boldsymbol{U} + \frac{\partial}{\partial z}\left(K \frac{\partial \boldsymbol{U}}{\partial z}\right) \tag{7.16b}$$

The diffusion coefficients are obtained from the turbulent kinetic energy and the dissipation rate of turbulent kinetic energy as:

$$K = C_\mu \frac{k^2}{\varepsilon}, \quad \frac{K}{K_T} = \sigma_k \tag{7.16c}$$

where $C_\mu = 0.09$ is a model constant and $\sigma_k = 1.4$ is the Prandtl number. The 2nd order closure provides the evolution of k and ε through (Svensson 1979)

$$\frac{\partial k}{\partial t} = \frac{\partial}{\partial z}\left(\frac{K}{\sigma_k} \cdot \frac{\partial k}{\partial z}\right) + P_s + P_b - \varepsilon \tag{7.16d}$$

$$\frac{\partial \varepsilon}{\partial t} = \frac{\partial}{\partial z}\left(\frac{K}{\sigma_\varepsilon} \cdot \frac{\partial k}{\partial z}\right) + \frac{\varepsilon}{k}(c_1 P_s + c_3 P_b - c_2 \varepsilon) \tag{7.16e}$$

where P_s and P_b are the shear and buoyancy production of turbulence, and the coefficients $\sigma_k, \sigma_\varepsilon, c_1, c_2$ and c_ε are model constants. The production terms are

$$P_s = K\left[\left(\frac{\partial u}{\partial z}\right)^2 + \left(\frac{\partial v}{\partial z}\right)^2\right], \quad P_b = K\frac{g}{\rho_0}\frac{\partial \rho}{\partial z} \tag{7.16f}$$

where $c_{1\varepsilon}, c_{2\varepsilon}$ and $c_{3\varepsilon}$ are model constants. The $k-\varepsilon$ model has thus six parameters, and with their standard values they are: $C_\mu = 0.09$, $c_1 = 1.44$, $c_2 = 1.92$, $c_3 = 0.8$, $\sigma_k = 1.0$ and $\sigma_\varepsilon = 1.3$.

The most uncertain part of this $k-\varepsilon$ model is the equation for the rate of dissipation of turbulent kinetic energy, which involves several parameters. The mixed layer physics with its depth comes out fairly well in the model but deeper, below the thermocline, horizontal processes become relatively speaking more significant. To reach the observed level of mixing in the lower layer, so-called 'deep mixing' functions have been added into the model for tuning. One-dimensional approach thus has limitations in that advection cannot be properly accounted for and interactions between the coastal zone and central basins are not solved. In the cooling process, in particular, advection and sinking of cold water from shallow shore areas to central basins complicates the one-dimensional picture.

Based on this 2nd order turbulence closure, a programme package 'PROBE' has been constructed to be utilized for several kinds of applications (Omstedt 2011). Cooling of lake waters in autumn has been widely examined with this model (Sahlberg 1983). In several basins good results have been obtained, and furthermore a group of one-dimensional models has been used as the basis of a connected box-model network. Figure 7.5 shows an example of the model simulation. The whole 50-m water column cools, and at temperatures below 4 °C surface layer starts to stratify and bottom water reaches temperatures down to 2 °C. The heat loss from the lake is at highest 300 W m^{-2} and almost continuously positive.

7.2 Thermal Structure and Circulation Under Ice-Cover

7.2.1 Water Body During the Ice Season

The physics of lakes is different in quality in the presence of full ice cover as compared with open water season (Fig. 7.6). A complete ice cover is a rigid lid, which almost closes the interaction between the water body and the atmosphere. The wind stress does not go through the ice, and therefore mechanical forcing is limited to surface pressure variations. Exchange of matter, including water, between the lake water body and atmosphere does

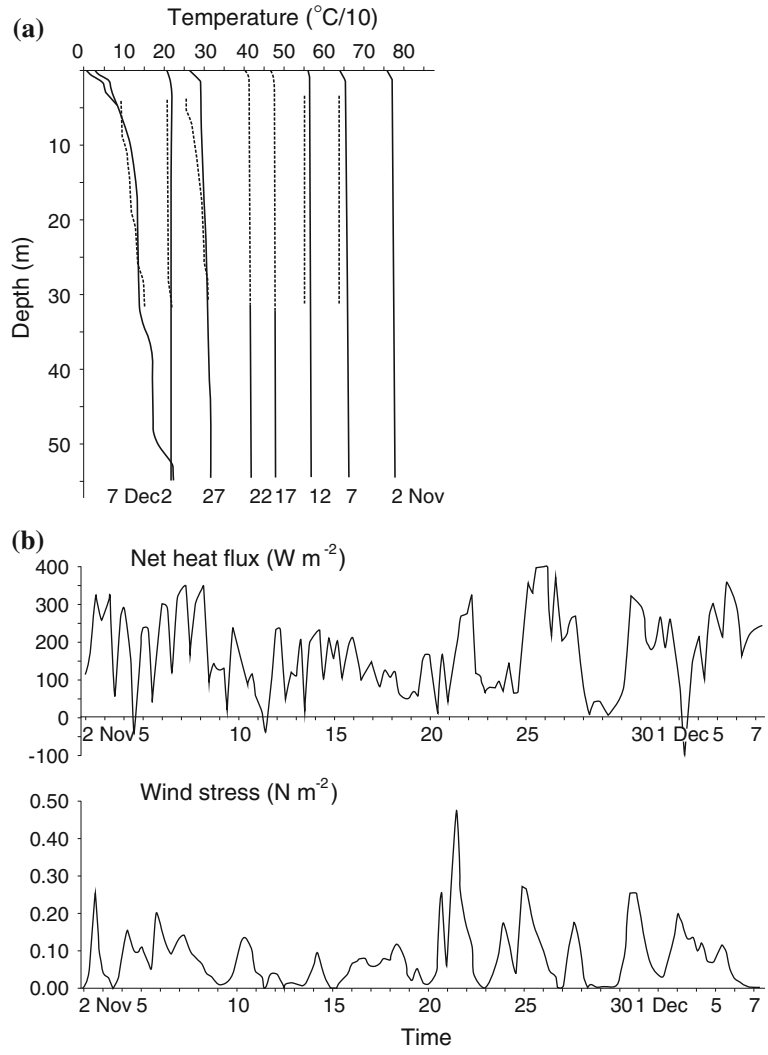

Fig. 7.5 Lake cooling simulation for Lake Väsman, November 2–December 7, 1981 by PROBE: **a** The simulated (*solid line*) and measured (*dashed line*) temperature profiles at every 5 days; **b** Net heat loss and wind stress (Sahlberg 1983). *Note* Temperature is given in tenths of a degree, the scale is from 0 to 8 °C

not take place. Thermal signals are, however, transmitted across the ice sheet. Sunlight penetrates ice or snow surface and reaches the water body, unless there is a thick snow cover on top, and heat can leak out from the lake slowly by molecular conduction through ice and snow. In summary, the modifying influence of a complete ice cover is on the lake physics as follows:

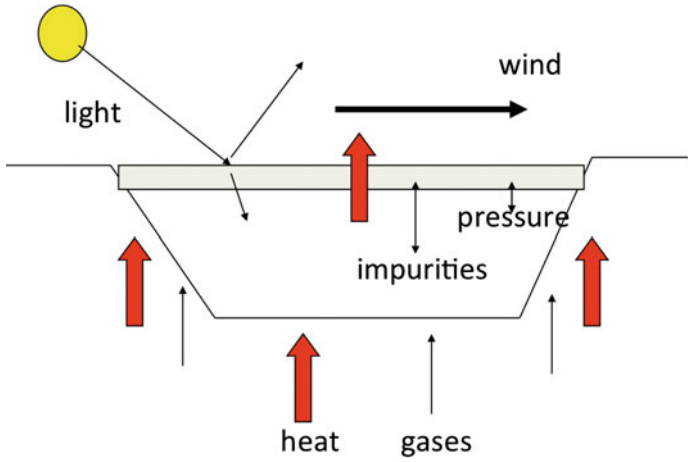

Fig. 7.6 Lake ice environment in the ice season

Quantity	Ice season compared to open water season
Wind stress	Removed
Surface pressure	No change
Solar radiation	Reduced by more than 50 %
Air-lake heat exchange	Reduced, realized mostly in phase changes
Water balance	Atmospheric exchange removed
Air-lake exchange of matter	Removed

Thus the ice cover largely isolates the lake with a degree of isolation depending on the ice coverage, ice thickness, and snow thickness. In the heat conservation law (Eq. 7.4) the main difference between ice-free and ice-covered lakes is in the surface boundary conditions. In the case of a stable ice cover, the temperature is at the freezing point and the current velocity is zero:

$$T = T_f, \quad \boldsymbol{u} = 0 \tag{7.17}$$

There is a weak loss of heat through the ice cover and gain from the bottom sediments. Circulation under ice cover is thermohaline. Whether the flow is laminar or turbulent is indicated by the Reynolds number $Re = UL/\nu$, where U and L are the velocity and length scales and $\nu \approx 1.8 \times 10^{-6}$ m^2 s^{-1} is the kinematic viscosity of water. The laminar–turbulent transition regime is at $Re \sim 10^3$–10^4. Therefore ice-free lakes are turbulent, but under compact ice cover $U \sim 10^{-3}$ m s^{-1}, and then the transition is at $L \sim$ 1–10 m.

The winter of seasonally freezing lakes can be divided into four phases (Kirillin et al. 2012b). The pre-winter, discussed in Sect. 7.1, forms the 1st phase. The 2nd phase is the

freeze-up, then follows the period of complete ice cover (Phase #3), and the fourth one is the ice decay period. The lengths of these phases largely depend on the lake size. In small and medium-size lakes Phases #2 and #4 take normally 2–3 weeks each, while the length of Phase #3 depends on the climate zone and can be from zero to more than 6 months.

Water renewal is slow in winter, especially if the soil is frozen and covered by snow. The inflow is then from brooks and rivers and from the ground beneath lakes (Bengtsson 1986, 1996). This is clearly illustrated by the inflow time series for Lake Vanajavesi (Fig. 7.7).

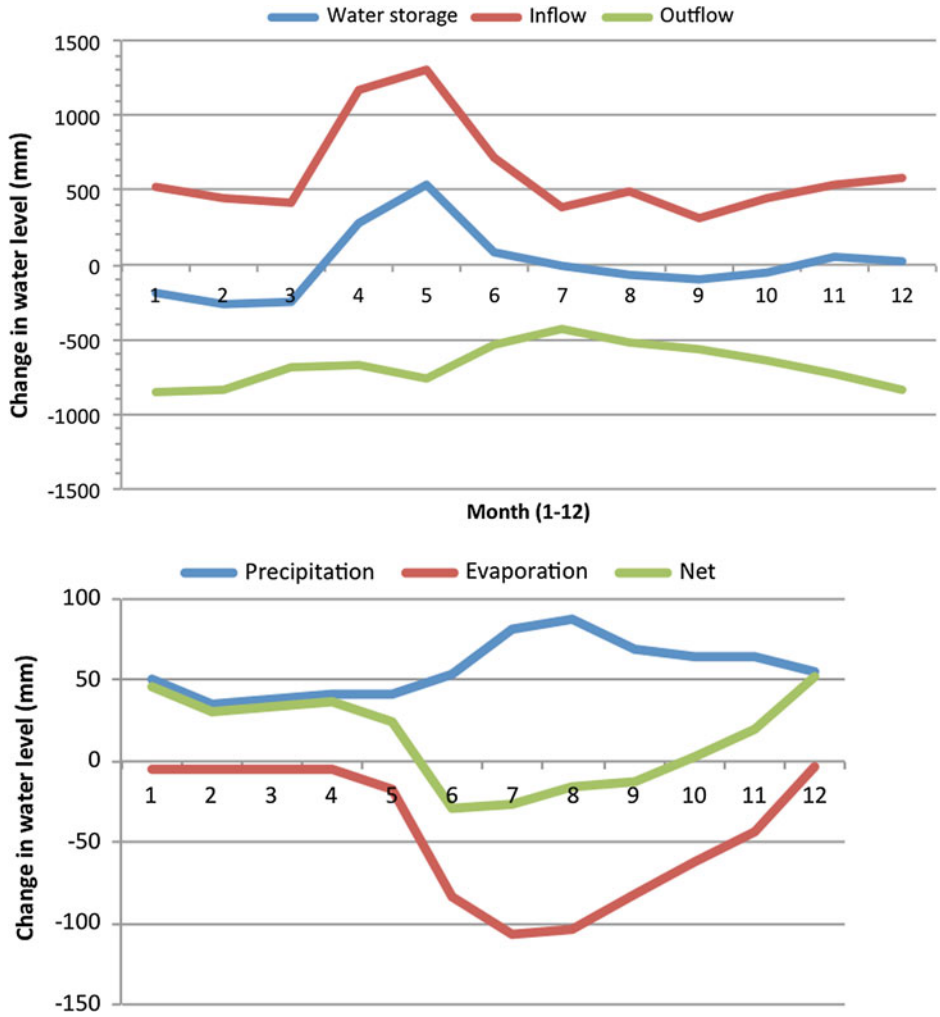

Fig. 7.7 Lake Vanajavesi, Southern Finland. *Top* monthly water balance, inflow and outflow; *Bottom* monthly precipitation, evaporation and their net value (Jokiniemi 2011)

A review of the river inflows under ice cover and their effect on the circulation was given by Bengtsson (1996). These effects are usually localized near in- and outlets; they affect the ice thickness, especially near the inlets, and they may alter the vertical stratification near the outlets by selective water withdrawal (Stigebrandt 1978). In small lakes, inflows can initiate a secondary, lake-wide, geostrophic circulation (Svensson and Larsson 1980). In deep lakes, inflows play an important role in the lake-wide lateral circulation and the deep-water formation. Hohmann et al. (1997) suggested that the inflow of River Selenga in Lake Baikal plunges down and initiates a thermobaric instability (see Sect. 7.1), which mixes the water column down to the lake bottom—the crucial process for the ventilation of the deep waters.

7.2.2 Stratification

The initial temperature conditions at the freeze-up are created in the autumn mixing and therefore then $T \le T_m$. The temperature at the ice–water interface is at the freezing point, $T_0 = T_f$, and if $T_m > T_f$, inverse thermal stratification forms. In freshwater lakes the upper layer temperature is close to the freezing point, $T_1 \ge T_0$ and the lower layer temperature is between the freezing point and the temperature of maximum density. Thus

$$T_f \le T_1 \le T_2 \le T_m \tag{7.18}$$

On top of the upper layer, just beneath the ice, there is a thin surface layer where diffusion is molecular and the temperature increases from T_f to T_1. In fresh-water lakes, we can take $T_f = 0$ °C and $T_m = 4$ °C. If the concentration of dissolved matter increases in the bottom water due to dissolution from the sediments, a thin bottom layer is formed into the lower layer (e.g., Malm 1998).

The stability of temperature stratification is described by the Rayleigh number:

$$Ra = \frac{g\alpha\Delta T d^3}{\kappa\nu} \tag{7.19}$$

where α is thermal expansion coefficient, ΔT is the temperature change across the layer of thickness d, $\kappa = 1.3 \times 10^{-7}$ m^2 s^{-1} is the thermal diffusivity, and $\nu = 1.8 \times 10^{-6}$ m^2 s^{-1} is the viscosity. Rayleigh number may be taken as the ratio of buoyant and viscous forces. When Rayleigh number exceeds a critical value of $\sim 10^3$, convection starts up. This may bring heat to the ice bottom.

Example 7.5. Assume that the temperature of the upper layer is 5 °C. Cooling the surface to 4 °C leads to molecular diffusion with the thickness of the cold layer increasing as $\delta = (\pi\kappa t)^{1/2}$ (see, e.g., Thorpe 2005). The Rayleigh number then grows proportional to time to the power of 3/2 and reaches the critical value. Since $\alpha \sim -¼ \times 10^{-4}$ °C^{-1}, Ra reaches the critical limit of 10^3 in 4 min.

Below the temperature of maximum density, further surface cooling is a stabilizing factor. After the ice cover has formed, solar radiation provides the strongest external forcing on the temperature stratification, especially in the ice decay phase after snowmelt. As soon as the solar heating can penetrate the ice sheet, stratification weakens and turns to convective mixing. The second factor is heating by the bottom sediments. Usually the bottom water temperature is below the temperature of maximum density in the beginning of winter, and sediment heat flux drives density currents down to greater depths. But in the case of strong geothermal heat flux, convective overturning may be triggered. The relative importance of the solar and sediment heat fluxes varies in the course of the winter.

The heat flux from bottom sediments has been examined from field data, e.g., by Kenney (1996), Malm (1998), and Terzhevik et al. (2009). Small boreal lakes reveal high inter-annual variability depending on snowfall and radiation conditions. The magnitude of the sediment heat flux is 1–10 W m^{-2} (Bengtsson 2011; Kirillin et al. 2012b), and it is a major factor in lake thermodynamics when the surface is protected by the ice cover. For a lake depth of 10 m, this heat flux would increase the mean water temperature by 0.06–0.6 °C $month^{-1}$. As a result, normally the water temperature increases in the lower layer during the ice season. Apart from strong geothermal heating, the surface temperature of the sediments is close to the temperature of maximum density of the lake water that limits the temperature level the heating may reach. For strong heating as observed in many geothermal lakes (100 W m^{-2} or more), the lake would stay open all the winter.

The latent heat released in ice growth must be conducted to the atmosphere through the ice and it does not influence on the temperature of the liquid water that remains. For a growth rate of 1 cm day^{-1}, the heat transfer is 35 W m^{-2}. In addition, there is an upward heat flux from the water body to the ice depending on the temperature gradient and water currents. This heat flux is conducted away through the ice or used for ice melting at the bottom of the ice. It has been estimated as 1–10 W m^{-2} (e.g., Jakkila et al. 2009; Yang et al. 2012), i.e. the magnitude is the same as is usually the magnitude of the heat flux from the sediments in boreal lakes. As a consequence, heat fluxes at the upper and lower surface of the water body largely compensate each other, and the temperature profile of the lake remains rather stable as long as solar radiation is absent or weak (see Fig. 7.8).

Sunlight starts to heat the surface water layer (see Sect. 3.5) when the snow cover is thin or absent and the sun is above the horizon long enough. In fresh and brackish water lakes this increases the water temperature in the upper layer and triggers convection (Fig. 7.8). However, in brackish waters, if ice is melted the salinity of the surface water decreases that adds, in turn, increases the stability of the stratification. The radiational heating can be up to 100 W m^{-2}, and it is used both for heating of the water and melting of the ice at the bottom surface. In freshwater lakes, convective mixing penetrates deeper with time into the stably stratified fluid below reaching the bottom as $T \rightarrow T_b$ beneath the immediate viscous boundary layer under the ice. This process raises the water temperature more in shallow areas, and circulation similar to the one forced by the sediment heat flux follows. It is the most energetic transport process in ice-covered lakes and dominates the circulation in spring and summer. Because of the strength of the solar heating, the water

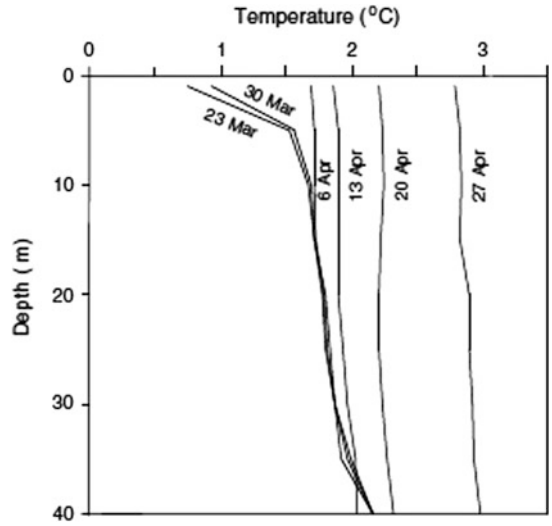

Fig. 7.8 Convective mixing in Lake Pääjärvi, spring 2004 (Jakkila et al. 2009)

column becomes in a short time isothermal, apart from the very thin boundary layer just beneath the ice to match the condition $T = T_f$ at the ice–water interface. Then, when the ice cover breaks, due to mixing, melting can take place fast and right after disappearance of ice the surface water temperature is well above zero.

The temperature effect on density is weak in the vicinity of the temperature of maximum density, and there is no (or, at most, weak) turbulence beneath a solid ice cover. Therefore, even in freshwater lakes ($S < 0.5$ ‰) the stratification is affected by vertical salinity gradients (Malm et al. 1997; Jonas et al. 2003). For a salinity difference of 0.1 ‰, the density difference is 0.08 kg m^{-3}, while in fresh water the density difference between the temperatures of 0 and 4 °C is 0.13 kg m^{-3}. As a result, the inflow water stratifies and spreads in a thin layer just beneath the ice, if it has lower salinity than the lake water. Apart from very deep zones, at the time of ice formation the temperature of bottom water is normally below the temperature of maximum density, $T_b < T_m$. Therefore the heat flux from sediments creates denser water, which flows down toward greater depths.

Assuming that the ice is salt-free, we have

$$S_1 = \frac{H}{H - h} S_0 \tag{7.20}$$

where S_0 and S_1 are the salinities before and after ice formation, respectively, H is the depth of the convective layer, and h is ice thickness. In the growth of ice, taking $H < 1$ m (Granin et al. 1999), for $h = 0.1$ m we have $S_1 > 1.1 \cdot S_0$, i.e. $\Delta\rho \sim S_0[‰] \times 0.8$ kg m^{-3}. Thus the higher the initial salinity is, the stronger the destabilizing influence will be. Melting gives an opposite, stabilizing effect, and therefore the depth H comes from molecular conduction and is much smaller than in the case of ice growth.

The meltwater has normally a very low salinity. The layer of low-saline surface water increases the vertical stability. But solar heating and inflow of low-salinity water may also produce a thermally unstable but non-convective layer with temperatures exceeding T_m in the very vicinity of the ice (Koźmiński and Wisznewski 1934; Jonas et al. 2003). This layer is not necessarily supported by stabilizing salinity gradient but can be also produced by vertical differences in the absorption rate of the solar radiation (Kirillin and Terzhevik 2011).

While dilution due to ice melting stabilizes the surface waters in spring, an opposite process takes place in the early winter, when salt release from newly formed ice destabilizes the upper water column and produces convection. In saline water, ice formation can drive deep convection, but in freshwater lakes the influence is soon compensated by the temperature increase beneath the ice. Convection driven by salt flux can play an important role in the survival of plankton under ice in winter (Jewson et al. 2009). In shallow lakes, the salt extruded from ice can be mixed across the water column and increase the average water density in the lake. Then in spring, the melt water from ice and snow forms a layer of lower density on the lake surface.

The salinity distribution may also affect the convection at the lake bottom. Near-bottom waters are often distinguished by increased content of dissolved salts released from the sediment or brought by groundwater inflow. If the resulting salinity stratification is strong enough, it can prevent ventilation of the near-bottom waters by the spring overturn and contribute to the deep anoxia development in the following summer (Mironov et al. 2002; Pieters and Lawrence 2009).

In large lakes, the area of shallow pelagial sediments is usually small compared to the entire surface of the lake bottom, and the heat seasonally stored in the sediment plays a minor role in driving the lake circulation. In addition, lakes of large surface area, especially those located in the dry continental climatic zones, remain snow-free for the entire ice-covered period (Lake Baikal is the most prominent example). There, convective mixing penetrates down to several tens or even hundreds meters depth (Farmer 1975; Shimaraev and Granin 1991; Weiss et al. 1991).

Another inflow-related effect, appearing in freshwater lakes only at temperatures close to T_m, is *cabbeling*—an increase of water density due to mixing of two water masses with differing temperatures and salinities (Kirillin et al. 2012b). The mixture of two such water masses is more dense than either of them, as seen in the convex shape of density isolines in *TS* space, and therefore diffusion induces convection. The effect is known to produce deep mixing in the ocean (called also as *double diffusive convection* in oceanography), but is usually negligible in freshwater lakes. At low temperatures, however, small differences in the salinity between near-shore waters and the core water masses are the source of the contraction by mixing.

7.3 Dynamics of Water Body Beneath Ice-Cover

7.3.1 Circulation

Thermohaline circulation[4] is the governing form of circulation in fully ice-covered lakes. It results from the evolution of water temperature and salinity that builds horizontal density gradients. The driving forces are the heat flux from the sediments and solar radiation. Other forms of circulation result from atmospheric pressure variations and, in lakes with significant through flow, from the boundary conditions. Except for the last case, water flow velocities are always very small, of the order of 1 mm s^{-1} (e.g., Huttula et al. 2010). Due to the very low levels, in practice it is very difficult to measure the circulation velocity field.

Circulation dynamics are based on the Navier-Stokes equation, equation of state, and conservation laws for mass, temperature and salinity (Gill 1982; Cushmann-Roisin 1994):

$$\frac{\partial \boldsymbol{u}}{\partial t} + \boldsymbol{u} \cdot \nabla \boldsymbol{u} + f\boldsymbol{k} \times \boldsymbol{u} = -\frac{1}{\rho}\nabla p + \nu \nabla^2 \boldsymbol{u} \tag{7.21a}$$

$$\rho = \rho(T, S, p) \tag{7.21b}$$

$$\nabla \cdot \boldsymbol{u} = 0 \tag{7.21c}$$

$$\frac{\partial \{T, S\}}{\partial t} + \boldsymbol{u} \cdot \nabla \{T, S\} = \nu \nabla^2 \{T, S\} + \{q, 0\} \tag{7.21d}$$

Thus we have seven unknowns and seven equations. In freshwater lakes, the salinity is normally ignored, but beneath the ice cover it may have a significant influence on density and consequently on the thermohaline circulation. Wind-driven circulation is driven by the wind stress, which steps into the surface boundary condition of the Navier-Stokes equation, while thermohaline circulation is driven by the pressure gradient. In partially ice-covered lakes, wind forcing through open water areas and drifting ice floes can generate a significant wind-driven circulation system (Fujisaki et al. 2012).

In fully ice-covered lakes, water velocities are small, and therefore advection and friction are small. Scaling analysis shows the basic characteristics. Denote U—velocity scale, T—time scale, H—vertical scale, and L—horizontal scale, and their typical values are $U \sim 1$ mm s^{-1}, $T \sim 10^5$ s (1 day), $H \sim 10$ m, and $L \sim 1$ km. Then we have for the terms in the Navier-Stokes equation (Table 7.2).

[4] The term thermohaline circulation comes from oceanography; 'thermo' refers to temperature and 'haline' to salinity. This circulation is driven by horizontal density gradients.

Table 7.2 Scaling the equation of motion of the water body in ice-covered lakes

Inertia	Advection acceleration	Coriolis	Pressure gradient (residual)	Viscous friction
$U\,T^{-1}$	$U^2\,L^{-1}$	fU	$g\Delta H/L$	UH^{-2}
10^{-8} m s^{-2}	10^{-9} m s^{-2}	10^{-7} m s^{-2}	10^{-7} m s^{-2}	10^{-11} m s^{-2}

To balance the equation, the pressure gradient must be of the same magnitude as the Coriolis acceleration and is thus obtained as the residual. It is clear by the continuity equation that vertical advection $\sim$ horizontal advection, and by $H \gg L$ that horizontal viscous friction is even smaller than vertical. The leading balance is between the Coriolis acceleration and the pressure gradient, i.e. thermohaline circulation in ice-covered lakes follows the geostrophic flow balance. This is also reflected in the small Rossby number $Ro = U/(Lf) \sim 10^{-2}$. There is a large difference in the circulation characteristics between ice-free and ice-covered lakes, since in ice-free conditions the flow is turbulent, and friction due to the wind forcing overcomes the Coriolis term.

Increasing the flow velocity to $U \sim 1$ cm s^{-1}, the importance of the advective acceleration increases but only at $U \sim 10$ cm s^{-1} it becomes comparable to the Coriolis acceleration. Taking the length scale as 100 m does not bring advection to the level of the geostrophic balance. For the time-scale of 10^4 s, local acceleration becomes equal to Coriolis acceleration, whatever is the flow velocity. But beneath an ice cover the flow is quite stable so that the local acceleration becomes a very small term. Since Rossby number is the ratio of advection to Coriolis acceleration, the geostrophic balance holds in frictionless stationary flow as long as $Ro \ll 1$.

The role of friction depends on the quality of the flow, which is described by the Reynolds number $Re = UH/\nu$. Taking $Re < 10^3$ and $Re > 10^4$ as the criteria for laminar and turbulent flow, respectively, it is seen that for $U \sim 1$ mm s^{-1}, laminar state follows for $H < 1$ m and turbulent state for $H > 10$ m. Thus laminar–turbulent transition conditions would be typical, while in extreme cases laminar or turbulent flow could be reached. The vertical kinematic friction can in general be expressed as

$$F_V = \frac{\partial}{\partial z}\left(K_V \frac{\partial \boldsymbol{u}}{\partial z}\right) \tag{7.22}$$

where K_v is kinematic viscosity, $K_\mathrm{v} = \mathrm{v} = 1.8 \times 10^{-6}$ m^2 s^{-1} (molecular viscosity) for laminar flow, $K_\mathrm{v} \sim 10^{-2}$–1 m^2 s^{-1} for turbulent flow, and for the laminar–turbulent transition regime $K_\mathrm{v} \sim 10^{-4}$ m^2 s^{-1} (Petrov et al. 2007). In the transition regime, the scale of the friction is not well known but anyway it is much lower than the other terms in the momentum equation; the influence is limited to the thin surface and bottom boundary layers.

The sediment heat flux creates thermohaline circulation just after freeze-up. Then this heat flux is at highest and horizontal density gradients form between shallow regions and pelagic zones. The circulation pattern consists of the downslope flow of the warm dense

water and the upward compensating flow in the lake interior (Mortimer and Mackereth 1958; Kirillin et al. 2012b). Estimations of flow rates by means of tracer experiments have revealed the values of 10^{-6} m s^{-1} for the vertical current velocity in the lake interior (Likens and Ragotzkie 1965) and 10^{-4} m s^{-1} for the downslope sinking in the bottom boundary layer (Welch and Bergmann 1985). The heat release from sediment was estimated in both cases as 3 W m^{-2}. Using radioactive tracers, Colman and Armstrong (1983) have estimated the average horizontal mixing rate as 4.7×10^{-5} m^2 s^{-1}. This means that the length scale of diffusion is 2 m in 1 day.

Since the amount of heat stored in the sediment is limited, the heat flux decreases and the stratification in the water column increases during the early stage of the ice-season. Hence, the number and size of circulation cells can change during a single winter. Terzhevik et al. (2009) estimated time scales of a non-stationary circulation driven by the sediment heat release by applying a simple model to temperature observations in Lake Vendyurskoe. For the initial heat flux of 5 W m^{-2}, they arrived at estimates for the downslope current velocity of 2×10^{-3} m s^{-1}, overturn time of about 7 days, and decay time of the circulation of 3–4 weeks.

Processes in the lake water body are occasionally reflected in the ice cover. In Lake Baikal rings are observed in the ice cover in some years (Granin 2010). Their diameter is close to the Rossby radius of deformation (5 km), and they are likely related to eruptions of mud volcanoes located at the lake bottom. Convective cells form gyres due to the Coriolis acceleration, which cause rings with thinner and porous ice to appear grey for observes above the ice cover (Fig. 7.9). The rings do not form every year. In small lakes specific small openings appear in the ice cover. Their diameter is less than 0.5 m, and they can be connected with methane release from lake bottom or with heavy snow accumulation. The snow load increases pressure in the ice, ice breaks, and if the flooded water contains heat the fracture grows into a small opening.

Fig. 7.9 Rings in the ice cover of Lake Baikal as observed from the International Space Station, April 2009. The diameter of the ring was 4.4 km. *Source* NASA

Rahm (1985) constructed a horizontally-integrated one-dimensional circulation model in an idealized lake with constant heat input from sediments and stably stratified water column. The model produced a two-cell circulation pattern in the vertical direction in the lake. In the upper layer, downward currents flowed along the bottom slope, and a compensating upwelling resulted in the middle of the lake. In the lower layer, there were upward boundary currents compensated by downwelling in the lake interior. The depth of the dividing level of no motion depended on the stratification and the angle of the bottom slope, but roughly speaking it was at the half-depth of the lake. Upward boundary currents were produced by diffusion-generated density gradients along the bottom slope—a mechanism described before in the deep ocean dynamics (Phillips 1970; Wunsch 1970)—and counteracted the downward currents produced by the sediment heat release. Likens and Ragotskie (1965) observed a similar two-cell structure in Tub Lake in 1961, but in the preceding year they found a simple one-cell circulation, with downward boundary currents and mid-lake upwelling throughout the entire lake. Hence, the circulation pattern can differ from year to year depending on the amount of heat stored in the sediment and on the stratification in the lake, both affected strongly by the conditions prior to ice coverage.

The effect of the Earth's rotation on the bottom-flux driven circulation has been largely neglected in most investigations of small and medium-size lakes. These effects were first discussed briefly by Likens and Ragotskie (1966). Recently, Huttula et al. (2010) applied a 3-dimensional model to simulate rotation-influenced density currents forced by heat flux from sediment of constant temperature (Fig. 7.10). An idealized cylindrical lake and Lake Pääjärvi, southern Finland acted as the study basins. The results demonstrated the formation of two vertically superimposed lake-wide gyres, coinciding roughly with the circulation cells in the model of Rahm (1985), and rotating in opposite directions.

Example 7.6. Consider a cylindrical basin with radius r and depth H. The geostrophic balance is written in polar coordinates (r, θ) as

$$fu_\theta = \frac{1}{\rho}\cdot\frac{\partial p}{\partial r}, \quad fu_r = -\frac{1}{\rho}\cdot\frac{\partial p}{r\partial\theta}$$
$$\frac{\partial p}{\partial z} = -g\rho$$

An axisymmetric solution has zero radial velocity, while the azimuthal component comes from the radial pressure gradient. High water in the middle produces clockwise gyre and vice versa. If there is a pressure compensation depth, the circulation would change sign. The 1st order correction to this balance gives a radial–vertical circulation pattern.

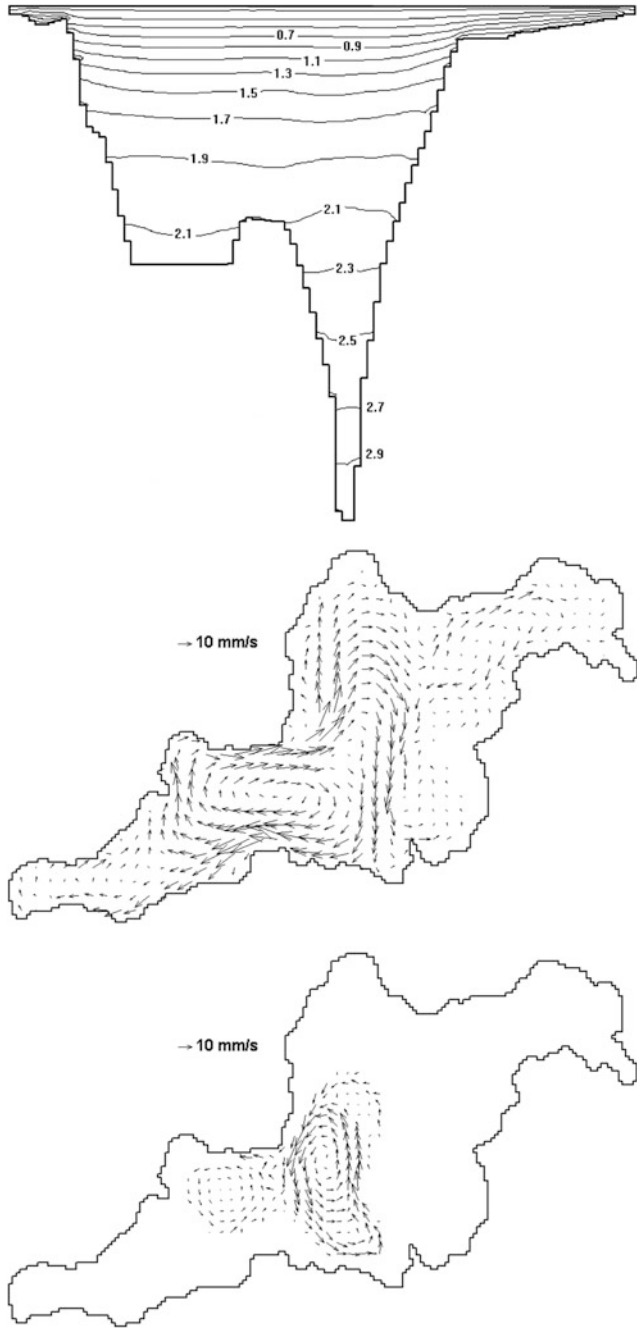

Fig. 7.10 Model simulation of the circulation in ice-covered Lake Pääjärvi. *Top*—temperature cross-section (°C), *Middle*—Current velocity at 2 m depth, *Bottom*—Current velocity at 20 m depth. The maximum depth is 80 m and the length of the lake is 10 km (Huttula et al. 2010)

7.3.2 Shallow Water Waves

Free oscillations of the entire water body, or barotropic seiches, are intrinsic features of lakes, observed also in the ice season (e.g., Falkenmark 1973). The wave speed is obtained from the shallow water theory as

$$c = \sqrt{gH} \tag{7.23}$$

Seiches are initiated by first tilting the lake surface level by wind or atmospheric pressure over the lake. When the wind or pressure force ceases, oscillation starts up and continues as a standing wave. In a narrow linear lake with depth H and length L, the period of uninodal (first mode) oscillation is $t_S = 2L/c$, known as the Merian's formula. In uninodal oscillation there is a node at the centre and antinodes at the ends of the lake.

In ice-covered lakes, seiches are induced by oscillation of the floating ice sheet (Bengtsson 1996; Malm et al. 1998; Petrov et al. 2006; Zdorovennova 2009; Kirillin et al. 2012b). The ice cover does not damp these oscillations (Sturova 2007; Zyryanov 2011), but the amplitudes are lower than in open water season because the seiches are excited by oscillations of the ice surface rather than by the wind-driven inclination of the lake surface.

The one-dimensional model can be also employed for seiches in two-dimensional lakes, with L as the length of the basin in the direction of the oscillation. In larger lakes the Coriolis acceleration starts to influence the direction of the wave motion. The scale of this influence is expressed by the ratio of the characteristic lake size to the Rossby radius of deformation, which is defined as

$$L_R = cf^{-1} \tag{7.24}$$

Barotropic motions in lakes with horizontal dimensions smaller than L_R are unaffected by the Earth's rotation. For $H \sim 40$ m and latitude 60°, we have $c \sim 20$ m s^{-1}, $f = 0.63 \times 10^{-4}$ s^{-1} and $L_R \sim 300$ km; for $H = 10$ m, $L_R \sim 150$ km. Therefore only in very large lakes Earth's rotation influences barotropic seiches. Exceptions are shallow lakes with large horizontal dimensions, e.g. Lake Erie and Lake Balkhash.

One of the first systematic observations of barotropic seiches was performed in ice-covered Swedish lakes by Bengtsson (1996). He reported of oscillating currents with periods of the first mode seiches and average magnitudes of 0.4 cm s^{-1}. Parallel estimations of horizontal dispersion revealed up to 10-fold increase in horizontal mixing associated with strong wind events, which were ascribed to the mixing intensification by seiches. In small, ice-covered Lake Vendyurskoe in Russian Karelia, flow velocity oscillations of several millimetres per second, driven by the longitudinal seiche, were found to exist during the entire ice-covered period (Malm et al. 1998; Malm 1999) accompanied by vertical oscillations of the ice cover. Atmospheric pressure variations have been identified as the main mechanism providing the kinetic energy to the

oscillations (Petrov et al. 2007). In Lake Baikal the flow velocities produced by seiches amount up to 1–2 cm s^{-1} with periods of 280 min (Zhdanov et al. 2001).

Ice-covered lakes have normally a stable stratification, and therefore they are also able to give a baroclinic response to external forcing (see Kirillin et al. 2012). By analogy with the barotropic oscillations, the length scale for the internal seiches is expressed by the internal Rossby radius

$$L_i = c_i f^{-1} \tag{7.25}$$

where c_i is the internal wave speed. For an idealized case of a two-layered fluid with layer thicknesses h_1 and h_2 and a density difference $\Delta\rho$ between them, the wave speed c_i is given by

$$c_i = \sqrt{g\frac{\Delta\rho}{\rho}\cdot\frac{h_1 h_2}{h_1 + h_2}} \tag{7.26}$$

For the density ratio of 10^{-2} and $h_1 \sim 1$ m, $h_1 \sim 9$ m, we have $c_i \sim 0.3$ m s^{-1}. If the stratification is continuous with a constant density gradient $\Delta\rho/H$ across the lake depth, Eq. (7.26) turns into

$$c_i = \frac{1}{\pi}NH = \frac{H}{\pi}\sqrt{\frac{g}{H}\frac{\Delta\rho}{\rho_0}} \tag{7.27}$$

where N is the Väisälä frequency. With the density ratio of 10^{-2} and lake depth of 10 m, Väisälä frequency is 0.099 s^{-1} and, consequently, $c_i \sim 0.3$ m s^{-1}.

Density stratification in ice-covered freshwater lakes is relatively weak, limited by the temperature difference $T_m - T_f$. Therefore $c_i \ll c$, and the baroclinic Rossby radius of deformation is $L_i \sim 5$ km, in weakly stratified lakes even less than that. Thus Earth's rotation plays an important role in baroclinic motions in even medium-size lakes. In the majority of ice-covered lakes, baroclinic waves are strongly influenced by the Coriolis acceleration and their dynamics resemble oceanic conditions rather than those in the same lakes in summer.

A thin (0.1–1.0 m) layer is formed in the very vicinity of the lake bottom, significantly warmer than the bulk water body, with high concentration of dissolved matter and high mixing rates produced by density currents and internal seiches (Malm 1999; Petrov et al. 2007; Kirillin et al. 2012b). This layer has also a high content of nutrients. Shear instabilities, produced by the density currents, and breaking of internal waves at the horizontal density interfaces are the major sources of mixing.

Periodic variations of the temperature field associated with large-scale internal waves have been registered in ice-covered lakes (Petrov et al. 2006; Kirillin et al. 2009; Zdorovennova 2009). Affected by the Earth's rotation, these oscillations take the form of

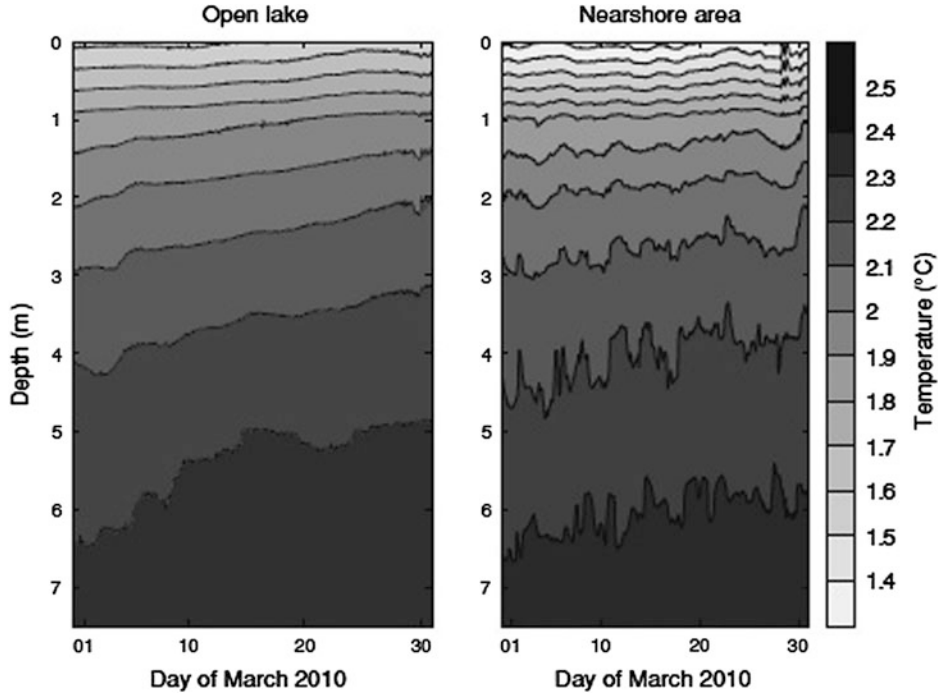

Fig. 7.11 Evolution of isotherms at two measurement points in Lake Pääjärvi, Finland, in March 2010. The short-term oscillations of isotherms associated with internal, basin-scale waves persist in the nearshore record only, demonstrating the Kelvin-type wave shape (Kirillin et al. 2012b)

inertial gravity waves traveling around the lake—analogs of Kelvin and Poincaré waves (Gill 1982) for enclosed basins. Such a deflection of the internal basin-scale waves implies important consequences to redistribution of the mixing energy. In contrast to planar seiches, Kelvin waves have their maximum amplitudes and current speeds near the lake shores (Fig. 7.11) affecting thus the water–sediment mass exchange in the littoral zone (Kirillin et al. 2009). Internal, basin-scale waves are known to be a major factor producing mixing in open-water lakes (Wüest and Lorke 2003); their contribution into mixing under ice is still unclear.

7.3.3 Melting Period

The melting period differs much from the mid-winter. It is dynamic, there is intensive ice–water interaction, and the decay of ice possesses a positive feedback via the evolution of albedo. Lake ice melts fast compared with its growth, the melt rate is 1–3 cm day^{-1}. A heat gain of 100 W m^{-2}, which is a high level, would melt 2.8 cm ice in 1 day. Ice is fresher than the lake water (e.g., Leppäranta et al. 2003b), and therefore the water salinity decreases beneath melting ice with a consequent stabilizing effect on the surface layer stratification.

In the melting period, a thin boundary-layer forms under the ice (surface layer), where temperature and salinity increase from T_0 and S_0 at the ice bottom to the bulk upper layer values T_1 and S_1. The presence of ice keeps the surface temperature at the freezing point, $T_0 = T_f(S_0)$ and beneath the surface the bulk temperature is $T_1 \geq T_f(S_1)$. As long as the salinity increases with depth, the temperature can reach $T_m(S)$ or even more in the surface layer. In the lower layer the temperature is determined by the depth of convection and the sediment heat flux. Just above the sediment there can be a more saline, dense layer as described above. In the temperatures below 6–8 °C very small salinity changes can compensate for the influence of temperature on the water density.

Solar radiation penetrating the ice is a major factor to drive convection (Farmer 1975; Mironov et al. 2002). It raises the temperature of the water beneath the ice sufficiently to initiate convective mixing. Solar forcing is an internal source term while the heat flux from sediments is a boundary flux. The solar heating extends to a surface layer with thickness of 1–10 m depending on the optical thicknesses of the ice and lake water (Leppäranta et al. 2003a; Arst et al. 2006; Jakkila et al. 2009). The resulting convection deepens and penetrates down to the lake bottom (or halocline if such exists) when the water temperature increases. Then the vertical heat transport predominates over the lateral exchange between shallow and deep parts of the lake.

Farmer (1975) performed the first systematic observations of radiatively-driven convection in the deep ice-covered freshwater Babine Lake (B.C., Canada) and presented an analysis of the convective mixing efficiency. Mironov et al. (2002) presented a comprehensive review on this topic. The buoyancy is defined as the relative weight

$$b = -g\frac{\rho_w - \rho_0}{\rho_0} \tag{7.28}$$

where ρ_0 is a fixed reference density. In freshwater lakes, the buoyancy conservation law is given by

$$\frac{\partial b}{\partial t} = \frac{\partial}{\partial z}\left(K_b \frac{\partial b}{\partial z}\right) - \frac{g\alpha}{\rho_w c_w} \cdot \frac{\partial Q_T}{\partial z} \tag{7.29}$$

where K_b is the diffusion coefficient of buoyancy, and α is the thermal expansion coefficient. Mironov et al. (2002) also proposed an appropriate scaling for the convection velocity w^* based on the kinetic energy budget integrated over the convective mixing layer:

$$\begin{aligned} w^* &= -\sqrt[3]{(H-\delta)B^*}, \quad B^* = B(\delta) + B(H) - \frac{2}{H-\delta}\int_\delta^H B(z)dz \\ B &= \frac{g\alpha Q_T}{\rho_w c_w} \end{aligned} \tag{7.30}$$

where B is the buoyancy flux, δ is the thickness of the surface boundary layer, and H is the depth of the convective layer. Accordingly, the velocity scale w^* is a measure of the kinetic energy of the convective motions and is representative for both the root-mean-square (rms) velocity u_{rms} of vertical convective water motions and the rate of the mixed layer deepening. The rms velocity was estimated from large eddy simulations as $0.7w^*$ by Mironov et al. (2002). Typical reported u_{rms} physical values are 2–3 mm s^{-1} (Farmer 1975; Kelley 1997) and support the above scaling.

The rate of deepening of a convective mixed layer is approximately given by (see Kirillin et al. 2012b)

$$\frac{dH}{dt} = -0.2\frac{w^{*^3}}{H\Delta b} \tag{7.31}$$

where Δb is the buoyancy jump at the bottom of the mixed layer. The reported rates of the mixed layer deepening are typically $\sim$0.5 m day^{-1} and increase up to several meters per day in deeper lakes. The background stratification enters into Eq. (7.31) through the buoyancy jump Δb. Therefore the past winter history influences on the convective layer development. A case with very fast development was registered in Lake Pääjärvi, Finland, in sunny weather in April 2011 after relatively long snowy winter (Fig. 7.12). As a result, a large amount of radiation penetrating into a weakly stratified water column deepened the mixed layer at the rate of more than 3 m day^{-1}. Then, a sharp temperature gradient at the bottom of the mixed layer was then produced, increasing the term ($H\Delta b$) in Eq. (7.31), and the deepening rate reduced to about 1 m day^{-1}.

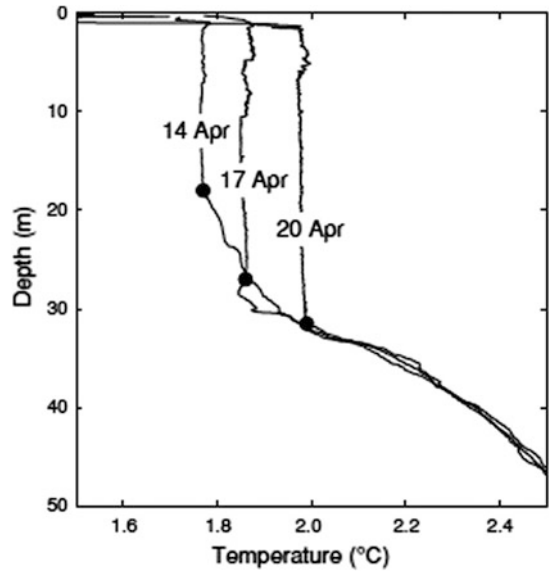

Fig. 7.12 Convective temperature profiles in the central part of Lake Pääjärvi, spring 2011 (Kirillin et al. 2012a). *Dots* mark approximate locations of the convectively mixed layer

Lateral heterogeneity in the solar heating of the upper layer can produce a secondary circulation pattern, whose character has been poorly investigated. The snow cover is unevenly distributed over the ice surface. In large lakes, the deep central parts remain often snow-free, whereas shore areas are snow-covered (Kouraev et al. 2008). In thin snow patches the albedo decreases faster, the ice surface becomes exposed, and increased irradiance beneath the ice results. Also in spring, the positive albedo feedback favours the development of a heterogeneous ice cover. In autumn the opposite is true, i.e. negative feedbacks favour homogenization of ice cover as seen in the small variability of ice thickness.

The differential solar heating of the water body yields horizontal temperature gradients and produces density currents (Zhdanov et al. 2001). Horizontal temperature transects were mapped by Forrest et al. (2008) in the convectively mixed layer of Pavilion Lake, and the result revealed remarkable differences in the temperature of the convective layer, ascribed by the authors to variations of the ice cover thickness. The patchy surface may create small-scale circulation patterns, too. Apart from variations in the ice and snow thickness, the depth differences between shallow and deep parts of lakes are able to produce lateral temperature gradients and initiate a density-driven circulation (Farmer 1975; Bengtsson 1986).

In freshwater lakes, it is possible that convective mixing raises the temperature of the whole water body to 4 °C, apart from the thin boundary layer beneath the ice, before ice breakup. This implies a fast final melting of ice after the porous ice sheet has broken. When the ice has disappeared, the temperature profile soon passes 4 °C, and stratification sets up leaving a very short time for convection in open water conditions. This way spring overturn mostly takes place under ice cover, and the renewal of oxygen in deep water remains limited.

7.4 Light Conditions

7.4.1 Optically Active Substances

Pure water is most transparent to blue light. In shorter and longer wavelengths, light absorption increases strongly (Fig. 7.14). Absorption by solid and liquid phases of pure water is similar but scattering is influenced by the size, shape and orientation of ice crystals (Warren 1982; Mullen and Warren 1988). Liquid water inside snow or ice traps radiation due to absorption and lower scattering, and the more there is liquid water, the higher is the absorption.

The optically active substances (OAS) in lake waters are, in addition to the pure water, coloured dissolved organic matter (CDOM),[5] suspended matter, and chlorophyll *a* (Fig. 7.13) (Arst 2003). CDOM absorbs strongly blue light with absorption decreasing

[5] Also known as the *yellow substance*.

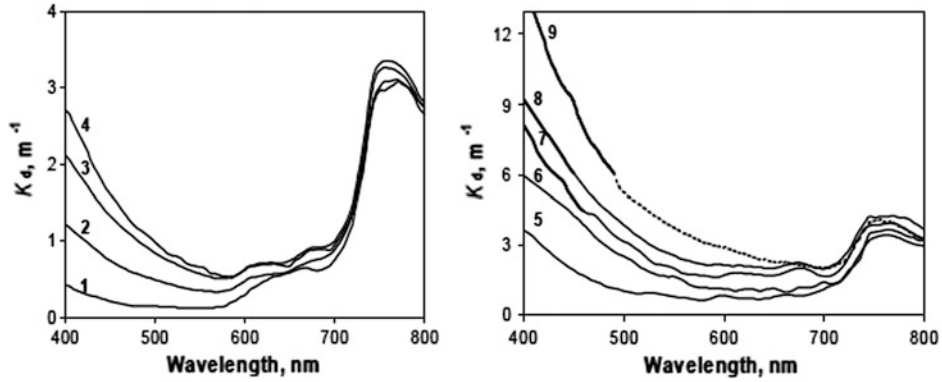

Fig. 7.13 Diffuse attenuation coefficients of light in selected lakes in Estonia and Finland: *1* Äntu Sinijärv, *2* Paukjärv, *3* Koorküla Valgjärv, *4* Vesijärvi, *5* Päijänne, *6* Lammi Pääjärvi, *7* Vôrtsjärv, *8* Tuusulanjärvi, *9* Valkea-kotinen (Arst et al. 2008)

exponentially with wavelength, and, consequently, CDOM moves the colour of the water from blue toward yellow wavelengths. The influence of suspended matter depends on the optical characteristics of particles, but normally radiation is absorbed and scattered with strength weakly decreasing with wavelength. Chlorophyll *a* absorbs strongly blue and red light (wavelength bands 430–440 and 660–690 nm); therefore plants have usually green colour. The absorption and scattering of the OAS can all be assumed additive, since the OAS concentrations are low enough.

Gas bubbles are the dominant optically active impurity in snow and ice. Due to a large number of air inclusions in snow, scattering and therefore light attenuation within the snow cover and snow-ice layer is strong, causing a drastic reduction of irradiance with depth. Also the OAS present in lake water are found in snow and ice. In highly humic lakes, a fraction of CDOM is captured in congelation ice growth and by flooding that adds to the absorption at short wavelengths. Suspended matter would be effectively captured into the ice sheet in frazil ice formation but this occurs rarely in frozen lakes. Since the size of gas bubbles is much larger than the wavelength of light, the attenuation of light when passing through ice is now strongly wavelength dependent.

Solar radiation penetrating the surface of a lake ice cover equals $Q_T = (1 - \alpha)\gamma Q_s$ and constitutes mostly photosynthetically active radiation (PAR) or visible light (see Sect. 4.1.2). The PAR-band attenuation coefficient is $\kappa_s \sim 10\ m^{-1}$ for snow and $\kappa_i \sim 1\ m^{-1}$ for congelation ice (Jakkila et al. 2009; Leppäranta et al. 2010). At $3 \cdot \kappa^{-1}$, or 0.3 m in snow and 3 m in ice (Fig. 7.14), 5 % of the light is left. Light attenuation in clear, bubble-free congelation ice is close to that in liquid lake water with similar attenuation spectra. Since the concentration of impurities is lower in congelation ice than in lake water, the ice may be even more transparent than the water especially in turbid and humic lakes. In contrast, gas bubbles in the ice scatter light, which lowers the light transmittance and flattens the attenuation spectrum.

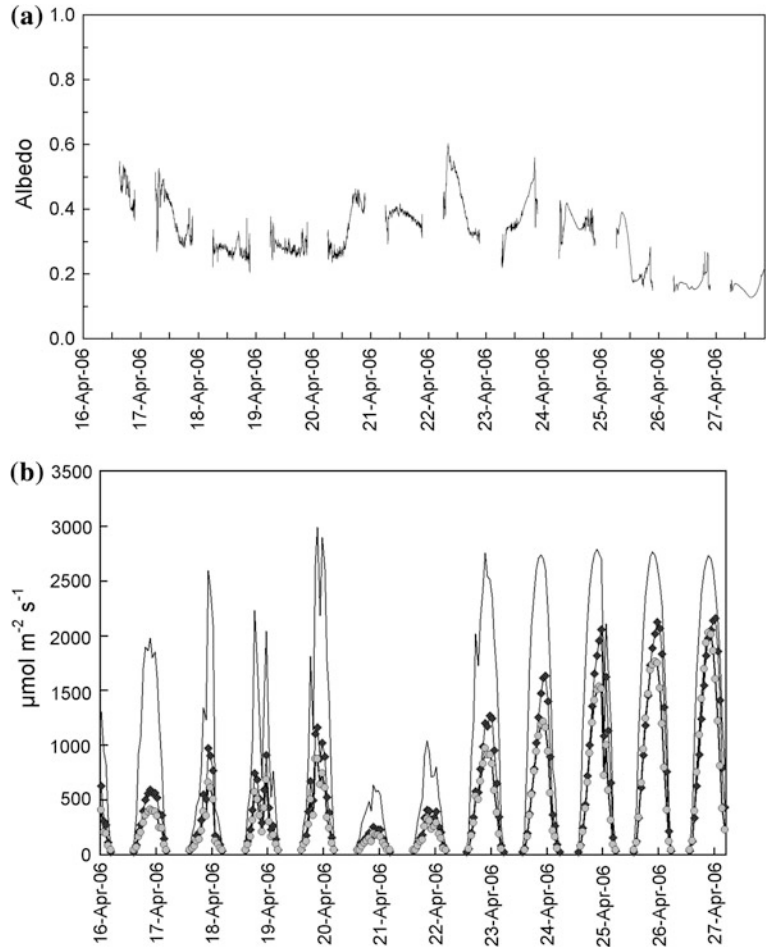

Fig. 7.14 Time series from the melting season in Lake Vendyurskoe, Russian Karelia, April 2006 (Leppäranta et al. 2010). **a** Albedo; **b** quantum downwelling PAR irradiance in the surface, snow-ice and congelation ice (the depths were 0, 14 and 39 cm at the beginning, and 0, 3, and 28 cm at the end due to surface melting)

For a normal three-layer ice sheet, the light transmittance is given by Eq. (3.24). For bare congelation ice the transmission is lowered due to the increased surface reflectance but a snow cover makes a big difference due to its very high reflectance and rapid light attenuation: e.g., adding 10 cm snow on a 50 cm ice sheet can reduce the irradiance level beneath the ice by an order of magnitude. In spring, sunlight plays a major role in the melting of the ice.

7.4.2 Light Below the Ice Cover

The level of downwelling irradiance beneath ice cover is (see Eq. 3.21)

$$\begin{aligned} E_d(z,\lambda) &= [1-r(\lambda)]E_d(0,\lambda)\int_0^z \exp[-K_d(w)]dw \\ &= [1-r(\lambda)]E_d(0,\lambda)\exp\left[-\sum_\ell h_{i\ell}K_{d,\ell}(\lambda)\right] \end{aligned} \tag{7.32}$$

where the lower index ℓ refers to optically different layers. The scalar irradiance E_0 is obtained in analogous manner.

Beneath the ice cover, light has penetrated the snow and ice layers, and its angular and spectral distributions are different from those above the surface. Due to the strong scattering, radiation is diffuse beneath the ice (Leppäranta et al. 2003a; Arst et al. 2006), and the spectral modification by ice and snow depends on their quality, thickness and OAS content (Arst et al. 2006). In the presence of congelation ice, the light spectrum is not white beneath the ice as it is at the surface. In open water and clear sky conditions, radiation becomes diffuse only at a distance from the surface.

A classical measure of the transparency of lake water is the Secchi depth.[6] It is defined as the depth where a white disc, diameter 30 cm, disappears from sight, and its value is about twice the optical thickness (e.g., Arst 2003). In principle, Secchi depth can also be defined for ice-covered lakes but due to light scattering by the ice sheet its observation may be difficult.

A suitable parameter to describe the angular structure of the light field is the ratio of planar to scalar irradiance $\Gamma = E_\mathrm{d}/E_\mathrm{o}$. This ratio not only represents the diffusiveness of light in the water but also the contribution of upwelling light to the formation of scalar irradiance. It can be easily evaluated for ideal cases: (1) For radiance turning horizontal $\Gamma \to 0$; (2) For diffuse irradiance (fixed radiance from all directions), $\Gamma = 1/4$; (3) For diffuse irradiance from upper hemisphere and zero from lower hemisphere, $\Gamma = 1/2$; and (4) For zenith radiance $\Gamma = 1$. A true diffuse irradiance is never observed in natural waters, and normally the downwelling irradiance is much stronger than the upwelling irradiance. In ice-free waters the ratio usually decreases with depth (Reinart 2000). Deeper in the water column in homogeneous water, the apparent optical properties reach their asymptotic values, usually $0.4 < \Gamma < 0.9$. The situation can be different in under-ice waters, because light having just penetrated the ice layer is considerably more diffuse than

[6] Introduced in 1865 by Italian astronomer Pietro Angelo Secchi (1818–1878).

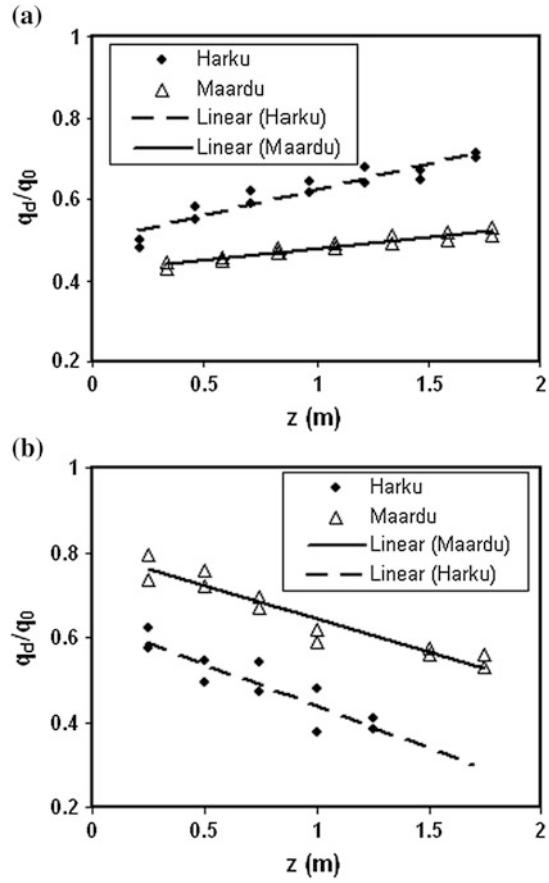

Fig. 7.15 Depth-dependence of the ratio of downwelling irradiance (q_d) to scalar irradiance (q_0) in the surface layer of Estonian lakes Harku and Maardu in, **a** winter with ice cover and **b** summer (Arst et al. 2006)

that below the surface of ice-free water (Arst et al. 2006). In contrast to ice-free situations, beneath ice scalar irradiance decreases with increasing depth more rapidly than planar irradiance, which means that diffuse attenuation coefficient is larger for the scalar irradiance than for the planar irradiance (Fig. 7.15).

Reflectance and transmittance are spectral quantities. Reflectance is the ratio of upwelling irradiance to downwelling irradiance just above the surface, and transmittance is the ratio of downwelling irradiance below the ice to downwelling irradiance just above the ice. They are illustrated for different lakes in Finland and Estonia in Fig. 7.16. It is seen that in the melting season they both are quite different from earlier winter situations. Reflectance is rather even across the optical band, and in a few humic lakes the absorption of short-wave radiation is strong.

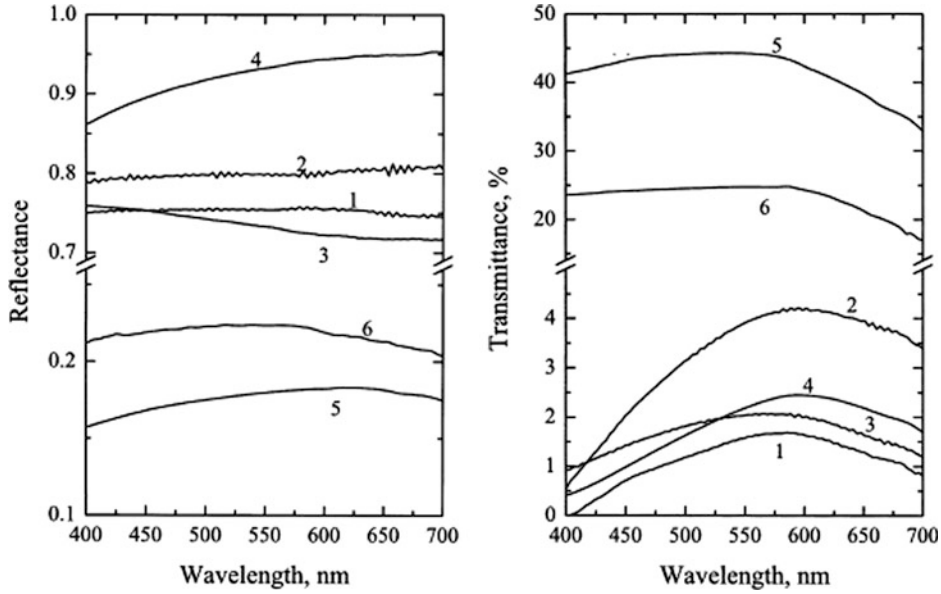

Fig. 7.16 Reflectance (*left*) and transmittance (*right*) in lakes *1*—Lovojärvi, *2*—Pääjärvi, *3*—Iso Valkjärvi, *4*—Vanajavesi, *5*—Peipsi, and *6*—Vesijärvi in the melting season. Lakes *1–3* are highly humic, and lakes *5–6* are snow-free

7.5 Wintertime Budgets of Gases and Nutrients

7.5.1 Oxygen

Ice-covered lakes behave as closed systems with regard to dissolved oxygen (DO). Without intense photosynthesis and water aeration, there is no oxygen supply, and the consumption of oxygen by bacterial plankton in decomposition of organic matter and the absorption of oxygen by bottom sediments control the DO content in a lake (Hargrave 1972). In general, the oxygen level is an excellent index of the health of the lake. The dimension of DO concentration is mass per volume, the unit is normally mg L^{-1} (milligrams per litre). Often the oxygen content is expressed as the percentage of its saturation level, which depends on the temperature (see Fig. 7.1).

In ice-covered lakes, oxygen renewal is marginal, and therefore the oxygen content decreases during the ice season (Fig. 7.17). The initial conditions at the instant of freezing are important, since the colder the water is after autumn mixing the more there is oxygen. Oxygen depletion is strongest in the lower layer, where anoxic conditions are reached particularly in long winters. The consumption of oxygen is higher in eutrophic lakes and therefore these are more likely to suffer in the ice season. Lakes, where such conditions are

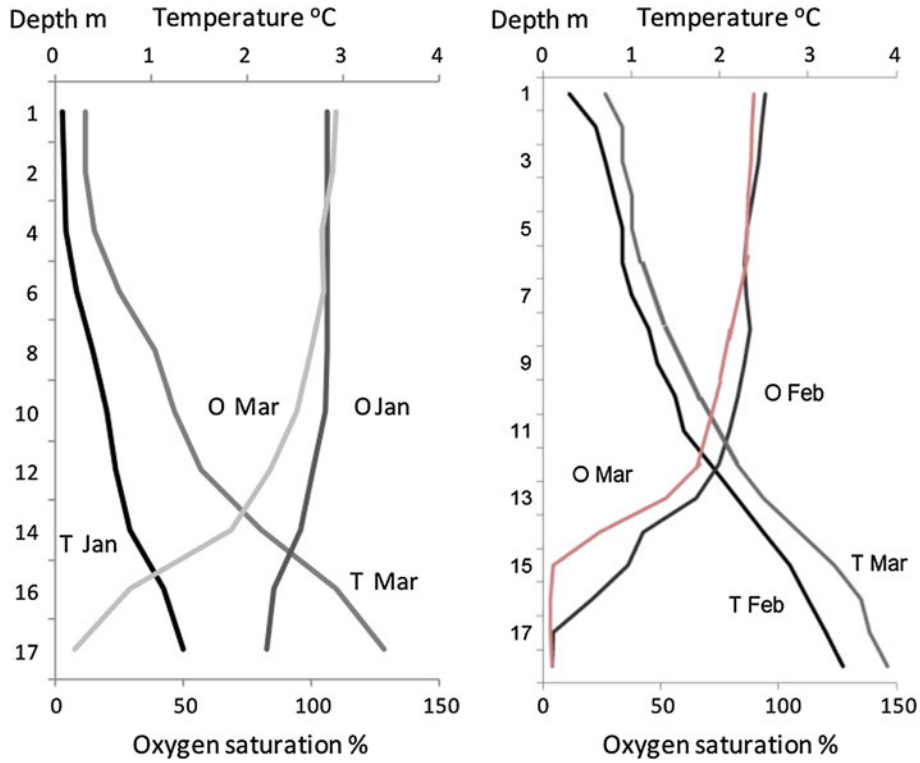

Fig. 7.17 Vertical distribution of water temperature (*T*) and oxygen saturation (*O*) in Lake Vanajavesi, Southern Finland in January 26 and March 18, 2008 (*left*), and February 10 and March 25, 2009 (*right*) (Leppäranta et al. 2012)

expected, are often equipped with an air pumping system to help their ecosystem to survive over the winter.

When DO concentration is high, bacterial destruction of organic matter is accompanied by extraction of carbon dioxide that is harmless to aquatic life. A decrease in the DO concentration or complete absence of DO in the lower layer leads to negative ecological consequences such as fish winterkill, loss of benthic organisms, activation of anaerobic processes with accumulation of dangerous compounds such as methane (CH_4), hydrogen sulphide (H_2S) and ammonia (NH_3) (Greenbank 1945; Barica and Mathias 1979). These gases, in particular hydrogen sulphide, are toxic.

The most dangerous anaerobic conditions develop in small, shallow lakes with prolonged or extensive snow and ice cover, limited water inflow, abundant aquatic macrophytes, and high primary productivity (Halsey 1968; Terzhevik et al. 2010). For example, the anaerobic zone of about one meter thick is formed in the bottom layers of the deep part of Lake Vendyurskoe, Russian Karelia every winter (Fig. 7.18).

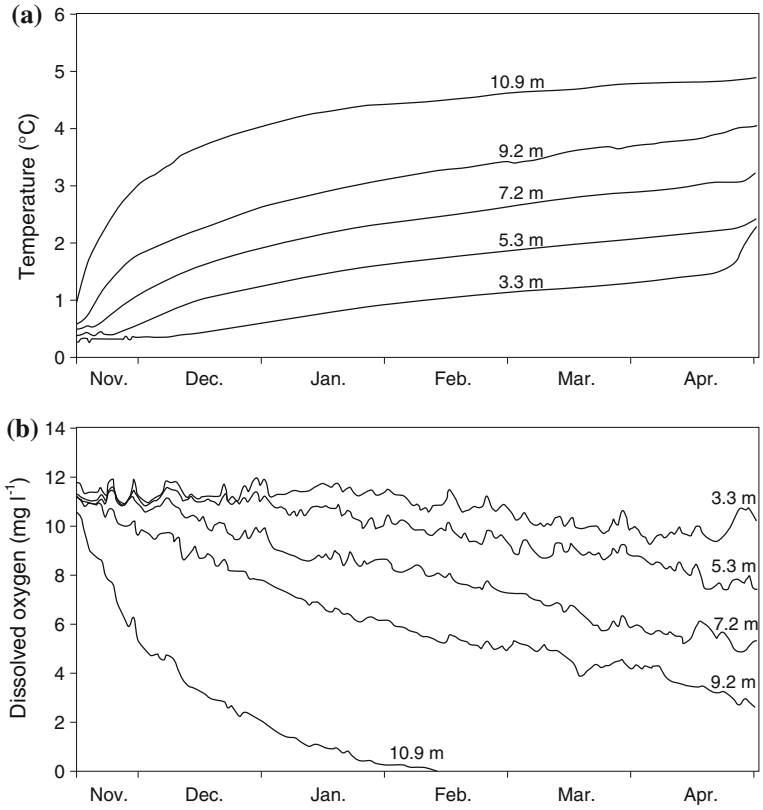

Fig. 7.18 Temperature (**a**) and dissolved oxygen concentration (**b**) in the *central part* of Lake Vendyurskoe, Russian Karelia, during the winter 2010–2011 at several depths (Redrawn from Terzhevik et al. 2010)

The life activity of bacterial plankton is the main consumer of DO and it is strongly dependent on the water temperature (Boylen and Brock 1973; Welch et al. 1976). However, it is normally assumed that in winter conditions the influence of temperature on the bacterial activity is not large and oxygen depletion depends only on the concentration of organic matter in the water column (Golosov et al. 2006). The biochemical oxygen demand of lake water (BOD) and lake sediment (SOD) are the main factors governing the oxygen depletion in ice-covered lakes. It is believed that SOD makes the major contribution (Greenbank 1945; Hargrave 1969), though no quantitative relation between SOD and BOD has been established (Ellis and Stefan 1989). Both BOD and SOD are strongly affected by physical conditions: vertical temperature stratification, near-bottom currents, and the heat release from sediments. SOD, defined as the rate at which DO is consumed from the water column due to the decomposition of organic matter in the bottom sediments, is controlled by mass transport and/or biochemical reactions in the upper sediment and in the diffusive boundary layer above (Higashino et al. 2004).

The diffusive boundary layer is a 0.2–1.2 mm thick film of water that coats cohesive sediments, through which molecular diffusion is the dominant transport mechanism for solutes (Boudreau and Jørgensen 2001). Bottom currents and associated mixing decrease the thickness of this layer, thereby increasing the flux of DO from overlying water to the sediment (Beutel 2001). Biochemical processes are, in turn, strongly dependent on temperature (Boylen and Brock 1973; Zeikus and Winfrey 1976).

Golosov et al. (2006) have shown that at low temperatures the sediment oxygen demand is especially sensitive to temperature variations: even several tenths of centigrade increase of the near-bottom temperature can essentially intensify oxygen consumption in the upper sediment and produce eventually anoxic conditions in the lower layer. Therefore, the capacity of bottom sediments to store heat and the heat flux from water to sediments in summer and autumn are critical factors for the oxygen conditions during the ice season. This gives one memory time scale of freezing lakes to be of the order of 6 months. Golosov et al. (2006) give examples of lakes where the temperature of the bottom water has increased from 0.5–1 °C in the beginning of the ice season to 4–5 °C at the end.

The oxygen consumption rate (oxygen depletion rate) is often used as a measure of combined effect of BOD and SOD, which is easily achieved from time records of DO concentrations as $(C_0 - C)/t$, where $C_0 = C_0(z)$ and $C = C(z; t)$ are the initial value and the time evolution of the DO concentration. Typical reported values of the oxygen consumption rate in ice-covered lakes range within 10^{-2}–1 mg O_2 L^{-1} day^{-1} (e.g., Puklakov et al. 2002), increasing towards the lake bottom. In shallow Lake Vendyurskoe, Russian Karelia the oxygen consumption rates varied in the beginning of the ice season from 0.4 mg O_2 L^{-1} day^{-1} in the upper layer to 1.0 mg O_2 L^{-1} day^{-1} in the vicinity of the water–sediment boundary (Terzhevik et al. 2010). Along with gradual decrease of oxygen concentration and development of the anoxic zone in the hypolimnion, the oxygen records demonstrated short-term fluctuations with periods from several minutes to several days (Fig. 7.19).

The evolution of the oxygen content under ice can be approached using a one-dimensional, vertical model (Golosov et al. 2006). It is based on the diffusion equation with a sink term. The boundary conditions are given by oxygen fluxes as absorption of oxygen at the bottom and no flux at the surface. The equation is written as

$$\frac{\partial C}{\partial t} = \frac{\partial}{\partial z}\left(K\frac{\partial C}{\partial z}\right) - \gamma(T)C \tag{7.33a}$$

$$z = 0 : \frac{\partial C}{\partial z} = 0; \quad z = H : K\frac{\partial C}{\partial z} = F_b \tag{7.33b}$$

where K is the diffusion coefficient, γ is the rate of oxygen consumption, H is depth, and F_b is the bottom absorption. The consumption rate varies from 10^{-8} s^{-1} in the upper water column to 10^{-7}–10^{-6} s^{-1} at the water-sediment boundary (Golosov et al. 2006). The upper layer has shown similar values in many lakes, but at the bottom the oxygen consumption

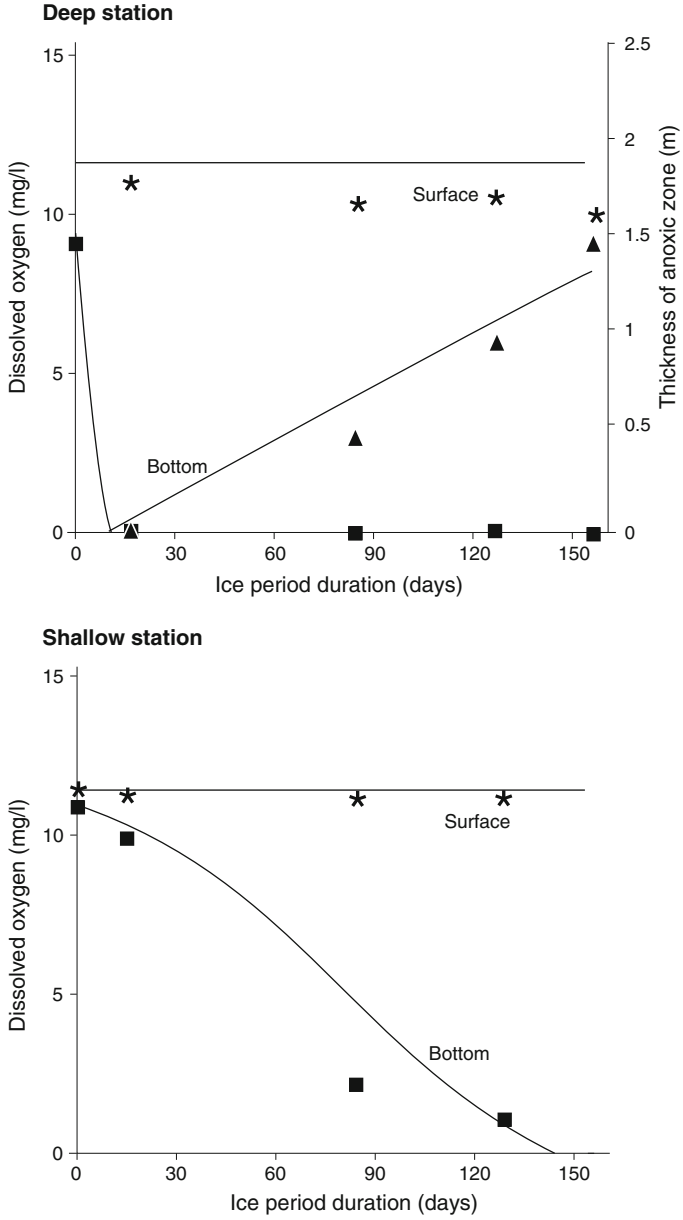

Fig. 7.19 Evolution of the DO concentration and of the anoxic zone thickness H in Lake Vendyurskoe. *Stars* and *squares* represent the DO concentrations measured under the ice cover and in the near-bottom water, respectively, and *triangles* mark the measured thickness of the anoxic zone (Prepared from Golosov et al. 2006)

depends strongly on the sediment composition. The molecular diffusion coefficient of oxygen is 2×10^{-9} m^2 s^{-1}. In the bottom boundary layer, the time-scale of oxygen consumption is much shorter than the time-scale of molecular diffusion.

Golosov et al. (2006) examined the evolution of vertical oxygen profile under lake ice using a self-similarity model, which also contained the surface layer of the bottom sediments. They used the Dirichlet boundary conditions: C_0 = constant at the surface, supported by their data, and $C = 0$ at the bottom. Initially $C = 0$ was reached at the depth δ beneath the sediment surface. The profiles of oxygen content and oxygen consumption were given as second or third order polynomials in the water and in the sediment, and the oxygen consumption depended on the water temperature. In the beginning, oxygen was fed from the water to the sediment, then the bottom became anoxic, and the anoxic layer grew upward from the bottom.

7.5.2 Methane

Lakes have been recognized as important sources of methane, which accounts for about 20 % of the greenhouse effect (see Kirillin et al. 2012b). There are four emission pathways: ebullition flux, diffusive flux, storage flux, and flux through aquatic vegetation. Isolation of lakes from the atmosphere by the ice cover can result in accumulation of methane bubbles beneath and inside the ice with subsequent increase of the emission after the ice break-up. Prokopenko and Williams (2005) suggested this effect to produce outbursts in Lake Baikal of several teragrams of methane for the whole lake area. Later, Schmid et al. (2007) demonstrated that most of the methane produced under ice is dissolved and oxidized in the deep water column of Lake Baikal. Though a slight increase of the methane concentration under ice was observed, the level did not exceed significantly the atmospheric concentrations. With certain care, the suggestion about the negligible methane emission on annual scales can be extrapolated to the majority of deep oligotrophic lakes.

Yet, depending on the trophic regime and the size of lakes, estimations of methane fluxes vary in a wide range, from micrograms to several grams carbon per square meter per year with the highest methane fluxes found in hypereutrophic lakes. Strayer and Tiedje (1978) reported of the methane fluxes in hypereutrophic Lake Wintergreen as high as 92 and 44 g cm^{-2} $year^{-1}$, due to ebullition and diffusion, respectively. The present evidence suggests that the majority of methane production occurs in anoxic sediment (Rudd and Hamilton 1978). Thus, an appreciable effect of the ice cover on methane production can be expected in shallow eutrophic lakes with significant duration of the ice-covered period. The winter anoxia, typical for such lakes, can significantly affect the methane production. Quantitative estimations of this effect and possible consequences of climate-driven changes in ice phenology on the methane emission are not yet available.

7.5.3 Nutrients

Circulation and mixing processes under ice, such as shear-driven resuspension at the water-sediment interface and pore-water convection, affect directly the nutrient release from the sediments. For open water conditions, several bulk estimates exist for nutrient supply by shear-driven resuspension (Kristensen et al. 1992; Hamilton and Mitchell 1996) and by convective mixing (Golosov and Ignatieva 1999; Kirillin et al. 2009) as a function of mixing intensity. These dependencies generally stay valid in ice-covered lakes, though reveal specific aspects. Anoxic conditions produce chemical and ecological consequences, such as release of phosphorus from the bottom sediments (Leppäranta et al. 2012).

First, the decoupling of wind, waves, currents and the sediment surface leads to an unhindered particle settling and incorporation into the sediment structure. Thus, the quiet winter conditions considerably reduce the entrainment of particulate and dissolved nutrients by resuspension, which in turn should favour the consolidation of sediment. Håkanson and Bryhn (2008) reported that the longer the particles have stayed at the bottom, the larger the potential gluing effect will be and the faster the settling velocity is if the particles are resuspended. Thus, the shorter the period of ice coverage the less is the degree of microbial gluing of surface sediment. Second, less consolidated sediment is more prone to wind/wave-induced bottom shear stresses. As a consequence, the 'start conditions' for the phytoplankton succession after ice thaw change considerably. It needs a lower critical bottom shear stress for resuspension, which is related to the entrainment of nutrients (algal recruitment), algal cells, and overwintering cyanobacterial cysts. Hence, climate-driven shortening of ice-cover duration would not only increase resuspension and related nutrient loading (Niemistö and Horppila 2007), but would also shorten the calm period for settling of particles and their integration into sediment as well as for its consolidation.

Another source of nutrients, specific for the ice-covered period only, is the ice sheet, which contains nutrients originating from the water body, sediments or atmospheric fallout. The capturing of impurities by the ice depends on the mode of ice growth, and their release to the water body occurs in the melting season (Leppäranta et al. 2003a). There is almost no research done on the nutrients in lake ice and their release into the water, the only publications concern Antarctic lakes (Fritsen and Priscu 1998).

Ice-Covered Lakes Environment

8

Saimaa ringed seal (*Pusa hispida saimensis*) in Lake Saimaa, Finland. Seals are very rarely seen in lake environments. After the last ice age the Baltic Sea evolved through several phases where, due to land upheaval, lakes with their ringed seal population were separated from marine waters and turned into freshwater basins. These relicts are still found from lakes Saimaa and Ladoga.

Photograph: Mr. Juha Taskinen, printed with permission.

Ice-covered lakes form a specific environment. Seasonally ice-covered lakes are common in a wide inhabited latitudinal zone in the northern hemisphere, while perennial lake ice can be found only in some remote polar and high mountain locations. The ice cover

M. Leppäranta, *Freezing of Lakes and the Evolution of their Ice Cover*,
DOI 10.1007/978-3-642-29081-7_8

sets limitations to ecosystems: light is absent or weak in mid-winter, oxygen is not renewed, and the water temperature is low. Also the renewal of the lake water mass and nutrients is reduced due to reduced inflows from the cold, frozen surroundings. For the society, frozen lakes are safety and traffic issues, and specific methods are needed for utilization of lakes and for near-shore construction efforts.

8.1 Winter Ecology

8.1.1 General

The biology of freezing lakes is much less known from field investigations for the ice season than for the summer. Most of the ice studies are concerned with polar lakes, while for boreal lakes there are just a few scattered publications (see Salonen et al. 2009). Primary production is weak in winter in boreal lakes, but as a whole the ecological conditions in spring and fall are linked through the winter rather than being independent, and therefore understanding the progress of the winter season is important.

Lake ecosystems cover phytoplankton, macrophytes, zooplankton, fish and amphibians. In a very few lakes there are seals, e.g. in Lake Saimaa and Lake Ladoga in Finland and Lake Baikal in Russia.[1] Freezing lakes provide specific aquatic habitats, and compared with lower latitudes, the food-web structure is simplified (e.g., Vincent et al. 2008). Arctic and Antarctic lake regions are dissimilar. In the Arctic they are found in northern extensions of continental land masses, while Antarctica is an isolated continent where lakes are proglacial. This is reflected in the colonization and biodiversity. Arctic lakes have more diverse compositions of biota, and in Antarctic lakes fish are absent and in many cases even zooplankton is missing. Microbial mats dominated by cyanobacteria are common in both polar regions but higher plants are not found in Antarctic lakes.

In cold regions, freezing brings limitations to biological activity. Primary production needs liquid water, carbon dioxide, photons and nutrients. The photosynthesis formula reads

$$6H_2O + 6CO_2 + \text{photons} \rightarrow C_6H_{12}O_6 + 6O_2 \tag{8.1}$$

The wavelength band of light used for photosynthesis is from 400 to 700 nm, called as the photosynthetically active radiation (PAR) band. It is nearly the same as the band of electromagnetic radiation visible to human eye. By photosynthesis, plants, algae and cyanobacteria use the energy of photons to transform water and carbon dioxide into sugar and oxygen.

Liquid water is available in lake environments, at least for a part of the year, by the definition of a lake. But in very shallow lakes and supraglacial lakes the whole water body

[1] Lake Saimaa and Ladoga seals are relicts from the time the lakes were connected to the ocean about 10,000 years ago, later isolated due to land uplift.

may freeze in winter. Normally, however, cold region lakes have liquid water and at least microbial activity throughout the year. Carbon dioxide dissolves easily in water and therefore the storage is renewed via the atmosphere in lakes, which possess an open water season.

The ice and snow layers also act as habitats of biota. As soon as there are liquid water layers or pockets in ice and snow cover, primary production takes place with its selective light absorption spectrum. This is typical in spring or summer, but also takes place in slush layers at the snow-ice interface and in the brine pockets on saline and brackish lakes. But the ice and ice margin ecosystems seem to be a minor factor in lakes not reaching the richness observed in polar sea ice environment.

Light can become a limiting factor to primary production. In the polar night there is no sunlight, and in the case of thick snow on ice the radiation can be attenuated too much before reaching the water body. Primary production uses light quanta, which is expressed in moles.[2] The rate of quanta flow in solar radiation is $\sim 10^3$ μmol m^{-2} s^{-1} at the Earth's surface. The level of quantum irradiance needed to maintain primary production is of the order of 25 μmol m^{-2} s^{-1} (see Arst 2003), which corresponds to irradiance power of around 5 W m^{-2}. If there is a dry, clean snow cover, irradiance just beneath the snow surface can be 50 W m^{-2} at noon in clear days, and that has attenuated to below 5 W m^{-2} at the depth of $z = \kappa^{-1} \log(10) \sim 25$ cm, where κ is the light attenuation coefficient of snow.

Under snow-free ice, there is enough light in the surface layer for photosynthesis, and an increase of the primary production under ice is often observed when the snow melts (Kelley 1997; Salonen et al. 2009). Hence, the physical-biological interactions are more manifold than in the preceding snow-covered period.

Primary production needs also nutrients, which are classified into macro- and micronutrients. The former category contains sodium, magnesium, phosphorus, sulphur, chlorine, potassium, calcium, iodine and silicon, while the latter contains e.g. iron, copper and zinc. Nutrient supply is a limiting factor. In winter, low temperature and freezing constraint the activity of soil microbes and slows geochemical processes that reduces the influx of nutrients via surface and groundwater runoff. In fully ice covered lakes, circulation and mixing are weak, and the water body is stratified. This factor further limits the cycling of nutrients within the water body. Also nutrients are lost in sedimentation, and due to the absence or weakness of turbulence at the bottom, less is gained by resuspension. In all, nutrient supply can bring a strongly limiting factor to primary production in ice-covered lakes. But ice-covered lakes, which receive nutrient enrichment from natural or human sources, can show high production rates.

Benthic photosynthetic communities may become dominant in ice-covered lakes, since conditions are more stable at the bottom. Sedimentation brings nutrients down from the water body, nutrients are released from the bottom sediments, and there are more active bacterial decomposition and nutrient recycling processes than in the overlying water body.

[2] The number of quanta in one mole equals the Avogadro's number $N_A = 6.022142 \times 10^{23}$.

These communities can grow into large stocks and fuel benthic food webs up to higher trophic levels including fish and birds.

The temperature of liquid water body is between 0 and 4 °C in ice-covered freshwater lakes. The low temperature is not a strictly limiting factor but it slows down the rate of metabolism and growth of living organisms. Since salinity depresses the freezing point, in brackish lakes the minimum temperature of liquid water is –1.3 °C while in saline lakes it can be much lower. In shallow lakes, which freeze almost throughout, salt rejection from growing ice depresses the freezing point and the remaining water layer can be highly saline. If a saline, ice-covered water body is stratified in salinity, solar radiation can heat the lower layer into quite high temperatures, as long as the salinity difference can prevent convection. By this mechanism, deep-water temperature has reached up to 14 °C in the Canadian High Arctic (Van Hove et al. 2006).

Lake ice as a habitat of biota has been investigated in the recent decades (Laybourn-Parry et al. 2012), but most of this research has involved perennial lakes in the Antarctica (e,g., Priscu et al. 1998). In general, inside ice and snow cover, the presence of liquid water is the limiting factor (Fig. 8.1). But as soon as there is liquid water, microbial life will occur. In the melting season there is always liquid water present inside ice due to internal melting, and earlier in the ice season flooding brings lake water to the snow-ice interface. Brackish and saline ice contains brine pockets, which serve as habitats of life. They have very low temperature and high salinity in cold winter periods. Sea ice biota in brine pockets has been widely examined in polar and brackish marine basins (e.g., Arrigo 2003; Rintala 2009).

8.1.2 Water Quality

The water balance, circulation and mixing together with the inflow and outflow of matter determine the water quality of lakes. Circulation dynamics result in transport and diffusion of water with its constituents, and geochemical and biochemical processes modify the lake water chemistry. The amount and composition of dissolved and particulate matter in the

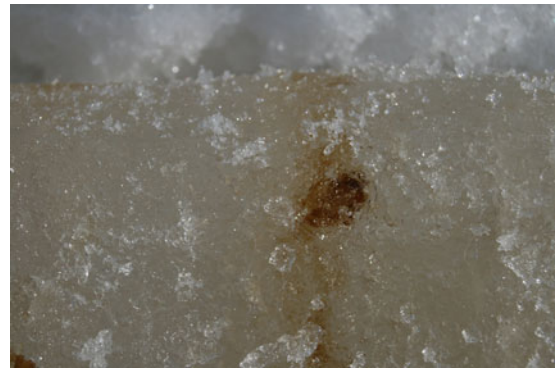

Fig. 8.1 Liquid humus water pocket inside a lake ice sheet. The size of the *brown* pocket is 5 mm

lake water is referred as the water quality. Salinity, pH, nutrients, chlorophyll, and harmful substances are particularly interesting. Fully ice-covered lake water bodies are characterized by low level and low range of temperature, stratification, weak thermohaline circulation, weak mixing, and often low level of sunlight. The water velocities are low, 1–10 mm s^{-1}, turbulence—if any—is weak, and consequently diffusion is slow. But if the ice cover is not stable, it has a major impact on circulation dynamics as wind stress can be transferred to some degree into the water body.

The concentration of dissolved matter (C_d) is normally estimated from the electric conductivity (σ) as C_d [mg L^{-1}] = 0.67 × $\sigma_{25°C}$ [μS cm^{-1}], where the lower index 25 °C gives the reference temperature for the conductivity. The concentration of dissolved matter is also expressed as salinity (S), which equals the relative mass of dissolved matter in a water parcel; in fresh and brackish waters 1 g L^{-1} corresponds to S = 1 ‰. The level of dissolved matter has a weak annual cycle due to consumption of nutrients. The quantity pH is a measure of the concentration of hydrogen ions. In exact terms, it is negative of the logarithm of the concentration of hydrogen ions, and therefore the higher the pH is the less there are free hydrogen ions. The pH of distilled water is 7, for acid water the pH is less and for basic water it is more.

Lake water contains dissolved gases, with saturation levels of different gases depending on the temperature (see Fig. 7.1 for oxygen). Solid ice cover is not permeable for gases, and therefore gas bubbles released from the water body or lake bottom get locked within a growing ice sheet. Oxygen is a key dissolved gas in water, and its concentration is an excellent single indicator of the health of a lake. The level of 2 mg L^{-1} is considered for lower boundary for an ecologically healthy lake environment, while at temperature of 1 °C the saturation level is 14.2 mg L^{-1} (Fig. 7.1). Oxygen is primarily renewed by the atmospheric flux, while the output of oxygen from primary production is a secondary factor. Therefore in the ice season the oxygen renewal is a major issue (Fig. 8.2).

Suspended matter concentration is changed by sedimentation and resuspension, inflow and outflow, and chemical processes within the water body. In winter the low level of water currents means that resuspension is weak that provides an internal cleaning mechanism. One implication is lower turbidity of the water mass. Major inflows of

Fig. 8.2 Ice fishing is a popular hobby in cold region lakes

suspended matter take place in the snow melting period, with meltwater flushing the soil surface, and after heavy rain events.

8.1.3 Quantum Irradiance

Attenuation of light in ice and water is wavelength-dependent as discussed in Sect. 3.4. At the depth z, the spectral distribution of scalar irradiance is (e.g., Arst 2003):

$$E_0(z;\lambda) = E_0(0;\lambda)\exp\left[-\int_0^z \kappa_0(z';\lambda)dz'\right] \tag{8.2}$$

where κ_0 is the attenuation coefficient of scalar irradiance. The energy of a photon is $E = hc_0/\lambda$, where $h = 6.6255 \times 10^{-34}$ J s is Planck's constant, and $c_0 = 2.9979 \times 10^8$ m s^{-1} is the velocity of light in vacuum, and consequently the quantum scalar irradiance is

$$q_0(z;\lambda) = \frac{\lambda}{hc_0}E_0(z;\lambda) \tag{8.3}$$

The scalar irradiance is taken since for the photosynthesis just the number of photons accounts for. The number of light quanta is obtained by integration of the photon flux:

$$q(z) = \int_{\lambda_1}^{\lambda_2} \frac{\lambda}{hc_0}E_0(z;\lambda)d\lambda \tag{8.4}$$

where λ_1 = 400 nm and λ_2 = 700 nm are the wavelength limits of the PAR band. The transformation between irradiance power and quanta units can be made by

$$qhc_0 = \tilde{\lambda}\widehat{E}_0, \tilde{\lambda} = \frac{1}{\widehat{E}_0}\int_{\lambda_1}^{\lambda_2} \lambda E_0(z;\lambda)d\lambda \tag{8.5}$$

where $\widehat{E}_0$ is the mean PAR irradiance and $\tilde{\lambda}$ = is the irradiance-weighted mean PAR-wavelength. For white light $\tilde{\lambda} = 550$ nm, and therefore $q/\widehat{E}_0 = 4.60$ µmol J^{-1} as normally used for the irradiance above a lake surface. This is a good approximation since the light spectrum is fairly even in the air. But within any lake, the light spectrum changes significantly with depth. Deeper in clean water $\tilde{\lambda} < 500$ nm, and deeper in humic or turbid water $\tilde{\lambda} < 600$ nm, and thus the bias of using the constant ratio of $q/\widehat{E}_0 = 4.60$ µmol J^{-1} is less than 20 %, often less than 10 %. In Finnish and Estonian lakes this ratio increases from 4.6 µmol/J at the surface to about 4.8–5.5 µmol/J deeper in the water (Reinart et al. 1998). Dry and clean snow or snow-ice keeps the even shape of the light spectrum, but congelation ice acts much as clear lake water.

In limnology as well as in oceanography the concept of *euphotic depth* is used to describe the maximum depth where photosynthesis can be maintained by the available light. This is usually taken as *the depth where the downwelling planar irradiance has gone down to 1 % of its level just below the surface* (see Smetacek and Passow 1990; Arst 2003). The definition has two shortcomings: it is relative rather than absolute, and it accounts for the radiation level and not for the photon flux. Therefore this euphotic depth serves just as a scaling depth of the photosynthetic layer. We can think that the magnitude of the noon irradiance is 500 W m^{-2} in high latitudes in spring and summer. For wet, bare ice surface the albedo is $\sim 1/3$, and therefore the 1 % level corresponds to the power of 3.3 W m^{-2} or to the photon flux of ~ 15 μmol m^{-2} s^{-1}. Depending on the water quality the photon flux can range by about 25 % for a fixed PAR irradiance power $\widehat{E}_0$. Also it has been suggested that in cold waters, when the rate of metabolism is lower, a smaller photon flux is sufficient to maintain photosynthesis.

In open water conditions, the euphotic depth is $z_e \sim \log(100) \cdot \kappa^{-1} \approx 4.61 \cdot \kappa^{-1}$, where κ is the mean PAR-band attenuation coefficient. However, it is best to consider the full spectral attenuation as a function of depth and integrate for the irradiance spectrally for any depth. Then the euphotic depth of photosynthesis can be more accurately evaluated. Thus,

$$\begin{aligned} \frac{\widehat{E}_d(z)}{\widehat{E}_d(0)} &= \int_{\lambda_1}^{\lambda_2} \frac{E_d(0;\lambda)}{\widehat{E}_d(0)} \exp\left[-\int_0^z \kappa(z';\lambda)dz'\right] d\lambda \\ &\approx \frac{1}{\lambda_2 - \lambda_1} \int_{\lambda_1}^{\lambda_2} \exp\left[-\int_0^z \kappa(z';\lambda)dz'\right] d\lambda \end{aligned} \tag{8.6}$$

where the last identity comes from the assumption that the spectrum of downwelling irradiance is even at the surface.

Example 8.1. Assume that the attenuation coefficient is independent of depth, κ(z; λ) = κ(λ). Then the spectral integral of the light attenuation can be approximately taken as the Riemann sum over an even division of PAR-band to n intervals

$$\frac{1}{\lambda_2 - \lambda_1} \int_{\lambda_1}^{\lambda_2} \exp(-\kappa z) d\lambda \cong \frac{\Delta\lambda}{\lambda_2 - \lambda_1} \sum_{i=1}^{m} \exp(-\kappa_i z) = \frac{1}{n} \sum_{i=1}^{m} \exp(-\kappa_i z)$$

where κ_i's are taken at the centre points of the intervals. With $n = 3$ and assuming $\kappa_2 \ll \kappa_1$, κ_3, euphotic depth is $z_e \approx 3.5 \cdot \kappa_2^{-1}$; but taking the mean attenuation coefficient for the whole PAR-band, we have $z_e \approx 4.61 \cdot [\frac{1}{2}(\kappa_1 + \kappa_3)]^{-1}$. For $\kappa_2 = 1$ m^{-1} and $\kappa_1, \kappa_3 = 10$ m^{-1}, these depths would be 3.5 and 0.46 m, respectively; for $\kappa_1, \kappa_3 = 3$ m^{-1}, they would be 3.5 and 2.0 m, respectively.

When using the concept of euphotic depth for ice-covered lakes, we can assume that the magnitude of downwelling irradiance above the surface is 500 W m^{-2} in spring or summer. But due to the high albedo, the magnitude of irradiance is low just beneath the surface; in case of dry snow surface it is just 50 W m^{-2}, and 1 % of that is only 0.5 W m^{-2}. This corresponds to the light quanta flux of about 2 μmol m^{-2} s^{-1}, which is too low for photosynthesis. Instead, a preferable euphotic depth would come as 1 % of the downwelling irradiance just above the surface. In the open water case the albedo is 0.07 and the scaling depth would be essentially the same whether the reference is taken just below or just above the surface. For ice-covered lakes, the euphotic depth z_e can thus be defined as:

$$\int_{\lambda_1}^{\lambda_2} \exp\left[-\int_0^{z_e} \kappa(\lambda)dz\right] d\lambda = \log[100(1-\alpha)] \tag{8.7}$$

If $z_e \leq h$, the thickness of snow and ice, photosynthesis is possible only in snow or ice provided that liquid water is present. Otherwise, $z_e > h$, and

$$z_e = h + \frac{1}{\kappa_{PAR}}\{\log[100(1-\alpha)] - T_i\}, T_i = \int_{\lambda_1}^{\lambda_2} \exp\left[-\int_0^{h} \kappa(\lambda)dz\right] d\lambda \tag{8.8}$$

where T_i is the transparency of the ice and snow sheet. Because of the albedo effect, the euphotic depth beneath bare ice is about half of that in the open water. If there is more than about 20 cm snow on the ice, no photosynthesis is possible in the upper layers of the water column. In cold lake water, photosynthesis can continue with even lower light level, and therefore the actual euphotic depth is more. Figure 8.3 shows planar and scalar irradiance beneath ice cover. The magnitude is 100 μmol m^{-2} s^{-1}, and scalar irradiance is higher but decreases faster with depth.

In high latitudes the diurnal and annual distribution of incoming solar radiation shows distinct characteristics compared to low latitudes. In the polar day or polar night the

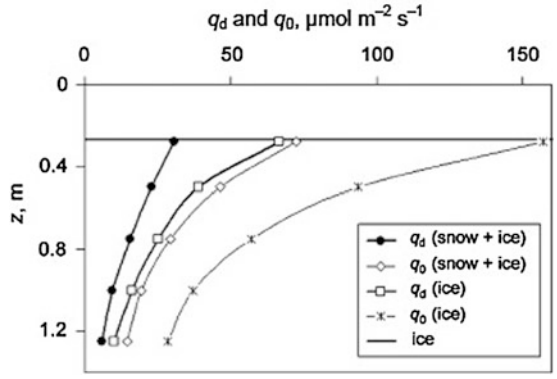

Fig. 8.3 Vertical profiles of downwelling planar (q_d) and scalar (q_0) PAR irradiance beneath 27 cm ice cover and zero or 1.5 cm snow cover (Arst et al. 2006). The site is Lake Ülemiste, Estonia, 15 February 2000

radiation is continuous or absent, respectively, and the solar altitude is limited by the zenith distance of the latitude plus inclination of the ecliptic ($\varepsilon = 23.5°$). At latitude ϕ, the solar altitude at midsummer noon and midwinter noon is $90° - \phi + \varepsilon$ or $90° - \phi - \varepsilon$, respectively; for $\phi = 60°$ these altitudes are 53.5° and 6.5°.

There is concern about the increase of UV-B (ultraviolet B-band, 280–320 nm) in high polar latitudes. This is photochemically and photobiologically the most active band of the solar irradiance on the surface of the Earth, and it disturbs the growth of biological organisms and causes DNA damage and mutations. UV-A (320–380 nm) is less energetic but can cause skin damage, while the shortest ultraviolet band UV-C is absorbed by the atmosphere and does not reach the Earth's surface.

8.1.4 Primary Production

Usually under ice phytoplankton community is sparse. Due to the poor light conditions, heterotrophic and mixotrophic species dominate over autotrophic ones. In spring, the growth of autotrophs starts as soon as the light intensity reaches the level, which is needed for photosynthesis. Sometimes there are dense algal populations just beneath the ice cover. All major taxonomical groups of algae can be represented under ice in winter.

Low light availability and low temperatures are the most obvious physical factors affecting primary productivity in ice-covered lakes. The biological response to these effects is discussed in detail by Sutter et al. (2012). The physical factors, whose effect on plankton is undoubtful, are the formation of liquid layers and pockets within the ice sheet as potential plankton habitats and convective mixing in the upper water column under ice. Both processes take place in the upper euphotic zone, which is especially thin in ice-covered lakes and are thereby highly relevant to the primary productivity.

Lake ice sheet may contain liquid water pockets, where primary production is possible provided that nutrients and light are available. The origin of the liquid water is lake water, snow and ice meltwater, or liquid precipitation. A common mechanism of formation of a liquid layer within the ice sheet is locking of the slush layer on ice surface by the snow-ice on top of it (see Chap. 4). The slush layer in lake ice sheet is a documented plankton habitat, though only few publications are available so far on slush layer algae (e.g., Felip et al. 1995; Leppäranta 2009a). Two other potential algae habitats are the freshwater pockets forming in the otherwise solid congelation ice during the melting season and the brine pockets in the ice cover of saline lakes. The latter are analogous to brine pockets in the sea ice and usually form when the lake water salinity exceeds 1–2 ‰ (e.g., Weeks 1998). Both environments can play an important role in the primary production as providing optimal light availability for the algae communities of ice-covered lakes. Information about the production in brine pockets is available mostly from the marine ecology (see Thomas and Dieckmann 2010). Also humus pockets in the lake ice sheet have been found in highly humic lakes (Salonen et al. 2009).

In addition to light conditions and temperature, convective mixing strongly affects the plankton growth under ice. Mixing conditions determine, to a large extent, supply of nutrients from the deeper lake layers as well as light availability for the plankton, especially for the non-motile diatom species (Matthews and Heaney 1987). There are also some reports on the direct effect of mixing on the diatom growth rates, though its mechanism is still less clear (Marra 1978). Several studies suggest strong correlation between radiatively-driven convection under ice and growth rate of diatoms (Matthews and Heaney 1987; Wilson and Wellman 1962; Kelley 1997). According to the reported observations, existence of convective layer under ice is the only mechanism supporting non-motile diatom species in the upper euphotic zone provided that vertical mixing velocities are larger than sinking velocities of the diatoms. However, the role of this early stage of plankton growth for subsequent diatom bloom after ice breakup is not yet clear.

8.2 Frozen Lakes at Settlements

8.2.1 Monitoring and Remote Sensing

Monitoring of ice conditions in freezing lakes has been an important issue for a long time. The principal questions have been the lake ice phenology and the thickness of ice, being related to safety, fishery, shipping and traffic on ice. Systematic monitoring of lake ice started in the 1800s, first by people interested in nature and then by environmental authorities. Example in Finland, competitions to predict the break-up date have been arranged in many lake site communities. Since lakes have limited size, phenology observations have been easy to perform in inhabited areas. These data are today extremely valuable for the research of lake ice climatology.

For the society the main question of lake ice is the safety issue, in particular for traffic, skiing and fishing. Travelling methods on lake ice have ranged from people walking on ice to trains, where the required ice thickness ranges from 5–125 cm. The additional questions are storage of material on ice, take lake ice for its latent heat as a cooler, and use lake ice as a source of fresh water. Lake ice can even be utilized for ice sculpture, especially when the ice is clear from gas bubbles and looks like glass.

Operational monitoring of ice conditions in lakes is ongoing in several countries based on ground observations. This is especially required for safety purposes. Ice thickness determines the bearing capacity in winter, but in spring deterioration of ice changes the quality and lowers the strength of the ice. A ground data based monitoring system is in use in the Finnish Environment Institute, which publishes a lake ice thickness map across the country based on about 30 ice thickness sites (Fig. 8.4). Also instructions and warnings are given for on-ice travelling and activities. Snow and ice thickness are monitored, for some lakes also the snow-ice and congelation ice fractions (Table 8.1).

Satellite remote sensing is based on emission and scattering of electromagnetic radiation from the Earth's surface. For ice mapping, the main channels are shown in Table 8.1.

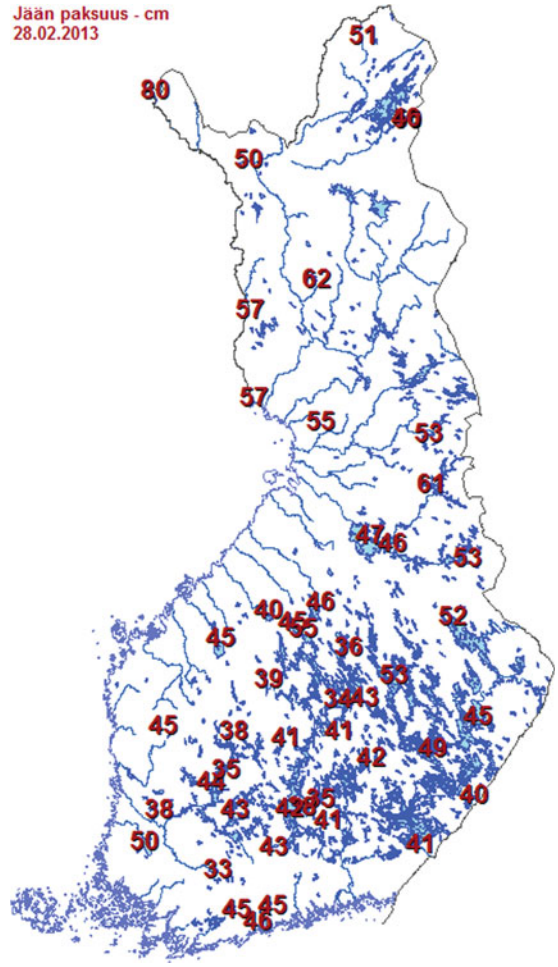

Fig. 8.4 Ice thickness (cm) in Finnish lakes on February 29, 2014. This information is available free to public in real time. Ms. Johanna Korhonen, Finnish Environment Institute. Printed by permission

Table 8.1 Windows of electromagnetic radiation used in satellite remote sensing of lake ice

Window	Observed	Information
Optical—near-IR	Reflectance	Quality of surface (ice/snow/water)
Thermal IR	Surface temperature	Ice and snow thickness
Microwave radiation	Brightness temperature	Quality of surface (frozen/liquid)
Radar	Backscatter	Surface roughness, kinematics

The great advantage in ice mapping is the strong contrasts between frozen and liquid surfaces across the electromagnetic spectrum from the visible light to microwaves. Therefore the horizontal properties of an ice cover are well revealed but information in the vertical direction is very small. The main limitation for remote sensing of lakes has been

the horizontal resolution of operational satellite systems. Therefore utilization of satellite remote sensing for lake ice monitoring was for long performed for large lakes only. In the last 10–20 years the situation has improved, in particular with Synthetic Aperture Radar (SAR). This method has problems with wet-surface ice and with thin, clear ice, which the radar signal penetrates through the ice leaving a weak backscatter. The strength of radar backscatter in general is related to the surface roughness and gas bubbles.

Physically the best channel for ice thickness is the thermal infrared, since the surface temperature does feel the thickness of ice (e.g., Leppäranta and Lewis 2007, 2015) but for the other windows the connections between surface layer and ice thickness are weak. SAR images have shown promises in distinguishing different lake ice types (Nghiem and Leshkevich 2007; Sobiech and Dierking 2013) but their connection to ice thickness is not very good. In the melting period, the contrasts weaken due to natural reasons. This is most unfortunate, since then the ice cover deteriorates fast and ice conditions change significantly on a daily basis.

In large freezing lakes, satellite remote sensing is a feasible method for ice monitoring (Nghiem and Leshkevich 2007; Filatov and Kondratyev 1999; Semovski et al. 2000). Then, in practice, ground-based mapping does not provide a full view of the ice cover. The Canadian Ice Service reports regularly of the ice conditions in the Great Lakes of North America, based on satellite data (Fig. 8.5).

8.2.2 Use of Lake Ice

Ice-covered lakes have been a part of the environment in northern settlements. Life has adjusted to the presence of the ice, and the ice itself has been utilized for its cold content. For long in the history, in Finland until the 1960s, ice blocks were taken in winter (Fig. 8.6) and stored under sawdust to survive through summer. It was especially the custom in dairy farms and food stores. In fact, machine-based cooling techniques have been introduced only at the end of 1800s.

Example 8.2. There are tales and stories about lake ice cover but one specific applied science story from northern Finland is claimed to be true. Children knew about a treasure at the bottom of a shallow lake. They could not get it up in summer but found a winter solution. As the ice grew, top layer was cut away and the growth rate became faster at the bottom. This way ice finally reached the bottom, and the treasure could be digged out.

Holes have been cut into the ice cover to maintain a free surface water spot. This acted as a source of liquid water for the household and farm production, and to wash clothes and linen (see Fig. 1.1). A particular activity has been bathing in an ice hole (Fig. 8.7), believed by many to be healthy, a way of strengthening oneself against cold. Fishing techniques were developed for ice conditions with nets and drags.

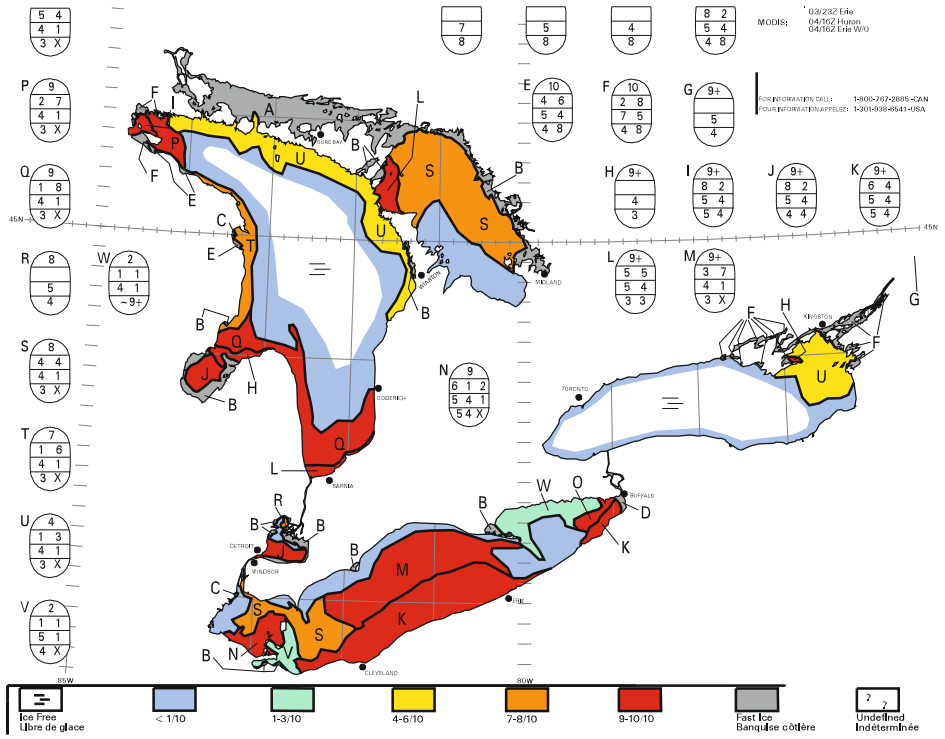

Fig. 8.5 Ice chart conditions in the Great Lakes on March 4, 2013 (Canadian Ice Service, Environment Canada). The "WMO egg code" symbols show total ice concentration on the first row and partition into subclasses with own concentration, stage of development and ice floe size in the next three *lines*. See http://ec.gc.ca/glaces-ice/

Fig. 8.6 Ice blocks are taken from the small lake, Kupparlampi in Hausjärvi commun, southern Finland, in the 1930s. This ice was used in summer to keep milk products cold in Jaakkola farm. *Photograph* by Kalle Kalervo. © Sarka, The Finnish Museum of Agriculture, Loimaa

Fig. 8.7 Ice-water bathing is a popular winter activity in northeast Europe. Here winter limnology students enjoy the bath at a sauna site in Lake Pääjärvi, Finland

8.2.3 Shoreline Erosion and Deformation

Lake ice influence on the shoreline geology has been widely examined by geographers since the 1800s. This shows up in erosion and specific coastal forms of freezing lakes. All lake ice covers produce shore ride-up due to thermal expansion. Since the linear thermal expansion coefficient of ice is $\sim 0.05 \times 10^{-3}$ °C^{-1}, the length scale of thermal expansion can be ~ 5 m in medium-size lakes. Thermal expansion deforms the soil and pushes stones ahead. In lakes, where the water level has been dropped, by nature or man, past shores can be identified from the ice-induced forms.

Thermal cracks are formed close to the shore and in medium-size or larger lakes also far offshore (von Cholnoky 1909; Helaakoski 1912). Their formation is influenced by the shoreline geometry so that many fractures are recurrent. Ice push on the shore creates a fringe, with structure depending on the bottom material and shore topography (Fig. 8.8). When such curved fringes collapse, they form tussocks in the shoreline zone. Helaakoski (1912) reported that ice pushes boulders up to ~ 1 m^3 volume, and the large boulders have left scouring lines to the shore area. In places boulder shore fields result from the transport.

In larger lakes mechanical events are also important. The ice cover may be broken by strong winds and pushed onshore, either piling up into ridges or riding up longer distances over land. Limitations to the shore processes come from the forcing. On the windward side of lakes, the wind force is $F = \tau_a L$, where τ_a is the wind stress and L is the fetch. For the wind speed of 10 m s^{-1}, in large lakes (100 km) $F \sim 30$ kN m^{-1}, which is able to break the ice of about ½ m thick at most and push onshore (see Sect. 5.4).

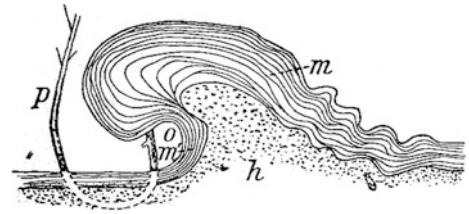

Fig. 8.8 A hollow (*o*) fringe form created by ice pushing a sand layer (*h*) beneath a surface peat layer (*m*) onshore. A young (10 years) birch trunk (*p*) is first upside down and curves up via the bottom mud layer. Lake Pyykösjärvi, Finland (Helaakoski 1912)

Ice driven mechanical shoreline erosion and deformation has been often observed in the Great Lakes of North America (Bolsenga 1988). The ice affects such constructions as shoreline houses, boathouses and docks. Normally a stable ice cover protects the shore, but when the shoreline ice is sufficiently thick, bottom scouring may take place and moving ice may encroach the shore zone. Ice features forming in the nearshore areas include the ice foot, a long continuous ridge of grounded ice, and ice ridges.

In very shallow zones, freezing may reach the bottom. In spring the buoyancy of ice may raise the bottom material with ice to surface and the mass appears as drifting 'mud floats' (Helaakoski 1912). This mechanism is also able to spread vegetation in the lake basin. Melting of permafrost results in subsurface shore erosion and cutting vegetation floats from the shore zone (Parsekian et al. 2011).

8.2.4 Sports on Lake Ice

Lake ice with the necessary bearing capacity has provided an excellent platform for winter sports. Skiing on lake has its roots in pre-historical times in northern Europe, and it developed sport as the side product during the 1800s. Although serious sports has moved to forests and mountains, snow-covered lake ice widely attracts recreational skiing community.

Skating has also long history, at least from the Medieval Times. In Central Europe it has been very popular in cold winters when the ice has the necessary bearing capacity. Further north, where winters are colder and longer snow accumulation brings often problems, but many communities keep a skating route open on the natural lake ice. In good skating winters, large areas of lakes are covered by bare ice and long distance free skating is possible (Fig. 8.9).

Fig. 8.9 Skating on Lake Vesijärvi ice, southern Finland. *Photograph* by Mr. Seppo Leinonen, printed with permission

In the modern times skiing and skating are still the most popular but other types of sports have also stepped into the picture. Ice sailing has become a wide activity, where due to the low friction considerable speeds can be achieved, and also ice is a very good platform for hang-gliding, towed by snow mobile to get the glider up. A few decades ago car and motorbike races were arranged on lake ice but due to environmental problems this has nearly stopped by now.

Ice fishing, i.e. fishing through a hole in the ice cover, is something between serious hobby and sport. Spring is a good ice fishing period but then the ice strength can be a major issue. Ice strength has a decreasing trend, and the daily cycle is remarkable as long as the night-time temperatures go below the freezing point. In large lakes, the ice may break and drift causing expensive rescue operations.

8.3 Lake Ice Engineering

8.3.1 Background

The presence of ice cover in a lake has positive and negative consequences to the living conditions in local settlements. First, the ice cover has been utilized for on-ice traffic as long as the region has been inhabited, but on the other hand the use of boats and ships has been prevented by the ice (Fig. 8.10). The feasibility of both these traffic methods are connected to the thickness of ice. Ice must be thinner than, say, h_1, for boats but thicker than, say, h_2, for on-ice traffic by cars or snow mobiles. In small and medium-size lakes the boats are small and usually $h_1 < h_2$ but in large lakes with major cargo vessels $h_1 > h_2$. In the former case, the time of ice growing from h_1 to h_2 is a difficult period especially for people living in islands, since all traffic is paused. Secondly, ice forces are of concern for offshore and onshore structures and ships. There is an extensive literature on the ice force problems (e.g., Ashton 1986; Sanderson 1988; Palmer and Croasdale 2012). Most work concerns marine ice but the knowledge and results can be applied for freshwater ice.

Fig. 8.10 Most lakes in Finland are closed from boat traffic in winter

8.3.2 Ice Loads

The magnitude of ice forcing on structures can be evaluated by simplified analyses. The force on a pier-type structure can be estimated by a Korzhavin (1962) type formula

$$F = K\sigma_0 bh \tag{8.9}$$

where K is a scaling coefficient, σ_0 is the compressive strength, b is the width of the pillar, and h is ice thickness. The coefficient K depends on the mechanical properties of ice and the geometry of the pier structure (Ashton 1986). For a narrow structure the ratio $\delta = b/h$ is an important parameter, $K = 2.5$ for $\delta = 1$ and $K \to 1$ for $\delta \gg 1$. For wide structures and wedge-shaped piers, $K = 1$ can be taken. For inclined structures $K < 1$ depending on the slope angle of the structure and ice-structure friction.

Fixed structures are designed to stand for the maximum forcing, and they range from simple docks to lighthouses. Ice load on ships provides resistance to ship's motion and at extreme may cause damage to ships. The resistance depends on the thickness, strength and density of the ice, and on the size and shape and the velocity of the ship.

8.3.3 On-Ice Traffic

A stable lake ice cover has served for traffic and transportation. A 5-cm thick ice sheet is capable to carry one person, a small car (1 ton) at 20-cm ice thickness, and a truck (10 tons) at 50-cm thickness. The bearing capacity increases proportional to the square of the ice thickness (see Sect. 5.3). When the ice thickness has reached 40 cm or more, car traffic is allowed on official ice roads. In Siberia, shortcut tracks for the railroad have been constructed across rivers. For heavy steam engine locomotives (100 tons), the thickness of ice would need to be at least 150 cm for safe crossing using the point load estimator, but the requirement can be lowered to with wooden supports beneath the track. Also lake ice cover has served as a runway for airplanes.

The fundamentals and the technology of ice roads and crossings under moving loads (road, railroad, and horse-drawn transportation) were developed during the World War II, as well as the creation of on-ice airfields. In the history a special place is occupied by the "Road of Life", laid on the ice cover of Ladoga Lake, that played a key role in the defence of Leningrad during the siege supplying the population with food and other essential goods (Fig. 8.11) (Bregman 1943; Ivanov 1949). After the war, there were growing needs for research of ice cover for the economic development of the northern territories, as well as for opportunities of storage and transport of military equipment.

Ice roads are kept by the local authorities wherever the ice grows thick enough. The traffic regulations in ice roads reflect the basic physics: for a given ice thickness, there is a maximum weight allowed proportional to the thickness of ice. There are two basic traffic rules for ice roads: First, a minimum distance is specified between cars, in order to avoid

Fig. 8.11 The road of life was the transport route across the frozen Lake Ladoga, which provided the only access to the besieged city of Leningrad in the winter months during the World War II. The road forms part of the World Heritage Site Saint Petersburg and Related Groups of Monuments. *Source* Wikimapia

more than one car loading the same site; second, the speed must be below the shallow water wave speed in the basin to avoid resonance between bending wave in the ice sheet and shallow water wave. In the official lake ice roads in Finland, ice roads are opened after the congelation ice thickness has exceeded 20 cm.

In more details, it has also been recommended to stick to the accepted speed, trying not to change it. If the ice strength is not high, then movement of caravans is unacceptable, and the speed of an individual car must be greater than the speed of the wave propagation. Also when the ice strength is not high, then the next car can start its movement only after a certain time necessary to provide a decay of ice cover vibrations. Near the coast, counter movements or cars are unacceptable, since due to reflection of waves superposition of amplitudes may follow.

There are techniques to strengthen or weaken the ice. Strengthening can be done by pumping water on ice or into snow on ice, and let the ice form naturally (Palosuo 1982). Weakening of ice by forced vertical convection by pumping air to lake bottom was made to small degree in the Second World War in Finland, and thereafter the method was utilized to keep ferry routes and log pools of sawmills ice-free (Vakkilainen 2001).

People in islands in cold regions had severe problems in the past when lake ice prevented both boat traffic and on-ice traffic. These periods are called *kelirikko* in Finnish language. Literally ‘kelirikko’ means ‘traffic conditions broken down’. The length of this period depends on the autumn or spring weather conditions and is therefore difficult to predict both for its timing and its length. Typically the length is about 1 month each year. Hovercrafts have been constructed for traffic on lake ice almost 100 years ago but they have not grown into any major industry for help in kelirikko period (Fig. 8.12). They are used by pilots in winter shipping in the Baltic Sea and in rescue operations.

8.3.4 Navigation

The main negative impact of a lake ice cover is to prevent boat traffic (Fig. 8.13). Only in large lakes, such as in the Great Lakes of North America, Lake Saimaa in Finland and Lake Vänern in Sweden, shipping can be continued in ice conditions. The advantage of

Fig. 8.12 Hovercraft used by the Finnish soldiers in World War II, Lake Ladoga in April 1942. SA-kuva (The Finnish Wartime Photograph Archive). *Photograph* by lieutenant T. Räisänen

Fig. 8.13 Winter shipping in Lake Saimaa, Finland. The main route goes from the Eastern Lake District of Finland to the Baltic Sea via Saimaa canal. Due to ice problems in the canal, the winter shipping is stopped in normal years for the mid-winter. *Photograph* by Mr. Seppo Piironen, printed by permission

winter shipping is to keep the same all-year transportation system for the industry, even though expenses can become high in the ice season.

Winter navigation in lakes has difficulties not present in marine conditions. When a ship channel is opened, local heat loss becomes large, and more ice is generated. Channels grow thicker and more difficult to get through. In shallow lakes, ship routes are in places narrow and it is not possible to start a new channel near the old one. Especially this is a problem in canals between lakes and between lakes and the sea. The more there is ice breaking the more ice is generated, and in canals it is not possible to push ice away. Example, Saimaa Canal from the Eastern Lake District of Finland to the Baltic Sea needs to be closed down for 2–3 months every winter. On the other hand, ice pressure, which is a major problem in sea ice fields, does not become a major issue in lakes where fetches are limited.

8.4 Climate Change Impact on Lake Ice Season

8.4.1 Background Physics

The principal seasonal ice characteristics are ice phenology, ice coverage, and ice thickness. Figure 8.14 shows a schematic picture of the evolution of an ice season. Ice grows slowly until mid-winter, and the melting in spring is fast. In the early and late winters there are periods when the ice is still weak and maybe broken by winds, shown as the unstable periods. In the stable phase, the ice cover is safe to walk and drive on, and its presence is useful to the community. If climate warms, the stable period becomes shorter, and the whole ice season may finally become unstable.

Ice phenology includes the dates of freezing and ice breakup; also in large lakes the period of full ice coverage and in very shallow lakes also the period of total freezing of the water body are accounted for. Ice time series analyses and mathematical models have been utilized to examine the sensitivity of ice season to climate and the expected changes in ice seasons for various climate scenarios. Simple analytical models (e.g., Leppäranta 1993, 2009a) can be used to provide the first-order predictions, and numerical models provide a better accuracy and more details about the ice cover structure.

Ice formation is generally governed by the intense radiative and convective heat loss from the warmer lake surface to the colder atmosphere. Convection and wind-driven mixing cool the water body to temperature below the temperature of maximum density, and then (in freshwater and brackish lakes) the lake surface layer becomes stable and the inverse thermocline develops. Surface cooling rate increases, especially at low winds, and the surface temperature quickly achieves the freezing point, followed by ice formation. Hence, the timing of freeze-up is strongly dependent on synoptic conditions—passages of cold air masses and strong winds—over the lake. Ice formation is generally correlated with synoptic variables, such as the local air temperature and wind, and is strongly dependent on the depth of the lake. The relation between freeze-up and air temperature is complicated since surface water temperature comes out from past air temperatures filtered with decreasing weights toward past and with memory time scale proportional to the depth of the lake or the depth of the mixed layer (see Sect. 7.1.3).

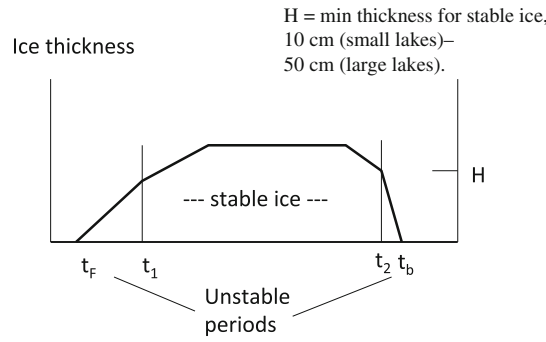

Fig. 8.14 A schematic picture of the course of a lake ice season

After ice cover formation, the main factors controlling the ice growth rate are the snow cover, heat fluxes at the upper and lower boundaries, and the thickness and structure of the accumulated ice. With this regard, an early appearance of snow cover can play a crucial role in decelerating the ice growth due to the low heat conductivity of snow. But high snow accumulation may lead to formation of superimposed ice that in turn tends to increase the resulting total ice thickness. Thermal stratification under lake ice is stable and water velocities are weak, so that heat transfer at the ice lower boundary is normally weak. As was shown in Sect. 4.3, a simple formula for the ice growth is provided by a semi-empirical law $h = F(S; a^*, b^*)$, where the freezing-degree-days S is the driving force and a^* and b^* are the tuning parameters. In Eq. (4.44) the theoretical values (a, b) are shown, and in semi-empirical modifications, to fit with observations of ice thickness, usually ½ $a < a^* < a$ and $b^* \sim b$. A climatic change would change the freezing-degree-days that is easy to evaluate, but first of all the coefficient a^* is the critical parameter and sensitive to snow accumulation.

The heat balance is fundamentally different during ice melting from that during lake cooling and ice growth (Jakkila et al. 2009). The stable stratification of atmospheric surface layer strongly reduces the sensible and latent heat exchange at the ice-air interface, and heat for melting is provided mostly by solar radiation. This fact implies also a strong influence of the surface albedo and, consequently, of snow layer in ice melting. Liquid precipitation is another major factor to deteriorate and melt the ice sheet. Solar radiation and rain also explain the fact that the timing of ice breakup is coherent at spatial scales of hundreds of kilometres (Magnuson et al. 2000). There is a degree of lake dependence via ice thickness, since the timing of breakup depends on how much there is ice to melt. The strong role of solar radiation also implies that the timing of ice breakup has much less variability between different years than in the case of freeze-up. Melting of ice follows spring warming and breakup date is reproducible by simple correlation models.

The sequence of an ice season, from first freezing to final break-up is not a simple cycle but there may be melt–refreeze events in between. In general, in milder climate the probability of melt−freeze events during ice season is larger, but this question has not been examined in detail. Ice formation and melting are not symmetric processes but ice is self-protecting. Once an ice cap has formed, it is difficult to melt it since solar radiation level is low, and lake heat storage is largely insulated by weak mixing conditions in lake water. Also albedo feedback from ice formation keeps the absorption of solar radiation low by ice cover.

The results from Chap. 4 and Sect. 7.1 can be examined for the impact of climate change on the ice season. The expected climate change at year 2100, as we understand it now from the IPCC (Intergovernmental Panel for Climate Change) scenario, is predicted to increase the air temperature by $\Delta T_a > 0$ and to change precipitation by ΔP (>0 or <0) in the lake ice zone.[3] The scenario varies from place to place and changes with time, along

[3] In Finland the predicted changes in the temperature and precipitation are 3–5 °C and 10–20 %, respectively (Finnish Meteorological Institute web site www.fmi.fi, August 2014).

with new model simulations. Therefore it is preferable to consider a general case: the sensitivity of lake ice seasons to climate change.

This sensitivity to air temperature is quite clear. Precipitation is a more difficult question, since the ice thickness cycle depends on the phase and timing of precipitation in addition to the total. Local snow accumulation and air temperature may have weak connections since in longer winters more precipitation comes down in the solid phase, but in general air temperature and snow accumulation can be considered independent predictors of ice thickness. However, indirect conditions exist in that air temperature must be low for solid precipitation to ground and the thicker the ice the more snow is needed for snow-ice growth. Thus, if the total ice thickness were to decrease under climate warming, the buoyancy of ice would be less and flooding events would become more common. In large lakes the mobility of ice is an additional question related to wind climate.

Figure 4.11 a gives insight into the influence of snowfall on the ice thickness. In the model a constant snowfall rate is assumed in a lake district where the ice thickness varies between 60 and 110 cm. If the rate of snowfall is less than 0.75 mm day^{-1}, increasing snowfall decreases the ice thickness due to insulation. At 0.25 mm day^{-1}, doubling the rate decreases the ice thickness by about 20 cm, and 20 % increase consequently would give 4 cm decrease. But if the rate of snowfall is more than 0.75 mm day^{-1}, increasing snowfall increases the ice thickness due to snow-ice formation. At 1.0 mm day^{-1}, doubling the rate increases the ice thickness by about 20 cm, and 20 % increase consequently would give 4 cm increase.

8.4.2 Analytic Modelling

Analytic models were derived for the relation between temperature and ice phenology, thickness and coverage (Sects. 4.3 and 7.1). In the first order modelling approach the surface heat balance is taken in the linear form (Sect. 4.1). Then a constant change ΔT_a can be employed for the air temperature level to examine the influence of an assumed climate change. This first-order approach is quite appropriate for examining the general variations in the ice season, since the simplifications in the surface heat budget are largely cancelled, i.e. the freezing date estimate is rather crude but we get better estimates for the change of the freezing date for a given climate change scenario. As a matter of fact, the parameters of the linearized heat balance depend on the wind speed, humidity and cloudiness, and therefore we can also examine the influence of systematic changes in these quantities on the ice season.

Whether a lake freezes or not, the condition for the length of the cold season ($T \leq 0$ °C) was given by Eq. (7.10) based on a parabolic curve for the winter air temperature. The climate change would shift the minimum temperature up by ΔT_a and then length of the cold season would be changed to

$$t_{c2} = t_c \sqrt{1 + \frac{\Delta T_a}{T_{a,\min}}} \tag{8.10}$$

where $T_{\mathrm{a,min}} < T_{\mathrm{f}} \leq 0$ °C is the winter minimum of air temperature. The change is not symmetric: warming reduces the length more than corresponding cooling increases. As shown in Sect. 7.1, the length of the cold season must be approximately more than twice the memory length, which is proportional to the depth of the mixed layer.

The case with the freezing date is straightforward. With linear atmospheric cooling, the temperature scenario is $T_a = \dot{T}_a t + \Delta T_a$, where $\dot{T}_a < 0$ is the rate of temperature decrease. It is directly seen that the freezing date would be shifted by

$$\Delta t_F = \frac{\Delta T_a}{|\dot{T}_a|} \tag{8.11}$$

Thus the freezing day shift not only depends on the air temperature change but also on the rate of atmospheric cooling. The predicted change is symmetric to the air temperature scenario. In continental tundra the cooling is faster than in maritime climate, and the climate change impact on the freezing date is consequently weaker. Example, in Finland the fall cooling rate is ~ 5 °C month^{-1}, and consequently the freezing day would shift by 6 days × (ΔT_{a} °C^{-1}).

For a change in the air temperature, the freezing-degree-days and consequently the maximum annual ice thickness would change. Using again the parabolic approximation for winter air temperature, the reduced ice thickness is

$$\frac{h_2}{h_1} = \frac{a_2^*}{a_1^*} \left(1 + \frac{\Delta T_a}{T_{a,\min}}\right)^{\frac{3}{4}} \tag{8.12}$$

where the lower indexes 1 and 2 refer to the present and future climate, respectively. If the parameter a^* is constant, typically in the range of 2–3 cm (°C·day)$^{-½}$, Eq. (8.12) gives about 10 cm for a change of 1 °C in air temperature. But since a^* may change due to changing snow conditions, snow may strengthen or even compensate for the change due to the air temperature. Evolution of ice coverage is obtained from the analytic models in Sect. 4.3, with the difference that the initial time has shifted as given by Eq. (8.11).

Melting of ice is tied to the radiation balance, and therefore the climate change impact is not directly clear. In fact three factors need to be considered. Firstly, as many statistical models assume, the length of the melting season is proportional to the positive degree-days. Secondly, the start of the melting depends on the atmospheric conditions and state of the surface, and therefore the start may become earlier if air temperature increases. So the shift in the breakup date must contain the shift in the zero upcrossing time of the radiation balance. Thirdly, if the ice thickness has decreased there is less ice to melt.

For the first factor, a linear model $T_a = \kappa t + \Delta T_a$ can be taken resulting with $\Delta R = ½ \kappa^{-1}(\Delta T_a)^2 + \Delta T_a t$. It is plausible that the second factor is somewhere between zero and the shift in the zero upcrossing time of air temperature, $0 \le \Delta t_m \le \kappa^{-1} \Delta T_a$. Then we have

$$t - (t_m + \Delta t_m) = \sqrt[3]{\frac{3}{\mu c}[\rho L(h_0 + \Delta h) - k_1(R + \Delta R)]} \tag{8.13}$$

The role of Δt_m is the strongest, since ice thickness change and positive degree-days change appear under the cube root. The cube root was obtained from a simple model for the increase of solar radiation and decrease of albedo during the melting period, and it could be changed into a general power law ν, $0 < \nu < 1$.

8.4.3 Numerical Modelling

A numerical model can be used to produce projections for the future ice seasons. If air temperature change only is considered, the first order analytic model is usually quite good, but to examine the influence of snow accumulation and qualitative changes, numerical models provide a more firm basis (e.g., Leppäranta 2009a; Yang et al. 2012).

An example is shown in Fig. 8.15 for southern Finland, where model simulations for a 'normal' winter are compared with those for winters where the mean air temperatures are 1 and 5 °C higher or lower than the present (1980–2010) baseline. In the numerical model, the lake freezes during the first strong cold spell. The observed, present average maximum annual ice thickness of 45 cm decreases by 5 cm for the first 1 °C warming, 20 cm for the next 3 °C warming, and 10 cm for the final 2 °C increase. The ice break-up date also shifts

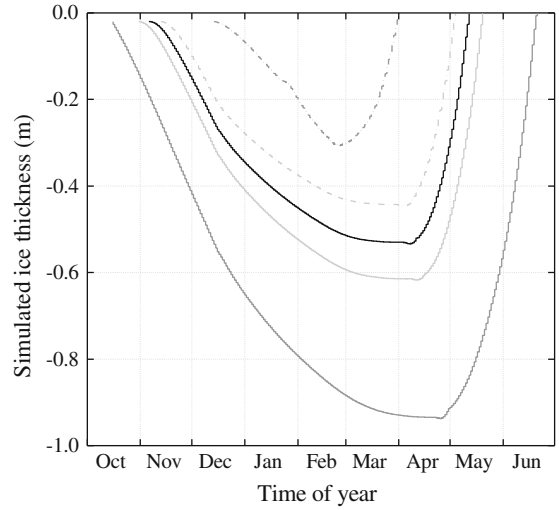

Fig. 8.15 Model sensitivity to the air temperature. The *black solid line* is the reference of present climate. The *grey solid lines* show the modelled ice thickness based on air temperature decrease by 5 and 1 °C, and the *grey dashed line* show modelled ice thickness based on air temperature increase by 5 and 1 °C (Yang et al. 2012)

to a much earlier date due to the earlier onset of melting, which reflects the change in the radiation balance and the fact that there is less ice to melt. The resulting ice break-up is 5 days earlier for the 1 °C warming, 25 days earlier for the 4 °C warming, and 75 days earlier for the 6 °C warming. This illustrates the high instability of the ice season to warming. In a warm climate, ice may form in mid-winter but since it is relatively thin it melts, if the weather becomes warmer, or breaks at significant wind load.

The results show that the 1 °C change brings the thickness curve down by 5–10 cm but has no effect on the form of the thickness cycle. With a 5 °C warming there are growth and decay periods through the winter and the maximum ice thickness is about 20 cm. In southern Finland the thickness of 20 cm is enough for a stable ice cover in small lakes, but in large or medium-size lakes stormy winds could break this cover and give rise to areas of open water at any time during the winter. This means a remarkable qualitative change in the lake ice seasons. The length of the ice season is only three months and the ice cover is also mechanically unstable throughout the winter.

8.4.4 Future Ice Seasons

Climate warming has taken place during the last 30 years as shown in the rise of Northern Hemispheric temperatures (IPCC 2001, 2007). Climate impact on lakes is thoroughly discussed in the book of George et al. (2009). The recent climate warming has affected the ice regime of lakes as shown by numerous publications. A review on the time series work was given by Adrian et al. (2009). Magnuson et al. (2000) reported trends of 5.8 days later freeze-up dates and 6.5 days earlier break-up dates per 100 years in lake and river ice in the northern hemisphere (1846–1995). Trends of the same order of magnitude were found in Berlin and Brandenburg lakes by Bernhardt et al. (2011). For the irregularly freezing Müggelsee, Berlin, trends were reported for later freezing (5.7 days) and earlier thawing (–6.8 days) for the period 1947–2007. Concurrently, the lake revealed increasing number of ice-free years, shortening in the total ice duration of –15.6 days (that is, longer duration of intermediate ice-free periods), and thinning of the ice cover. In Lake Kilpisjärvi, Arctic tundra in northern Finland, since 1964 the trend has been later freezing by 11.5 days and earlier ice breakup by 5.0 days per 50 years (Lei et al. 2012).

Notably, trends in the earlier breakup are sometimes reported to be stronger than those in the freezing date (Korhonen 2006; Jensen et al. 2007), despite ice melting in spring is driven, as we have shown above, by absorption of solar radiation, which is affected by the global warming only via the albedo. Prokacheva and Borodulin (1985) examined the variability of lake ice seasons in Northwest Russia, in particular Lake Ladoga. No clear connection was found with sunspots (Wolff index) in Lake Ladoga. Spatial coherence in was seen with large lakes in the region, with Lake Onega, Lake Il'men, Lake Peipsi and Rybinski Reservoir. Thus, climatic factors other than higher local air temperature in spring affect the ice-off. They may include decreased ice thickness due to milder autumn/winter conditions, trends in winter precipitation affecting the snow amount, or more cloudy

Fig. 8.16 In the past cold periods lakes in Central Europe were covered by ice with bearing capacity to travel and enjoy. *Painting* by Jakob Grimmer, from Wikimedia

spring conditions directly affecting the radiation input at the lake surface. Apparently, physical mechanisms of the global warming impact on the ice phenology include time-delayed effects and feedbacks not resolved to date.

The projected changes in the climate will have a significant effect on the qualitative characteristics of the ice as well as the quantitative changes described above (Fig. 8.16). In geographical terms, the ice season regimes can be grouped into three zones: ephemeral ice zone, unstable ice zone, and stable ice zone. In the first zone, ice comes and goes in one season, in the second the ice breaks at times and results in periods when the lake is partially open while in the third zone the whole lake has stable ice cover from the date of first freezing until the ice cover becomes rotten in spring. The boundaries of the zones will move north when the climate becomes warmer. The extent of the ephemeral zone is dictated by the mean and variance of air temperature whilst that of the unstable zone is dictated by the thickness of ice. With decreasing ice thickness, the period of the ice being breakable increases and finally the ice cover is breakable during the whole ice season. Today, only very large lakes at around 60ºN in European climate have unstable ice cover but if the ice thickness is reduced to 20–30 cm or less, medium size lakes will also be unstable.

Consequently the implications of a warming climate to the lake ice season are first shorter season and then thinner ice. However, depending on the snowfall conditions, snow-ice formation may increase to counter at least part of the effect of rising air temperatures. Thinner ice also means more breakable ice with more areas of open water, which changes fluxes of heat and moisture between the lake and the atmosphere and may generate frazil ice. Frazil ice formation may, in turn, lead to accumulation of sediments in the ice cover via frazil capturing of particles in the water body and via anchor ice formation. From the point of view of lake ecology, shorter ice season and presence of openings mean less oxygen deficit problems. But the openings will also create a new type of winter environment in lakes, which have hitherto been completely covered with ice.

Future of Frozen Lakes

9

Lake ice has changed from a key factor of living conditions in the cold regions to a site for winter activities, such as ice fishing, skiing and skating, and ice sailing.

M. Leppäranta, *Freezing of Lakes and the Evolution of their Ice Cover*,
DOI 10.1007/978-3-642-29081-7_9

9.1 Role of Ice Cover

Lake ice forms in cold regions, where the air temperature goes below the freezing point in winter. Ice is normally seasonal but in high latitudes and high altitudes permanently ice-covered lakes are found. The presence of seasonal lake ice may last more than half a year, and its thickness can reach up to 2 m. The snow and ice season modifies the hydrological year in cold regions by its influence on the annual distribution of runoff and by the problems caused by ice to the management of water resources. The research of freezing lakes has experienced a major rise after the year 2000, much due to environmental and climate problems in addition to basic science (Fig. 9.1).

Lake ice is a degree more simple as compared with sea ice and river ice (Fig. 9.2). Lake ice cover is mostly immobile and circulation in the water body beneath the ice cover is weak, and in particular, freshwater lake ice is poor in impurities. But lakes with strong through flow may have river ice type processes (Ferrick and Prowse 2002; Shen 2006), ice structure in brackish and saline lakes is similar to sea ice, and drift ice occurs in very large lakes. Our knowledge of ice in saline waters comes mainly from marine research (e.g., Wadhams 2000; Weeks 2010), and these results are to a large degree applicable for saline lakes. Hypersaline lakes would require specific lake water analyses for ice research rather than extrapolation of the sea ice knowledge.

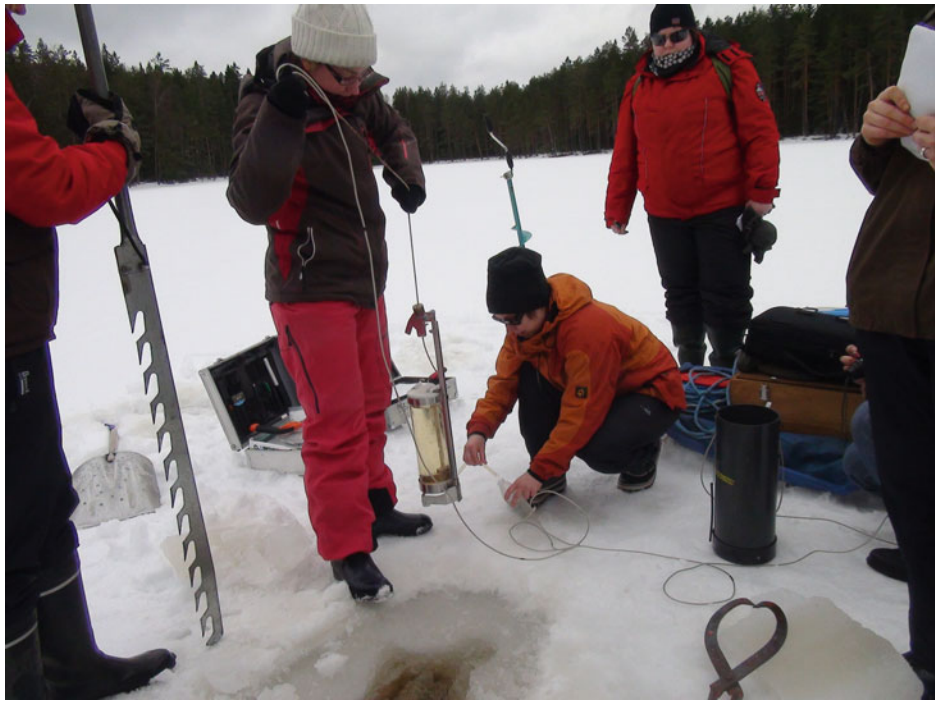

Fig. 9.1 Students taking water samples from beneath lake ice

Fig. 9.2 Lake Baikal ice season is quite complicated due to its great depth and horizontal scale. In large lakes in general the ice shows significant horizontal displacements due to forcing from winds or water currents. *Photograph* by Oleg Timoshkin, printed by permission

Frozen lakes have belonged to people's normal life in the cold regions. Solid ice cover has been an excellent base for traffic across lakes and to transport cargo, provided the ice has been thick enough. Indeed, ice cover has isolated island inhabitants from the mainland in periods, when the ice is too weak to walk but still limits boating. Until about mid-20th century, when refrigerators were not common, the cold content of lake ice was utilized by storing lake ice for summer. Openings were sawed into the lake ice cover for household water and for washing clothes at the site. For ice-covered lakes, special techniques were developed for domestic and commercial winter fishing.

This book, *Freezing of Lakes and the Evolution of Their Ice Cover*, presents an up-to-date (year 2014) status of knowledge of the physics of lake ice with applications. It is based on a review of the literature and the research of the author during the last 20 years. The focus is in fresh-water lakes, with river ice and sea ice results utilized where helpful. The role of dissolved substances of the parent water is explained here based on the results of sea-ice research.

A historical view is embedded with material from the more than 100 years long period in lake ice research. Earlier literature of the physics of ice-covered lakes is quite sparse. The important books include Barnes (1928), Shumskii (1956), Pivovarov (1973), Michel (1978), and Ashton (1986), and also the book of Pounder (1965) contains much general material on ice in natural waters. Pivovarov (1973) presented a scientific monograph on freezing lakes and rivers with weight on the liquid water body, while Ashton (1986) had a more engineering point of view on this topic [see also Ashton (1980) for an overview

paper on lake ice]. Ice engineering aspects are covered in Ashton (1986) and Palmer and Croasdale (2012). More recent material is given in the article collections of polar lakes (Vincent and Laybourn-Parry 2008), limnology by George (2009), and in the reviews of the physics (Kirillin et al. 2012) and fish (Shuter et al. 2012) of frozen lakes.

The Chap. 1 introduces the topic with a brief historical overview. Chapter 2 presents lakes, their classification, and the zones of ice-covered lakes. Ice formation and the structure and properties of lake ice are treated in Chap. 3, with ice impurities and ice mass balance. Chapter 4 contains lake ice thermodynamics from the freezing of lakes to ice melting, with thermodynamic models included. Lake ice mechanics is the topic of Chap. 5 including engineering questions such as ice forces and bearing capacity of ice. A section is included on drift ice in large lakes. Glaciers and pro-glacial lakes are treated in Chap. 6. Quite exotic lakes are introduced, in particular lakes at the top and bottom of glaciers and ice sheets. Chapter 7 focuses on the water body beneath lake ice cover with water balance, stratification, and circulation. Applications are treated in Chap. 8, considering the ecology of lake water bodies with limitations brought by the ice and life inside the ice cover also discussed. Environmental and practical questions are treated as well as the impact of climate change on lake ice seasons. Final closing words are written in Chap. 9, and the list of references follow in chapter backmatter. Study problems with solutions are given as examples in the text. Useful constants and formulae have been collected in an Annex.

9.2 Science and Technology Needs

Scientific research on lake ice was commenced in the 1800s, and at the same time lake ice monitoring was commenced in northern Europe. Ice engineering problems were included in research from the late 1800s, concerning shipping, ice forces on structures, and the bearing capacity of ice. Also from the early stage of limnology the ecology of frozen lakes has gained attention, especially in the Central Europe. In large lakes the ice may break and drift considerable distances which influences on the evolution of the winter conditions in lakes and utilization of the lakes (Fig. 9.2). In all, the research of ice-covered lakes turned out to be for long, until about 1970s, scattered and occasional. Thereafter, more effort was put on polar lakes when the access to reach them was better and measurement techniques were feasible.

The leading topics are now the impact of climate change on lakes and the ecology of freezing lakes. Also together with free access high or moderate resolution satellite imagery, such as Aqua/Terra and Envisat, monitoring of lake ice cover has expanded to medium-size lakes.

The annual ice cycle depends on the atmospheric mass and heat fluxes and is particularly sensitive to air temperature and snowfall. Furthermore, the sensitivity of modelled thickness increase is in general inversely proportional to the thickness. Therefore when the ice is thin we need a more sophisticated model to simulate the growth of ice. The connection between ice thickness and snow accumulation is quite complicated since the

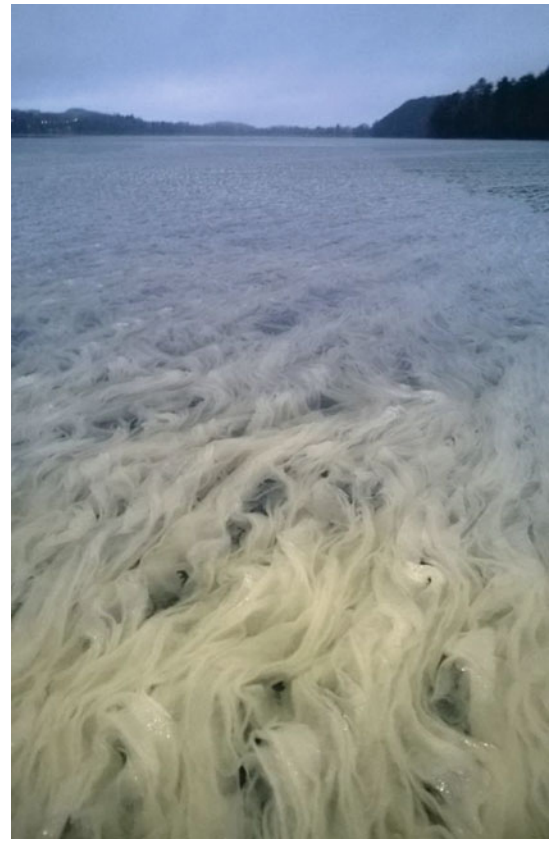

Fig. 9.3 Snow on lake ice is the main present problem in thermodynamic ice models. The *photograph* shows strange spaghetti-like surface structure formed during a snowstorm on an open lake, Lake Suolijärvi in Tuulos, Finland. *Photograph* by Mr. Vesa Kaloinen, Tuulos, printed with permission

timing of the snowfall is critical (Fig. 9.3). Also the ice break-up date depends on the structure and thickness of the ice and snow and needs a physically realistic model, with stratigraphy, to explore its variability. The main weakness in the present thermodynamic lake ice models is indeed in the accounting for snow properties and processes. Another question is the ice melting, which takes place at both boundaries and in the interior, the partitioning depending on the ice structure and solar radiation.

The modelling problem for lake ice thickness can be approached with semi-analytic or numerical methods. Semi-analytic methods are based on the degree-days and provide the first order approximation of the freezing—ice growth—melting cycle from which simple relations between winter climate and ice season characteristics can be derived. Numerical models are designed to include the full ice physics in the analysis. In these models the stratigraphy of ice, snow physics and atmospheric forcing can be treated in a realistic way,

and the evaluation of climate change consequences becomes more reliable than with semi-analytic models. Slush layers are well reproduced and the physical representation of melting ice is more realistic.

In addition, mechanical models are used to examine the breakage of ice, a factor, which is a critically important to the character of lake ice seasons. Mechanical models have not been much discussed in the lake ice literature over the last 25 years. Ice drift models have been constructed for marine basins, down to the size of 100 km, but in lakes this work has been quite limited. The main area of lake ice drift modelling has been the Great Lakes of North America, where shipping has needed more such information. A major characteristic of lake ice drift is that it consists of short-term displacements between immobile states that require a very close approximation to plastic behaviour in the modelling. The occurrence of ice displacements in a given basin depends on the ice thickness, and therefore climate warming may influence the quality of ice cover.

In the lake water body, physical phenomena and processes are very different under ice cover from the open water conditions. The ice cover cuts the transfer of momentum from the wind to the water body that damps turbulence and mixing. The surface water temperature is at the freezing point, and there is very little vertical transfer of heat, apart from geothermal lakes. In all, the temperature structure and circulation are quite stable.

In fully ice-covered lakes the water flow under ice can be in laminar or laminar-turbulent transition state that makes the ice–water body interaction a difficult problem for observation techniques and modelling. Even though the water velocities are small, they are stable and result in significant long-term transport of water with its impurities. However, in very large lakes, the ice sheet may experience episodic movements and disturb the water body. In spring, solar radiation provides a strong downward flux of heat, which constitutes the strongest heat flux into fully ice-covered lakes, and the ice melt water with its impurities is released into the water column.

Research on winter biology of lakes has largely increased (Salonen et al. 2009; Shuter et al. 2012). Questions of life in extreme conditions have brought in more research of lakes with perennial ice and pro-glacial lakes (Vincent and Laybourn-Parry 2008; Keskitalo et al. 2013), especially in the Antarctic continent (Fig. 1.3). The ecosystem of subglacial lakes has been largely unknown (Christner et al. 2006), but in austral summer 2012–2013 the first water samples ever were taken from these lakes showing signs of bacterial life beneath the ice sheet (Shtarkman et al. 2013).

Lake ice belongs to the part of cryosphere, which closely interacts with human living conditions. The ice cover has caused problems but people have learnt to live with them and also to utilize the ice. Especially, in the present time this is true for on-ice traffic and recreation activities. Ice fishing has become a widely enjoyed winter hobby. Apart from fishing, winter sports such as skiing, skating and ice sailing are now popular winter activities on frozen lakes. In the past, lake ice was used to store perishable products, when it was removed during the winter and stored for the summer. On the negative side, the freezing of lakes makes boating impossible and limits their use for commercial and recreational transport. The bearing capacity of ice is a major safety question. It increases

Fig. 9.4 Travelling on ice is always risky. To prepare for crossing by foot, skiing or skating, it is good to take a sharp stick to test ice and ice picks to get up after ice breakage, also rope to help others. *Photograph* by Finnish Swimming and Lifesaving Federation, printed with permission

with ice thickness squared so that for a skier or skater 5 cm is enough. When the thickness of the ice is very close to the limiting minimum, special care must be taken because of the natural variability of ice thickness and the resonance effects with shallow water waves for moving loads (Fig. 9.4).

9.3 What Will Be?

Lakes are normally frozen at latitudes higher than 40–50° and at high altitudes in winter. In these northern and southern caps there are open water lakes due to geothermal heat, great depth or high salinity. Perennial lake ice is rare and found only in specific high polar and high altitude environments. The annual course of the thermal structure of lakes is forced by local climatology, and the boundaries of lake ice zones consequently vary along the climate variations. The low latitude limit is the 0 °C isothermal where very shallow lakes still may freeze over.

The physics of ice-covered lakes is presently rather well understood (Kirillin et al. 2012). The main questions are connected to the melting of ice and to the mechanical displacements and drift of the ice cover. New-level, coupled ice–liquid water body models are needed to improve our understanding of ice season processes and phenomena. The coupling takes place via the solar radiation and heat loss from the lake to the atmosphere, which both depend on the thickness of the ice. Two- and three-dimensional modelling of ice-covered lakes is required more with appropriate process-based links to the seasonal dynamics of the lakes.

The climate change question focuses for the physics on the ice phenology and maximum annual ice thickness. In large lakes, ice concentration is as well examined. The expected changes can be qualitative as seasonally freezing lakes may change into occasionally freezing lakes, and ice may disappear from sites at the climatological ice margin.

Lake ecosystems need to adapt to changes in lake ice climatology. The connection between lake ecology and physics is strong in that the ice cover structure and properties provide information about light level in the water, presence of open water spots, and liquid water within the ice sheet. Rapid changes bring stresses through light and temperature conditions as well as through budgets of oxygen and nutrients. Climate change issues also necessitate a better understanding of the role played by a lake ice cover in the emission of greenhouse gases, especially methane, into the atmosphere, and in the global carbon budget.

The impact of these changes on the ecological status of lakes is less clear and is the topic of future investigations. The key questions are the physical implications of lake ice fracturing and the influence of the projected changes in the ice structure on the transfer of light. When a lake is frozen, the circulation in the water column is weak and driven by solar radiation and heat flux from the lake bottom. These weak circulations are, however, known to be ecologically important since they influence the oxygen budget, regulate the growth of phytoplankton and have a major effect on the winter survival of lake fish.

For human living conditions, shorter ice seasons, while extending the open water season, would severely or even drastically limit the traditional on-ice activities. A key point is the stable ice period when the thickness of the ice is above the critical level of about 30 cm. Then the ice is a stable platform for on-ice traffic, fishing, and recreation. Even a modest warming will have a major impact on the ice season viewed from this practical viewpoint. On the other hand, the lakes would be open for a much longer period and allow the extension of many water-based activities. For the ice cover to be "useful", it has to be thick enough to serve as a solid platform. Lakes in the ephemeral zone, and to a lesser extent those in the unstable zone, are not useful in that sense. A warming by 2–3 °C may reduce the ice thickness about 20 cm that would mean below the critical level throughout southern Finland and corresponding climatic zones. Even then, the length of the ice season could still be 3 months (see Yang et al. 2012). If there were a continuous warming climatic trend, these qualitative changes would become obvious toward the end of the 21st century.

To understand more about the winter conditions in freezing lakes, further research is ongoing on lake ice physics, ecology and engineering. It is expected that this research will continue growing in the near future. The main motivation is the impact of environmental loads and climate changes on the ice conditions. Lake ice seasons are of concern in The Global Lake Ecological Observatory Network (GLEON), Society of Limnology has established a Working Group on Winter Limnology, and lake ice sessions are run in the Ice Symposium series of the Ice Committee of the International Association of Hydro-Environment Research (IAHR).

Annex: Physics Data

A.1 Properties of Ice Ih and Liquid Water

1. Basic properties of freshwater ice as a function of temperature (see Table A.1).

Table A.1

	0 °C	–10 °C	–20 °C	–30 °C
Density (kg m^{-3})	916.7	918.7	920.3	921.6
Thermal expansion coefficient, volume (10^{-6} $°C^{-1}$)	159	155	149	143
Adiabatic compressibility (10^{-5} MPa^{-1})	13.0	12.8	12.7	12.5
Specific heat (kJ kg^{-1} $°C^{-1}$)	2.11	2.03	1.96	1.88
Thermal conductivity (W m^{-1} $°C^{-1}$)	2.14	2.3	2.4	2.5
Dielectric constant	91.6	94.4	97.5	99.7
Latent heat of melting (kJ kg^{-1})	333.5			
Thermal emissivity	0.97			

2. Dependence of melting point on pressure (see Table A.2).

Table A.2

Pressure (bar)	1	10	100	1,000
Melting point (°C)	0.00	–0.06	–0.74	–8.80

M. Leppäranta, *Freezing of Lakes and the Evolution of their Ice Cover*,
DOI 10.1007/978-3-642-29081-7

3. Properties of liquid freshwater references (at pressure 1 bar) (see Table A.3).

Table A.3.

Molecular weight (g mol^{-1})	18.016	
Gas constant for vapour (J °C $^{-1}$ kg^{-1})	461	
Temperature of maximum density (°C)	3.98	
Boiling point (°C)	100	
Triple point	0.1 °C, 611.73 Pa	
Thermal emissivity	0.97	
	0 °C	10 °C
Density of water (kg m^{-3})	999.84	999.70
Viscosity (N s m^{-1})	1.793×10^{-3}	1.307×10^{-3}
Surface tension (N m^{-1})	75.64	74.23
Specific heat of water (kJ kg^{-1} °C^{-1})	4.2176	4.1921
Thermal conductivity (W m^{-1} °C^{-1})	0.561	0.580
Relative permittivity	87.90	83.96
Latent heat of evaporation (MJ kg^{-1})	2.49	2.47

4. Equation of state of sea water

$$\rho(T,0,0) = 999.842594 + 6.793952\times10^{-2}T - 9.095290\times10^{-3}T^2 + 1.001685\times10^{-4}T^3 - 1.120083\times10^{-6}T^4 + 6.536332\times10^{-9}T^5$$

$$\Delta(T,S,0) = \rho(T,0,0) + S(0.824493 - 4.0899\times10^{-3}T + 7.6438\times10^{-5}T^2 - 8.2467\times10^{-7}T^3 + 5.3875\times10^{-9}T^4) + S^{3/2}(-5.72466\times10^{-3} + 1.0227\times10^{-4}T - 1.6546\times10^{-6}T^2) + 4.8314\times10^{-4}S^2$$

$$\rho(T,S,0) = \rho(T,0,0) + \Delta(T,S,0)$$

$$\rho(T,S,p) = \frac{\rho(T,S,0)}{1 - p/K(T,S,p)}$$

$$K(T,0,0) = 19652.21 + 148.206T - 2.327105T^2 + 1.360477\times10^{-2}T^3 - 5.155288\times10^{-5}T^4$$

$$K(T,S,0) = K(T,0,0) + S(54.6746 - 0.603459T + 1.09987\times10^{-2}T^2 - 6.1670\times10^{-5} + S^{3/2}(7.944\times10^{-2} + 1.6483\times10^{-2}T - 5.3009\times10^{-4}T^2)$$

$$K(T,S,p) = K(T,S,0) + p(3.239908 + 1.43713\times10^{-3}T + 1.16092\times10^{-4}T^2 - 5.77905\times10^{-7}T^3) + pS(2.2838\times10^{-3} - 1.0981\times10^{-5}T - 1.6078\times10^{-6}T^2) + 1.91075\times10^{-4}pS^{3/2} + p^2(8.50935\times10^{-5} - 6.12293\times10^{-6}T + 5.2787\times10^{-8}T^2) + p^2S(-9.9348\times10^{-7} + 2.0816\times10^{-8}T + 9.1697\times10^{-10}T^2)$$

Values for checking are $\rho(0, 5, 0) = 999.96675$ kg m^{-3}, $\rho(35, 5, 0) = 1027.67547$ kg m^{-3}, and $\rho(0, 5, 0) = 1062.53817$ kg m^{-3}.

A.2 Physical Information of the Environment

1. General physics constants

Gravitational constant	$G = 6.67 \times 10^{-11}$ N m^2 kg^{-2}
Avogadro's number	$N_A = 6.022142 \times 10^{23}$
Planck's constant	$h = 6.626068 \times 10^{-34}$ J s
Boltzmann's constant	$k_B = 1.3807 \times 10^{-23}$ J K^{-1}
Stefan-Boltzmann constant	s = 5.670400×10^{-8} W m^{-2} K^{-4}
Velocity of light in vacuum	$c_o = 2.99792458 \times 10^8$ m s^{-1}
Universal gas constant	$R = 8.3145$ J K^{-1} mol^{-1}
Celcius—Kelvin conversion	T [K] = T [°C] + 273.15

2. Earth

Equatorial radius	6378.140 km
Polar radius	6356.755 km
Surface area	5.101×10^{14} m^2
Mean density	5515 kg m^{-3}
Standard acceleration due to gravity	$g = 9.80665$ m s^{-2} (at 45° latitude)
Period of rotation	23 h 56 min 4.10 s
Rotation rate	$\Omega = 0.7292 \times 10^{-5}$ s^{-1}
Inclination of rotation axis	23°27'

3. Sun

Solar constant	$Q_{sc} = 1367$ W m^{-2}
Sunlight (400–700 nm) fraction	$\gamma \approx 0.48$ (range 0.44–0.50)

The Sun–Earth distance (r)

$$\left(\frac{AU}{r}\right)^2 = 1.000110 + 0.034221\cos j + 0.001280\sin j + 0.00719\cos 2j + 0.000077\sin 2j$$

where $AU = 149.60 \cdot 10^9$ m is the astronomical unit equal to the mean Earth–Sun distance, and $j = (J–1) \cdot 2\pi/365$, J is the day of year ($J = 1.0$ on January 1st, 00.00 h).

The solar zenith angle (Z)

$$\cos Z = \sin\phi\ \sin\delta\ +\ \cos\phi\ \cos\delta\cos\tau$$
$$\sin\delta\ = \sin\varepsilon \sin(j - 80 \times 2\pi/365)$$
$$\tau\ = \tau_{\mathrm{GMT}} - \Lambda/15^{\circ}\ +\ \Delta t$$

where ϕ is the latitude, δ is the declination, τ is the local solar hour angle (zero at solar noon), $\varepsilon = 23°27'$ is the inclination of ecliptic, τ_{GMT} is GMT (Greenwich Mean Time), Λ is longitude, and Δt is time correction, $|\Delta t| < 30$ min, available in astronomical tables.

4. Atmosphere

Average molecular mass	28.97 g mol^{-1}
Standard atmospheric pressure	1013.25 mbar = p_0
Gas constant of air	R_a = 287.04 J kg^{-1} $°\mathrm{C}^{-1}$
Specific heat of air (constant pressure)	c_p = 1.004 kJ kg^{-1} $°\mathrm{C}^{-1}$
Thermal conductivity	2.4 $\cdot 10^{-2}$ W m^{-1} $°\mathrm{C}^{-1}$ ($p_{0,}$ 0 °C)
Density of dry air	$\rho_a = p_a/(R_a T)$, p_a – air pressure 1.293 kg m^{-3} at 0 °C and $p_a = p_0$
Atmospheric transmissivity	$T_{tr} \approx 0.9$
Dry air	
Specific heat at constant pressure	c_p = 1004 J $°\mathrm{C}^{-1}$ kg^{-1}
Specific heat at constant volume	c_v = 717 J $°\mathrm{C}^{-1}$ kg^{-1}
Thermal conductivity (0 °C)	2.40 × 10^{-2} J m^{-1} $°\mathrm{C}^{-1}$ s^{-1}

The saturation water vapour pressures (mbar)
Over liquid water surface (e_w) and over ice surface (e_i) as functions of temperature (°C) are given by

$$\log_{10} e_w(T) = \frac{0.7859 + 0.03477T}{1 + 0.00412T}$$

$$\log_{10} e_i(T) = \log_{10} e_w(T) + 0.00422T \qquad (T \leq {}^{\circ}\mathrm{C})$$

The relation between specific humidity (q) and water vapour pressure is

$$q = \frac{0.622e}{p_a}$$

David R. Line, ed. (2001) *CRC Handbook of Chemistry and Physics*. 82nd edition 2001–2002. CRC Press 2001, Boca Raton, Fl.

Petrenko, V.F., and Whitworth, R.W. (1999) *Physics of Ice*. Oxford University Press. Oxford, U.K.

Gill, A. (1982) *Atmosphere–Ocean Dynamics*. Academic Press, London, U.K.

References

Abel's, G. (1893) Beobachtungen der täglichen Periode der Temperatur im Schnee und Bestimmung des Wärmeleitungsvermögens des Schnees als Funktion seiner Dichtigkeit. *Kaiserliche Akademie der Wissenschaften. Repertorium für Meteorologie*, **16**, 1–53.

Adams, W.P., Doran, P.T., Ecclestone, M., Kingsbury, C.M. and Allan, C.J. (1989) A rare second-year—lake ice cover in the Canadian High Arctic. *Arctic* **42**(4), 299–306.

Adrian. R., O'Reilly, C., Zagarese, H., Baines, S.B., Hessen, D.O., Keller, W., Livingstone, D.M., Sommaruga, R., Straile, D., Van Donk, E., Weyhenmeyer, G.A., and Winder. M. (2009) Lakes as sentinels of climate change. *Limnology and Oceanography*, **54**, 2283–2297. doi: 10.4319/lo.2009.54.6_part_2.2283.

Alestalo, J. (1980) Systems of ice movement on Lake Lappajärvi, Finland. *Fennia*, **148**, 27–39.

Alestalo, J., and Häikiö, J. (1979) Forms created by thermal movement of lake ice in Finland in winter 1972–73. *Fennia*, **157**(2), 51–92.

Anderson, D.L. (1961) Growth rate of sea ice. *Journal of Glaciology*, **3**, 1170–1172.

Andreas, E.L. (1998) The atmospheric boundary layer over polar marine surfaces. In: M. Leppäranta (ed.), *The Physics of ice-covered seas*, Vol. 2, pp. 715–773. Helsinki University Press, Helsinki. (Available at https://helda.helsinki.fi/handle/10138/39286).

Arakawa, H. (1954) Five centuries of freezing dates of Lake Suwa in Central Japan. Archiv für Meteorologie, Geophysik und Bioklimatologie, B, **6**, 152–166.

Arp, C., and Jones, B. (2011) The hydrology and ice cover of Teshekpuk Lake in changing Arctic climate. Alaska Section of the American Water Resources Association 2011 Conference Proceedings (http://www.awra.org/state/alaska/proceedings/2011abstracts/).

Arrigo, K.R. (2003) Primary production in sea ice. In: D.N. Thomas and G.S. Dieckmann, *Sea ice. An introduction to its physics, chemistry and biology,* pp. 153–183. Blackwell Publishing, Oxford, UK.

Arst, H. (2003) *Optical properties and remote sensing of multicomponental water bodies*. Springer/Praxis. Chichester, U.K., 231 pp.

Arst, H., Erm, A., Leppäranta, M., and Reinart, A. (2006) Radiative characteristics of ice-covered freshwater and brackish water bodies. *Proceedings of the Estonian Academy of Sciences. Geology*, **55**(1), 3–23.

Arst, H., Erm, A., Herlevi, A., Kutser, T., Leppäranta, M., Reinart, A., and Virta, J. (2008) Optical properties of boreal lake waters in Finland and Estonia. *Boreal Environment Research*, **13**(2), 133–158.

Ashton, G. (1980) Freshwater ice growth, motion, and decay. In: S. Colbeck (ed.), *Dynamics of Snow and Ice Masses*, pp. 261–304. Academic Press, New York.

Ashton, G. (ed.) (1986) *River and Lake Ice Engineering*. Water Resources Publications, Littleton, Colorado, 485 pp.

Ashton, G. (1989) Thin ice growth. *Water Resources Research*, **25**(3), 564–566.

M. Leppäranta, *Freezing of Lakes and the Evolution of their Ice Cover*,
DOI 10.1007/978-3-642-29081-7

Assur, A. (1958) Composition of sea ice and its tensile strength. In: Thurston, W. (ed.), *Arctic Sea Ice*, pp. 106–138. US National Academy of Science/National Research Council: Publ. No. 598.

Bajracharya, S.M., and Mool, P. (2009) Glaciers, glacial lakes and glacial lake outburst floods in the Mount Everest region, Nepal. *Annals Glaciology*, **50**(53), 81–86.

Bar-Cohen, Y., Sherrit, S., Chang, Z., Wessel, L., Bao, X., Doran, P.T., Fritsen, C.H., Kenig, F., McKay, C.P., Murray, A., and Peterson, T. (2004) Subsurface ice and brine sampling using an ultrasonic/sonic gopher for life detection and characterization in the McMurdo Dry Valleys. *Proceedings of the SPIE Smart Structures Conference San Diego, CA*. SPIE Vol. 5388-32.

Barica. J., and Mathias, J.A. (1979) Oxygen depletion and winterkill risk in small prairie lakes under extended ice cover. *Journal of the Fishery Research Board of Canada*, **36**, 980–986.

Barnes, H.T. (1928) *Ice engineering*. Montreal Renouf Publishing Co., Montreal, Canada.

Bates, R.E., and Bilello, M.A. (1966) Defining the cold regions of the Northern Hemisphere. Technical Report 178. US Army Cold Regions Research and Engineering Laboratory, Hanover, NH.

Bengtsson, L. (1986) Dispersion in ice-covered lakes. *Nordic Hydrology*, **17**,151–170.

Bengtsson, L. (1996) Mixing in ice-covered lakes. *Hydrobiologia*, **322**, 91–97.

Bengtsson, L. (2011) Ice-covered lakes: environment and climate—required research. *Hydrological Processes*, **25**, 2767–2769. doi: 10.1002/hyp.8098.

Bergdahl, L. (2002) Islaster på vindkraftverk till havs. Rapport nr 2002:1, Vatten Miljö Transport. Chalmers University of Technology, Göteborg, Sweden.

Bergdahl, L., and Wernersson, L. (1978) Calculated and expected thermal ice pressure in five Swedish lakes. Department of Hydraulics, Chalmers University of Technology, Göteborg, Sweden, Report Series B:7.

Bernhardt, J., Engelhardt, C., Kirillin, G., and Matschullat, J. (2011) Lake ice phenology in Berlin-Brandenburg from 1947–2007: observations and model hindcasts. *Climatic Change* doi: 10.1007/s10584-011-0248-9.

Bernshteyn, S. (1929) The railway ice crossing. *Trudy Nauchno-Tekhnicheskogo Komiteta Narodnogo Komissariata Putei Soobshcheniya*, **84**, 36–82.

Beutel, M.W. (2001) Oxygen consumption and ammonia accumulation in the hypolimnion of Walker Lake, Nevada. *Hydrobiologia*, **466**, 107–117.

Blenckner, T., Järvinen, M., and Weyhenmeyer, G.A. (2004) Atmospheric circulation and its impact on ice phenology in Scandinavia. *Boreal Environment Research*, **9**, 371–380.

Bolsenga, S.J. (1988) Nearshore Great Lakes ice cover. *Cold Regions Science and Technology*, **15**, 99–105.

Boudreau, B.P., Jørgensen, B.B. (2001) *The benthic boundary layer: transport processes and biogeochemistry.* Oxford University Press.

Boylen, C.W., and Brock, T.D. (1973) Bacterial decomposition processes in Lake Wingra sediments during winter. *Limnology and Oceanography*, **18**, 628–634.

Bregman, G.R., and Proskuryakov, B.V. (1943) *Ice crossing-Sverdlovsk*. Gidrometeoizdat, 151 p.

Brunt, D. (1932) Notes on the radiation in the atmosphere. *Quarterly Journal of the Royal Meteorological Society*, **58**(247), 389–420.

Buckley, E.R. (1900) Ice ramparts. *Transactions of the Wisconsin Academy of Sciences, Arts and Letters*, Vol. 13, 141–157.

Caldwell, D.C. (1978) The maximum density points of pure and saline water. *Deep Sea Research*, **25**(2), 175–181.

Carmack, E., and Weiss, R. (1991) Convection in Lake Baikal: an example of thermobaric instability. In: Chu PC, Gascard JC (eds.), *Deep convection and deep water formation in the oceans*. Elsevier, Amsterdam, pp. 215–228.

Cheng, B. (2002) On modeling of sea ice thermodynamics and air-ice coupling in the Bohai Sea and the Baltic Sea. *Finnish Institute of Marine Research Contributions* 5, 38 pp.

Cheng, B., Vihma, T., and Launiainen, J. (2003) Modelling of the superimposed ice formation and subsurface melting in the Baltic Sea. *Geophysica*, **39**, 31–50.

Cheng, B., Zhang, Z., Vihma, T., Johansson, M., Bian, L., Li, Z., and Wu, H. (2008) Model experiments on snow and ice thermodynamics in the Arctic Ocean with CHINAREN 2003 data. *Journal of Geophysical Research*, **113**, C09020, doi: 10.1029/2007JC004654.

Chikita, K., Jha, J., and Yamada, T. (1999) Hydrodynamics of a supraglacial lake and its effect on the basin expansion: Tsho Rolpa, Rolwaling Valley, Nepal Himalaya. *Arctic, Antarctic, and Alpine Research,* **31**(1), 58–70.

Cholnoky, von, E. (1909) Das Eis des Balatonsees. E. Höezel, Wien.

Christner, B.C., Royston-Bishop, G., Foreman, C.M., Arnold, B.R., Tranter, M., Welch, K.A., Lyons, W.B., Tsapin, A.I., Studinger, M., and Priscu, J.C. (2006) Limnological conditions in subglacial Lake Vostok, Antarctica. *Limnology and Oceanography*, **51**(6), 2485–2501.

Colman, J.A., and Armstrong, D.E. (1983) Horizontal diffusivity in a small, ice-covered lake. *Limnology and Oceanography*, **28**, 1020–1026.

Coon, M.D. (1974) Mechanical behaviour of compacted Arctic ice floes. *Journal of Petroleum Technology*, **257**, 466–479.

Coon, M.D., Maykut, G.A., Pritchard, R.S., Rothrock, D.A., and Thorndike, A.S. (1974) Modeling the pack ice as an elastic-plastic material. *AIDJEX Bulletin*, **24**, 1–105.

Coon, M.D. (1980) A review of AIDJEX modeling. In: R.S. Pritchard (ed.), *Proceedings of ICSI/ AIDJEX Symposium on Sea Ice Processes and Models* (pp. 12–23). University of Washington, Seattle.

Coon, M.D., Knoke, G.S., Echert, D.C., and Pritchard, R.S. (1998) The architecture of an anisotropic elastic-plastic sea ice mechanics constitutive law. *Journal of Geophysical Research* **103**(C10), 21,915–21,925.

Cox, G.F.N. (1984) A preliminary investigation of thermal ice pressures. *Cold Regions Science and Technology*, **9**, 221–229.

Cox, G.F.N., and Weeks, W. F. (1983) Equations for determining the gas and brine volumes in sea-ice samples. Journal of Glaciology, **29**(102), 306–316.

Croley T.E., II, and Assel R.A. (1994) A one-dimensional ice thermodynamics model for the Laurentian Great Lakes. *Water Resources Research*, **30**(3), 625–639, doi: 10.1029/93WR03415.

Curry, J.A., and Webster, P.J. (1999) *Thermodynamics of Atmospheres and Oceans.* International Geophysics Series **65**. Academic Press, London, U.K., 467 pp.

Cushman-Roisin, B. (1994) *Introduction to Geophysical Fluid Dynamics.* Prentice-Hall, Englewood Cliffs, NJ.

Dammert, P.G., Leppäranta, M., and Askne, J. (1998) SAR interferometry over Baltic sea ice. *International Journal of Remote Sensing*, **19**(16), 3017–3037.

Davis, R.O. and Selvadurai, A.P.S. (2002) *Plasticity and geomechanics*. Cambridge University Press, Cambridge, U.K.

Dera, J. (1990) *Marine Physics*. Elsevier, Amsterdam, 516 pp.

DeWalle, D.R. and Rango, A. (2008) *Principles of snow hydrology*. Cambridge University Press, Cambridge, UK.

Doran, P.T., Priscu, J.C., Lyons, W.B., Powell, R.D., Andersen, D.T., and Poreda, R.J. (2004) Paleolimnology of extreme cold terrestrial and extraterrestrial environments. In Pienitz, R., Douglas, M.S.V., and Smol, J.P. (eds.), *Developments in Palaeoenvironmental Research*. Dordrecht: Springer. Long-Term Environmental Change in Arctic and Antarctic Lakes, Vol. 8, pp. 475–507.

Doran, P.T., Wharton Jr., R.A., Lyons, W.B. (2004) Paleolimnology of the McMurdo Dry Valleys, Antarctica. *Journal of Paleolimnology*, **10**(2), 85–114.

Doronin, Yu.P. (1970) On a method of calculating the compactness and drift of ice floes. *Trudy Arkticheskii i Antarkticheskii Nauchno-issledovatel'skii Institut* **291**, 5–17 [English transl. 1970 in AIDJEX *Bulletin* **3**, 22–39].

Duguay, C.R., and Lafleur. P.M. (2003) Determining depth and ice thickness of shallow sub-Arctic lakes using space-borne optical and SAR data. *International Journal of Remote Sensing*, **24**(3), 475–489.

Duguay, C.R., Flato, G.M., Jeffries, M.O., Ménard, P., Morris, K. and co-authors. 2003. Ice-cover variability on shallow lakes at high latitudes: model simulations and observations. Hydrological Processes, **17**, 3464–3483.

Duguay, C.R., Prowse, T.D., Bonsal, B.R., Brown, R.D., Lacroix, M.P., and Menard, P. (2006) Recent trends in Canadian lake ice cover. *Hydrological Processes*, **20**, 781–801.

Dunkle, R.V., and J.T. Bevans (1956) An approximate analysis of the solar reflectance and transmittance of a snow cover. *Journal of Meteorology*, **13**, 212–216.

Efremova, T., and Palshin, N. (2011) Ice phenomena terms on the water bodies of northwestern Russia. *Meteorology and Hydrology*, **36**(8), 559–565.

Ellis, C.R., and Stefan, H.G. (1989) Oxygen demand in ice covered lakes as it pertains to winter aeration. *Water Resources Bulletin*, **25**, 1169–1176.

Falkenmark, M. (ed.) (1973) Dynamic studies in Lake Velen. International Hydrological Decade – Sweden, Report 31. Swedish Natural Science Research Council, Stockholm, Sweden.

Farmer, D.M. (1975) Penetrative convection in the absence of mean shear. *Quarterly Journal of the Royal Meteorological Society*, **101**, 869–891. doi: 10.1002/qj.49710143011.

Farmer, D.M., and Carmack, E. (1981) Wind mixing and restratification in a lake near the temperature of maximum density. *Journal of Physical Oceanography*, **11**, 1516–1533.

Fedorova, I.V., Savatyugin, L.M., Anisimov, M.A., and Azarova, N.S. (2010) Change of the Schirmacher oasis hydrographic net (East Antarctic, Queen Maud Land) under deglaciation conditions. *Ice and Glacier*, **3**(111), 63–70. Moscow, Nauka.

Felip, M., Sattler, B., Psenner, R., and Catalan, J. (1995) Highly active microbial communities in the ice and snow cover of high mountain lakes. *Applied Environmental Microbiology,* **61**, 2394–2401.

Ferrick., M.G., and Prowse, T.D. (eds.) (2002) Special issue: Hydrology of ice-covered rivers and lakes. *Hydrological Processes* **16**(4), 759–958.

Fierz, C., Armstrong, R.L., Durand, Y., Etchevers, P., Greene, E., McClung, D.M., Nishimura, K., Satyawali, P.K., Sokratov, S.A. (2009) The international classification for seasonal snow on the ground. In: IHP-VII Technical Documents in Hydrology. IACS Contribution (1), Vol. 83. UNESCO-IHP, Paris.

Filatov, N.N., and Kondratyev, K.Ya. (1999) *Limnology and remote sensing*. Springer-Praxis Series in Remote Sensing, Springer-Verlag.

Flato, G.M., and Brown, R.D. (1996) Variablility and climate sensitivity of landfast Arctic sea ice. *Journal of Geophysical Research*, **101**, 25767–25777.

FMI (1982) Solar radiation measurements 1971–1980. *Meteorological Yearbook of Finland.* Part 4:1 (pp. 71–80). Finnish Meteorological Institute, Helsinki.

Forrest, A.L., Laval, B.E., Pieters, R., and Lim, D.S.S. (2008) Convectively driven transport in temperate lakes. *Limnology and Oceanography*, **53**, 2321–2332.

Fritsen, C.H., and Priscu, J.C. (1998) Cyanobacterial assemblages in permanent ice covers on antarctic lakes: Distribution, growth rate, and temperature response of photosynthesis. *Journal of Phycology*, **34**, 587–597.

Fritsen, C.H., Ackley, S.F., Kremer, J.N., and Sullivan, C.W. (1998) Flood-freeze cycles and microalgal dynamics in Antarctic pack ice. *Antarctic Research Series*, **73**. American Geophysical Union, pp. 1–21.

Fujisaki, A., Wang, J., Hu, H., Schwab, D.J., Hawley, N., and Rao, Y.R. (2012) A modeling study of ice–water processes for Lake Erie applying coupled ice-circulation models. *Journal of Great Lakes Research*, **38**(4), 585–599.

Futter, M.N. (2003) Patterns and trends in Southern Ontario lake ice phenology. *Environ Monit Assess*, **88**, 431–444.

Gamayunov, A.I. (1960) Vertical pressure of solid ice cover, caused by rising water level [in Russian]. *Gidrotekhnicheskoe Stroitel'stvo* 9, 40–42. (cited by Ashton, 1986).

George, G. (ed.) (2009) *The impact of climate change on European lakes*. Springer-Verlag, Berlin, Germany.

Gibson, J. A. E., Wilmotte, A., Taton, A., Van de Vijver, B., Beyens, L., and Dartnall, H. J. G. (2006) Biogeographic trends in Antarctic lake communities. In Bergstrom, D., Huiskes, A., and Convey, P. (eds.), *Trends in Antarctic Terrestrial and Limnetic Ecosystems*. The Netherlands: Kluwer.

Gill, A. (1982) *Atmosphere–Ocean Dynamics.* Academic Press, London, U.K., 662 pp.

Glen, J.W. (1955) The creep of polycrystalline ice. *Proceedings of the Royal Society of London*, **228A**, 519–538.

Glen, J.W. (1958) The flow law of ice. *International Association of Scientific Hydrology* **47**, 171–183.

Gold, L.W. (1971) Use of ice covers for transportation. *Canadian Geotechnical Journal*, **8**, 170.

Goldstein, R., Leppäranta, M., Onishchenko, D., and Osipenko, N. (2014) Bearing capacity of ice cover. *EOLLS*, in press.

Golosov, S., and Ignatieva, N. (1999) Hydrothermodynamic features of mass exchange across the sediment–water interface in shallow lakes. *Hydrobiologia*, **408/409**, 153–157.

Golosov, S., and Kirillin, G. (2010) A parameterized model of heat storage by lake sediments. *Environmental Modelling Software*, **25**, 793–801.

Golosov, S., Maher, O.A., Schipunova, E., Terzhevik, A., Zdorovennova, G., and Kirillin, G. (2006) Physical background of the development of oxygen depletion in ice-covered lakes. *Oecologia* (online) doi: 10.1007/s00442-006-0543-8.

Gothus, Olaus Magnus (1539) *Carta Marina.* Available at National Land Survey, Finland.

Götzinger, G. (1909) Studien über das Eis des Lunzer Unter- und Obersees. *Int Rev ges Hydrobiol Hydrogr*, **2**, 3–386.

Gow, A.J. (1986) Orientation textures in ice sheets of quietly frozen lakes. *Journal of Crystal Growth*, **74**, 247–258.

Gow, A.J., and Govoni, J.W. (1983) Ice growth on Post Pond, 1973–1982. CRREL Report 83–4. U. S. Army Cold Regions Research and Engineering Laboratory, Hanover, NH.

Granberg, H.B. (1998) Snow on sea ice. In Leppäranta, M. (ed.), *Physics of ice-covered seas*, Vol. 1, pp. 195–230. Helsinki, University of Helsinki Press. (Available at https://helda.helsinki.fi/handle/10138/39286).

Granin, N.G. (2010) The ringed Baikal. *Science First Hand* **27**(3), 26–27. The Siberian Branch of Russian Academy of Sciences, Novosibirsk, Russia.

Granin, N., Gnatovskiy, R.Y., Zhdanov, A., Zehanovsky, V.V., and Gorbunova, L.A. (1999) Convection and mixing under the ice of Lake Baikal. *Sibirskij Ecologicheskij Zhurnal* **6**, 597–600 (in Russian).

Greenbank, J. (1945) Limnological conditions in ice-covered lakes, especially as related to winter-kill of fish. *Ecological Monographs*, **15**, 343–391.

Grenfell, T. C. and Maykut, G. A. (1977) The optical properties of ice and snow in the Arctic Basin. *Journal of Glaciology*, **18**, 445–463.

Grenfell, T.C., and Perovich, D.K. (1981) Radiation absorption coefficient of polycrystalline ice from 400–1400 nm. *Journal of Geophysical Research*, **86**(C8), 7447–7450.

Haapala, J., and Leppäranta, M. (1996) Simulations of the Baltic Sea ice season with a coupled ice-ocean model. *Tellus* **48A**, 622–643.

Haapala, J., and Leppäranta, M. (1997) The Baltic Sea ice season in changing climate. *Boreal Environment Research* **2**, 93–108.

Håkanson, L., Bryhn, A. C. (2008) A dynamic mass-balance model for phosphorus in lakes with a focus on criteria for applicability and boundary conditions. *Water, Air, & Soil Pollution*, **187**, 119–147.

Hällström, G.G. (1839) Specimina mutanti currente seculo temporis, quo glacies fluminun annuae dissolutae sunt. *Acta Acad Sci Fenn*, **1**, 129–149.

Halsey, T.G. (1968) Autumnal and over-winter limnology of three small eutrophic lakes with particular reference to experimental circulation and trout mortality. *Journal of the Fishery Research Board of Canada*, **25**, 81–99.

Hamilton, D.P., and Mitchell, S.F. (1996) An empirical model for sediment resuspension in shallow lakes. *Hydrobiologia,* **317**, 209–220.

Hargrave, B.T. (1969) Similarity of oxygen uptake by benthic communities. *Limnology and Oceanography*, **14**, 801–805.

Hargrave, B.T. (1972) A comparison of sediment oxygen uptake, hypolimnetic oxygen deficit and primary production in Lake Esrom, Denmark. *Verhandlungen des Internationalen Verein Limnologie*, **18**, 134–139.

Helaakoski, A. (1912) Havaintoja jäätymisilmiöiden geomorfologisista vaikutuksista [Beobachtungen über die geomorfologischen Einflüsse der Gefriererscheinungen]. *Suomalaisen Maantieteellisen Yhdistyksen julkaisuja* 9, 109 pp.

Henneman, H.E. and Stefan, H.G. (1999) Albedo models for snow and ice on a freshwater lake. *Cold Regions Science and Technology*, **29**(1), 31–48.

Henderson, P., and Henderson, G.M. (2009) *The Cambridge handbook of earth science data*. Cambridge University Press, Cambridge, UK. 276 pp.

Hertz, H. (1884) Über das Gleichgewicht schimmender elastischen Platten. *Wiedmanns Annalen der Physik und Chemie,* **22**, 449–455.

Heron, R., and Woo, M.K. (1994) Decay of a High Arctic lake-ice cover: observations and modelling. *Journal of Glaciology*, **40**, 283–292.

Hibler, W.D., III (1979) A dynamic-thermodynamic sea ice model. *Journal of Physical Oceanography*, **9**, 815–846.

Hibler, W.D., III (1980) Modelling a variable thickness sea ice cover. *Monthly Weather Review*, **108** (12), 1943–1973.

Hibler, W.D., III (2001) Sea ice fracturing on the large scale. *Engineering Fracture Mechanics*, **68**, 2013–2043.

Hibler, W.D., III and Schulson, E.M. (2000) On modeling the anisotropic failure and flow of flawed sea ice. *Journal of Geophysical Research* **105**(C7), 17105–17120.

Higashino, M., Gantzer, C.J., and Stefan, H.G. (2004) Unsteady diffusional mass transfer at the sediment/water interface: theory and significance for SOD measurement. *Water Resources*, **38**, 1–12.

Hodgson, D.A. (2012) Antarctic lakes. In *Encyclopedia of Lakes and Reservoirs*, eds. L. Bengtsson, R.W. Herschy and R.W. Fairbridge, pp. 26–31. Springer, Berlin.

Hoffman, M.J., Catania, G.A., Neumann, T.A., Andrews, L.C. and Rumrill, J.A. (2011) Links between acceleration, melting, and supraglacial lake drainage of the western Greenland Ice Sheet. *Journal of Geophysical Research* **116**, F04035, doi:10.1029/2010JF001934.

Hohmann, R., Kipfer, R., Peeters, F., Piepke, G., Imboden, D.M., and Shimaraev, M.N. (1997) Processes of deep-water renewal in Lake Baikal. *Limnology and Oceanography*, **42**, 841–855.

Holton, J.R. (1979) *An introduction to dynamic meteorology*. Academic Press, New York.

Homén, Th, (1903) Die Temperaturverhältnisse in den Seen Finnlands. Förh. vid Nat. fork. mötet i Helsingfors 1902.

Hopkins, M. (1994 On the ridging of intact lead ice. *Journal of Geophysical Research* **99**(C8), 16,351–16,360.

Huang, W.-F., Li, Z., Han, H., Niu, F., Lin, Z., and Leppäranta, M. (2012) Structural analysis of thermokarst lake ice in Beiluhe Basin, Qinghai–Tibet Plateau. *Cold Regions Science and Technology*, **72**, 33–42.

Humphreys, W.J. (1934) The 'sinking' of lake and river ice. *Monthly Weather Review*, **62**(4), 133–134.

Hunter, S.C. (1976) *Mechanics of Continuous Media*. Ellis Horwood, Chichester, UK.

Huss, M., Bauder, A., Werder, M., Funk, M., and Hock, R. (2007) Glacier-dammed lake outburst events of Gornersee, Switzerland. *Journal of Glaciology*, **53**(181), 189–200.

Hutchinson, G.E. (1957) *A treatise on limnology, v. 1. Geography, Physics and Chemistry*. Wiley, 1015 p.

Hutchinson, G.E., and Löffler, H. (1956) The thermal classification of lakes. Proceedings of National Academy of Science of the USA, 42, 84–86.

Huttula, T., Pulkkanen, M., Arkhipov, B., Leppäranta, M., Solbakov, V., Shirasawa, K., and Salonen, K. (2010) Modelling circulation in an ice covered lake. *Estonian Journal of Earth Sciences*, **59**(4), 298–309.

Iqbal, M. (1983) *An Introduction to Solar Radiation.* Academic Press, Orlando, FL. 390 pp.

Isaksson, E., and Karlén, W. (1994) Spatial and temporal patterns in snow accumulation, western Dronning Maud Land, Antarctica. *Journal of Glaciology*, **40**(135), 399–409.

Ivanov, K.E. (1949) Carrying capacity of the ice cover and the construction of roads on the ice. *Publishing House of the Northern Sea Route*, Moscow. 182p.

Jakkila, J., Leppäranta, M., Kawamura, T., Shirasawa, K., and Salonen, K. (2009) Radiation transfer and heat budget during the melting season in Lake Pääjärvi. *Aquatic Ecology*, **43**(3), 681–692.

Jensen, O.P., Benson, B.J., Magnuson, J.J., Card, V.M., Futter, M.N., Soranno, P.A., and Stewart, K.M. (2007) Spatial analysis of ice phenology trends across the Laurentian Great Lakes region during a recent warming period. *Limnology and Oceanography*, **52**, 2013–2026.

Jevrejeva, S., Drabkin, V.V., Kostjukov, K., Lebedev, A.A., Leppäranta, M., Mironov, Ye.U., Schmelzer, N. and Sztobryn, M. (2004) Baltic Sea ice seasons in the twentieth century. *Climate Research*, **25**, 217–227.

Jewson, D., Granin, N., Zhdanov, A., and Gnatovsky, R. (2009) Effect of snow depth on under-ice irradiance and growth of Aulacoseira baicalensis in Lake Baikal. *Aquatic Ecology*, **43**, 673–679. doi: 10.1007/s10452-009-9267-2.

Jokiniemi, A. (2011) The water balance of Lake Vanajavesi. BSc thesis, Department of Physics, University of Helsinki.

Jonas, T., Terzhevik, A.Y., Mironov, D.V., and Wüest, A. (2003) Radiatively driven convection in an ice-covered lake investigated by using temperature microstructure technique. *Journal of Geophysical Research*, **108**(C6), 3183. doi: 10.1029/2002JC001316.

Joughin, I., Das, S.B., King, M.A., Smith, B.E., Howat, I.M., and Moon, T. (2008) Seasonal speedup along the western flank of the Greenland ice sheet. *Science* **320**(5277), 781–783.

Kagan, B.A. (1995) *Ocean-Atmosphere Interaction and Climate Modelling*. Cambridge University Press, 377 p. Cambridge, UK.

Karetnikov, S., and Naumenko, M.A. (2008) Recent trends in Lake Ladoga ice cover. *Hydrobiologia*, **599**, 41–48.

Karetnikov, S., and Naumenko, M.A. (2011) Lake Ladoga ice phenology: Mean condition and extremes during the last 65 years. *Hydrological Processes*, **25**(18), 2859–2867.

Karetnikov, S., Leppäranta, M., and Jokiniemi, A. (2015) Climatology of the ice season in Lake Ladoga. Manuscript.

Kärkäs, E. (2000) The ice season of Lake Pääjärvi, southern Finland, *Geophysica* **36**, 85–94.

Kaup, E. (1994) Annual primary production of phytoplankton in Lake Verkhneye, Schirmacher Oasis. Antarctica. *Polar Biology,* **14**, 433–439.

Kaup, E., Loopmann, A., Klokov, V., Simonov, I., and Haendel, D. (1988) Limnological investigations in the Untersee Oasis (Queen Maud Land, East Antarctica). In Martin, J. (ed.), *Limnological studies in Queen Maud Land (East Antarctica). Valgus*, Tallinn, 6–14.

Kawamura, T., Shirasawa, K., Ishikawa, N., Lindfors, A., Rasmus, K., Ehn, J., Leppäranta, M., Martma, T., and Vaikmäe, R. (2001) A time series of the sea ice structure in the Baltic Sea. *Annals of Glaciology*, **33**: 1–4.

Kawamura, T., Granskog, M.A., Lindfors, A., Ehn, J., Martma, T., Vaikmäe, R., Ishikawa, N., Shirasawa, K. and Leppäranta, M. (2002) Study on brackish ice in the Gulf of Finland – effect of salt on sea ice structure. *Proceedings of the 15th IAHR Ice Symposium*, Vol. 2, pp. 165–172. Dunedin, New Zealand.

Kelley, D.E. (1997) Convection in ice-covered lakes: effects on algal suspension. *Journal of Plankton Research* **19**(12), 1859–1880. doi: 10.1093/plankt/19.12.1859.

Kenney, B. (1996) Physical limnological processes under ice. *Hydrobiologia*, **322**, 85–90.

Kerr, A.D. (1975) Ice forces on structures due to a change in the water level. *Proceedings of the IAHR Ice Symposium 1975*, pp. 419–427.

Keskitalo, J., Leppäranta, M., and Arvola, L. (2013) First records on primary producers of epiglacial and supraglacial lakes in the western Dronning Maud Land, Antarctica. *Polar Biology* **36**(10), 1441–1450. doi: 10.1007/s00300-013-1362-0.

Kirillin, G. (2010) Modeling the impact of global warming on water temperature and seasonal mixing regimes in small temperate lakes. *Boreal Environment Research*, **15**, 279–293.

Kirillin, G., and Terzhevik, A. (2011) Thermal instability in freshwater lakes under ice: effect of salt gradients or solar radiation? *Cold Regions Science and Technology*, **65**, 184–190. doi: 10.1016/j.coldregions.2010.08.010.

Kirillin, G., Engelhardt, C., Golosov, S., and Hintze, T. (2009) Basin-scale internal waves in the bottom boundary layer of ice-covered Lake Müggelsee, Germany. *Aquatic Ecology*, **43**, 641–651. doi: 10.1007/s10452-009-9274-3.

Kirillin, G., Rizk, W., and Leppäranta, M. (2012a) Convective mixing by solar radiation under lake ice. In: Li, Z., Lu, P. (eds) *Ice research for a sustainable environment. Proceedings of 21st IAHR international symposium on ice*, Dalian University of Technology Press, Dalian, China, pp. 1201–1211. ISBN: 978-7-89437-020-4.

Kirillin, G., Leppäranta, M., Terzhevik. A., Granin, N., Bernhardt, J., Engelhardt, C., Efremova, T., Golosov, S., Palshin, N., Sherstyankin, P., Zdorovennova, G., and Zdorovennov, R. (2012b) Physics of seasonally ice-covered lakes: a review. *Aquatic Sciences*, **74**, 659–682. doi: 10.1007/s00027-012-0279-y.

Kolmogorov, A. (1949) Geometric selection of crystals [in Russian]. *Doklady Akademii Nauk SSSR*, **65**(5), 681–684.

Korhonen, J. (2006) Long-term changes in lake ice cover in Finland. *Nordic Hydrology*, **37**, 347–363.

Korzhavin, K.N. (1962) Vozdeystviye l'da na inzhenertrye sooruzheniya [The Action of Ice on Engineering Structures]. *Izdatel'stvo Sibirskogo Otdel*, Akademiya Nauk SSSR, Novosibirsk.

Kouraev, A.V., Papa, F., Mognard, N.M., Buharizin, P.I., Cazenave, A., Cretaux, J.-F., Dozortseva, J., and Remy, F. (2004) Sea ice cover in the Caspian and Aral Seas from historical and satellite data. *Journal of Marine Systems*, **47**, 89–100.

Kouraev, A.V., Shimaraev, M.N., Buharizin, P.I., Naumenko, M.A., Crétaux, J.F., Mognard, N., Legrésy. B., and Rémy, F. (2008) Ice and snow cover of continental water bodies from simultaneous radar altimetry and radiometry observations. *Surveys in Geophysics*, **29**, 271–295. doi: 10.1007/s10712-008-9042-2.

Kourzeneva, E., Samuelsson, P., Ganbat, G., and Mironov, D. (2008) Implementation of lake model FLake in HIRLAM. *HIRLAM Newsletter,* No. 54, 54–61.

Koźmiński, Z., and Wisznewski, J. (1934) Über die Vorfrühlingthermik der Wigry-Seen. *Archiv für Hydrobiologie*, **28**, 198–235.

Kottek, M., Grieser, J., Beck, C., Rudolf, B., and Rubel, F. (2006) World Map of the Köppen-Geiger climate classification updated. *Meteorologische Zeitschrift*, **15**(3), 259–263.

Korvin, G. (1992) *Fractal models in the Earth sciences*. Elsevier, Amsterdam.

Kristensen, P., Søndergaard, M., and Jeppesen, E. (1992) Resuspension in a shallow eutrophic lake. *Hydrobiologia*, **228**, 101–109.

Krzywicki, H. J., and Chinn, K. S. K. (1966). Human body density and fat of an adult male population as measured by water displacement. Defense Documentation Center. Retrieved 2012-08-07.

Kubat, I., Sayed, M., Savage, S.B., and Carrieres, T. (2009) Numerical simulations of ice thickness redistribution in the Gulf of St. Lawrence. *Cold Regions Science and Technology*, **60**(1), 15–28.

Lal, A.M.W., and Shen, H.T. (1993) A mathematical model for river ice processes. CRREL Report 93-4. Cold Regions Research Laboratory, Hanover, NH, U.S.A.

Landau, L.D., and Lifschitz, E.M. (1976) *Mechanics*, 3rd edn. Pergamon Press, Oxford, UK.

Langway, C.C. (1958) Ice fabrics and the universal stage. Techn. Rep. 62. U.S. Army Snow, Ice, and Permafrost Research Establishment, Hanover, N.H.

Launiainen J., and Cheng B. (1998) Modelling of ice thermodynamics in nature water bodies. *Cold Regions Science and Technology*, **27**, 153–178.

Launiainen, J., and Vihma, T. (1990) Derivation of turbulent surface fluxes – an iterative flux-profile method allowing arbitrary observing heights. *Environmental Software*, **5**(3), 113–124. (doi: 10.1016/0266-9838(90)90021-W).

Laybourn-Parry, J., Tranter, M. and Hodson, A.J. (2012) *The ecology of snow and ice environments*. Oxford University Press, New York, N.Y.

Lei, R., Leppäranta, M., Erm, A., Jaatinen, E., and Pärn, O. (2011) Field investigations of apparent optical properties of ice cover in Finnish and Estonian lakes in winter 2009. *Estonian Journal of Earth Sciences*, 60(1), 50–64.

Lei, R., Leppäranta, M., Cheng, B., Heil, P., and Li, Z. (2012) Changes in ice-season characteristics of a European Arctic lake from 1964 to 2008. *Climatic Change*, doi: 10.1007/s10584-012-0489-2.

Leppäranta, M. (1983) A growth model for black ice, snow ice and snow thickness in subarctic basins. *Nordic Hydrology,* **14**(2), 59–70.

Leppäranta, M. (1993) A review of analytical sea ice growth models. *Atmosphere–Ocean,* **31**(1), 123–138.

Leppäranta, M. (2009a) Modelling of growth and decay of lake ice. In: G. George (Ed.), *Climate change impact on European lakes*, Springer-Verlag.

Leppäranta, M. (2009b) A two-phase model for thermodynamics of floating ice. *Proceedings of the 6th Workshop on Baltic Sea Ice Climate*, Report Series in Geophysics 61, pp. 146–154. Department of Physics, University of Helsinki, Helsinki, Finland.

Leppäranta, M. (2011) *The drift of sea ice, 2nd edition*. Springer-Praxis, Heidelberg, Germany.
Leppäranta, M. (2013) Land-ice interaction in the Baltic Sea. *Estonian Journal of Earth Sciences* **62** (1), 2–14.
Leppäranta, M. (2014) Interpretation of statistics of lake ice time series for climate variability. *Hydrology Research*, in press.
Leppäranta, M., and W.D. Hibler III (1985) The role of plastic ice interaction in marginal ice zone dynamics. *Journal of Geophysical Research* **90**(C6), 11,899–11,909.
Leppäranta, M., and Kosloff, P. (2000) The thickness and structure of Lake Pääjärvi ice. *Geophysica*, **36**(1–2), 233–248.
Leppäranta, M., and Lewis, J.E. (2015) Surface temperature and thickness of ice in Lake Peipsi as observed from MODIS data. Manuscript.
Leppäranta, M., and Manninen, T. (1988) Brine and gas content of sea ice with attention to low salinities and high temperatures. Internal Report 1988(2), 15 p. Finnish Institute of Marine Research, Helsinki, Finland.
Leppäranta, M. and Myrberg, K. (2009) *Physical oceanography of the Baltic Sea*. Springer-Praxis, Heidelberg, Germany.
Leppäranta, M. and A. Seinä (1985) Freezing, maximum annual ice thickness and breakup of ice on the Finnish coast during 1830–1984. *Geophysica*, **21**(2), 87–104.
Leppäranta, M., and Uusikivi, J. (2002) The annual cycle of the Lake Pääjärvi ice. *Lammi Notes 29*.
Leppäranta, M., and Wang, K. (2008) The ice cover on small and large lakes: scaling analysis and mathematical modelling. *Hydrobiologica*, **599**, 183–189.
Leppäranta, M., Reinart, A., Arst, H., Erm, A., Sipelgas, L., and Hussainov, M. (2003a) Investigation of ice and water properties and under-ice light fields in fresh and brackish water bodies. *Nordic Hydrology*, **34**(3), 245–266.
Leppäranta, M., Tikkanen, M., and Virkanen, J. (2003b) Observations of ice impurities in some Finnish lakes. *Proceedings of the. Estonian Academy of Science. Chemistry*, **52**(2), 59–75.
Leppäranta, M., Terzhevik, A., and Shirasawa, K. (2010) Solar radiation and ice melting in Lake Vendyurskoe, Russian Karelia. *Hydrology Research*, **41**(1), 50–62.
Leppäranta, M., Heini, A., Jaatinen, E., and Arvola, L. (2012) The influence of ice season on the physical and ecological conditions in Lake Vanajanselkä, southern Finland. *Water Quality Research Journal of Canada* 47(3-4), 287–299.
Leppäranta, M., Järvinen, O., and Lindgren, E. (2013a) Mass and heat balance of snow patches in Basen nunatak, Dronning Maud Land in summer. *Journal of Glaciology* **59**(218), 1093–1105.
Leppäranta, M., Järvinen, O., and Mattila, O.-P. (2013b) Structure and life cycle of supraglacial lakes in the Dronning Maud Land. *Antarctic Science,* 25(3), 457–467.
Levänen, S. (1894) Solfläckarnes inflytande på islossingstiderna i Finlands floder och på vattenståndet i finska viken [The influence of sunspots to ice breakup in Finnish rivers and to water level elevation in the Gulf of Finland]. *Fennia* **9**(4). Societas geographica Fenniae, Helsinki. Finland.
Li, Z., Huang, W.-F., Jia, Q., and Leppäranta, M. (2011) Distributions of crystals and gas bubbles in reservoir ice during growth period. *Water Science and Engineering*, **4**(2), 204–211. doi: 10.3882/j.issn.1674-2370.2011.02.008.
Liang , Y.-L., Colgan, W., Lv, Q., Steffen, K., Abdalati, W., Stroeve, J., Gallaher, D., and Bayou, N. (2012) A decadal investigation of supraglacial lakes in West Greenland using a fully automatic detection and tracking algorithm. *Remote Sensing of Environment*, **123**, 127–138.
Likens, G.E., and Ragotzkie, R.A. (1965) Vertical water motions in a small ice-covered lake. *Journal of Geophysical Research*, **70**, 2333–2344. doi: 196510.1029/JZ070i010p02333.
Lindholm, T., Rönnberg, O. and Östman, T. (1989) Husövikenen flada i Ålands skärgård. *Svensk Botanisk Tidskrift* **83**, 143–147.

Liston, G.E., and Hall, D.K. (1995) An energy-balance model of lake-ice evolution. *Journal of Glaciology*, **10**, 373–382.

Livingstone, D.M. (2000) Large scale climatic forcing detected in historical observations of lake-ice break-up. *Verhandlungen der Internationalen Vereinigung für Theoretische und Angewandte Limnologie*, **27**(5), 2775–2783.

Louis, J.-F. (1979) A parametric model of vertical eddy fluxes in the atmosphere. *Boundary-Layer Meteorology*, **17**, 187–202.

Lumb, F.E. (1964) The influence of cloud on hourly amounts of total solar radiation at the sea surface. *Quarterly Journal of the Royal Meteorological Society*, **90**(383), 43–56.

MacDonell S., and Fitzimons, S. (2008) The formation and hydrological significance of cryoconite holes. *Progress in Physical Geography*, **32**(6), 595–610.

McPhee, M. (2008) *Air-ice-ocean interaction: turbulent boundary layer exchange processes*. Springer, Berlin.

Magano, C., and Lee, C.W. (1966) Meteorological classification of natural snow crystals. *Journal of the Faculty of Science, Hokkaido University*, Ser. VII, **2**(4), 321–335.

Magnuson, J.J., Robertson, D.M., Benson, B.J., Wynne, R.H., Livingstone, D.M., Arai, T., Assel, R. A., Barry, R.G., Card, V., Kuusisto, E., Granin, N.G., Prowse, T.D., Stewart, K.M., and Vuglinski, V.S. (2000) Historical trends in lake and river ice cover in the northern hemisphere. *Science* **289**,1743–1746 and Errata 2001 *Science* **291**:254.

Makkonen, L., Törnqvist, J., Kuutti, J. (2010) Vibrations of buildings induced by thermal cracking of lake ice. *Proceedings of the 20th IAHR Ice Symposium*, Lahti, Finland, 14–18 June 2010.

Maksym, T., and Jeffries, M.O. (2000) A one-dimensional percolation model of flooding and snow ice formation on Antarctic sea ice. *Journal of Geophysical Research*, **105**(C11), 26313–26331.

Malm, J. (1998) Bottom buoyancy layer in an ice-covered lake. *Water Resources Research*, **34**, 2981–2993.

Malm, J. (1999) Some properties of currents and mixing in a shallow ice-covered lake. *Water Resources Research*, **35**, 221–232.

Malm, J., Terzhevik, A., Bengtsson, L., Boyarinov, P., Glinsky, A., Palshin, N., and Petrov, M. (1997) Temperature and salt content regimes in three shallow ice-covered lakes. 2. Heat and mass fluxes. *Nordic Hydrology*, **28**, 129–152.

Malm, J., Bengtsson, L., Terzhevik, A., Boyarinov, P., Glinsky, A., Palshin, N., and Petrov, M. (1998) Field study on currents in a shallow, ice-covered lake. *Limnology and Oceanography*, **43**, 1669–1679.

Marra, J. (1978) Effect of short-term variation in light intensity on photosynthesis of a marine phytoplankter: a laboratory simulation study. *Marine Biology*, **46**, 191–202.

Marszelewski W., and Skowron, R. (2006) Ice cover as an indicator of winter air temperature changes: case study of the Polish Lowland lakes. *Hydrological Sciences Journal* **51**, 336–349.

Martin, S. (1981) Frazil ice in rivers and oceans. *Annual Reviews in Fluid Mechanics,* **13**, 379–397.

Mase, G.E. (1970) *Continuum Mechanics* (Schaum's outline series). McGraw-Hill, New York.

Masolov, V. N., Popov, S. V., Lukin, V. V., Sheremetyev, A. N., and Popkov, A. M. (2006). Russian geophysical studies of Lake Vostok, Central East Antarctica. In *Antarctica*, pp. 135–140. Springer, Berlin and Heidelberg.

Matthews, P.C., and Heaney, S.I. (1987) Solar heating and its influence on mixing in ice-covered lakes. *Freshwater Biology*, **18**, 135–149.

Maurer, J. (1924) Severe winters in southern Germany and Switzerland since the year 1400 determined from severe lake freezes. *Monthly Weather Review*, **52**, 222. [Translater from German original in *Meteorologische Zeitschrift*, **41**, 85–86.

Maykut, G.A., and Untersteiner, N. (1971) Some results from a time-dependent, thermodynamic model of sea ice. *Journal of Geophysical Research,* **76**, 1550–1575.

Melentyev, V.V., Tikhomirov, A.I., Kondratyev, K.Ya., Johannessen, O.M., Sandven, S., Pettersson, L.H. (1997) Study of freeze-up phase change on large temperate zone inland water bodies and possibilities of their microwave diagnostics [in Russian]. *Earth Observations and Remote Sensing*, 3, 61–72.

Melnik, N.G., Lazarev, M.I., Pomazkova, G.I., Bondarenko, N.A., Obolkina, L.A., Penzina, M.M., and Timoshkin, O.A. (2008) The cryophilic habitat of micrometazoans under the lake ice in Lake Baikal. *Fundamental and Applied Limnology*, **170**, 315–323.

Menzies, J. (ed.) (1995) *Modern glacial environments. Processes, dynamics and sediments.* Butterworth–Heinemann, Oxford, UK.

Metge, M. (1976) Thermal cracks in lake ice. PhD thesis, Queen's University, Kingston, Ontario.

Meyer, G.H., Morrow, M.B., Wyss, O., Berg, T.E. and Littlepage, J.L. (1962) Antarctica: The microbiology of an unfrozen saline pond. *Science,* **138**, 1103–1104.

Michel, B. (1978) *Ice mechanics*. 499 p. Laval University Press, Québec, Canada.

Michel, B. (1978b) Mechanical model of creep of polycrystalline ice. *Canadian Geotechnical Journal*, **15**(2), 155–170.

Michel, B., and Ramseier, R.O. (1971) Classification of river and lake ice. *Canadian Geotechnical Journal*, **8**(36), 36–45.

Mironov, D.V., Golosov, S.D., Zilitinkevich, S.S., Kreiman, K.D., and Terzhevik, A.Yu. (1991) Seasonal changes of temperature and mixing conditions in a lake. *Modeling Air-Lake interaction. Physical Background*, S. S. Zilitinkevich, Ed. Springer-Verlag, Berlin, pp. 74-90.

Mironov, D., Terzhevik, A., Kirillin, G., Jonas, T., Malm, J., and Farmer, D. (2002) Radiatively driven convection in ice-covered lakes: Observations, scaling, and a mixed layer model. *Journal of Geophysical Research*, **107**(C4). doi: 10.1029/2001JC000892.

Mironov, D., Terzhevik, A., Beyrich, F., and Heise, E. (2004) A lake model for use in numerical weather prediction systems. *Research Activities in Atmospheric and Oceanic Modelling*, J. Cote, Ed., Report No. 34, April 2004, WMO/TD-No. 1220, 4.23–4.24.

Mishra, V., Cherkauer, K.A., Bowling, L.C., and Huber, M. (2011) Lake Ice phenology of small lakes: Impacts of climate variability in the Great Lakes region. *Global and Planetary Change*, **76**, 166–185.

Mortimer, C., and Mackereth, F. (1958) Convection and its consequences in ice-covered lakes. *Verh Int Ver Limnol* **13**, 923–932.

Mosier, A.C., Murray, A.E., and Fritsen, C.H. (2007) Microbiota within the perennial ice cover of Lake Vida, Antarctica. *FEMS Microbiology Ecology*, **59**(2), 274–278.

Mueller, D.R., Van Hove, P., Antoniades, D., Jeffries, M.O., and Vincent, W.F. (2009) High Arctic as sentimental ecosystems: Cascading regime shifts in climate, ice cover, and mixing. *Limnology and Oceanography*, **54**(6, part 2). 2371–2385.

Mullen P.C., and Warren, S.G. (1988) Theory of the optical properties of lake ice. *Journal of Geophysical Research*, **93**(D7), 8403–8414.

Müller-Stoffels, M., Langhorne, P.J., Petrich, C., Kempema, E.W. (2009) Preferred crystal orientation in fresh water ice. *Cold Regions Science and Technology*, **56**, 1–9.

Munro-Stasiuk, M.J. (2003) Subglacial Lake McGregor, south-central Alberta, Canada. *Sedimentary Geology*, **160**, 325–350.

Nghiem, S.V., and Leshkevich, G.A. (2007) Satellite SAR remote sensing of Great Lakes ice cover, Part 1. Ice backscatter signatures at C band. *Journal of Great Lakes Research*, **33**, 722–735.

Niemistö, J., and Horppila, J. (2007). The contribution of ice cover to sediment resuspension in a shallow temperate lake - possible effects of climate change on internal nutrient loading. *Journal of Environmental Quality*, **36**, 1318–1323.

Niiler, P.P., and Kraus, E.B. (1977) One-dimensional models of the upper ocean. In: E.B. Kraus (ed.), *Modelling and prediction of the upper layers of the ocean*, pp. 143–172. Pergamon Press, Oxford, U.K.

Nolan, M. (2013) Quantitative and qualitative constraints on hind-casting the formation of multi-year lake-ice covers at Lake El'gygytgyn. *Climate of the Past*, **9**, 1253–1269.

Nye, J.F. (1973) The physical meaning of two-dimensional stresses in a floating ice cover. *AIDJEX Bulletin*, 21, 1–9.

Omstedt A. (2011) *Guide to process based modelling of lakes and coastal seas*. Springer-Praxis books in Geophysical Sciences. Springer-Verlag, Berlin Heidelberg.

Omstedt. A. and Svensson, U. (1984) Modeling supercooling and ice formation in a turbulent Ekman layer. *Journal of Geophysical Research* **89**(C1), 735–744.

Osborn, M., and Mitchell, S.A. (2007) The battle on ice. *ANQ*, **20**(3), 70–74.

Osterkamp, T.E. (1977) Frazil ice nucleation by mass-exchange processes at the air-water interface. *Journal of Glaciology*, **19**(81), 619–625.

Ovsienko, S. (1976) Numerical modeling of the drift of ice. *Izvestiya, Atmospheric and Oceanic Physics*, **12**(11), 1201–1206.

Palmer, A., Croasdale, K. (2012) *Arctic offshore engineering*. World Scientific Publishing, Singapore.

Palmer, S.J., Dowdeswell, J.A., Christoffersen, P., Young, D.A., Blankenship, D.D., Greenbaum, J. S., Benham, T., Bamber, J., and Siegert, M.J. (2013) Greenland subglacial lakes detected by radar. *Geophysical Research Letters*, **40**, 6154–6159. doi: 10.1002/2013GL058383.

Palosuo, E. (1961) Crystal structure of brackish and fresh-water ice. Snow and Ice Commission Publication 54, pp. 9–14. IASH, Gentbugge, Belgium.

Palosuo, E. (1965) Frozen slush on lake ice. *Geophysica*, **9**(2), 131–147.

Palosuo, E. (1982) Jään vahvistaminen Finlandia-82 hiihdon lähtöpaikalla [Strengthening of the ice at start of the Finlandia-82 ski event]. Report Series in Geophysics 16. Department of Physics, University of Helsinki.

Panfilov, D.F. (1960) Approximate method to analyze the bearing capacity of an ice cover. *Izvestiya Vsesoyuznogo Nauchno-Issledovatel'skogo Instituta Gidrotekhniki*, **65**, 221–224.

Parmerter, R.R. (1975) A model of simple rafting in sea ice. *Journal of Geophysical Research*, **80** (15), 1948–1952.

Parsekian, A.D., Jones, B.M., Jones, M., Grosse, G., Walter Anthony, K.M., and Slater, L. (2011) Expansion rate and geometry of floating vegetation mats on the margins of thermokarst lakes, northern Seward Peninsula, Alaska, USA. *Earth Surface Processes and Landforms,* **36**(14), 1889–1897.

Paterson, W. (1999) *Physics of glaciers, 3rd ed*. Butterworth–Heinemann, Oxford, UK.

Patterson, J. C., and Hamblin, P. F. (1988) Thermal simulation of a lake with winter ice cover. *Limnology and Oceanography*, **33**, 323–338.

Paulson, C.A. (1970) The mathematical representation of windspeed and temperature profiles in the unstable atmospheric boundary layer, *Journal of Applied Meteorology,* **9**, 857–861.

Perovich, D. K. (1990) Theoretical estimates of light reflection and transmission by spatially complex and temporally varying sea ice covers. *Journal of Geophysical Research*, **95**(C6), 9557–9567, doi: 10.1029/JC095iC06p09557.

Perovich, D.K. (1998) The optical properties of sea ice. In Leppäranta, M. (ed.), *Physics of ice-covered seas*, Vol. 1, pp. 195–230. Helsinki, University of Helsinki Press. (Available at https://helda.helsinki.fi/handle/10138/39285).

Perovich, D.K., and Polashenski, C. (2012) Albedo evolution of seasonal Arctic sea ice. *Geophysical Research Letters* **39**, L08501, doi: 10.1029/2012GL051432.

Petrenko, V.F., and Whitworth, R.W. (1999) *Physics of Ice.* Oxford University Press, 373 pp. Oxford, U.K.

Petrov, M.P., Terzhevika, A.Yu., Zdorovennov, R.E., and Zdorovennova, G.E. (2006) The thermal structure of a shallow lake in early winter. *Water Research*, **33**, 135–143.

Petrov, M., Terzhevik, A., Zdorovennov, R., and Zdorovennova, G. (2007) Motion of water in an ice-covered shallow lake. *Water Resources* **34**(2), 113–122. doi: 10.1134/S0097807807020017.

Phillips, O.M. (1970) On flows induced by diffusion in a stably stratified fluid. *Deep Sea Research*, **17**, 435–443. doi: 10.1016/0011-7471(70)90058-6.

Pieters, R., and Lawrence, G.A. (2009) Effect of salt exclusion from lake ice on seasonal circulation. *Limnology and Oceanography*, **54**, 401–412.

Pirazzini, R., Vihma, T., Granskog, M. A. and Cheng, B. (2006) Surface albedo measurements over sea ice in the Baltic Sea during the spring snowmelt period. *Annals of Glaciology*, **44**, 7–14.

Pirinen, P., Simola, S., Aalto, J., Kaukoranta, J.-P., Karlsson, P., and Ruuhela, R. (2012) Tilastoja Suomen ilmastosta 1981–2010 [Statistics on the climate in Finland]. Finnish Meteorological Institute, Report 2012:1 [in Finnish and in English]. Available at https://helda.helsinki.fi/handle/10138/35880.

Pivovarov, A.A. (1973) *Thermal conditions in freezing lakes and rivers*. Wiley, New York, N.Y. 136 pp. [Translated from Russian].

Pounder, E.R. (1965) *Physics of ice*. Pergamon Press, Oxford, UK.

Priscu, J.C. (ed.) (1998) *Ecosystem dynamics in a polar desert: the McMurdo Dry Valleys Antarctica.* Research Series vol. 72. American Geophysical Union, Washington DC.

Priscu, J.C., and Foreman, C.M. (2009) Lakes of Antarctica. In: Gene E. Likens, (Editor) *Encyclopedia of Inland Waters*. volume 2, pp. 555–566. Oxford: Elsevier.

Pritchard, R.S. (1975) An elastic-plastic constitutive law for sea ice. *Journal of Applied Mechanics*, **42E**, 379–384.

Pritchard, R.S. (1980) Simulations of nearshore winter ice dynamics in the Beaufort Sea. In: R.S. Pritchard (ed.), *Proceedings of ICSI/AIDJEX Symposium on Sea Ice Processes and Models* (pp. 49–61). University of Washington, Seattle.

Prokacheva, V.G., and Borodulin, V.V. (1985) Long-term fluctuations of ice cover in Lake Ladoga. *Meteorologiya i Gidrologiya,* **10**, 86–93.

Prokopenko, A.A., and Williams, D.F. (2005) Depleted methane-derived carbon in waters of Lake Baikal, Siberia. *Hydrobiologio*, **544**, 279–288.

Puklakov, V.V., Edel'shtein, K.K., Kremenetskaya, E.R., and Gashkina, N.A. (2002) Water self purification in the Mozhaisk Reservoir in winter. *Water Resources*, **29**(6), 655–664.

Pulkkanen, M., and Salonen, K. (2013) Accumulation of low oxygen water in deep waters of ice-covered lakes cooled below 4 °C. *Inland Waters*, 3(1), 15–24.

Rahm, L. (1985) The thermally forced circulation in a small, ice-covered lake. *Limnology and Oceanography*, **30**, 1122–1128.

Raj, K. B. G., Kumar, K.V., Mishra, R. and Muneer, A. M. (2014) Remote sensing based assessment of glacial lake growth on Milam Glacier, Goriganga Basin, Kumaon Himalaya. *Journal of Geologial Society of India*, **83**, 385–392.

Ramseier, R.O. (1971) Mechanical properties of snow ice. *Proceedings of POAC 1971*, vol. 1, pp. 192–210.

Reed, R.K. (1977) On estimating insolation over the ocean. *Journal of Physical Oceanography*, **7**, 482–485.

Reinart, A., and Pärn, O. (2006) Ice conditions of a large shallow lake (Lake Peipsi) determined by observations, an ice model, and satellite images. *Proceedings of the Estonian Academy of Sciences. Biology and Ecology*, **55**(3), 243–261.

Reinart A., Arst, H., Blanco-Sequeiros, A., and Herlevi, A. (1998) Relation between underwater irradiance and quantum irradiance in dependence on water transparency at different depths in the water bodies. *Journal of Geophysical Research*, **103**(C4), 7749–7752.

Reinart A., Arst, H., Nõges, P., and Nõges. T. (2000) Comparison of euphotic layer criteria in lakes. *Geophysica,* **36**(1–2), 141–159.

Rignot, E., Rivera, A., and Casassa, G. (2003) Contribution of the Patagonia icefields of South America to sea level rise. *Science,* **302**, 434–437.

Rintala, J. M. (2009). A systematic-ecological approach to Baltic Sea ice studies of algae and protists. PhD thesis, University of Helsinki, Faculty of Biosciences.

Robertson, D.M., Ragotszkie, R.A., and Magnuson, J.J. (1992) Lake ice records used to detect historical and future climatic change. *Climate Change*, **21**, 407–427.

Rodhe, B. (1952) On the relation between air temperature and ice formation in the Baltic. *Geografiska Annaler,* **1–2**, 176–202.

Rogers, S.O., Shtarkman, Yu.M., Koçer, Z.A., Edgar, R., Veerapaneni, R., and D'Elia, T. (2013) Ecology of subglacial Lake Vostok (Antarctica), based on metagenomic/metatranscriptomic analyses of accretion ice. *Biology* **2013**, 2, 629-650; doi:10.3390/biology2020629.

Rothrock, D.A. (1975) The mechanical behavior of pack ice. *Annual Review of Earth Planetary Science*, **3,** 317–342.

Rothrock, D.A. (1986). Ice thickness distribution – measurement and theory. In: N. Untersteiner (ed.), *The Geophysics of Sea Ice* (pp. 551–575). Plenum Press, New York.

Rudd, J.W., and Hamilton, R.D. (1978) Methane cycling in a eutrophic shield lake and its effects on the whole lake metabolism. *Limnology and Oceanography*, **23**, 337–348.

Rumyantsev, V., Viljanen, M., and Slepukhina, T. (1999) The present state of Lake Ladoga, Russia – a review. *Boreal Environment Research*, 4, 201–214.

Ruuhijärvi, R. (1974) A general description of the oligotrophic lake Pääjärvi, southern Finland, and the ecological studies on it. *Annales Botanici Fennici*, **11**, 95**–**104.

Sahlberg, J. (1983) A hydrodynamical model for calculating the vertical temperature profile in lakes during Cooling. *Nordic Hydrology*, **14**(4), 239–254.

Salonen, K., Leppäranta, M., Viljanen, M., and Gulati, R. (2009) Perspectives in winter limnology: closing the annual cycle of freezing lakes. *Aquatic Ecology*, **43**(3), 609–616.

Saloranta, T. (2000) Modeling the evolution of snow, snow ice and ice in the Baltic Sea, *Tellus*, **52**A, 93–108.

Sanderson, T.J.O. (1988) Ice Mechanics. Risks to O.shore Structures. Graham & Trotman, Boston.

Saucier, F.J., Roy, F., Gilbert, D., Pellerin, P., and Ritchie, H. (2003) Modeling the formation and circulation processes of water masses and sea ice in the Gulf of St. Lawrence, Canada. *Journal of Geophysical Research*, **108**(C8), 3269, doi: 10.1029/2000JC000686.

Schmid, M., Budnev, N.M., Granin, N.G., Sturm, M., Schurter, M., and Wüest, A. (2008) Lake Baikal deepwater renewal mystery solved. *Geophysical Research Letters*, **35**, L09605. doi: 10.1029/2008GL033223.

Schulson, E.M., and Duval, P. (2009) *Creep and fracture of ice*. Cambridge University Press, Cambridge, U.K.

Schwerdtfeger, P. (1963) The thermal properties of sea ice. *Journal of Glaciology*, **4**(36), 789-807.

Semovski, S.V., Mogilev, N.Yu., and Sherstyankin, P.P. (2000) Lake Baikal ice: analysis of AVHRR imagery and simulation of under-ice phytoplankton bloom. *Journal of Marine Systems* **27**, 117–130.

Semtner, A. J. (1976) A model for the thermodynamic growth of sea ice in numerical investigations of climate. *Journal of Physical Oceanography*, **6**, 379–389.

Sergeev, B.N. (1929) Creation of winter crossing of wagons on the ice and behavior of a layer of ice under load. *Trudy Nauchno-Tekhnicheskogo Komiteta Narodnogo Komissariata Putei Soobshcheniya*, **84**, 5–35.

Shen, H.T., Chen, Y.C., Wake, A., and Crissman, R.D. (1993) Lagrangian discrete parcel simulation of two-dimensional river ice dynamics. *International Journal of Offshore and Polar Engineering* **3**(4), 328–332.

Shen, H.T. (2006) A trip through the life of river ice – research progress and needs. *Proceedings of the 18th IAHR International Symposium on Ice, pp.* 85–91. Hokkaido University, Sapporo, Japan.

Shen, H.T., and Yapa, P.D. (1985) A unified degree-day method for river ice cover thickness simulation. *Canadian Journal of Civil Engineering,* **12**(1), 54–62.

Sherstyankin, P.P. (1975) *The experimental investigations of under ice light field of Lake Baikal* [in Russian]. *Moscow Nauka*.

Shimaraev, M., and Granin, N. (1991) Temperature stratification and the mechanism of convection in Lake Baikal. *Doklady of the Academy of Sciences of Russia*, **321**, 381–385 (in Russian).

Shimaraev, M.N., Gnatovskii, R.Yu., Blinov, V.V., and Ivanov, V.G. (2011) Renewal of deep waters of Lake Baikal revisited. *Doklady Earth Sciences*, **438**, 652–655. doi: 10.1134/S1028334X11050096.

Shirasawa, K., Leppäranta, M., Saloranta, T., Polomoshnov, A., Surkov, G., and Kawamura, T. (2005) The thickness of landfast ice in the Sea of Okhotsk. *Cold Regions Science and Technology,* **42**, 25–40.

Shirasawa, K., Leppäranta, M., Kawamura, T., Ishikawa, M., and Takatsuka, T. (2006) Measurements and modelling of the water – ice heat flux in natural waters. *Proceedings of the 18th IAHR International Symposium on Ice, pp.* 85–91. Hokkaido University, Sapporo, Japan.

Shtarkman, Y.M., Koçer, Z.A., Edgar R, Veerapaneni, R.S., D'Elia. T., Morris, P.F., and Rogers, S. O. (2013) Subglacial Lake Vostok (Antarctica) accretion ice contains a diverse set of sequences from aquatic, marine and sediment-inhabiting bacteria and eukarya. PLoS ONE 8(7): e67221.

Shumskii, P.A. (1956) *Principles of Structural Glaciology* [in Russian]. English transl. 1964 by Dover Publications, Inc.

Shuter, B.J., Finstad, A.G., Helland, I.P., Zweimüller, I., and Hölker, F. (2012) The role of winter phenology in shaping the ecology of freshwater fish and their sensitivities to climate change. *Aquatic Sciences,* **74**(4), 637–657.

Siegert, M., Ellis-Evans, J.C., Tranter, M., Mayer, C., Petit, J.-R., Salamatink, A., and Priscu, J.C. (2001) Physical, chemical and biological processes in Lake Vostok and other Antarctic subglacial lakes. *Nature,* **414**, 603–609.

Simojoki, H. (1940) Über die Eisverhältnisse der Binnenseen Finnlands. *Mitteilungen des Meteorologischen Instituts der Universität Helsinki* **43**, 194 pp. + annexes. [in German].

Simojoki, H. (1959) Kallaveden pitkä jäähavaintosarja [A long series of ice observations for Lake Kallavesi]. *Terra*, **71**, 156–161.

Simojoki, H. (1978) The history of geophysics in Finland 1828–1918. *The History of Learning and Science in Finland 1828–1918*, No. 5b, Societas Scientarum Fennicae, Helsinki.

Smetacek, V., and Passow, U. (1990) Spring bloom initiation and Sverdrup's critical-depth model. *Limnology and Oceanography*, **35**, 228–234.

Smith, R.C., and K. S. Baker, K.S. (1981) Optical properties of the clearest natural waters (200–800 nm). *Applied Optics*, **20**, 177–184.

Sobiech, J., and Dierking, W. (2013) Observing lake- and river-ice decay with SAR: advantages and limitations of the unsupervised k-means classification approach. *Annals of Glaciology*, **54**(62), 65–72.

Sokratova, I.N. (2011) Hydrological investigations in the Antarctic oases. *Russian Meteorology and Hydrology*, **36**(3), 207–215.

Stefan, J. (1891) Über die Theorie der Eisbildung, insbesondere uber Eisbildung im Polarmeere. *Annalen der Physik, 3rd Ser*, **42,** 269–286.

Stigebrandt, A. (1978) Dynamics of an ice covered lake with throughflow. *Nordic Hydrology*, **9**, 19–244.

Strayer, R.F., and Tiedje, J.M. (1978) In situ methane production in a small, hypereutrophic, hard-water lake: Loss of methane from sediments by vertical diffusion and ebullition. *Limnology and Oceanography*, **23**(6), 1201–1206.

Sturova, I.V. (2007) Effect of ice cover on oscillations of fluid in a closed basin. *Izvestiya Atmospheric and Oceanic Physics*, **43**(1), 112–118. doi: 10.1134/S0001433807010136.

Svensson, U. (1979) The structure of the turbulent Ekman layer. *Tellus*, **31**, 340–350.

Svensson, U., and Larsson, R. (1980) A one-dimensional numerical model study of some basic features of the flow in ice-covered lakes. *Journal of Hydraulic Research*, **18**, 251–267.

Tennekes, H., and Lumley, J.E. (1972) *A First Course in Turbulence.* MIT Press.

Terzhevik, A., Golosov, S., Palshin, N., Mitrokhov, A., Zdorovennov, R., Zdorovennova, G., Kirillin, G., Shipunova, E., and Zverev, I. (2009) Some features of the thermal and dissolved oxygen structure in boreal, shallow ice-covered Lake Vendyurskoe, Russia. *Aquatic Ecology*, **43** (3), 617–627. doi: 10.1007/s10452-009-9288-x.

Terzhevik, A.Y., Palshin, N.I., Golosov, S.D., Zdorovennov, R.E., Zdorovennova, G.E., Mitrokhov, A.V., Potakhin, M.S., Shipunova, E.A., and Zverev, I.S. (2010) Hydrophysical aspects of oxygen regime formation in a shallow ice-covered lake. *Water Resources*, **37**, 662–673. doi: 10.1134/S0097807810050064.

Thomas, D.N., and Dieckmann, G.S. (2010) *Sea ice*, 2nd ed. Wiley–Blackwell, Chichester, West Sussex, United Kingdom.

Thorndike, A.S., Rothrock, D.A., Maykut, G.A., and Colony, R. (1975) The thickness distribution of sea ice. *Journal of Geophysical Research,* **80**, 4501–4513.

Thorpe, S.A. (2005) *The turbulent ocean.* Cambridge University Press, Cambridge, UK.

UNESCO (1981) The Practical Salinity Scale 1978 and the International Equation of State of Seawater 1980. Technical Papers in Marine Science, 36.

Vakkilainen, P. (2001) Hydrology at technical universities. *Geophysica*, **37**(1–2), 205–213.

Van Hoeve, P., Belzile. C., Gibson, J.A.E., and Vincent, W.F. (2006) Coupled landscape-lake evolution in the Canadian High Arctic. *Canadian Journal of Earth Sciences*, **43**, 533–546.

Vanderploeg, H.A., Bolsenga, S.J., Fahnenstiel, G.L., Liebig, J.L., and Gardner, W.S. (1992) Plankton ecology in an ice-covered bay of Lake Michigan: utilization of a winter phytoplankton boom by reproducing copepods. *Hydrobiologia* **243/244**, 175–183.

Veillette, J., Martineau, M.-J., Antoniades, D., Sarrazin, D., Vincent, W.F. (2010) Effects of loss of perennial lake ice on mixing and phytoplankton dynamics: insights from High Arctic Canada. *Annals of Glaciology*, **51**(56).

Venkatesh, S., El-Tahan, H., Comfort, G., and Abdelnour, R. (1990) Modelling the behaviour of oil spills in ice-infested waters. *Atmosphere–Ocean* **28**(3), 303–329.

Verescagin, G. (1925) A selection of works from Lake Baikal Expedition. *Doklady Acad Sci SSSR*, **12**, 161–164 [in Russian].

Vihma, T. (1995a) Atmosphere-surface interactions over polar oceans and heterogeneous surfaces. *Finnish Marine Research* **264**, 41pp + 7 articles, Finnish Institute of Marine Research, Helsinki. (PhD Thesis).

Vihma, T. (1995b) Subgrid parameterization of surface heat and momentum fluxes over polar oceans. *Journal of Geophysical Research*, **100**, 22,625–22,646.

Vincent, C., Descloitres, M., Garambois, S., Legchenko, A., Guyard, H., and Gilbert, A. (2012) Detection of a subglacial lake in Glacier de Tête Rousse (Mont Blanc area). *Journal of Glaciology*, **58**(211). doi: 10.3189/2012JoG11J179.

Vincent, W.F. and Laybourn-Parry, J. (eds.) (2008) *Polar lakes and rivers. Limnology of Arctic and Antarctic aquatic ecosystems.* Oxford University Press, Oxford, UK.

Vincent, W.F., Hobbie, J.E., and Laybourn-Parry, J. (2008) Introduction to the limnology of high-latitude lake and river ecosystems. In: Vincent, W.F. and Laybourn-Parry, J. (eds.), *Polar lakes and rivers. Limnology of Arctic and Antarctic aquatic ecosystems*, pp. 1–23. Oxford University Press, Oxford, UK.

Vincent, F., Raucoules, D., Degroeve, T., Edwards, G., and Abolfazl Mostafavi, A. (2012) Detection of river/sea ice deformation using satellite interferometry: limits and potential. *International Journal of Remote Sensing*, **25**(18), 3555–3571.

Wadhams, P. (2000) *Ice in the ocean.* Gordon & Breach Science, Amsterdam.

Wake, A., and Rumer, R.R. (1983) Great lakes ice dynamics simulation. *Journal of Waterway, Port, Coastal and Ocean Engineering*, **109**, 86–102.

Wand, U., Schwarz, G., Bruggemann, E., and Brauer, K. (1997) Evidence for physical and chemical stratification in Lake Untersee (central Dronning Maud Land, East Antarctica). *Antarctic Science*, **9**(1), 43–45.

Wang, C., Shirasawa, K., Leppäranta, M., Ishikawa, M., Huttunen, O., and Takatsuka, T. (2005) Solar radiation and ice heat budget during winter 2002–2003 in Lake Pääjärvi, Finland. *Verhandlungen der Internationalen Vereinigung für Theoretische und Angewandte Limnologie*, **29**, 414–417.

Wang, J., Mysak, L.A., and Ingram, R.G. (1994) A numerical simulation of sea-ice cover in Hudson Bay. *Journal of Physical Oceanography*, **24**, 2515–253.

Wang, J. Hu, H., and Bai, X. (2010) Modeling Lake Erie ice dynamics: Process studies. *Proceedings of the 20th IAHR International Symposium on Ice,* University of Helsinki, Finland.

Wang, K., Leppäranta, M., and Kouts, T. (2003) A model for sea ice dynamics in the Gulf of Riga. *Proceedings of Estonian Academy of Sciences. Engineering*, **9**(2), 107–125.

Wang, K., Leppäranta, M., and Reinart, A. (2006a) Modeling ice dynamics in Lake Peipsi. *Verh. Internat. Verein. Limnol.*, **29**, 1443–1446.

Wang, K., M. Leppäranta and T. Kouts (2006b) A study of sea ice dynamic events in a small bay. *Cold Regions Science and Technology* **45**: 83–94.

Warren S.G. (1982) Optical properties of snow. *Reviews in Geophysics and Space Physics*, **20**(1), 67–89.

Webb, E.K. (1970) Profile relationships: The log-linear range and extension to strong stability. *Quarterly Journal of Royal Meteorological Society*, **96**, 67–90.

Weeks, W.F. (1998) Growth conditions and structure and properties of sea ice. In: M. Leppäranta (ed.), *The physics of ice-covered seas*, Vol. 1, pp. 25–104. Helsinki University Press, Helsinki. (Available at https://helda.helsinki.fi/handle/10138/39285).

Weeks, W.F. (2010) *On sea ice*. University of Alaska Press, Fairbanks, Alaska.

Weeks, W.F., and Gow, A.J. (1978) Preferred crystal orientations in the fast ice along the margins of the Arctic Ocean. *Journal of Geophysical Research,* **83**(C10), 5105–5121.

Weeks, W.F., and Lofgren, G. (1967) The effective solute distribution coefficient during the freezing of NaCl solutions. In: H. Oura (ed.), *Proceedings of the International Conference on Low Temperature Science. Physics and Snow and Ice,* I(1), 579–597. Institute of Low Temperature Science, Sapporo, Japan.

Weeks, W.F., Gow, A.J., Kosloff, P., and Digby-Argus, S. (1990) The internal structure, composition and properties of brackish ice from the Bay of Bothnia. CRREL Monograph 90–1, 5–15.

Weiss, R.F., Carmack, E.C., and Koropalov, V.M. (1991) Deep-water renewal and biological production in Lake Baikal. *Nature* **349**, 665–669. doi: 10.1038/349665a0.

Welch, H., Dillon, P., and Sreedharan, A. (1976) Factors affecting winter respiration in Ontario lakes. *Journal of Fishery Research Board of Canada*, **33**, 1809–1815.

Welch, H.E., and Bergmann, M.A. (1985) Water circulation in small arctic lakes in winter. *Canadian Journal of Fishery and Aquatic Science*, **42**, 506–520.

Wilson, A.T., and Wellman, H.W. (1962) Lake Vanda: An Antarctic lake. *Nature*, **196**, 1171–1173.

Wing, L. (1943) Freezing and thawing dates of lakes and rivers as phenological indicators. *Monthly Weather Review*, **71**, 149–155.

Winther, J.-G., Elvehøy, H., Bøggild, C.E., Sand, K., and Liston, G. (1996) Melting, runoff and the formation of frozen lakes in a mixed snow and blue-ice field in Dronning Maud Land, Antarctica. *Journal of Glaciology*, **42**(141), 271–278.

WMO, 1970. WMO sea-ice nomenclature. Report N:o 147. World Meteorological Organization, Geneve, Switzerland.

Wüest, A., and Lorke, A. (2003) Small-scale hydrodynamics in lakes. *Annual Reviews of Fluid Mechanics*, **35**, 373–412. doi: 10.1146/annurev.fluid.35.101101.161220.

Wunsch, C. (1970) On oceanic boundary mixing. *Deep Sea Research*, **17**, 293–301. doi: 10.1016/0011-7471(70),90022-7.

Wyman, M. (1950) Deflections of an infinite plate. *Canadian Journal of Research,* **A28**, 293–302.

Yang, Y., Leppäranta, M., Li, Z., and Cheng, B. (2012) An ice model for Lake Vanajavesi, Finland. *Tellus* A, **64**, 17202, DOI: 10.3402/tellusa.v64i0.17202.

Yang, Y., Cheng, B., Kourzeneva, E., Semmler, T., Rontu, L., Leppäranta, M., Shirasawa, K., and Li, Z. (2013) Modelling experiments on air-snow-ice interactions over an Arctic lake. *Boreal Environment Research*, **18**, 341–358.

Yen, Y.-C. (1981) Review of thermal properties of snow, ice and sea ice. CRREL Report 81-10. U. S. Army Cold Regions Research and Engineering Laboratory, Hanover, NH.

Zeikus, J.G., and Winfrey, M.R. (1976) Temperature limitation of methanogenesis in aquatic sediments. *Applied Environmental Microbiology*, **31**, 99–107.

Zhdanov, A.A., Granin, N.G., and Shimaraev, M.N. (2001) The generation mechanism of under-ice currents in Lake Baikal. *Doklady Earth Science*, **377A**, 329–332.

Zilitinkevich, S. S., Kreiman, K. D., and Terzhevik, A. Yu. (1992) The thermal bar. *Journal of Fluid Mechanics* **236**(1), 27–42.

Zillman, J.W. (1972) A study of some aspects of the radiation and heat budgets of the Southern Hemisphere oceans. In *Meteorological Studies*, 26. Bureau of Meteorology, Department of Interior, Canberra, Australia, 562 pp.

Zintz, K., Löffler, H., and Schröder, H.G. (2009) *Der Bodensee. Ein Naturraum im Wandel*. Thorbecke, Ostfildern.

Zotikov, I.A. (2006) *The Antarctic subglacial Lake Vostok*. *Glaciology, biology and planetology*. Springer Praxis books, Springer Berlin Heidelberg.

Zubov, N.N. (1942) Basics devices roads ice cover. *Gidrometeoizdat*, 74 p.

Zubov, N.N. (1945) *L'dy Arktiki* [Arctic Ice]. Izdatel'stvo Glavsermorputi, Moscow. [English translation 1963 by U.S. Naval Oceanographic Office and American Meteorological Society, San Diego].

Zdorovennova, G. (2009) Spatial and temporal variations of the watersediment thermal structure in shallow ice-covered Lake Vendyurskoe (Northwestern Russia). *Aquatic Ecology*, **43**, 629–639. doi: 10.1007/s10452-009-9277-0.

Zyryanov, V.N. (2011) Under-ice seiches. *Water Resources*, **38**, 261–273. doi: 10.1134/S0097807811020163.